

**Ground-state structures and vibrational free  
energy in first-principles models of  
substitutional-alloy thermodynamics**

by

Gerardo Damián Garbulsky

Submitted to the Department of Materials Science and Engineering  
in partial fulfillment of the requirements for the degree of

Doctor of Philosophy in Materials Science

at the

MASSACHUSETTS INSTITUTE OF TECHNOLOGY

June 1996

© Massachusetts Institute of Technology 1996. All rights reserved.

Author .....  
Department of Materials Science and Engineering  
May 3, 1996

Certified by .....  
Gerbrand Ceder  
Associate Professor of Materials Science  
Thesis Supervisor

Accepted by .....  
Michael F. Rubner  
TDK Professor of Materials Science and Engineering  
Chair, Departmental Committee on Graduate Students

MASSACHUSETTS INSTITUTE  
OF TECHNOLOGY

JUN 24 1996

ARCHIVES



*A mis viejos, Susy y Gusty*



# Ground-state structures and vibrational free energy in first-principles models of substitutional-alloy thermodynamics

by

Gerardo Damián Garbulsky

Submitted to the Department of Materials Science and Engineering  
on May 3, 1996, in partial fulfillment of the  
requirements for the degree of  
Doctor of Philosophy in Materials Science

## Abstract

We explore three areas of the first-principles studies of substitutional alloy thermodynamics: the parameterization of the configurational energy of the alloy, the search for the ground states, and the inclusion of the vibrational degrees of freedom in the lattice models.

We develop a method for obtaining effective cluster interactions (ECI's) in substitutional alloys from total-energy calculations, based on linear-programming techniques. The method reproduces not only the formation energies, but also the ground-state line and relative energies of different structures. We show that long-range interactions are necessary to reproduce the ground-state line of the fcc Pd-rich superstructures in the Pd-V system.

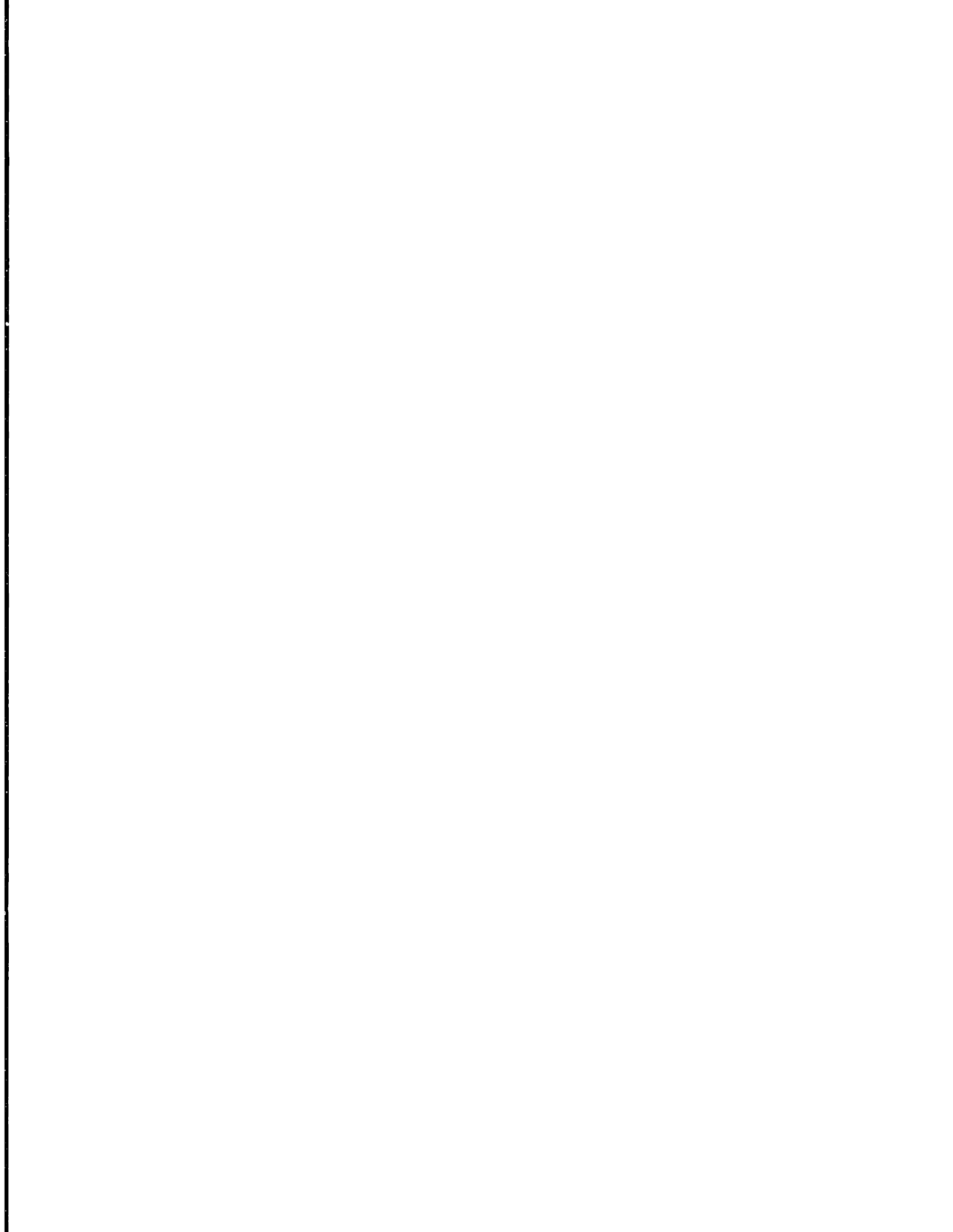
We review existing methods to obtain the ground states of a lattice model and develop a method that can solve problems with long-range ECI's. We find solutions to two ground-state problems on the fcc lattice: ternary alloys with first- and second-neighbor ECI's and binary alloys with first- through fourth-neighbor ECI's.

A deep understanding of alloy thermodynamics requires not only a model of the substitutional excitations, but also of the other degrees of freedom in the alloy. We show that, with very few assumptions, the effects of *lattice vibrations* can be included in the lattice models used to study alloy phase stability. We illustrate the formalism by applying it to several systems: a one-dimensional alloy, "isotopic" alloys, Ar-Kr alloys, and MgO-CaO pseudobinary mixtures. The predicted MgO-CaO phase diagram is in very good agreement with experimental data. By using available experimental information on intermetallic alloys, we estimate that the lattice vibrations may reduce transition temperatures by  $\sim 30\%$  in some systems.

First-principles techniques are required if reliable predictions are sought. We evaluate the Debye approximation, usually used in first-principles studies, and show that it fails to capture the configuration dependence of the vibrational free energy. We develop a new method, based on the calculation of a few spring constant parameters, and apply it to study Si-Ge alloys.

Thesis Supervisor: Gerbrand Ceder

Title: Associate Professor of Materials Science



## Summary

We explore three areas in the study of alloy thermodynamics: the parameterization of the substitutional energy of the alloy, the search for the ground states of the resulting lattice Hamiltonian, and the inclusion of the vibrational degrees of freedom in the lattice models.

We develop a method for obtaining effective cluster interactions (ECI's) in substitutional binary alloys from first-principles total-energy calculations, based on linear-programming techniques. The method reproduces not only the formation energies, but also the ground-state line and relative energies of different structures. Using the new method, we show that long-range pair interactions (seventh- or eighth-neighbor pairs) are necessary to reproduce the ground-state line of the fcc Pd-rich superstructures in the Pd-V system.

The study of the ground-state structures is the first step in the calculation of the thermodynamic properties of an alloy. We use the polyhedron method to approximately solve the ground-state problem of ternary alloys on the fcc lattice with first- and second-neighbor interactions. To our knowledge, this is the largest ground-state problem solved to date, with 323,188 vertices in the ground-state polytope. Although most of the vertices do not correspond to real structures, we find 31 *exact* ternary ground states.

We show that the complexity of the polyhedron method grows in such a way that solutions for alloys with more than a few ECI's will not be obtained in the near future. For this reason, we develop a method, that we call "enumeration" method, that is capable of finding approximate solutions of the ground-state problem for *any* interaction range. The method is based on an exhaustive enumeration of ordered structures with relatively small unit cells, and the construction of the convex hull of the resulting points in correlation space. We apply the enumeration method to study the ground-state configurations of binary fcc alloys with first- through fourth-neighbor ECI's. Our solution shows that previous approximate solutions underestimated the number of possible ground-state structures by an order of magnitude.

To be able to make reliable predictions of phase stability of alloys, all the important contributions to the free energy have to be included in the models. We show that with very few assumptions the effects of lattice vibrations can be included in the lattice models used to study alloy phase stability.

For temperatures of the order of, or larger than, the Debye temperatures of the system, the effect of the lattice vibrations, in the harmonic approximation, can be included in the ECI's with a term linear in temperature. These high-temperature "vibrational" ECI's depend on the spring constant disorder but not on the masses of the atoms.

We illustrate the formalism by applying it to several model systems. A linear chain with only nearest-neighbor springs is solved exactly in the high-temperature limit, and an elastic approximation is used for the low-temperature limit. The accuracy of this approximation is verified with a numerical study.

In "isotopic" alloys, where two isotopes of the same element are mixed together, there is no chemical difference between the species. However, due to the different

masses of the isotopes, the vibrational frequencies depend on the arrangement of the atoms, and a small phase-separation tendency is induced. We estimate the consolute temperatures of these systems to be extremely low (in the milli-Kelvin range).

The Ar-Kr system is used to illustrate the change in the predicted phase diagram of an ordering alloy when the lattice vibrations are included in the model. The order-disorder transition in this system is reduced by 12% by the lattice vibrations.

With the use of Lennard-Jones potentials, we study the trends in the effect of lattice vibrations with chemical affinity and size mismatch of the alloy species. We found that although for most alloy systems the lattice vibrations will reduce the predicted transition temperatures, there are some combinations of chemical affinity and size mismatch for which the opposite is true. By using available experimental information on intermetallic alloys, we estimate that the lattice vibrations may reduce transition temperatures by  $\sim 30\%$  in some systems.

The MgO-CaO system is highly ionic and the ions are almost spherical. This allows us to use a simplified first-principles method to compute phonon frequencies for ordered structures. The computed phase diagram with the effect of vibrations is in very good agreement with available experimental data.

Because complete computations of the phonon density of states from first principles are difficult, simpler models for the vibrational free energy have been used to incorporate these effects into phase diagram calculations. We systematically investigate the accuracy of these approximations by studying model systems for which the vibrational free energy can be computed exactly in the harmonic approximation. We find that the Debye approximation, usually used in first-principles studies, fails to capture the configuration dependence of the vibrational free energy. We explain the reason for this failure.

We develop a new method to include the lattice vibrations in the alloy models from first principles, based on the calculation of a few spring-constant parameters. This method produces reliable, quantitative predictions and does not require the calculation of the full phonon dispersion relations. To illustrate the applicability of the new method to real systems, we study Si-Ge alloys.



# Acknowledgments

I am very grateful to my advisor, Professor Gerbrand Ceder, for his encouragement and support. His guidance throughout my thesis work helped me learn a great deal about science. Doing research, teaching, and hiking with “Gerd” will be some of the most enduring memories from my days at MIT.

I thank the members of my thesis committee, Prof. Samuel M. Allen and Prof. Mehran Kardar for their support and comments on this manuscript.

Alberto Pignotti, my mentor in Buenos Aires, supported my plans of coming to MIT from the early days. For that and his friendship, I thank him very much.

Several people gave us the technical support that made this thesis possible. David Avis and Komei Fukuda taught us about vertex–enumeration techniques. I enjoyed the interaction with them during the ground–state project very much. I thank Kenneth Clarkson for his help in the early stages of the ground–state project. John Joannopoulos and Kyeongjae Cho provided us with the pseudopotential codes used in chapter 6. Their assistance in learning to use the codes was a great help for my thesis work. Mark van Schilfgaarde is gratefully acknowledged for providing us with the LMTO–ASA codes, used in chapter 2. Steve Steiner developed the computer graphics that made the interpretation of the ground–state structures in chapter 3 possible. Harold Stokes is acknowledged for the phonon calculations with the self–consistent potential–induced breathing method. For some of the Lennard–Jones calculations, we used the General Utility Lattice Program, developed by Julian Gale. Finally, Mei-Yin Chou and Siqing Wei provided valuable suggestions for the calculations of force constants in the Si–Ge system.

Hanging out with Chris Wolverton, Ryan McCormack, Mark Asta, and Carlos Amador at the APS, MRS, and TMS meetings was a pleasure and privilege. Comments and suggestions from Efthimios Kaxiras, Alex Zunger, and Didier de Fontaine are greatly appreciated.

The discussions with present and past members of our research group gave me extra motivation for my every–day work. They are: Shuba, Anton, Axel, Kadri, Craig B., Adro, Patrick and Gerd.

I could not possibly enumerate all the ways in which Patrick Tepesch and Adrián Kohan helped me during my Ph.D. work. It was not just in trying to get the pseudopotential code to converge or challenging every one of my arguments, but also in giving me the motivation and energy that made my years at MIT a great experience. For all that and their friendship, I thank them from the bottom of my heart.

The friends I made during these years in Boston helped me enjoy myself very

much. They are Patrick, Kate, Roby, Sandra, Ale, Daniel, Pampa, Marce, Juanπ, Flor, Felipe, Sally, Yair, Analia, Alain, Pablo, Maria, and Ariel.

I was very lucky to have my friend Julio and his wife Vicki nearby. I thank Adro, Cari, Luigi, and Adri because they made me look forward to the weekends. With the help from all of them, I could balance my life between work and sharing time with the people I love.

Coming to MIT would not have been possible without the support of my beloved family in Argentina. The frequent visits of Iaia Tituña Tomasa, Iaio Quique, Susy, Gusty, Marto, Vivi, Fabio, Melu, Maru, and Guidín made me feel close to home, in spite of the 6,000 miles that keep us apart. I also enjoyed the visits of Adrian P., Sergio, Jorge, Estela, and Gabri very much.

I dedicate this thesis to my parents Susy and Gusty. Their commitment to my education from the very early days is the pillar on which I am constructing my professional career. Although they would rather have had me with them in Argentina, they supported my plans unconditionally. For all this and their love, I will always be indebted to them.

But, most of all, I would like to thank my beloved wife, Marce (La Chitrula). She is not only the prettiest woman on Earth and nearby planets, but also the best company. Her support made this thesis possible. I could not imagine going through these years without her.

Finally, I would like to acknowledge my financial support. During my first year at MIT, I had the support of the Roberto Rocca Fellowship. It gave me enough time to shop around and find a research group and topic that made my stay at MIT a real joy. Subsequently, I had support, at different times from: the AT&T New Research Fund, the National Science Foundation (MRL Contract DMR90-22933 and DMR-9400334), the Charles Reed Fund at MIT. Finally, during the spring of 1995, I was supported by a teaching assistantship of the Department of Materials Science and Engineering.

# Contents

<b>Abstract</b>	<b>5</b>
<b>Summary</b>	<b>7</b>
<b>Acknowledgments</b>	<b>9</b>
<b>Contents</b>	<b>11</b>
<b>List of Figures</b>	<b>15</b>
<b>List of Tables</b>	<b>23</b>
<b>1 Introduction</b>	<b>27</b>
1.1 Computational materials science . . . . .	27
1.1.1 Computer power . . . . .	28
1.1.2 Advances in solid state physics . . . . .	28
1.1.3 Computational materials science: achievements and limitations	31
1.2 Alloy theory . . . . .	33
1.2.1 Building the alloy Hamiltonian . . . . .	36
1.2.2 Ground states of the lattice Hamiltonian . . . . .	37
1.2.3 Free energies and phase diagrams . . . . .	37
1.3 Contributions made in this thesis . . . . .	38
<b>2 The lattice-model Hamiltonian</b>	<b>41</b>
2.1 The cluster expansion . . . . .	42
2.2 Review of methods to compute the effective cluster interactions . . .	47
2.3 A new method to obtain the effective cluster interactions . . . . .	48
2.4 Application to the Pd-V system . . . . .	51
<b>3 Ground states in alloys</b>	<b>59</b>
3.1 The ground-state problem . . . . .	61
3.1.1 Two types of ground-state problems . . . . .	61
3.1.2 Frustration and the configurational polytope . . . . .	62
3.2 The polytope method . . . . .	66
3.2.1 The method . . . . .	66
3.2.2 Successes of the polytope method . . . . .	71

3.2.3	Application of the polytope method to fcc binary alloys with first- through fourth-neighbor pair interactions . . . . .	74
3.2.4	Application of the polytope method to fcc ternary alloys with first- and second-neighbor pair interactions . . . . .	77
3.3	The enumeration method . . . . .	84
3.3.1	The method . . . . .	84
3.3.2	Application of the enumeration method to fcc binary alloys with first- through fourth-neighbor pair interactions . . . . .	86
3.4	Conclusions . . . . .	88
3.5	Future perspectives . . . . .	91
<b>4</b>	<b>Lattice vibrations and phase stability: Formalism and trends</b>	<b>93</b>
4.1	Coarse-graining of the partition function . . . . .	94
4.1.1	From the continuous to the lattice Hamiltonian . . . . .	94
4.1.2	The $\vec{\sigma}$ -ensemble free energy . . . . .	96
4.1.3	The vibrational free energy . . . . .	98
4.1.4	The vibrational effective cluster interactions . . . . .	100
4.2	The vibrating binary chain . . . . .	102
4.3	The size of the effect of lattice vibrations on phase stability . . . . .	106
4.4	Conclusions . . . . .	108
<b>5</b>	<b>Lattice vibrations and phase stability: Classical-potential models</b>	<b>109</b>
5.1	Classical potentials . . . . .	110
5.2	The “isotopic” alloy . . . . .	110
5.3	The Ar-Kr system . . . . .	114
5.3.1	The phase diagram . . . . .	115
5.3.2	What frequencies are responsible for $\Delta \overline{\ln(\omega)}$ ? . . . . .	122
5.4	Trends . . . . .	122
5.5	Conclusions . . . . .	125
<b>6</b>	<b>Lattice vibrations and phase stability: First-principles methods</b>	<b>129</b>
6.1	The MgO-CaO pseudobinary system . . . . .	130
6.2	Approximate schemes . . . . .	133
6.2.1	Debye model . . . . .	133
6.2.2	Local harmonic model . . . . .	135
6.3	Evaluation of simplified models . . . . .	136
6.4	Alternative frameworks for <i>ab-initio</i> calculations . . . . .	140
6.5	A proposed new approach . . . . .	143
6.6	The Si-Ge alloy system . . . . .	149
6.7	Conclusions . . . . .	161
<b>7</b>	<b>Conclusions</b>	<b>163</b>
<b>8</b>	<b>Future research</b>	<b>167</b>

<b>A Building alloy configurations with specified values of correlation functions</b>	<b>171</b>
<b>B The Ising mapping of the alloy Hamiltonian: a toy model</b>	<b>175</b>
<b>C Classical potentials</b>	<b>181</b>
C.1 Pair potentials . . . . .	131
C.1.1 Limitations of pair potentials . . . . .	184
C.2 Multibody potentials . . . . .	184
<b>D Generating k-points to perform integrals over the Brillouin zone</b>	<b>187</b>
D.1 Introduction . . . . .	187
D.2 Primitive cells . . . . .	187
D.2.1 Brute Force . . . . .	187
D.2.2 Using the symmetry . . . . .	188
D.2.3 The Chadi-Cohen scheme . . . . .	188
D.3 Superstructures . . . . .	188
<b>Bibliography</b>	<b>190</b>



# List of Figures

1-1	Exponential growth in computer power. a) Number of transistors in the Intel microprocessors for personal computers [1]. b) Computational speed of Intel microprocessors in million instructions per second (MIPS). c) Time needed to perform a series of molecular-dynamics simulations on the fastest computer manufactured by different companies [2]. . . . .	29
1-2	Examples of temperature-composition phase diagrams of <i>substitutional</i> binary alloys. a) Cu-Au is a system in which the Cu and Au atoms arrange themselves on a face centered cubic lattice for all the composition range in the solid-state part of the phase diagram. b) In Cu-Zn alloys the substitutional alloy description applies, for example, to the shaded region, where the Cu and Zn atoms are distributed on a body centered cubic lattice. . . . .	34
1-3	Steps to compute the temperature-composition phase diagram of a substitutional alloy from first principles. . . . .	35
2-1	Examples of two-dimensional lattices. <sup>2</sup> The lattices extend infinitely in space. Only a portion of the lattice is shown. Lattices <i>a</i> and <i>b</i> have one lattice site per primitive unit cell, while lattice <i>b</i> and <i>c</i> have two and three lattice sites per primitive unit cell respectively. . . . .	42
2-2	Schematic representation of the mapping of the substitutional state of the alloy onto a configuration of the spin variables. . . . .	43
2-3	Examples of clusters on the simple-square two-dimensional lattice. The dark sites belong to the clusters. $\alpha$ , $\beta$ , and $\gamma$ are first, second, and third neighbor pair clusters; $\epsilon$ and $\zeta$ are three-site clusters, or "triplets," and $\delta$ is a four-site cluster. . . . .	44
2-4	Schematic representation of the quantities needed for the calculation of the effective cluster interactions using the new method. The ground-state line (dashed line) is the lower convex hull of the set of formation energies in the energy-composition plane. The other quantities are: $\Delta E_j/N$ : formation energy per atom of structure <i>j</i> , $\delta_j$ : error assigned to $\Delta E_j/N$ , $\Lambda E_j/N$ : energy difference (per atom) between structure <i>j</i> and the ground-state line at the composition of structure <i>j</i> . . . . .	49

2-5	Direct formation energies of the 42 ordered structures computed with the LMTO-ASA method. The ground-state line is shown and the ground-state structures on the Pd-rich side are labeled with their prototype structure ( $\text{Pt}_8\text{Ti}$ and $\text{MoPt}_2$ ) or Strukturbericht notation ( $\text{DO}_{22}$ and $\text{L1}_0$ ).	52
2-6	Effective cluster interactions for the Pd-V system computed with the new method. The pair clusters are indicated with the shell number, while the multi-site clusters are drawn explicitly.	55
2-7	Ground-state line on the Pd-rich side of the Pd-V system. The cluster expansion obtained with the new method reproduces the LMTO results, while the CW method incorrectly produces two extra ground states ( $\text{A}_5\text{B}$ and $\text{Ni}_4\text{Mo}$ ) that are only metastable in the LMTO results. The curves obtained with the new method and with the CW method have been shifted down by 50 and 100 meV/atom respectively for clarity.	56
2-8	Energy differences between the Pd-rich structures and the tielines defined by the sequence fcc-Pd, $\text{Pt}_8\text{Ti}$ -type, $\text{DO}_{22}$ , $\text{MoPt}_2$ -type, and $\text{L1}_0$ . On the abscissa, the Pd-rich structures are ordered in increasing distance to the tielines as obtained with the LMTO method. For the LMTO results and the energy parameterization of the new method these tielines define the ground-state line, and all the energy differences are positive. The energy parameterization obtained with the new method reproduces the ground states and fits the structures with energies close to the ground-state line better than structures with high energy. The CW results fail to reproduce the ground states (negative points in this plot) and the fits to the low-energy structures are worse than the ones obtained with the new method, while the high-energy structures are well reproduced.	57
3-1	Ground-state structures of the Ising model on the square-lattice with point ( $V_1$ ) and nearest-neighbor pair ( $V_2$ ) interactions ( $E(\vec{\sigma}) = V_1\langle\sigma_1\rangle + 2V_2\langle\sigma_2\rangle$ ). The stability map shows the range of interactions for which each of the structures is the ground state of the system.	60
3-2	Correlation functions of the ground-state structures of the simple-square lattice with point and nearest-neighbor ECI's ( $\langle\sigma_1\rangle$ is the point correlation function and $\langle\sigma_2\rangle$ is the nearest-neighbor pair correlation function). The correlation functions of the ground-state structures are the vertices of the shaded triangle.	63
3-3	Frustration effect in the triangular lattice with nearest-neighbor pair interactions. If the ECI is positive, then the number of A-B nearest-neighbor pairs has to be maximized in order to minimize the energy of the system. However, due to the topology of the triangular lattice, not all nearest-neighbor pairs can be of the A-B type.	64
3-4	Configurational polytope of the triangular lattice with nearest-neighbor ECI's. The vertices of the polytope correspond to the possible ground-state structures.	65



3-5	Schematic representation of the polytope method for the determination of the possible ground states of a lattice model. Every point inside the exact configurational polytope corresponds to one or more configurations on the lattice (constructible points), while there is no configuration with correlation functions outside the exact configurational polytope (inconstructible points). The constraints of the polytope method define a polytope that contains the exact solution, but may also contain inconstructible points (e.g., vertices 2 and 5). In other words, the polytope method approaches the exact solution from outside in the space of the correlation functions. . . . .	67
3-6	Example of the calculation of the $v$ -matrix and probability constraints for the triangular maximal cluster in the two-dimensional triangular lattice. The bold numbers on the table constitute the $v$ -matrix, obtained through equation 3.5. The probabilities of the configurations $J$ on the maximal cluster are linear combinations of the correlation functions. The coefficients of these linear functions are the rows of the $v$ -matrix. The condition of positive probability implies then a linear constraint on the correlation functions (shown below the table). . . .	69
3-7	Definitions of clusters on the fcc lattice. The 14-point cluster is composed of all the atoms in a conventional fcc unit cell and the 13-point cluster by one atom and its 12 nearest neighbors. . . . .	70
3-8	Steps for the determination of the ground-state structures of a lattice model using the polytope method. . . . .	72
3-9	Size distribution of the ternary ground-state structures found with the polytope method and constructed using the method of appendix A. .	81
3-10	$\{001\}$ projections of the ternary ground-state superstructures of fcc with first- and second-neighbor interactions. White, grey and black circles correspond to A, B and C atoms respectively. Large circles are in $\{00n\}$ planes, and small ones in $\{00n + 1/2\}$ planes. Half-shaded circles correspond to atoms alternating in the $[001]$ direction, while circles with a shaded quadrant correspond to particles occupying every fourth site in the $[001]$ direction. Rotations of the shaded parts indicate different $\{00z\}$ planes. The structures are labelled with the number of atoms in their primitive unit cells and letters to distinguish between structures with the same number of atoms. Structures 8c1, 8c2 and 8c3 correspond to the same vertex in the configurational polytope and have the same energy for the range of interactions used. . . . .	82

3-11	Schematic representation of the enumeration method for the determination of the possible ground states of a lattice model. Every point inside the exact configurational polytope corresponds to one or more configurations on the lattice (constructible points), while there is no configuration with correlation functions outside the exact configurational polytope (inconstructible points). The polytope of the enumeration method is the convex hull of the set of points in correlation-function space correspondent to ordered configurations with small unit cells. Since by construction all the vertices of the enumeration-method polytope correspond to constructible configurations, the exact solution is approached from inside in the enumeration method. Vertices 2, 4, and 6 in this example correspond to unit cells with more than $N_{max}$ atoms and therefore are not obtained with the enumeration method. Compare this figure with the schematic representation of the polytope method in figure 3-5. . . . .	87
3-12	Size distribution of the ground-state configurations found by Kanamori and Kakehashi in reference [3]. . . . .	88
3-13	Results of the enumeration method applied to the fcc lattice with four pair interactions. . . . .	89
3-14	Projections on the (001) plane of the new ground-state configurations with up to 8 atoms per unit cell. Each configuration is labeled according to the number of atoms in its primitive unit cell. Refer to the conventions in figure 3-10. . . . .	90
4-1	Comparison of the zero-temperature nearest-neighbor pair VECI computed with equation 4.23 and numerical results. The 137 different systems scan the sets of parameters $0.3 < \gamma_{BB}, \gamma_{AB} < 3$ and $1 < M_B < 3$ , while keeping $\gamma_{AA} = 1$ and $M_A = 1$ . The systems are ordered in the horizontal axis in increasing value of $V_2$ as obtained numerically. It can be seen that equation 4.23 underestimates the absolute value of the VECI for large VECI's. . . . .	104
4-2	Nearest-neighbor VECI as a function of temperature for a linear chain with $\gamma_{AA} = 1$ , $\gamma_{BB} = 3$ , $\gamma_{AB} = 1.2$ , $M_A = 1$ , $M_B = 1.5$ . Debye temperatures for different configurations are also indicated. . . . .	105
4-3	Rough estimate of the effect of lattice vibrations on the predicted phase stability for some alloys systems. The vibrational ECI for the other systems were estimated from experimental measurements of vibrational entropy [4, 5, 6, 7, 8]. . . . .	108
5-1	Cluster expansion coefficient of the average frequency $\bar{\omega}$ for a system with $\epsilon = 1\text{eV}$ , $\rho = 1\text{\AA}$ , and $M_A = 1\text{a.u.}$ as a function of the isotopic mass ratio $M_B/M_A$ . . . . .	113
5-2	Formation energies of the selected ordered structures in the Ar-Kr system. Average spin of $-1$ (1) corresponds to pure Ar (Kr). . . . .	115

5-3	Formation of the logarithmic average of the frequencies of the selected ordered structures in the Ar–Kr system. Average spin of $-1$ ( $1$ ) corresponds to pure Ar (Kr). . . . .	117
5-4	Subclusters of the tetrahedron and octahedron clusters on the fcc lattice. The “point” subcluster is not shown. . . . .	118
5-5	Chemical and vibrational effective cluster interactions for the Ar–Kr system. The labels of the clusters are explained in figure 5-4. The energy is expressed in units of temperature (Kelvin), which is obtained from the units of energy dividing by the Boltzmann constant. . . . .	119
5-6	Comparison of the direct and cluster–expanded (C.E.) energies for the 16 ordered structures studied in the Ar–Kr system. The closer the points are to the dashed line, the better the fit. . . . .	120
5-7	Comparison of the direct and cluster–expanded (C.E.) values of $\overline{\Delta \ln(\omega)}$ for the 16 ordered structures studied in the Ar–Kr system. The closer the points are to the dashed line, the better the fit. . . . .	120
5-8	Phase diagram of the Ar–Kr system computed with the ECI’s of figure 5-5 and using the cluster variation method in the tetrahedron–octahedron approximation. The lattice vibrations reduce the order–disorder transition temperature of the $L1_0$ phase by 12%. . . . .	121
5-9	Temperature–dependent contribution of the lattice vibrations to the total ECI’s in the Ar–Kr system. The number of terms refers to the configuration–dependent terms in equation 4.16. . . . .	123
5-10	Contribution to the formation value of the logarithmic average of the frequencies for some ordered configurations in the Ar–Kr system. The plots correspond to the following structures in the Strukturbericht notation: a) $L1_0$ , b) $L1_1$ , c) Ar–rich $L1_2$ , d) Kr–rich $L1_2$ , e) Ar–rich $DO_{22}$ , and f) Kr–rich $DO_{22}$ . . . . .	124
5-11	Trends in the effect of lattice vibrations on phase stability. The shaded region corresponds to the set of LJ parameters that define systems in which the lattice vibrations tend to increase the transition temperatures. . . . .	126
6-1	Solid part of the CaO–MgO phase diagram computed with and without vibrational effects A few experimental data points [9] are represented with filled circles. . . . .	131
6-2	Contribution to $\overline{\Delta \ln(\omega)}$ for some ordered structures in the MgO–CaO system. The plots correspond to the following structures: a) Ca–rich $L1_2$ , b) $L1_0$ , c) Mg–rich $L1_2$ , d) $2 \times 2 \times 2$ Ca cell with one Mg impurity, and e) $2 \times 2 \times 2$ Mg cell with one Ca impurity. . . . .	132
6-3	Comparison of the exact value of $\overline{\Delta \ln(\omega)}$ with the prediction of the Debye, MJS, mMJS, and LH models for the 16 ordered structures. The closer the points lie to the dashed line, the better the approximation. . . . .	138
6-4	Contribution of the masses to the value of $\overline{\Delta \ln(\omega)}$ in the MJS and Debye models, for an alloy of composition $1/2$ , as a function of the mass ratio, $M_A/M_B$ . . . . .	140

6-5	Convergence error in $\overline{\Delta \ln(\omega)}$ as a function of the number of fcc Chadi-Cohen k-points. . . . .	142
6-6	Steps for the calculation of $\overline{\Delta \ln(\omega)}$ (written as $D\langle \ln(w) \rangle$ in the flow-chart) from first-principles for an ordered configuration $\vec{\sigma}$ in a substitutional alloy, with the new method. . . . .	145
6-7	Conventional unit cell of the diamond structure. The origin of the systems of coordinates used to describe the atomic positions is conventionally taken at the lower-right atom in the figure. The conventional cell has 8 atoms, while the primitive cell has 2 atoms. . . . .	150
6-8	Conventional unit cell of the zinc-blend (ZB) ordered structure on the diamond lattice. One of the alloy species (dark-grey shaded atoms) forms an fcc arrangement, while the other (light-gray shaded atoms) occupies half of the tetrahedral interstitial sites, forming another fcc arrangement. . . . .	151
6-9	Convergence properties of the force along $x$ for the structures with the nearest-neighbor bonds contracted by 1% of the lattice constant. In the first plot, the absolute value of the forces is shown. In the second, we show the difference between the force computed with a given energy cutoff ( $E_c$ ) and the force at $E_c = 600$ eV. . . . .	156
6-10	Convergence of $\overline{\ln(\omega)}$ for Si, Ge, and ZB, and $\overline{\Delta \ln(\omega)}$ for ZB as a function of the energy cutoff ( $E_c$ ) in the pseudopotential calculations. The values of $\overline{\ln(\omega)}$ were obtained by fitting to only one spring-constant-tensor parameter. . . . .	157
6-11	Vibrational density of states for Si computed with the 15 force-constant-tensor parameters, shown in table 6.10. . . . .	159
6-12	Convergence of the formation value of the first three even moments of the VDOS for the zinc-blend configuration in Si-Ge alloys, with respect to the number of spring-constant parameters. The labels of the spring constant parameters correspond to the tensors shown in table 6.6. . . . .	160
A-1	Number of distinct unit cells of superstructures of fcc, as a function of the number of atoms in the cell. . . . .	172
B-1	One-dimensional potential used to study the accuracy of the Ising mapping of the alloy Hamiltonian. The parameters $\gamma_A$ and $\gamma_B$ are the second derivatives of the potential at the minima. . . . .	176
B-2	Exact probability of finding the system in $\vec{\sigma}_A$ , as a function of the migration barrier, $E_m - E_0$ , for different values of the "spin flip energy," $E_0$ , when $\omega_A = \omega_B$ . Both energies are expressed in units of the temperature, $T$ . The asymptotic value for large $E_m - E_0$ corresponds to the Ising solution of equation B.3. . . . .	177

- B-3 Rough estimate of the error in the transition temperature of a phase transition due to the Ising mapping of the alloy Hamiltonian. The ratio of transition temperatures is shown as a function of the migration barrier,  $E_m - E_0$ , for different values of the "spin flip energy,"  $E_0$ , when  $\omega_A = \omega_B$ . Both energies are expressed in units of the temperature,  $T$ . 178
- C-1 Possible types of energy functions and functionals for the description of the energy of an assembly of atoms. After figure 1 in reference [10]. The arrows point in the direction of increasing complexity. . . . . 182



# List of Tables

2.1	Formation energies of ordered structures in the Pd-V fcc system, as computed with the LMTO-ASA method (see text for details). Kn structures refer to the n-th structure in reference [3] and Gn structures refer to possible ground-state structures reported in reference [11]. The other structures are identified by either their prototype structure, their Strukturbericht notation, or a conventional name. For some structures, alternative names are shown. All the formation energies are in meV/atom. The composition is expressed by the chemical formula of the structure. The fourth column contains the reference number where a picture of the structure can be found. . . . .	53
3.1	Summary of solutions of the ground-state problem for some three-dimensional lattices using the polytope or similar method. The results are for binary alloys, unless otherwise stated. . . . .	73
3.2	New solutions of ground-state problems obtained in this thesis using the polytope method. . . . .	74
3.3	Size of the ground-state problem in the polytope method for different ranges of the interactions and clusters used to account for the frustration of the fcc lattice. The vertices in the high-dimensional space correspond to the polytope before being projected to the correlation space of the interactions in the truncated cluster expansion, while the vertices in the low-dimensional space are the possible ground states of the truncated Hamiltonian. . . . .	76
3.4	Experimental prototypes have been found for three of the structures shown in figure 3-10. . . . .	81
5.1	Transition temperatures at composition 1/2 of isotopic mixtures. The masses of the two most abundant isotopes are in atomic units and the temperatures in $10^{-3}$ Kelvin. . . . .	113
5.2	Parameters of the Lennard-Jones potentials used to model the Ar-Kr system, from [12]. . . . .	114

5.3	Direct formation energy ( $\Delta E$ ) (in meV/atom) and logarithmic average of the vibrational frequencies ( $\overline{\Delta \ln(\omega)}$ ) (dimensionless) for the 16 ordered configurations on the fcc lattice in the Ar–Kr system, modeled with LJ potentials. The structures are identified by either their prototype structure, their Strukturbericht notation, or a conventional name. The composition is expressed by the chemical formula of the structure. The fifth column contains the reference number where a picture of the structure can be found. . . . .	116
6.1	Sets of Lennard–Jones parameters for the model alloy systems. In all cases, $\epsilon_{AA} = 1$ and $R_{AA} = 1$ without loss of generality. Set number 1 corresponds to a simplified model of the Ar–Kr system [12]. . . . .	136
6.2	Average values of $\Delta E$ and $\overline{\Delta \ln(\omega)}$ for the 16 ordered structures considered, using the sets of LJ parameters of table 6.1. The energies are in units of $\epsilon_{AA}$ . . . . .	137
6.3	Root mean square (RMS) error of the prediction of the value of $\overline{\Delta \ln(\omega)}$ for 16 ordered structures using the Debye, MJS, mMJS, and LH models, for the sets of LJ parameters shown in table 6.1. . . . .	137
6.4	Number of k–points for the different ordered structures as a function of the iteration number in the Chadi–Cohen scheme [13]. . . . .	141
6.5	Distances (in units of $a$ , the conventional–cell lattice constant), and coordinates of the first 8 neighbor atoms to the atom at the origin, in the diamond lattice. Neighbors 7a and 7b are at the same distance to the origin, but are crystallographically distinct. . . . .	150
6.6	Self and pair spring–constant tensors for the first 8 neighbor pairs in the diamond lattice, as shown in table 6.5. For each neighbor (N), the number of independent parameters of the tensor is shown (P), together with the general form of the spring–constant tensor expressed in the cartesian basis. . . . .	153
6.7	Self and pair spring–constant tensors for the first 8 neighbor pairs in the ZB structure. The splitting of the orbits of the diamond pairs is explicitly shown. The pairs are identified by the coordinates of the atoms of a representative pair (in units of $a/4$ ). For each pair, the number of independent parameters of the tensor is shown (Param), together with the general form of the spring–constant tensor expressed in the cartesian basis. . . . .	154



6.8	Perturbations used to compute the forces on the atoms to obtain the equations for the spring constant parameters. In all cases, the unit cells are supercells along the supercell direction given. Only the atom at the origin is perturbed, along the direction shown in the table by $0.01a$ , where $a$ is the lattice constant of the conventional cell. The space groups of the perturbed structures are given by their conventional name and their number in the International Tables for Crystallography [14]. Since ZB has the same primitive unit cell as Si and Ge, the perturbations for the three structures are the same. The only difference is that twice as many perturbation were computed for ZB: shifting a Si atom and shifting a Ge atom. . . . .	155
6.9	Comparison of the predictions of the pseudopotentials used in this thesis for Si and Ge with experimental results and other theoretical calculations. Experimental measurements for the ZB structure are not available (N/A). . . . .	157
6.10	Spring constant parameters for Si, Ge, and ZB in $\text{eV}/\text{\AA}^2$ . The labels for the parameters are from tables 6.6 and 6.7. Note that the fifth neighbor spring constant tensor has one more parameter due to the lower symmetry of ZB. . . . .	158
D.1	Number of Chadi-Cohen $k$ -points for several lattices. . . . .	188



# Chapter 1

## Introduction

The science and engineering of materials is at the early stages of a major transformation. Historically, the research and development of new materials has been done through the traditional interplay of experimentation and theory. After many experiments, often guided by trial and error, a material has been developed to achieve the desired properties. This is an expensive process, that gives limited insight on how the final properties of the material are determined. The powerful tools of atomistic modeling and simulation are adding a new dimension to the research in materials science. They allow for a deeper understanding of the properties of materials and open the road for a new generation of engineered materials with improved performance. Computational methods are already complementing laboratory experiments, and are likely to replace them in many applications in the future.

The present thesis makes a small contribution towards making computational materials science a useful discipline for the development of new materials and the understanding of their properties. In this chapter, we describe the field of modeling and simulation in materials science and engineering and situate our work within the framework of current research. In section 1.1, we describe the development and achievements of computational material science, and argue that the combined advances in solid state physics and computer power are responsible for the rise of the new discipline. The application of computational tools to the development and understanding of alloys is discussed in section 1.2. Finally, the chapter ends with a description of how this thesis fits in the framework of alloy theory (section 1.3).

### 1.1 Computational materials science

According to the current understanding of nature, the behavior of matter at the length scales of every-day human life, is completely determined by the electromagnetic forces through which nuclei and electrons interact, together with the laws of quantum and statistical mechanics. Any phenomenon that takes place between distances of Angstroms and meters is completely described by this simple set of principles. Under most circumstances, the influence of the other forces of nature (i.e., gravitational, weak, and strong nuclear forces) is too small to affect the understand-

ing of the properties of the materials that surround us.<sup>1</sup>

If we were able to solve the equations of quantum and statistical mechanics that describe the behavior of materials, we would know everything there is to know about them. However, the energetics and time evolution of materials are determined by  $\sim 10^{23}$ , coupled, non-linear differential equations; while complex sums over the high dimensional phase space of the systems are needed to obtain the thermodynamic properties. These equations can be solved exactly for very simplified and idealized systems (that usually do not resemble anything in nature). These few solutions, together with empirical theories and a large amount of experimentation, dominated the science and engineering of materials until the invention of the computer. The amazing increase in computational power and the breakthroughs in solid state physics that produced sensible approximations to deal with the complexity of these systems created the field of computational materials science. In the rest of this section, we analyze these developments in more detail, and describe areas of materials science in which modeling and simulation techniques are already having a big impact.

### 1.1.1 Computer power

One of the sources for the development of computational materials science is the dramatic improvement of computer power in the last decades. Almost any measure of performance of computer power has experienced an exponential growth since the 1940's. Memory and speed have doubled every one to two years for the past 40 years [1]! These amazing developments, unparalleled in any other area of human endeavor, have dramatic implications for the applicability of computers to science. Problems that were deemed too difficult to solve a decade ago, are feasible today, and will be trivial in 10 years. Figure 1-1 shows examples of this growth.

Although there have been several predictions of this exponential growth slowing down due to different kinds of forecasted limitations, they have all been disproved by technological innovations. It is currently argued that economic constraints may be the first factor to limit the exponential growth of computer power [15]. However, there is no evidence that the trend is leveling off.

### 1.1.2 Advances in solid state physics

The dramatic improvement in computer power would not be revolutionary for materials science, if it weren't for the recent series of advances in solid state physics that paralleled the developments in the computer world. Even the most powerful computer would be incapable of attacking the most basic problems without the extra insight that simplified the quantum and statistical mechanics of materials.

Since the atomic nuclei are much more massive than the electrons, the latter can be assumed to respond instantaneously to changes in the positions of the former. This is known as the Born–Oppenheimer or “adiabatic” approximation [16], and it

---

<sup>1</sup>One notable exception is the growth of high quality crystals in a gravitational field that produces inhomogeneities in composition.

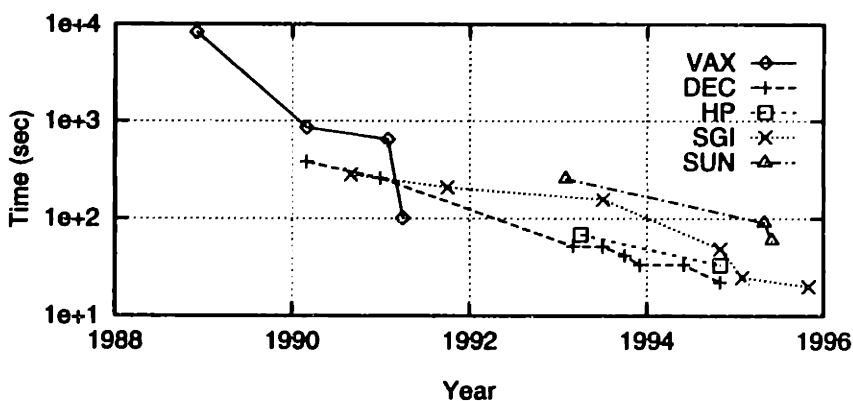
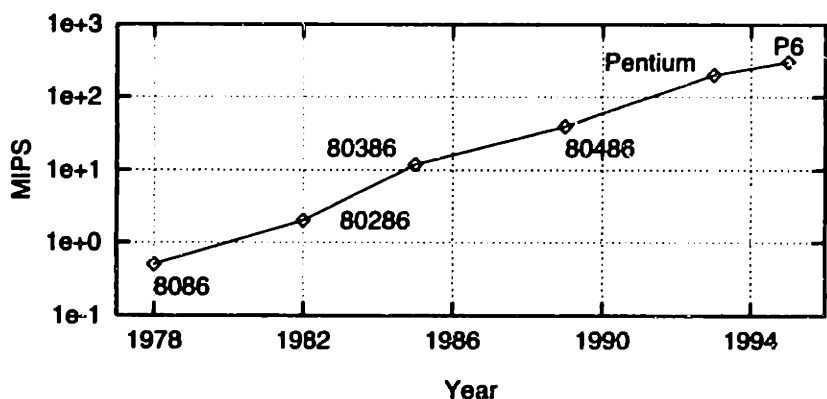
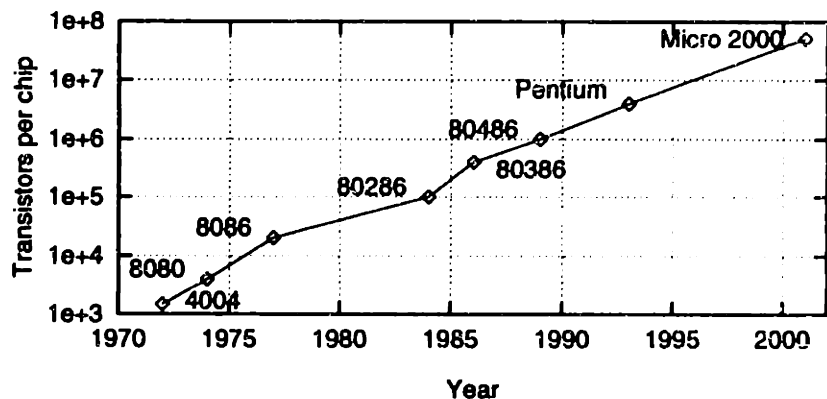


Figure 1-1: Exponential growth in computer power. a) Number of transistors in the Intel microprocessors for personal computers [1]. b) Computational speed of Intel microprocessors in million instructions per second (MIPS). c) Time needed to perform a series of molecular-dynamics simulations on the fastest computer manufactured by different companies [2].

has been successfully applied to most problems in solid state physics. Furthermore, the nuclei can be assumed to behave classically, with well defined positions and momenta, and to obey Newton's equations of motion.<sup>2</sup> With these approximations, the quantum mechanical problem is reduced to solving the Schrödinger equation for all the electrons, with the nuclei assumed to be fixed at their current positions.

The quantum mechanical problem of computing the electronic energy of an arrangement of atoms can be mapped exactly onto the problem of a single "quasi-particle" in a non-local effective potential. This is known as density functional theory [17, 18, 19]. Although this is a major simplification of the problem, the resulting equations are still too difficult to solve, mainly due to the non-local characteristics of the so-called exchange and correlation potentials of the electrons. The local density approximation (LDA) [18] solves this difficulty by assuming that the exchange and correlation potentials can be expressed as a local functional of the electronic density. With the LDA, and the aid of powerful computers, the electronic structure and energetics of simple systems can be computed with a high degree of accuracy. This includes systems of a few atoms, or periodic arrangements with unit cells composed of at most a few hundred atoms. Calculations of lattice constants, elastic properties, and energy differences between different crystal structures are in good agreement with experimental observations.

The LDA equations can be solved using a variety of techniques. These techniques differ in: the choice of the basis sets used for the description of the wave functions, whether or not the techniques are self-consistent, and whether the equations are solved for all the electrons of the system or just the valence electrons. The realization that only the valence electrons are affected when atoms are brought close together led to the development of frozen core methods, such as the pseudopotential method [20], used in chapter 6 of this thesis. By "freezing in" the core electrons, the quantum mechanical problem is further simplified without losing much accuracy.

The study of systems at non-zero temperature adds a new dimension to the complexity of the problem. The calculation of thermodynamic properties requires complex summations over all possible configurations of the system. Therefore, in order to use modeling and simulation to solve the thermodynamics of solid state systems, other developments were necessary.

Early on, mean field methods [21] were used to estimate the free energy of very simple model systems. These methods neglect the statistical correlations between atoms. With the advent of the computer, improvements over the mean field methods became possible. The cluster variation method [22] for substitutional alloys, for example, treats the statistical correlations within a finite distance, and neglects them beyond it.

Other simulation methods that try to sample the relevant part of the phase space of the system were developed and extensively used. Among these, the most notable are the Monte Carlo and the molecular dynamics methods. In the Monte Carlo

---

<sup>2</sup>An exception to this rule is the so-called quantum solids, like solid He. In these systems, even the zero-point vibrational amplitude of the atoms is comparable to the interatomic distance and therefore any classical picture of the nuclei fails.

method [23], points in phase space of the system are generated with different statistical distributions (i.e., canonical, grand-canonical, etc.) using a stochastic process. On the other hand, the molecular dynamics method [24, 25] simulates the actual time evolution of the system, by integrating Newton's equations of motion for the atomic nuclei in the force fields generated by the electronic clouds.

In recent years, the new developments in computational materials science have led to the creation of new journals devoted to modeling and simulation. Some of the new journals, with the dates they first appeared are Macromolecular theory and simulations (January, 1994), Modelling and simulation in materials science and engineering (October, 1992), Molecular simulation (1992), Computational Materials Science (October 1992), Materials theory "e-print" archive at Los Alamos National Laboratory,<sup>3</sup> (October 1994) etc. Of course, the number of publications using computational modeling and simulations has also increased in traditional journals in physics, chemistry, and materials science.

### 1.1.3 Computational materials science: achievements and limitations

Although the field of computational materials science is relatively new, it has already made important contributions towards a better understanding of materials properties. The main driving forces for the new developments are the following advantages of modeling and simulations over traditional experiments:

- greater **control** of experimental variables,
- attainability of **extreme experimental conditions**,
- access to detailed **information** about the system,
- lower **cost**,
- greater **flexibility**.

In traditional experimental settings the variables that define a system are not always under complete **control**. For example, it is practically impossible to have 100% purity in the samples to be studied, or to have a single crystal free of point defects. These limitations are naturally absent in atomistic computer simulations, where one has complete control over the system under study.

There is a limit to the maximum pressure attainable in the laboratory. This technological difficulty precludes experimental studies of materials at very high pressures, with important applications in geophysics. In computer simulations, the pressure can usually be adjusted to any desired value without difficulty. The same is true of other variables, such as vacuum levels, high and low temperature, etc., for which **extreme conditions** are easily obtained in computer simulations.

Not all the **information** about the state of the system under study is available with traditional experimental techniques. For example, diffraction techniques are

---

<sup>3</sup>Universal Resource Locator: <http://xxx.lanl.gov/archive/mtrl-th>

capable of measuring some properties of the short range order in disordered binary alloys. However, the exact distribution of atoms around a given atom is very difficult to obtain with current technology. A computer simulation contains all this information, which is readily available for analysis when the system is modeled.

The cost of the equipment and materials necessary to perform sophisticated experiments increases as the researcher needs more control and wishes to extract more information about the system under study. On the other hand, the price of the fastest computers is approximately constant in time, or even decreasing in some cases. If these trends continue, and the sophistication of experimental techniques keeps increasing, it is very likely that modeling studies will replace traditional experimentation for economic reasons.

Finally, computer simulations have an inherent **flexibility** that traditional experiments lack. Once a simulation is prepared, changing one atomic species in the system or adding a new component in a complex alloy is not difficult. Even studying "what if" situations can help give insight into the mechanism underlying a given phenomenon. For example, the value of the atomic mass of an element could be continuously varied to see how it influences the vibrational properties. Of course, since there are only a few stable isotopes of any element, it is not possible to achieve this using real experiments.

Applications of atomistic computer simulation can be found in different areas of materials science. Essentially, every phenomenon that takes place at the atomic level is amenable to simulation. These are some of the materials science problems that have been studied with computer modeling: point defects, dislocations, grain boundaries, simple inter-phase boundaries, segregation, phase stability of elements and alloys, mechanisms for melting, diffusion, electronic properties, optical properties, heat transfer, crystal growth, kinetics of phase transformations and simple processing, elastic properties, mechanics properties, simple 2-D fracture, dielectric properties, ferroelectric properties, polymer folding, superconductivity, superfluidity, percolation, critical phenomena, quasicrystals, catalysis, chemical reactions, adsorption.

However, not all news is good about modeling and simulation in materials science. The approximations and simplifications necessary to obtain a solvable set of equations present a serious concern about computational studies. These approximations are of two different types: a) known effects that are not supposed to contribute significantly to the properties being computed, and b) unknown effects. Examples of the former class of approximations are the adiabatic approximation that decouples the electronic problem from the time evolution of the nuclear coordinates (this approximation is "harmless" in most cases), and the approximation of neglecting the contribution of lattice vibrations to the free energy of alloys (this approximation is not good for some systems, as shown in this thesis, in chapters 4, 5, and 6). For the latter type of approximations, we can mention the effect of unknown impurities in real systems. These unknown conditions are sometimes important for determining the properties of the materials under study. In these cases, the modeling techniques are bound to fail.

The second limitation the modeling and simulation techniques suffer from is that the studies are currently limited to systems of a few hundred atoms using first-



principles techniques, or to a few million atoms when empirical approaches are used. This allows one to study small systems (e.g., molecules, quantum dots), periodic systems (perfect solids), point defects (using supercell approximations [20]), etc. However, atomistic simulations of mesoscopic problems are prohibitively expensive. These problems include microstructure formation, complex inter-phase boundaries, processing, fracture, etc. There is some hope that these problems will be solved as a result of the forecasted increase in computer power. However, most of the methods currently used scale with the size of the input as " $N^3$ ." This means that when the size of the system increases by a factor of 2, either the time necessary to solve it, or the memory necessary to store it in the computer increases by a factor  $2^3 = 8$ . Or, in other words, if we could build computers 1000 times faster than the fastest computer available today, we could solve problems only 10 times larger than the problems we can solve today. There is a great deal of interest within the scientific community to avoid this  $N^3$  scaling by developing new methods that scale only linearly with  $N$  [26, 27]. Although these methods are more computationally expensive than traditional methods for the systems currently attainable, they may be the way of the future, when computers are able to function some orders of magnitude faster.

## 1.2 Alloy theory

There are very few applications for materials made of just one element from the periodic table. When two or more species are combined, the "menu" of possible properties increases dramatically, allowing the materials engineer to fine-tune materials for specific applications. An understanding of the mixing properties of different kinds of atoms is therefore very important for the development of improved materials.

"Alloy theory" studies the behavior of systems composed by two or more atomic species, using computational or theoretical tools. In this thesis we are concerned with the *thermodynamic* properties of *substitutional* alloys. In a *substitutional* alloy, the thermodynamically stable phases can be thought of as different arrangements of the atomic species on the sites of a lattice. There are some examples of alloy systems in which this is the case for the complete composition range. However, almost every alloy system is *substitutional* in some limited range of composition. Examples of both cases are shown in figure 1-2. We will further restrict the scope of the present thesis to *solid state phases* of the alloys. The properties of liquid and gaseous phases will not be considered.

The ultimate goal of alloy theory is to produce an "alloy machine." This alloy machine would require as input the set of sought properties of a material, and would produce as output the composition and processing conditions of a material with those properties. Of course, we are very far from achieving this goal, and will be satisfied with a much more modest objective: given the atomic numbers and masses of two or more species, compute the thermodynamic properties of the alloys they form. When only this information is used, and no experimental input is required, the calculations are called "first-principles" or "*ab-initio*."

Of all the thermodynamic properties of an alloy, its temperature-composition

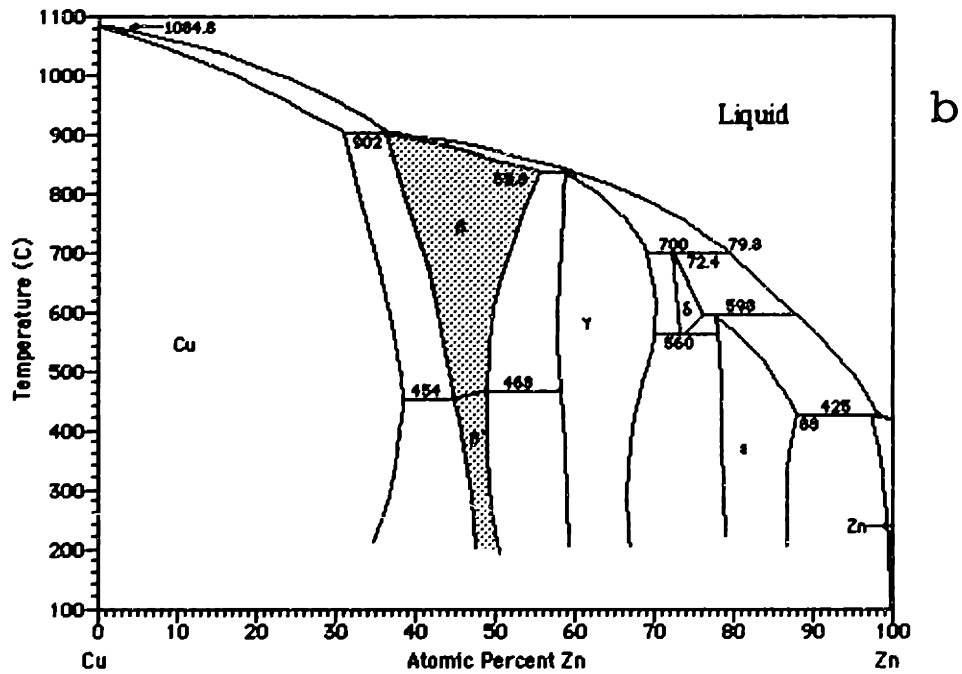
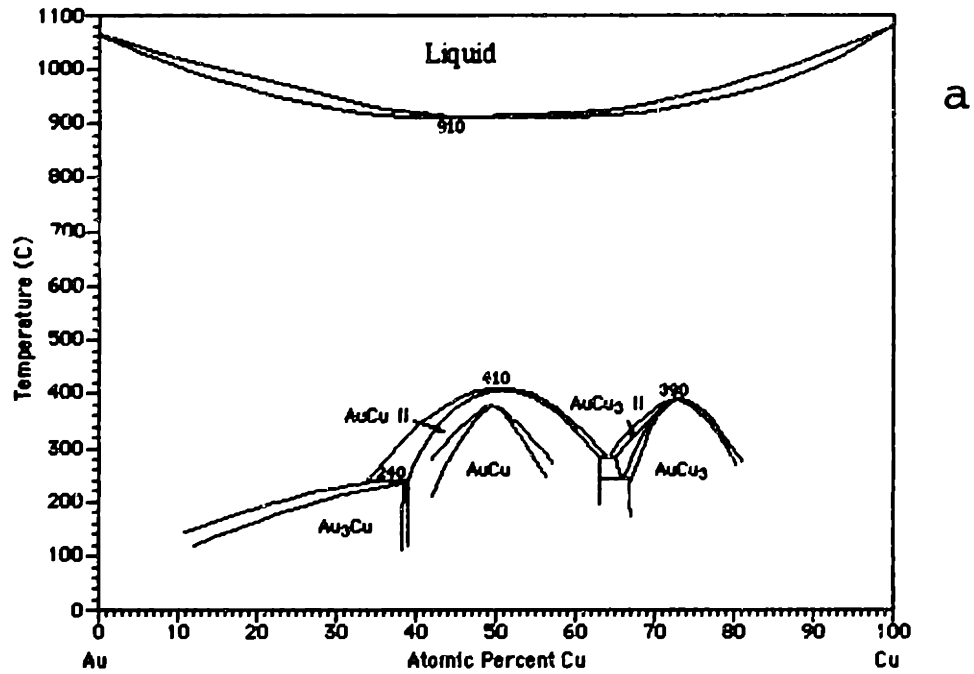


Figure 1-2: Examples of temperature–composition phase diagrams of *substitutional* binary alloys. a) Cu–Au is a system in which the Cu and Au atoms arrange themselves on a face centered cubic lattice for all the composition range in the solid–state part of the phase diagram. b) In Cu–Zn alloys the substitutional alloy description applies, for example, to the shaded region, where the Cu and Zn atoms are distributed on a body centered cubic lattice.

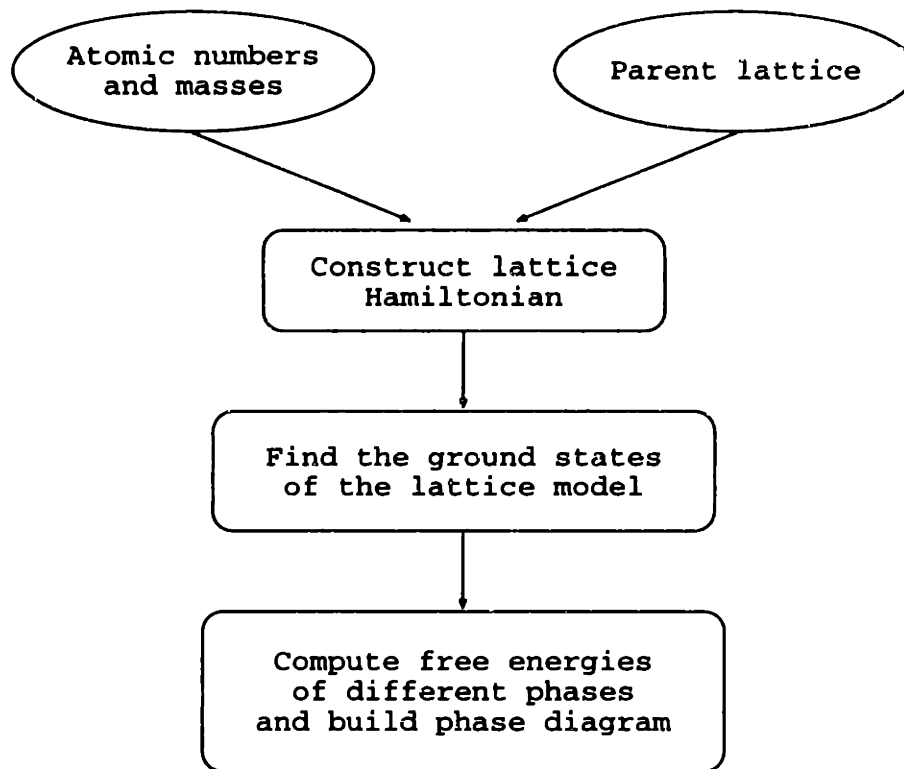


Figure 1-3: Steps to compute the temperature–composition phase diagram of a substitutional alloy from first principles.

phase diagram is probably the most compact and useful piece of information. Although it only contains equilibrium data, the type and location of the stable phases can give the materials engineer information about the final microstructure of an alloy after processing. The steps usually taken to compute the temperature–composition phase diagram of a substitutional alloy from first principles are shown in figure 1-3.

For systems that are not completely substitutional, such as Cu–Zn (see figure 1-2), the process can be carried out for more than one parent lattice, to obtain the free energies of phases that cannot be interpreted as ordering on the same lattice. Once these free energies are obtained, the complete solid–state part of the phase diagram can be computed.

The first two steps in the flowchart of figure 1-3 constitute the input of the problem. For first–principles studies, only the atomic numbers and masses of the species are required. If we restrict ourselves to substitutional alloys, then the lattice on which the two or more species will order is also part of the input to the problem. This restriction does not imply that the atoms are constrained to sit motionless on the exact lattice sites. As will be discussed further in this thesis, the only requirement for a valid mapping of the alloy Hamiltonian onto a lattice model is that every microstate of the alloy be uniquely mapped onto a substitutional state of the lattice [28]. Therefore, the lattice model can accommodate not only substitutional excitations, but also relaxations away from ideal lattice sites, lattice vibrations, electronic excitations, etc.

In the rest of this section, we describe the techniques used to accomplish the three main steps in the flowchart of figure 1-3.

### 1.2.1 Building the alloy Hamiltonian

The first step in the calculations is the construction of the Hamiltonian of the lattice model. The simplest approach is to assign an energy to every arrangement of the alloy species on the *ideal lattice sites*. This energy can be computed using a variety of methods with a wide range of sophistication and accuracy, from the full *ab-initio* quantum-mechanical methods to very simple empirical potentials.<sup>4</sup> This was the approach used in the early studies of phase stability. For simple alloy systems, it predicted phase diagrams in *qualitative* agreement with experiment [29].

Very rapidly, researchers realized that, even with the most sophisticated energy methods, the results did not converge to the experimental measurements. The predictions could be significantly improved when the constraint of the atoms sitting at the ideal lattice sites was lifted. Even for substitutional alloys, the size mismatch between the different atomic species will induce some *relaxation* away from the ideal lattice sites. When these relaxation effects are taken into account, the predicted phase diagrams of many alloy systems improve dramatically, in some cases giving results that are in *quantitative* agreement with experiment [30, 31].

If the predictions of the computational models are to compete in accuracy with the experimental techniques, further improvements are necessary. The next step to improve the models of alloy thermodynamics, is to consider not only the substitutional exchanges that the lattice model naturally account for, but also other kinds of excitations. Even with very crude approximations for the vibrational and electronic excitations, better agreement with experiment was achieved [30, 31, 32, 33]. In this thesis, we develop systematic methods for including the lattice vibrations in the studies of alloy phase stability.

In 1984, an important breakthrough made all these developments possible: the *cluster expansion*. Sanchez, Ducastelle, and Gratias [34] proved that any property of a substitutional alloy that only depends on the distribution of atoms on the lattice can be expanded exactly in a basis of so-called cluster functions. Furthermore, for properties that only depend on the local arrangement of atoms, this cluster expansion can be truncated, keeping only the terms that describe the local environments. When the property of interest is the energy of the substitutional arrangement, the cluster expansion has the form of a generalized Ising Hamiltonian, with a few coupling parameters. Therefore, the problem of computing the energy of any possible arrangement of atoms on a lattice is reduced to the knowledge of these few parameters.

Various methods have been devised to obtain the coupling parameters of the generalized Ising Hamiltonian of the alloy. The most popular and powerful method is originally due to Connolly and Williams [35] and was later generalized by other authors [36, 37, 38]. This method is usually referred to as the Connolly-Williams (CW) method or “structure inversion method” (SIM). The basic idea behind the

---

<sup>4</sup>In which case the computation is not a “first-principles” study.

SIM is to compute the energy of a few simple periodic arrangements of atoms on the lattice and then obtain the coupling parameters of the cluster expansion by a least-squares procedure. The SIM can very easily accommodate atomic relaxations and non-substitutional excitations.

Other methods to obtain the coupling parameters include the “direct configurational averaging” (DCA) and the “coherent potential approximation” (CPA) with the “generalized perturbation method” (GPM). In the DCA method, the coupling parameters are obtained by an explicit average of the energy over all possible configurations of the alloy [39, 40]. In the CPA-GPM scheme, an approximation of the alloy with random occupancy of the lattice sites by the atomic species is built, and the ordering energies are computed through a perturbative approach [41]. Currently, neither of these two methods is capable of modeling the atomic relaxations away from ideal lattice sites. Although some attempts have been made to remove this limitation, it is not clear whether the DCA and the CPA-GPM can compete with the SIM in studies of complex alloy systems.

Once the cluster expansion is obtained, the alloy problem is reduced to the calculation of the thermodynamics of the resulting lattice model. Before calculating the free energy of the alloy it is convenient to know the stable phases  $T = 0\text{K}$ , i.e., the ground states of the lattice model.

### 1.2.2 Ground states of the lattice Hamiltonian

The stable phases at  $T = 0\text{K}$ , or ground states, are those arrangements of atoms on the lattice that minimize the energy of the system. For very simple systems, these structures can be obtained by simple inspection of the lattice Hamiltonian. For example, in the ferromagnetic Ising model, the minimum energy structures correspond to all spins “up” or all spins “down.” For the antiferromagnetic Ising model on the simple square lattice, for example, the ground state is the “checkerboard” ordering.

Two kinds of difficulties arise when the simple Ising model with nearest-neighbor interactions is generalized to model alloys. First, the connectivity of the lattice may introduce “frustration” effects. For example, in an antiferromagnetic Ising model on a triangular lattice, the energy would be minimized if we could find a distribution of spins that only had unlike spins as nearest neighbors. However, this is not possible due to the topology of the lattice, that contains triangles of nearest neighbors. The second difficulty that arises when studying alloys is that the Hamiltonian usually contains interactions that go beyond the nearest-neighbor distance.

Several methods have been developed to find the ground state structures of a lattice model. These methods have been successful in studying a number of alloy systems and will be discussed in chapter 3.

### 1.2.3 Free energies and phase diagrams

The phase diagram of the alloy is determined by the competition for stability of all the possible phases of the alloy. Any statistical mechanical method should, at least, include the phases that are stable at  $T = 0\text{K}$  (ground states), the disordered state

(which is stable in the high temperature limit), and other phases that are in close competition with the ground states. Two methods have been widely used to compute phase diagrams of alloys: the Monte Carlo method and the cluster variation method (CVM). In the Monte Carlo method [23], the equilibrium state of the system is simulated using a stochastic approach. In its most basic formulation, it does not produce free energies, and the stable phases are obtained by inspection of the equilibrium structures during the simulation. The CVM [22, 41], on the other hand, is an extension of the mean field method to compute free energies of any given phase of the alloy. After the free energies of all the phases that compete for stability are computed, the phase diagram is obtained by minimizing the free energy of the alloy.

Most of the phase transitions in alloys are first-order transitions and therefore there is no need to perform studies of critical phenomena. Even for alloys that present second-order transitions, we are interested in the transition temperatures and compositions, and can obtain these properties with enough accuracy, using the CVM [42].

### 1.3 Contributions made in this thesis

In spite of all the recent improvements in alloy theory, there are still some problems to be solved before the predictions of phase stability become quantitatively reliable. In this thesis we address some of these problems. We made contributions in three different areas of alloy theory: the construction of the lattice model Hamiltonian, the determination of the ground-state structures of the lattice model, and the inclusion of the vibrational degrees of freedom in studies of phase stability.

In chapter 2, we show that the traditional methods to build the lattice Hamiltonian from the energies of ordered arrangements of the alloy can fail to capture important features of the energetics of the alloy. A new method, based on linear programming techniques, is proposed to overcome these limitations. We apply the new method to the study of the Pd-V alloy, and show that long range pair interactions are necessary to obtain a good parameterization of the energetics of the system.

The state-of-the-art methods to find the ground-state structures of the alloy lattice model are reviewed in chapter 3. We show that, although very successful for simple alloys, these methods fail when the interaction range is beyond the second or third neighbor. We developed a new method that can approximately solve the ground state problem for complex alloys and applied it to the binary alloys on the fcc lattice with first- through fourth-neighbor pair interactions. The limits of the exact traditional methods are illustrated with the solution of the ground state problem of the ternary alloys on the fcc lattice with first- and second-neighbor interactions.

The effect of lattice vibrations on the phase stability of substitutional alloys is studied in chapters 4, 5, and 6. We show that non-substitutional degrees of freedom, like the lattice vibrations and the electronic excitations, can be accounted for in a lattice model of the alloy. This is done by a coarse-graining procedure with very few assumptions (chapter 4). We apply the new formalism to study a variety of systems, ranging from very simple model systems, to more complex systems where

first-principles quantum-mechanical computations are necessary:

- Empirical potentials are used to study model systems (including a crude model of Ar-Kr alloys). From these studies, we conclude that the size of the effect of lattice vibrations on phase stability can be large and therefore should be included in the studies of phase stability (chapters 4 and 5).
- A simple first-principles method is applied to the study of the MgO-CaO system. Our prediction of the phase diagram is in very good agreement with experiments (chapter 6).
- We study different approximations to do *ab-initio* calculations, and develop a new method that produces more reliable results than traditional techniques. This new method is applied to study the Si-Ge system (chapter 6).

Finally, chapter 7 summarizes the conclusions of this thesis, and chapter 8 outlines suggested future work to continue improving the models of alloy phase stability.





# Chapter 2

## The lattice–model Hamiltonian

The construction of the lattice Hamiltonian is the first step in the first–principles calculations of phase diagrams of substitutional alloys (see figure 1-3). Once the input to the alloy problem is specified (atomic numbers and masses of the alloy species and the parent lattice on which the atoms will order), the next step is to compute the energy of every possible arrangement of the atoms on the lattice. The justification of the mapping of the quantum–mechanical, continuous Hamiltonian onto the lattice model Hamiltonian is deferred to chapter 4. For now, it suffices to assume that the thermodynamical properties of the alloy are well described by the lattice model, with an energy associated with every possible substitutional state.<sup>1</sup> Since only the substitutional energy is considered in the alloy Hamiltonian and other contributions are neglected (i.e., lattice vibrations, electronic and magnetic excitations, etc.), the terms “energy” and “Hamiltonian” are used interchangeably throughout *this chapter*.

The calculation of the energy for all possible configurations of the lattice model is beyond the capabilities of any energy method. For a binary alloy with  $N$  sites, there are  $2^N$  possible configurations, most of which are non–periodic. Since  $N$  is a large number when modeling macroscopic behavior, even with the most simple empirical potential model we would not be able to compute all the  $2^N$  energies.

The development of the *cluster expansion* technique solved this problem by reducing such computation to the knowledge of a few energy parameters. In this chapter, we describe the cluster expansion for substitutional alloys, review the schemes used for the calculation of the energy parameters of the lattice–model Hamiltonian, and develop a new method that overcomes some of the limitations of the previous formulations. We apply the new method to the study of the energetics of Pd–V alloys.

---

<sup>1</sup> As described in chapter 1, the lattice model does not imply that the atoms are fixed at their ideal lattice positions. In fact, the energy corresponding to any substitutional state is the ground–state energy of all the microstates of the alloy that are mapped onto that substitutional state. This is achieved, in practice, initializing the system with the atoms at the ideal lattice sites and relaxing the atomic coordinates until the energy is minimized (locally). These ideas are further discussed in chapter 4.

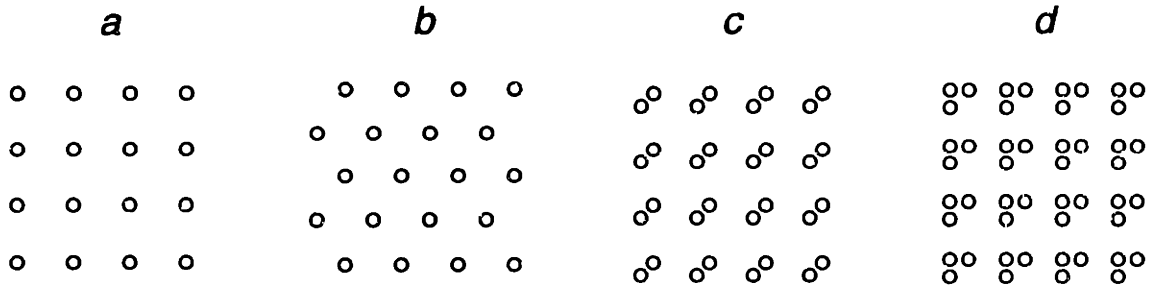
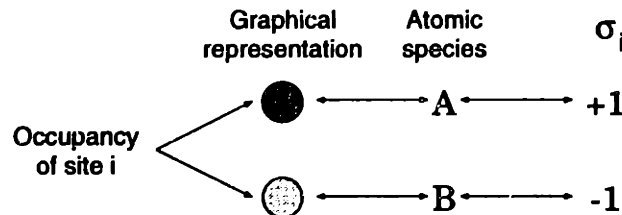


Figure 2-1: Examples of two-dimensional lattices.<sup>2</sup> The lattices extend infinitely in space. Only a portion of the lattice is shown. Lattices *a* and *b* have one lattice site per primitive unit cell, while lattice *b* and *c* have two and three lattice sites per primitive unit cell respectively.

## 2.1 The cluster expansion

The ordering phenomena in a substitutional alloy take place on a periodic structure of sites in space. These points in space form inter-penetrating Bravais lattices.<sup>2</sup> Examples of two-dimensional lattices are shown in figure 2-1. The lattices can have one or more sites per primitive unit cell. Examples of lattices with one lattice site per unit cell are lattices *a* and *b* in figure 2-1, and the face- and body-centered-cubic lattices in three dimensions. In lattices with more than one site per unit cell, such as lattices *c* and *d* in figure 2-1 and the hexagonal-closed-packed three-dimensional lattice, not all the sites are connected by lattice translations.

Our goal in this section is to review a systematic way of describing the possible arrangements of the atomic species on the sites of the lattice, and any function of such arrangement (e.g., the energy or volume per atom of the system). We will restrict the considerations in this chapter to binary alloys (only two atomic species form the alloy). For extensions to multicomponent alloys, the reader is referred to published studies [34, 45, 46, 47]. To formally describe the substitutional state of a binary alloy, we define a variable,  $\sigma_i$ , for every site *i* of the alloy as:



The complete substitutional state of an *N*-site alloy is then described by a binary

<sup>2</sup>From the crystallographic point of view, a lattice has, by definition, only one site per unit cell [43]. However, in this thesis we will refer to “lattices” as any periodic *structure* of sites. This allows us to refer to the hexagonal-closed-packed (hcp) structure as a lattice, when in fact it is composed by two inter-penetrating simple-hexagonal Bravais lattices. This is common practice in the field of lattice models [44].

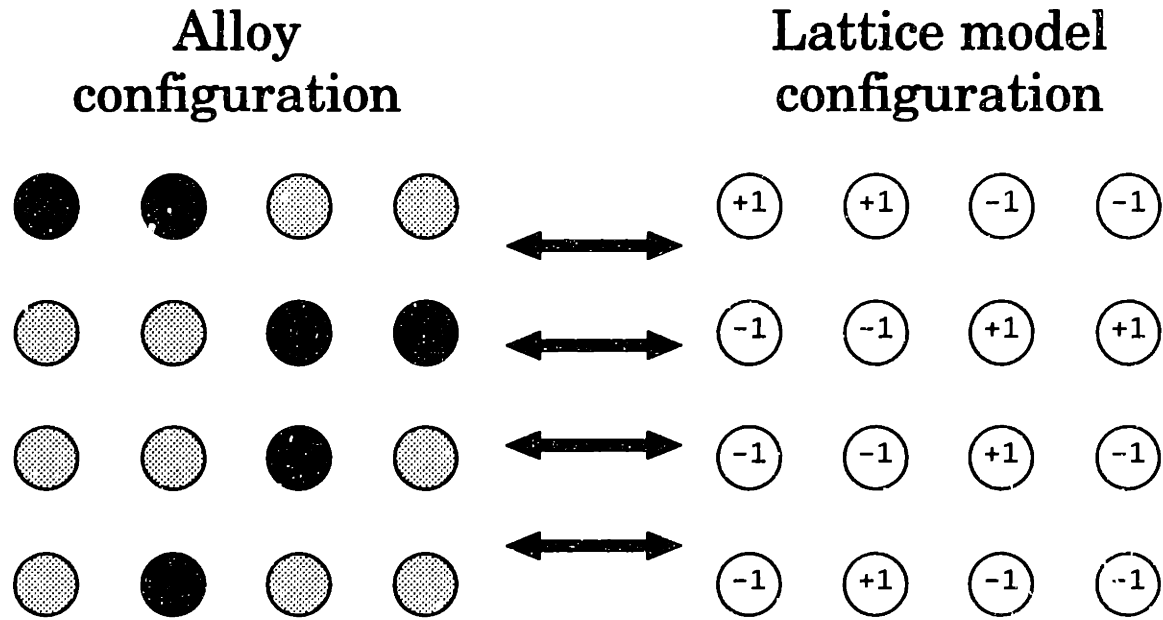


Figure 2-2: Schematic representation of the mapping of the substitutional state of the alloy onto a configuration of the spin variables.

vector,  $\vec{\sigma} = (\sigma_1, \sigma_2, \dots, \sigma_N)$ . The variables  $\sigma_i$  are usually called “spins” in analogy with the magnetic problem. Figure 2-2 schematically shows the mapping of the substitutional state of the lattice onto an Ising-like state of a set of spin variables.

In order to describe any function of configuration, such as the energy, volume, etc., we need to introduce some definitions. Consider two arbitrary scalar functions of configuration,  $f(\vec{\sigma})$  and  $g(\vec{\sigma})$ . The scalar product between these functions is defined as

$$\langle f, g \rangle \equiv \frac{1}{2^N} \sum_{\vec{\sigma}} f(\vec{\sigma})g(\vec{\sigma}), \quad (2.1)$$

where the sum is over all  $2^N$  possible configurations of the lattice model.

A *cluster*  $\alpha$  is a subset of the sites of the lattice. Examples of clusters on the simple-square two-dimensional lattice are shown in figure 2-3. For every cluster,  $\alpha$ , we define a *cluster function*,  $\sigma_\alpha$ , as the product of the spin variables on the sites of the cluster, i.e.,

$$\sigma_\alpha \equiv \prod_{i \in \alpha} \sigma_i, \quad (2.2)$$

where Greek subindices represent clusters and Roman subindices label lattice sites. The cluster functions are functions of configuration, i.e.,  $\sigma_\alpha = \sigma_\alpha(\vec{\sigma})$ , and take on the values  $+1$  or  $-1$ , depending on the values of the spins on the cluster. The definition is extended to the “empty” cluster (a cluster that contains no lattice sites), for which  $\sigma_\emptyset \equiv 1$ .

The most important property of the cluster functions is that they form an or-

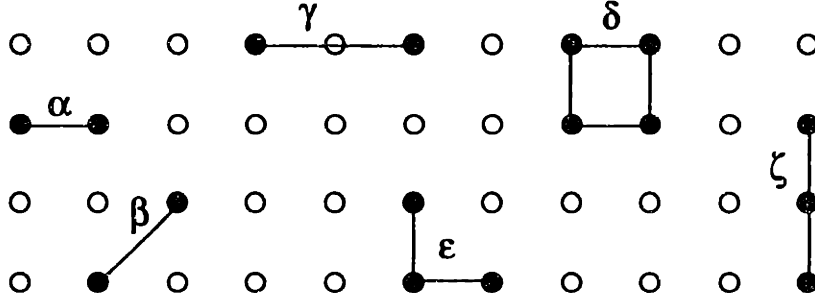


Figure 2-3: Examples of clusters on the simple-square two-dimensional lattice. The dark sites belong to the clusters.  $\alpha$ ,  $\beta$ , and  $\gamma$  are first, second, and third neighbor pair clusters;  $\epsilon$  and  $\zeta$  are three-site clusters, or “triplets,” and  $\delta$  is a four-site cluster.

*thonormal basis of the functions of configuration.* To prove this property, we need to show that: a) the cluster functions are normalized, b) they are orthogonal, and c) they are complete in the space of functions of configuration.

The normalization of the cluster functions is easily proved:

$$\langle \sigma_\alpha, \sigma_\alpha \rangle = \frac{1}{2^N} \sum_{\vec{\sigma}} \sigma_\alpha(\vec{\sigma}) \sigma_\alpha(\vec{\sigma}) = \frac{1}{2^N} \sum_{\vec{\sigma}} 1 = 1, \quad (2.3)$$

because there are  $2^N$  different configurations  $\vec{\sigma}$ .

To prove the orthogonality of the cluster functions, we define the following operations between arbitrary clusters  $\alpha$  and  $\beta$ . The union of clusters ( $\alpha \cup \beta$ ) produces a new cluster that contains the lattice sites that are in cluster  $\alpha$  or in cluster  $\beta$ . The intersection of clusters ( $\alpha \cap \beta$ ) produces a new cluster composed of the lattice sites that are both in  $\alpha$  and  $\beta$ . Finally,  $\alpha \Delta \beta \equiv \alpha \cup \beta - \alpha \cap \beta$  is the cluster of lattice sites that belong to  $\alpha$  or  $\beta$ , but not to both. It follows from equations 2.1 and 2.2 that

$$\begin{aligned} \langle \sigma_\alpha, \sigma_\beta \rangle &= \frac{1}{2^N} \sum_{\vec{\sigma}} \sigma_\alpha(\vec{\sigma}) \sigma_\beta(\vec{\sigma}) \\ &= \frac{1}{2^N} \sum_{\vec{\sigma}} \prod_{i \in \alpha} \sigma_i \prod_{j \in \beta} \sigma_j \\ &= \frac{1}{2^N} \sum_{\vec{\sigma}} \sigma_{\alpha \Delta \beta} \sigma_{\alpha \cap \beta}^2 \\ &= \frac{1}{2^N} \sum_{\vec{\sigma}} \sigma_{\alpha \Delta \beta} \\ &= 0, \end{aligned} \quad (2.4)$$

provided that  $\alpha \cup \beta - \alpha \cap \beta$  is non-empty (note that  $\alpha \cup \beta - \alpha \cap \beta = \emptyset$  if and only if  $\alpha = \beta$ ). The last equality in equation 2.4 follows from the fact that, for any non-empty cluster  $\gamma$ , there are equal number of configurations with  $\sigma_\gamma = +1$  and  $\sigma_\gamma = -1$ . The normalization and orthogonality of the cluster functions are usually

condensed in the expression

$$\langle \sigma_\alpha, \sigma_\beta \rangle = \delta_{\alpha\beta}. \quad (2.5)$$

Finally, the cluster functions form a complete set, i.e., any function of configuration can be written as a linear combination of cluster functions. This is proved in the literature [34] by showing that the completeness relation is satisfied, i.e.,

$$\frac{1}{2^N} \sum_{\alpha} \sigma_{\alpha}(\vec{\sigma}) \sigma_{\alpha}(\vec{\sigma}') = \delta_{\vec{\sigma}\vec{\sigma}'}, \quad (2.6)$$

where the sum is over all possible clusters. However, it suffices to realize that there are  $2^N$  cluster functions and that the dimensionality of the space of functions of configuration is also  $2^N$ . Since the cluster functions are independent (in fact they are orthogonal), they form a basis of the space of functions of configuration.

These properties of the set of *all* cluster functions allow any function  $f$  of configuration  $\vec{\sigma}$  to be expressed as linear combination of the cluster functions,

$$f(\vec{\sigma}) = \sum_{\alpha} F_{\alpha} \sigma_{\alpha}(\vec{\sigma}), \quad (2.7)$$

where the expansion coefficients,  $F_{\alpha}$  are the projection of the function  $f$  onto the cluster function  $\sigma_{\alpha}$ ,

$$F_{\alpha} = \langle \sigma_{\alpha}, f \rangle. \quad (2.8)$$

Expression 2.7 is usually referred to as the *cluster expansion* of property  $f$ . Any property of the alloy that depends on the substitutional state,  $\vec{\sigma}$ , and is uniquely determined by it, can be “cluster-expanded.” Examples of such properties are the energy, volume, elastic properties, etc.<sup>3</sup> In particular, the energy of the alloy can be cluster-expanded,

$$E(\vec{\sigma}) = \sum_{\alpha} V_{\alpha} \sigma_{\alpha}(\vec{\sigma}). \quad (2.9)$$

The expansion coefficients of the energy,  $V_{\alpha}$ , are usually called *effective cluster interactions* (ECI's), and, as in 2.8, can be obtained by projecting the energy of the system onto the corresponding cluster function:

$$V_{\alpha} = \langle \sigma_{\alpha}, E \rangle. \quad (2.10)$$

Since the cluster functions form a basis of the space of functions of configuration, the cluster expansion of the energy is exact. However, there are  $2^N$  ECI's in equation 2.9, and obtaining them is equivalent to computing the energy of all the  $2^N$  configurations of the lattice. Therefore, simplifications are necessary to make the problem tractable.

The first reduction in the number of parameters in the cluster expansion is obtained by considering the symmetry of the lattice. If there is a symmetry operation in

---

<sup>3</sup>On the other hand, thermodynamic properties, such as the configurational entropy, are not just functions of the current substitutional state, but are ensemble properties and therefore cannot be expanded as in 2.7.

the space group of the lattice that maps cluster  $\alpha$  onto cluster  $\beta$ , then the correspondent ECI's will have the same numerical value, i.e.,  $V_\alpha = V_\beta$ . For instance, all the nearest-neighbor pairs in the face-centered-cubic lattice are equivalent by symmetry and therefore have the same ECI's. By grouping all the symmetry-equivalent ECI's in equation 2.9, the cluster expansion of the energy per lattice site can be reduced to,

$$\frac{E(\vec{\sigma})}{N} = \sum'_\alpha m_\alpha V_\alpha \langle \sigma_\alpha \rangle(\vec{\sigma}), \quad (2.11)$$

where  $m_\alpha$  is the number of clusters per lattice site that are equivalent to cluster  $\alpha$  by the symmetry of the lattice,  $\langle \sigma_\alpha \rangle$  is the average of the cluster functions over the equivalent clusters (sometimes referred to as "correlation functions"), and the prime indicates that the summation is only performed over non-equivalent clusters  $\alpha$ .

Although equation 2.11 is simpler than equation 2.9, it is still too complex to be practical. In fact, in the thermodynamic limit ( $N \rightarrow \infty$ ), there is an infinite number of ECI's in equation 2.11. In order to make the cluster expansion a useful tool for the calculation of alloy phase diagrams, it is necessary to introduce approximations that simplify this expression. In many metallic alloys the energy of the system depends *mostly* on the types of local atomic environments present in the alloy. When this is the case, the energy can be described with cluster functions that comprise a small number of lattice sites that are located close together. Therefore the cluster expansion can be truncated to keep only a finite number of small clusters. This is usually symbolized with a maximal cluster,  $\alpha_{max}$ , beyond which the cluster expansion is truncated:

$$\frac{E(\vec{\sigma})}{N} = \sum'_{\alpha \leq \alpha_{max}} m_\alpha V_\alpha \langle \sigma_\alpha \rangle(\vec{\sigma}). \quad (2.12)$$

The truncated cluster expansion of the energy is the Hamiltonian used for studies of alloy phase stability. It usually includes the empty, point, a few pair and some multi-site cluster functions. It has the form of a generalized Ising Hamiltonian, with not just nearest neighbor couplings (or ECI's), but also further neighbor and multi-site interactions.

The truncation of the cluster expansion is not always well justified, and more sophisticated parameterizations of the substitutional energy of an alloy are sometimes necessary. They include reciprocal-space treatments [37], schemes where the long-ranged elastic effects are analyzed separately from the local contributions to the energy [38], or formulations where the ECI's are volume-dependent [48]. However, we have recently proved [49] that even for systems with long-ranged interactions between the atoms, like purely "Coulombic" systems where point charges interact electrostatically, short-ranged real-space parameterizations of the energy are possible.

Formal extensions of the cluster expansion technique to multicomponent systems are straightforward [34]. However, the complexity of the formalism grows dramatically with the number of species, making multicomponent alloys much more difficult to study than binary alloys. We have recently shown [50] that for the special case of ionic systems, where cations and anions mix on separate sublattices, the quaternary problem (two cations and two anions) can be reduced to a binary problem, making

the calculations feasible.

In the next section, we review the methods that have been used to compute the ECI's in equation 2.12 for the parameterization of the energy of alloys.

## 2.2 Review of methods to compute the effective cluster interactions

At least three approaches have been used in the past to compute the ECI's. The Connolly–Williams (CW) method<sup>4</sup> takes advantage of the fact that if a few ECI's are enough to parameterize the energy, then their values can be determined by fitting a truncated cluster expansion (equation 2.12) to the energy of a small set of ordered structures on the lattice (we will refer to the energy of ordered structures, when computed with any energy method, as the “direct” energies of the structures, as opposed to the “cluster-expanded” energies obtained with equation 2.12, once the ECI's are known). In its first formulation [35], the CW method consisted of fitting the values of  $n$  ECI's to the direct energy of  $n$  ordered arrangements on the lattice. These direct energies can, for example, be computed from first-principles within the local density approximation. Subsequent improvements [36] use more ordered structures than ECI's, and through a least-squares fit obtain a more stable set of ECI's, avoiding the sometimes ill-conditioned inversions. When considering a set of  $p$  ordered structures with direct energies  $E_j$ ,  $j = 1, \dots, p$ , the  $n$  ECI's ( $n \leq p$ ) are obtained by solving

$$\sum_{j=1}^p \omega_j \left[ \frac{E_j}{N} - \sum_{\alpha=1}^n m_{\alpha} V_{\alpha} \langle \sigma_{\alpha} \rangle_j \right]^2 = \text{minimum}, \quad (2.13)$$

where  $\omega_j$  is the weight assigned to the  $j^{\text{th}}$  structure. Because the cluster expansion requires only a one-to-one correspondence between atomic positions and lattice sites, it can also model configurations where the atoms relax away from their ideal lattice sites. In the CW method, the effect on the energy of the atomic relaxations is taken into account by relaxing the geometry of the ordered structures used in the fit.

The direct configurational averaging (DCA) method uses recursion techniques to compute the local density of states and the ECI's through a real space average, usually in the tight-binding approximation [39, 40]. In this method, the ECI's are computed one at a time, using their definition [34], as in equation 2.10. For example, for a pair ECI, it can be easily shown that equation 2.10 reduces to

$$V_{\text{pair}} = \frac{1}{4} (\langle E_{AA} \rangle + \langle E_{BB} \rangle - \langle E_{AB} \rangle - \langle E_{BA} \rangle), \quad (2.14)$$

where  $\langle E_{IJ} \rangle$  is the average energy of all the configurations  $\vec{\sigma}$  with atom  $I$  in the first site and atom  $J$  in the second site of the pair cluster. Similar expressions can be

---

<sup>4</sup>The Connolly-Williams method is sometimes referred to as the “structure inversion method” or SIM.

obtained for multi-site clusters. At its present stage, the DCA method does not take atomic relaxations into account.

Finally, the coherent potential approximation (CPA) [41] can be used to describe the disordered system by an effective medium and the ECI's are obtained perturbing this effective medium, with the so-called generalized perturbation method (GPM) [41]. The CPA is a mean-field description of the electronic structure of a completely disordered alloy, constructed by a self-consistent procedure that assures that, on average, the scattering of electrons by the atoms of the alloy vanishes. The GPM is a real-space perturbation method that produces concentration-dependent ECI's, from a reference medium, like the CPA. Although the CPA-GPM method has been able to predict general trends, its ability to include atomic relaxations has not yet been proved.

## 2.3 A new method to obtain the effective cluster interactions

Because atomic relaxations can play a very important role in determining the phase stability of an alloy system [37], the CW method has gained popularity (of the three methods described above, CW is the only one that takes the effect of atomic relaxations into account). Although now widely applied, the least-squares fitting procedure used in the CW method to extract the value of the ECI's from the direct energies of ordered structures has the following serious limitations: a) The CW method only fits the ECI's to the absolute direct formation energies of ordered structures. However, ground-state and phase-diagram predictions depend on *subtle differences* in direct formation energies of different ordered structures. b) The CW method does not necessarily reproduce the relative stability of the input structures one fits to (see for example [51]). This may cause structures that were metastable with the direct energy calculation, to become stable with the cluster expansion. These structures would be present in a phase diagram computed with the cluster expansion, whereas it is clear from the direct energy calculation that they should not be. c) The CW method is incapable of determining what truncation of the cluster expansion is needed to reproduce the desired features of the direct formation energies of the system.

The method we have developed [52] overcomes the limitations of the CW method mentioned above. The philosophy of the method is to reproduce not only the direct formation energies, but also the ground states and relative values of the direct formation energies of a set of ordered structures. The new method only guarantees that none of the metastable structures included in the fit will become ground states when their energies are computed with the cluster expansion. However, other structures not included in the fit may be ground states of the system. In the rest of this section, we describe the new method, and then apply it to the study of the energetics of the Pd-V system.

A schematic representation of the input quantities of the new method is shown in



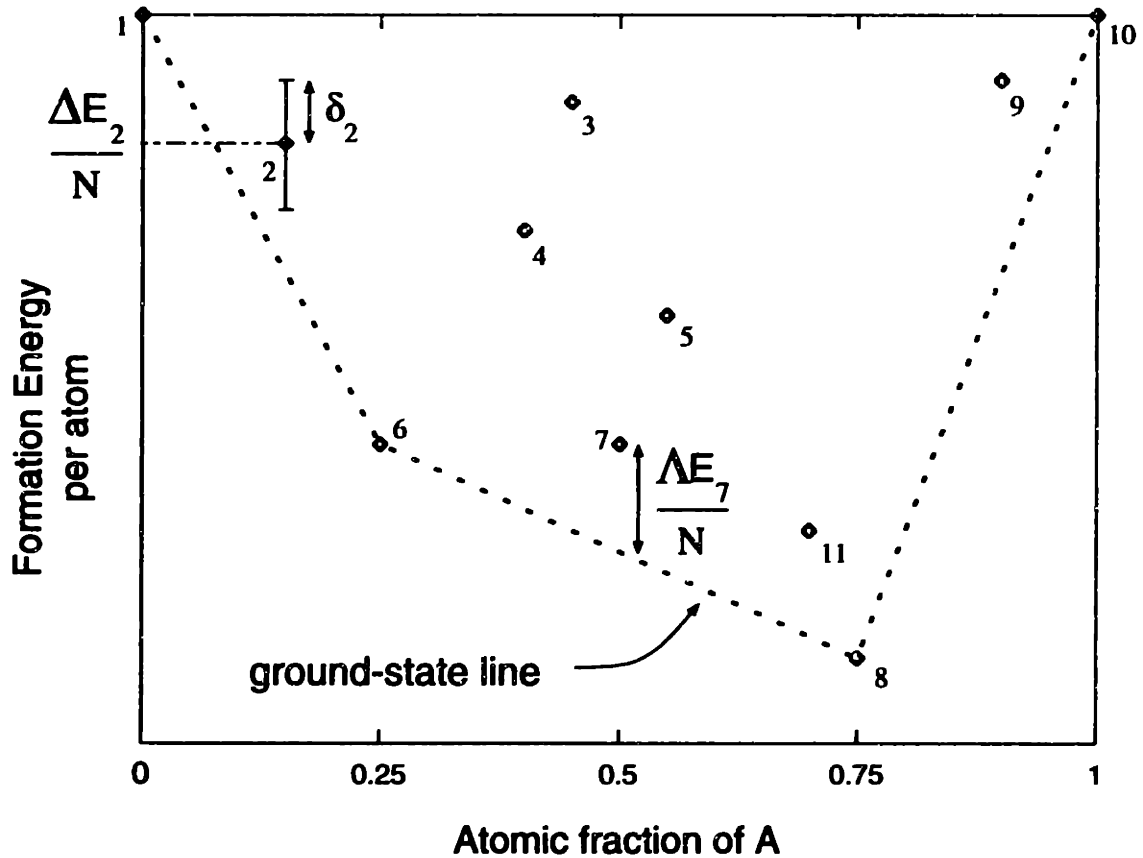


Figure 2-4: Schematic representation of the quantities needed for the calculation of the effective cluster interactions using the new method. The ground-state line (dashed line) is the lower convex hull of the set of formation energies in the energy-composition plane. The other quantities are:  $\Delta E_j/N$ : formation energy per atom of structure  $j$ ,  $\delta_j$ : error assigned to  $\Delta E_j/N$ ,  $\Lambda E_j/N$ : energy difference (per atom) between structure  $j$  and the ground-state line at the composition of structure  $j$ .

figure 2-4. As in the CW method, the direct formation<sup>5</sup> energies of a set of  $p$  ordered structures of A and B atoms arranged on a common parent lattice ( $\Delta E_j/N$ ,  $j = 1, \dots, p$ ) are required. Each direct energy is assigned an error bar  $\delta_j$ , i.e.,  $\Delta E_j/N \pm \delta_j$ . This error bar can be determined either by the error of the method used to obtain the direct energy or by the maximum error accepted in the cluster expanded energy.

The method also requires information about the ground-state line as obtained from the total energy method that we wish the cluster expansion to reproduce. The ground-state line of a set of ordered structures, is defined as the lower convex hull

<sup>5</sup>For an ordered structure with composition  $c$  (atomic fraction of A), the formation value of a quantity  $Q$  is defined as:  $\Delta Q = Q - [cQ_A + (1 - c)Q_B]$ . It can be easily shown that the thermodynamic properties of the alloy system will be the same if the lattice Hamiltonian is defined as the energy or the formation energy. For convenience, the formation energy is used.

of the energies of those structures in the energy–composition plane (see figure 2-4). It represents the sequence of thermodynamically stable structures (among the set of ordered structures chosen<sup>6</sup>) at  $T = 0\text{K}$ . In the schematic example of figure 2-4, structures 1, 6, 8, and 10 define the ground state line of the 11 structures shown. Each segment of the direct ground–state line is characterized by the composition and energy of the two ordered ground–state structures at the ends of the segment.

The final input of the new method is the set of lattice–averaged cluster functions ( $\langle\sigma_\alpha\rangle_j$ ,  $j = 1, \dots, p$ ,  $\alpha$ =empty cluster, point cluster, pairs, multiplets) for the ordered structures considered. These averages are easily computed from the description of the unit cell of the ordered structures.

With the truncation of the cluster expansion symbolized by  $\alpha_{max}$ , we impose the following constraints on the ECI's:

$$\sum_{\alpha}^{\alpha_{max}} m_{\alpha} V_{\alpha} \langle\sigma_{\alpha}\rangle_j \leq \frac{\Delta E_j}{N} + \delta_j \quad j = 1, \dots, p \quad (2.15)$$

$$\sum_{\alpha}^{\alpha_{max}} m_{\alpha} V_{\alpha} \langle\sigma_{\alpha}\rangle_j \geq \frac{\Delta E_j}{N} - \delta_j \quad j = 1, \dots, p \quad (2.16)$$

$$\sum_{\alpha}^{\alpha_{max}} m_{\alpha} V_{\alpha} I_{j_a}^{ab} \geq \epsilon \quad \begin{array}{l} j = 1, \dots, p \\ j \neq a, j \neq b, \end{array} \quad (2.17)$$

where

$$I_{j_a}^{ab} = \langle\sigma_{\alpha}\rangle_j - \frac{(\langle\sigma_1\rangle_b - \langle\sigma_1\rangle_j) \langle\sigma_{\alpha}\rangle_a + (\langle\sigma_1\rangle_j - \langle\sigma_1\rangle_a) \langle\sigma_{\alpha}\rangle_b}{\langle\sigma_1\rangle_b - \langle\sigma_1\rangle_a}. \quad (2.18)$$

Equations 2.15 and 2.16 require that the cluster expanded energies be within the error bars of the direct energies. Equation 2.17 imposes the linear constraints to reproduce the a–b segment of the direct ground–state line.  $\langle\sigma_1\rangle_j$  is the lattice average of the point cluster function, related to the concentration through  $\langle\sigma_1\rangle_j = 2c_j - 1$ , and  $\epsilon$  is a small number (smaller than the energy differences involved in the problem). Other constraints can be added to require that relative stabilities of ordered structures be reproduced in the cluster expansion.

Equations 2.15, 2.16, and 2.17 are linear inequalities in the space of ECI's, and can therefore be solved using any standard linear programming technique [53]. If the linear programming problem has a feasible solution in the space of ECI's, then the cluster expansion with these ECI's reproduces the required properties of the direct formation energies. If the volume of the polyhedron of feasible points is large, some of the constraints can be tightened to produce a better energy parameterization. If there is no feasible point, the truncation of the cluster expansion did not include enough terms to reproduce the direct energies. Then, there are two alternatives: a) relax the constraints (increase the error bars or take out segments of the ground–state line), or

---

<sup>6</sup>The thermodynamically stable structures at  $T = 0\text{K}$  of the lattice model are the lower convex hull of *all* the  $2^N$  states of the lattice model. When a subset of structures is computed, one obtains an approximation for the exact ground–state line of the system. In chapter 3, the ground–state problem of the lattice model is analyzed in detail.

b) include more ECI's and look for a feasible point in the new space of interactions. Both of these alternatives can be carried out automatically by a computer program. One of the strengths of this method is, therefore, that it exactly recognizes whether a given truncation of the cluster expansion can reproduce the desired features of the direct formation energies.

The most important features of the substitutional excitation spectrum of the stable phases are determined by the distance of other metastable ordered structures to the ground-state line in the energy-composition plane. For metastable structures that are close to the direct ground-state line, a small relative error in the formation energy could imply a big relative error in its cluster-expanded distance to the ground-state line, greatly altering the free energies of the stable phases and, therefore, the phase diagram. By requiring that the cluster expansion reproduce these distances, this problem can be avoided and a better description of the energetics of the system can be obtained. This can be done in the present method by introducing linear constraints of the form:

$$\frac{\Delta E_j}{N} - \lambda_j \leq \sum_{\alpha}^{a_{max}} m_{\alpha} V_{\alpha} I_{j\alpha}^{ab} \leq \frac{\Delta E_j}{N} + \lambda_j \quad \begin{array}{l} j = 1, \dots, p \\ j \neq a, j \neq b, \end{array} \quad (2.19)$$

where  $I_{j\alpha}^{ab}$  is the quantity defined in equation 2.18,  $\Delta E_j/N$  is the direct energy difference per atom between structure  $j$  and the a-b ground-state tieline at the same composition, and  $\lambda_j$  is the error bar assigned to this quantity.

## 2.4 Application to the Pd-V system

To illustrate the method, we studied the Pd-V substitutional alloys on the fcc lattice. Much work has been recently reported on this alloy system [54, 55, 56, 57, 40, 58, 33]. Part of the theoretical interest in Pd-V alloys was motivated by a study indicating that relatively long-range interactions are needed to describe the energetics of the ordering processes [54]. Since we are studying the energy of substitutional arrangements on the fcc lattice, our studies are relevant for the Pd-rich concentrations of the system. On the V-rich side of the phase diagram, the stable phases are not based on the fcc lattice.

We computed the direct formation energies of 42 ordered structures in the Pd-V system using the linear muffin tin orbital (LMTO) method in the atomic sphere approximation (ASA) [59]. The LMTO is a self-consistent all-electron method, based on the local density approximation [18]. In the ASA, the electrostatic potential around every ion is spherically averaged, greatly reducing the complexity of the problem. The results are shown in table 2.1 and figure 2-5. Figures of the unit cells of the structures can be found in references [41, 40, 3, 11].

The calculations were self-consistent and semi-relativistic. We used equal atomic sphere radii for Pd and V, "combined corrections" to the ASA, and  $17^3$  points in the Brillouin zone for k-space integrations. The von Barth-Hedin form for the exchange and correlation potential was used. In these calculations, only global volume relaxations are taken into account. The size mismatch between Pd and V is only 3%, so

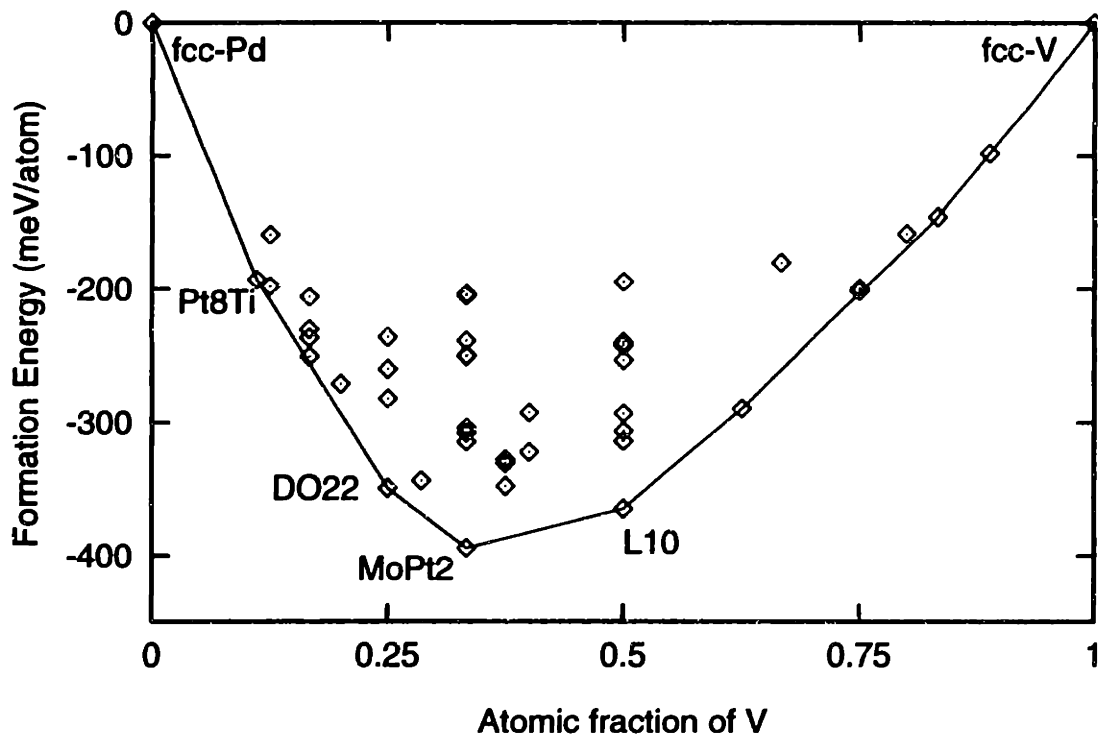


Figure 2-5: Direct formation energies of the 42 ordered structures computed with the LMTO-ASA method. The ground-state line is shown and the ground-state structures on the Pd-rich side are labeled with their prototype structure ( $\text{Pt}_8\text{Ti}$  and  $\text{MoPt}_2$ ) or Strukturbericht notation ( $\text{DO}_{22}$  and  $\text{L}_{10}$ ).

the effect of other relaxations is expected to be small.

Of the 42 structures, 18 coincide with the ones studied by Wolverton [58] using similar techniques. The formation energies for these structures differ from the ones in reference [58] by less than 4 meV/atom, except for  $\text{W}_1$  ( $\text{Pd}_5\text{V}_3$ ) and  $\text{W}_1$  ( $\text{Pd}_3\text{V}_5$ ), for which the differences are 13.5 and -6.5 meV/atom respectively. To our knowledge, the energies of the other 24 structures have not been reported before. Since we are interested in the energetics of Pd-rich configurations, we chose more Pd-rich than V-rich structures.

We first apply the new method to find a suitable truncation of the cluster expansion that can reproduce the ground-state line of the direct energies of the structures computed with the LMTO-ASA. The ground-state structures in the Pd-rich part of the system, as obtained with the LMTO-ASA method, are: fcc-Pd,  $\text{Pt}_8\text{Ti}$ -type,  $\text{DO}_{22}$ ,  $\text{MoPt}_2$ -type, and  $\text{L}_{10}$  (see figure 2-5). It is important to stress that we are not making use of the *values* of the direct formation energies in this stage. We are only asking what truncation of the cluster expansion can give the desired ground-state line. We find that the direct ground-state line cannot be reproduced with the ECI's used for this system in the past [54, 55, 56, 57, 40, 58, 33]. These include pairs up to the fourth neighbor, 4 triplets, and 2 quadruplets. By adding pair ECI's, the direct ground-state line can be reproduced only when the seventh- or eighth-neighbor pair

Structure	Energy	Comp.	Ref.	Structure	Energy	Comp.	Ref.
CuPt	-240.2	PdV	[41]	L1 <sub>0</sub>	-364.9	PdV	[41]
A <sub>2</sub> B <sub>2</sub>	-242.6	PdV	[41]	G4c=Z2	-314.3	PdV	[11]
MoPt <sub>2</sub>	-394.1	Pd <sub>2</sub> V	[41]	MoPt <sub>2</sub>	-179.8	PdV <sub>2</sub>	[41]
DO <sub>22</sub>	-349.7	Pd <sub>3</sub> V	[41]	DO <sub>22</sub>	-199.6	PdV <sub>3</sub>	[41]
L1 <sub>2</sub>	-281.8	Pd <sub>3</sub> V	[41]	L1 <sub>2</sub>	-201.4	PdV <sub>3</sub>	[41]
Ni <sub>4</sub> Mo=K15	-270.7	Pd <sub>4</sub> V	[3]	Ni <sub>4</sub> Mo=K15	-157.8	PdV <sub>4</sub>	[3]
W8=K13	-236.6	Pd <sub>5</sub> V	[40]	W8=K13	-145.5	PdV <sub>5</sub>	[40]
Pt <sub>8</sub> Ti=K4	-192.9	Pd <sub>8</sub> V	[3]	Pt <sub>8</sub> Ti=K4	-98.2	PdV <sub>8</sub>	[3]
W1	-348.3	Pd <sub>5</sub> V <sub>3</sub>	[40]	W1	-289.3	Pd <sub>3</sub> V <sub>5</sub>	[40]
K8	-158.6	Pd <sub>7</sub> V	[3]	K9	-197.9	Pd <sub>7</sub> V	[3]
K12	-250.5	Pd <sub>5</sub> V	[3]	K19	-344.0	Pd <sub>5</sub> V <sub>2</sub>	[3]
K21	-314.8	Pd <sub>2</sub> V	[3]	K22	-304.1	Pd <sub>2</sub> V	[3]
K29	-328.2	Pd <sub>5</sub> V <sub>3</sub>	[3]	K30	-331.1	Pd <sub>5</sub> V <sub>3</sub>	[3]
K33	-292.3	Pd <sub>3</sub> V <sub>2</sub>	[3]	K42	-205.3	Pd <sub>2</sub> V	[3]
A <sub>5</sub> B	-230.6	Pd <sub>5</sub> V	[41]	G3a	-239.0	Pd <sub>2</sub> V	[11]
G3b	-308.0	Pd <sub>2</sub> V	[11]	G4a	-236.3	Pd <sub>3</sub> V	[11]
G4b	-259.8	Pd <sub>3</sub> V	[11]	G4d	-194.6	PdV	[11]
G4e	-253.2	PdV	[11]	G5a	-322.6	Pd <sub>3</sub> V <sub>2</sub>	[11]
G6a	-293.0	PdV	[11]	G6b	-206.0	Pd <sub>5</sub> V	[11]
G6c	-306.6	PdV	[11]	G6d	-249.6	Pd <sub>2</sub> V	[11]
G6e	-203.7	Pd <sub>2</sub> V	[11]	G6f	-250.4	Pd <sub>2</sub> V	[11]

Table 2.1: Formation energies of ordered structures in the Pd-V fcc system, as computed with the LMTO-ASA method (see text for details). Kn structures refer to the n-th structure in reference [3] and Gn structures refer to possible ground-state structures reported in reference [11]. The other structures are identified by either their prototype structure, their Strukturbericht notation, or a conventional name. For some structures, alternative names are shown. All the formation energies are in meV/atom. The composition is expressed by the chemical formula of the structure. The fourth column contains the reference number where a picture of the structure can be found.

is included. This result could not have been obtained with the CW method.

We decided to include clusters beyond the eighth-neighbor pair, to verify the convergence of the cluster expansion. We included pairs up to the eleventh-neighbor distance, 5 triplets and 3 quadruplets, for a total of 20 ECI's (there are two ninth neighbors not related by symmetry). The empty and point ECI's are determined by requiring that the formation energies of fcc-Pd and fcc-V be zero.

The set of 20 ECI's is fitted imposing the following linear constraints: a) the cluster expanded formation energies of the ground-state structures in the Pd-rich side should be within 15 meV/atom of the LMTO values; b) the ground-state line as predicted by the LMTO results on the Pd-rich side should be reproduced by the cluster expansion; c) the direct energy differences between the Pd-rich structures and the ground-state line should be well reproduced by the cluster expansion when this difference is relatively small; and d) the formation energy of the V-rich structures should be reproduced within 50 meV/atom. The resulting values for the ECI's are shown in figure 2-6.

These ECI's capture the essential features of the energetics of the Pd-V system. Although the pair ECI's decay with distance, the 8<sup>th</sup> neighbor ECI's is rather large. Our linear programming technique gives clear evidence that this is necessary to reproduce the LMTO ground-state line. Figure 2-7 shows that this set of ECI's indeed reproduces the ground-state structures obtained with the LMTO method. The energy differences between the metastable Pd-rich structures and the ground-state line are shown in figure 2-8. It can be seen that the important low-lying structures are better fitted than the high-energy ones.

For comparison, we also used the CW method to fit the same set of ECI's. Even with the 20 ECI's used, the CW method failed to correctly reproduce the ground-state line. Three of the structures (Ni<sub>4</sub>Mo, A<sub>5</sub>B and K12) that were above the ground-state line in the direct LMTO results, are "pushed" below the ground-state line by the CW cluster expansion. Of course, a better CW fit could be obtained by adjusting the weights of the different structures in the least-squares fit (see equation 2.13). However, in the CW method, there is no systematic way of achieving this, and even more important, no *a-priori* knowledge that a good fit is possible. The CW results are compared to the ones obtained with the new method in figures 2-7 and 2-8.

Since the Ni<sub>4</sub>Mo and A<sub>5</sub>B structures are ground states of the CW energy parameterization, they would be stable phases in a phase diagram computed with these ECI's, contrary to what the LMTO computations predict. The stability of the Ni<sub>4</sub>Mo and A<sub>5</sub>B phases, and a relatively poor fit to the low-energy metastable structures would greatly affect the topology of the phase diagram. This problem is naturally avoided in the new method, requiring that the direct ground-state line and the direct energies of structures close to it be well reproduced by the cluster expansion.

Before using a cluster expansion (obtained with either the CW method or the new method) to compute the phase diagram of an alloy system, the ground states of the system should be computed with the same cluster expansion. If any of the ground state structures is not within the set of structures used to derive the ECI's, its cluster expanded energy should be checked against the direct energy method. If it is not a ground state in the direct energy method or if its energy is badly reproduced by the

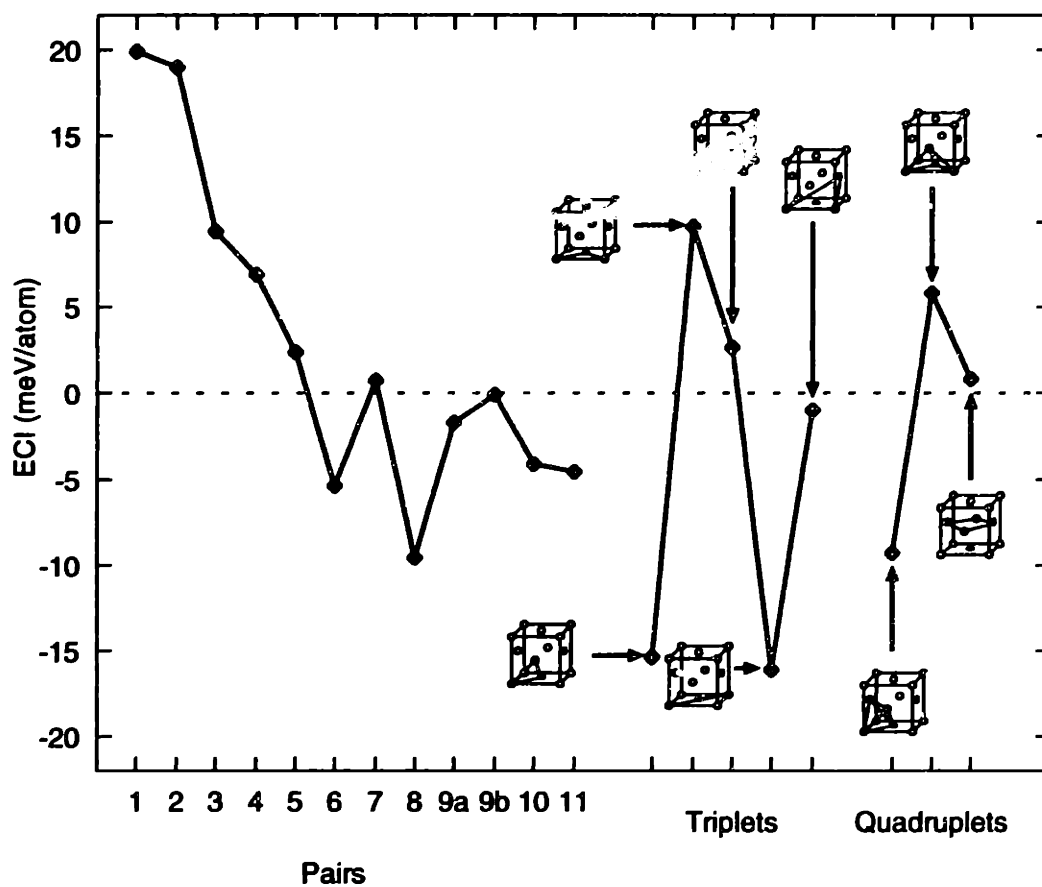


Figure 2-6: Effective cluster interactions for the Pd-V system computed with the new method. The pair clusters are indicated with the shell number, while the multi-site clusters are drawn explicitly.

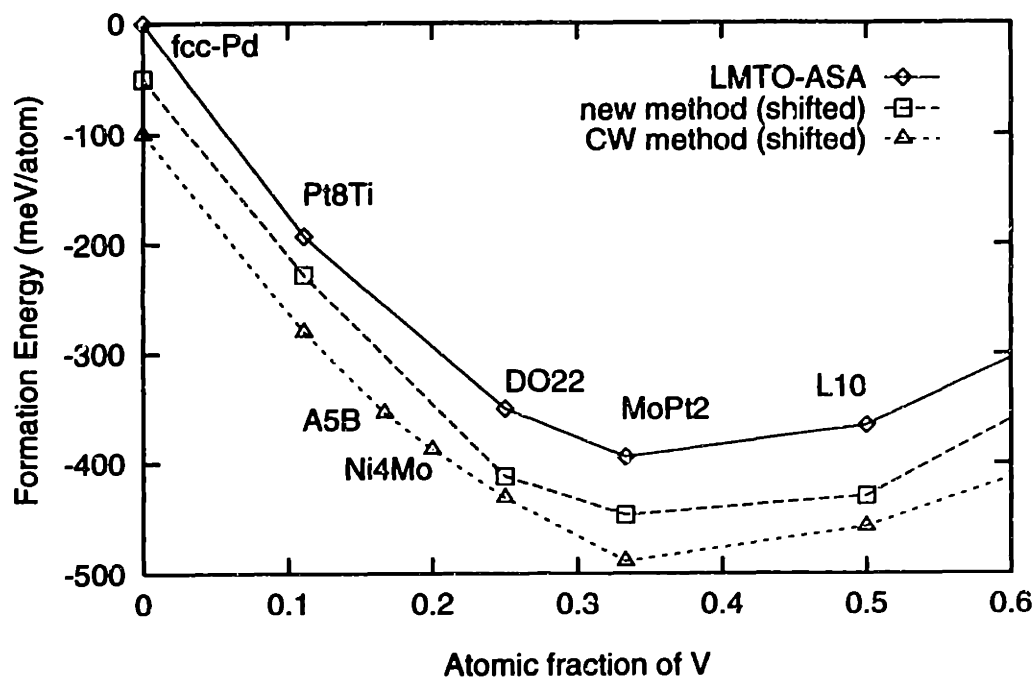


Figure 2-7: Ground-state line on the Pd-rich side of the Pd-V system. The cluster expansion obtained with the new method reproduces the LMTO results, while the CW method incorrectly produces two extra ground states (A<sub>5</sub>B and Ni<sub>4</sub>Mo) that are only metastable in the LMTO results. The curves obtained with the new method and with the CW method have been shifted down by 50 and 100 meV/atom respectively for clarity.



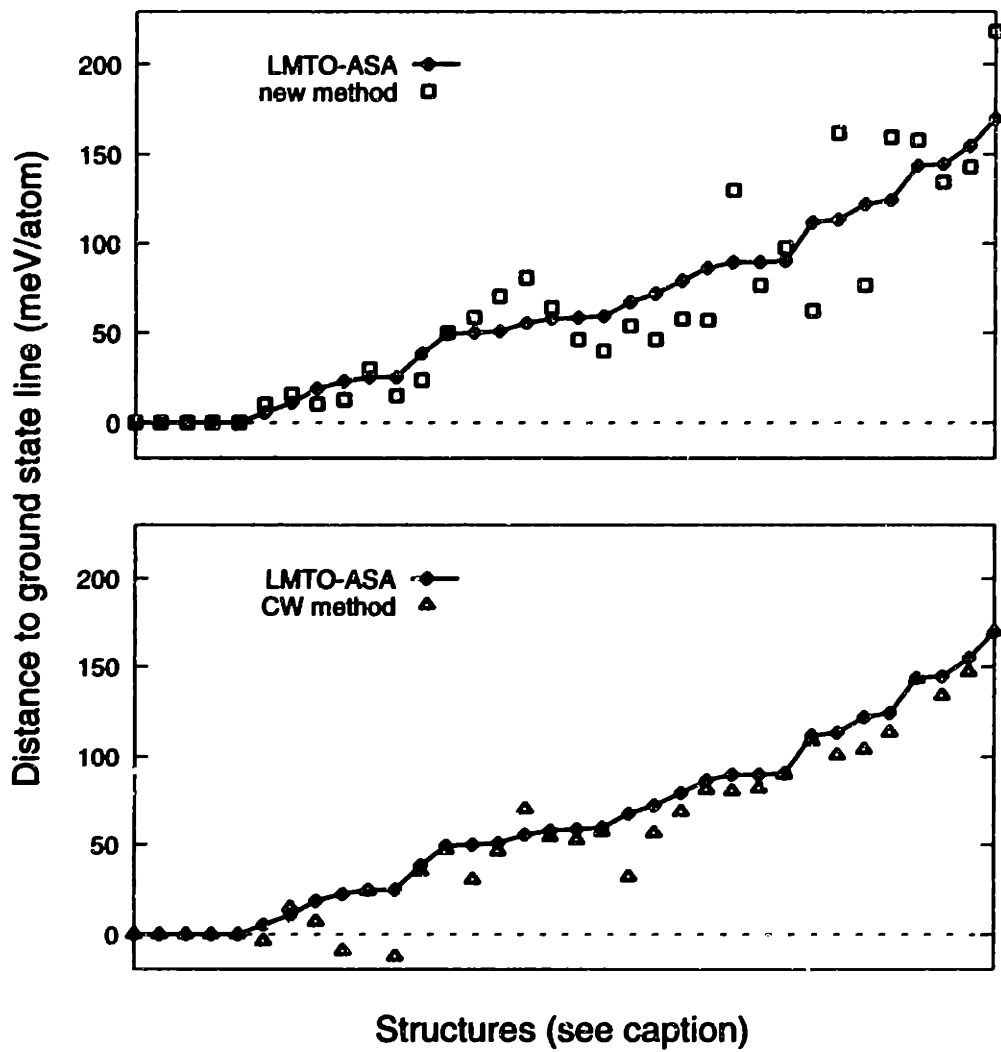


Figure 2-8: Energy differences between the Pd-rich structures and the tielines defined by the sequence fcc-Pd,  $Pt_3Ti$ -type,  $DO_{22}$ ,  $MoPt_2$ -type, and  $L1_0$ . On the abscissa, the Pd-rich structures are ordered in increasing distance to the tielines as obtained with the LMTO method. For the LMTO results and the energy parameterization of the new method these tielines define the ground-state line, and all the energy differences are positive. The energy parameterization obtained with the new method reproduces the ground states and fits the structures with energies close to the ground-state line better than structures with high energy. The CW results fail to reproduce the ground states (negative points in this plot) and the fits to the low-energy structures are worse than the ones obtained with the new method, while the high-energy structures are well reproduced.

cluster expansion, the ECI's should be recomputed including this structure in the set of structures the cluster expansion is fitted to.

In summary, the new method to get ECI's from the direct formation energies of ordered structures overcomes the limitations of the Connolly-Williams approach by taking into account the relative stabilities of different structures and the ground-state line of the alloy system. These relative energies can have a strong effect on the predicted phase diagram of the alloy system, specially for ordering systems with many structures close to or on the ground-state line. By applying the method to the Pd-V alloy system, we found that relatively long-range interactions (seventh- or eighth-neighbor pairs) are needed to reproduce the ground-state line obtained with the LMTO-ASA method. By truncating the cluster expansion at the eleventh-neighbor distance, we found a set of ECI's that reproduces most of the subtle energy differences in the Pd-V system. Finally, the method can be easily extended to the k-space formulation [37], and to volume-dependent ECI's.

# Chapter 3

## Ground states in alloys

The first step towards understanding the thermodynamic properties of substitutional alloys is the study of the ground states of the lattice models. The ground-state structures are the configurations of atoms on the lattice that have lowest energy, and therefore, are stable at  $T = 0\text{K}$ .

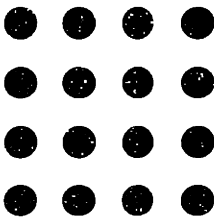
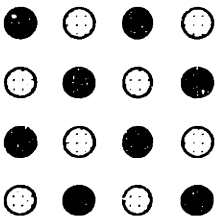
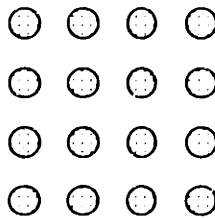
It is well known, for example, that in the lattice model on the square two-dimensional lattice, with point and nearest-neighbor pair effective cluster interactions (ECI's),<sup>1</sup> the ground states of the system are all atoms of the same type (ferromagnetic) or the "checkerboard" ordering (antiferromagnetic), depending on the values of the ECI's (see figure 3-1). If the lattice is not the square lattice or the range of the ECI's is longer than the nearest-neighbor distance, the problem of finding the lowest energy structures becomes non-trivial.

In this chapter, we explore some of the techniques that have been developed to solve the general ground-state problem. The ground-state problem for alloys is characterized in sections 3.1.1 and 3.1.2. The traditional methods used to solve the ground-state problem, reviewed in section 3.2.1, are based on linear programming (LP) techniques, and have been very successful at finding the possible ground-state arrangements for a variety of lattice models. In this chapter, we will take advantage of the power of the so-called polytope method, together with recently developed LP algorithms, to find approximate solutions for two ground-state problems: binary alloys on the fcc lattice with first- through fourth-neighbor pair interactions (section 3.2.3), and ternary alloys on the fcc lattice with first- and second-neighbor pair interactions (section 3.2.4). To our knowledge, these problems are the largest ground-state problems solved to date with the polytope method (in a sense to be further specified below).

Most of the "interesting" alloy systems require relatively long-ranged cluster expansions for an accurate description of their energetics (e.g., the Pd-V system discussed in chapter 2). As we will discover throughout this chapter, the complexity of the polytope method grows with the interaction range, in such a way that the

---

<sup>1</sup>This model is equivalent to the original Ising model where the pair ECI is minus the Ising coupling between spins and the point ECI corresponds to the external magnetic field [60].

	A	B	C
			
$\langle \sigma_1 \rangle$	+1	0	-1
$\langle \sigma_2 \rangle$	+1	-1	+1
$E/N$	$V_1 + 2V_2$	$-2V_2$	$-V_1 + 2V_2$

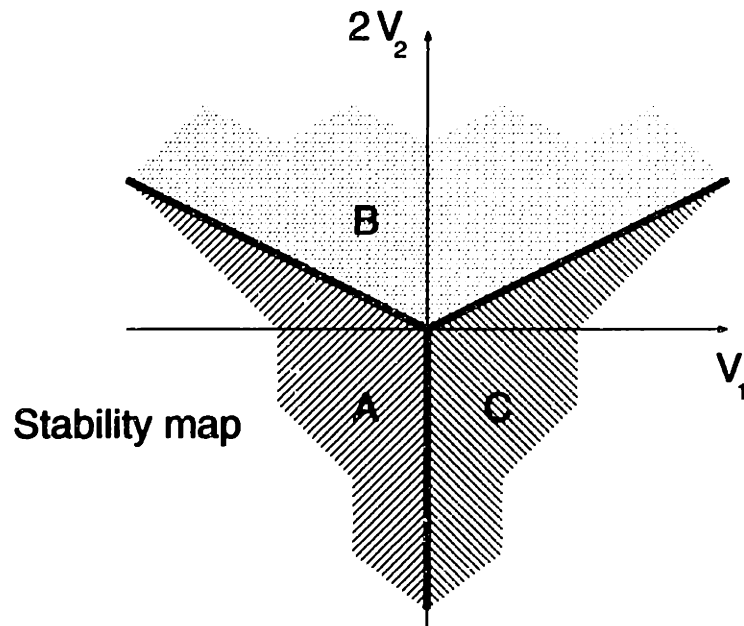


Figure 3-1: Ground-state structures of the Ising model on the square-lattice with point ( $V_1$ ) and nearest-neighbor pair ( $V_2$ ) interactions ( $E(\vec{\sigma}) = V_1\langle\sigma_1\rangle + 2V_2\langle\sigma_2\rangle$ ). The stability map shows the range of interactions for which each of the structures is the ground state of the system.

ground–state problems become intractable<sup>2</sup> for systems with interactions beyond the second– or third–neighbor distance. To be able to study these complex systems, we developed a new method, that we call *enumeration method*, that approximately solves the ground–state problem for any interaction range. This method is described in section 3.3.1 and is applied to the binary fcc alloy with first– through fourth–neighbor pair interactions in section 3.3.2, obtaining an increase of an order of magnitude in the number of possible ground–state structures with respect to the results of the polytope method.

The chapter concludes with a summary (section 3.4) and a discussion of the future perspectives of ground–state determination methods (section 3.5).

## 3.1 The ground–state problem

### 3.1.1 Two types of ground–state problems

There are two types of problems related to the ground–state search. The first and simpler problem consists of finding the ground–state structures as a function of composition for a given alloy system, once the ECI’s in the cluster expansion of the energy are known. An example of this first type of problems would be:

“find the ground–state structures as a function of composition for an alloy on the simple–cubic lattice, modeled with the following cluster expansion:

$$E(\vec{\sigma}) = 20 \frac{\text{meV}}{\text{atom}} \langle \sigma_1 \rangle + 8 \frac{\text{meV}}{\text{atom}} \langle \sigma_2 \rangle,$$

where  $\langle \sigma_i \rangle$  is the  $i^{\text{th}}$  nearest–neighbor averaged cluster function.”

In the second and more general problem, one tries to find all possible ground–state structures for a given truncation of the cluster expansion, and for any value of the ECI’s; for example:

“find *all* possible ground states of a simple–cubic lattice model with first– and second–neighbor interactions.”

The first kind of problems is of interest when the energetics of the alloy system is already understood, and well modeled by the cluster expansion. The second kind is very useful for determining the terms that should be kept in the cluster expansion so that a certain sequence of ground states vs. composition can be obtained. As a by–product, the range of ECI’s for which these structures are the ground states of the system is obtained.

---

<sup>2</sup>These problems are intractable with the computer power currently available. As computers get faster, more problems will be solved. However, due to the rapid increase in complexity with interaction range (“exponential scaling”), not much improvement is expected with the polytope method (see section 1.1.3, page 32).

In this thesis, we are concerned with the second kind of ground-state problems. Since the first kind of problems is a subset of the second kind, some of our conclusions are also valid for the former. However, special techniques to solve ground-state problems for specific alloy systems have been developed [56] and are currently being perfected [61].

### 3.1.2 Frustration and the configurational polytope

Given a truncation of the cluster expansion for the energy of the system, symbolized with  $\alpha_{max}$  (see section 2.1),

$$\frac{E(\vec{\sigma})}{N} = \sum'_{\alpha \leq \alpha_{max}} m_{\alpha} V_{\alpha} \langle \sigma_{\alpha} \rangle(\vec{\sigma}), \quad (3.1)$$

the ground-state problem consists of finding all possible arrangements,  $\vec{\sigma}$ , that minimize the energy of the system for some range of values of the ECI's,  $V_{\alpha}$ . The averaged cluster functions (or correlation functions) on cluster  $\alpha$  are defined as

$$\langle \sigma_{\alpha} \rangle \equiv \left\langle \prod_{i \in \alpha} \sigma_i \right\rangle, \quad (3.2)$$

where  $\langle \rangle$  indicates the average over all the clusters equivalent to cluster  $\alpha$  under a symmetry operation of the lattice. The correlation functions  $\langle \sigma_{\alpha} \rangle$  can take values between  $-1$  and  $+1$ . This follows trivially from the fact that  $\langle \sigma_{\alpha} \rangle$  is the average of products of  $\pm 1$  spins  $\sigma_i$ . This means that the correlation functions of any arrangement have to lie within the hypercube defined by the above restrictions. Since the energy of the system is a linear function of  $\langle \sigma_{\alpha} \rangle$  (equation 3.1), one is tempted to conclude that the possible ground states are those structures with lattice-averaged cluster functions with values  $-1$  and  $+1$ . In fact, the energy would be minimized by structures with

$$\langle \sigma_{\alpha} \rangle = \begin{cases} -1 & \text{if } V_{\alpha} > 0 \\ +1 & \text{if } V_{\alpha} < 0 \end{cases}. \quad (3.3)$$

Let us consider, however, the simple-square binary alloy described in figure 3-1. The correlation functions of the three possible ground-state structures are shown in figure 3-2. Any point outside the triangle defined by connecting the correlation functions of these three structures does not correspond to any configuration  $\vec{\sigma}$  on the simple-square lattice. For example, it is impossible to find a configuration with  $\langle \sigma_1 \rangle = 1$  and  $\langle \sigma_2 \rangle = -1$ , because if  $\langle \sigma_1 \rangle = 1$ , then all the nearest-neighbor pair clusters will be of the kind A-A and therefore  $\langle \sigma_2 \rangle = 1$ . From this analysis, we conclude that not all the correlation functions can be adjusted *independently* between  $-1$  and  $+1$ .

Can the above analysis on the simple-square lattice be extended to other lattices with the same interaction range? Consider, for example, the triangular lattice with point and nearest-neighbor ECI's. It is easy to show that it is impossible to build a configuration with  $\langle \sigma_2 \rangle = -1$ , where  $\sigma_2$  is the nearest-neighbor pair cluster function.

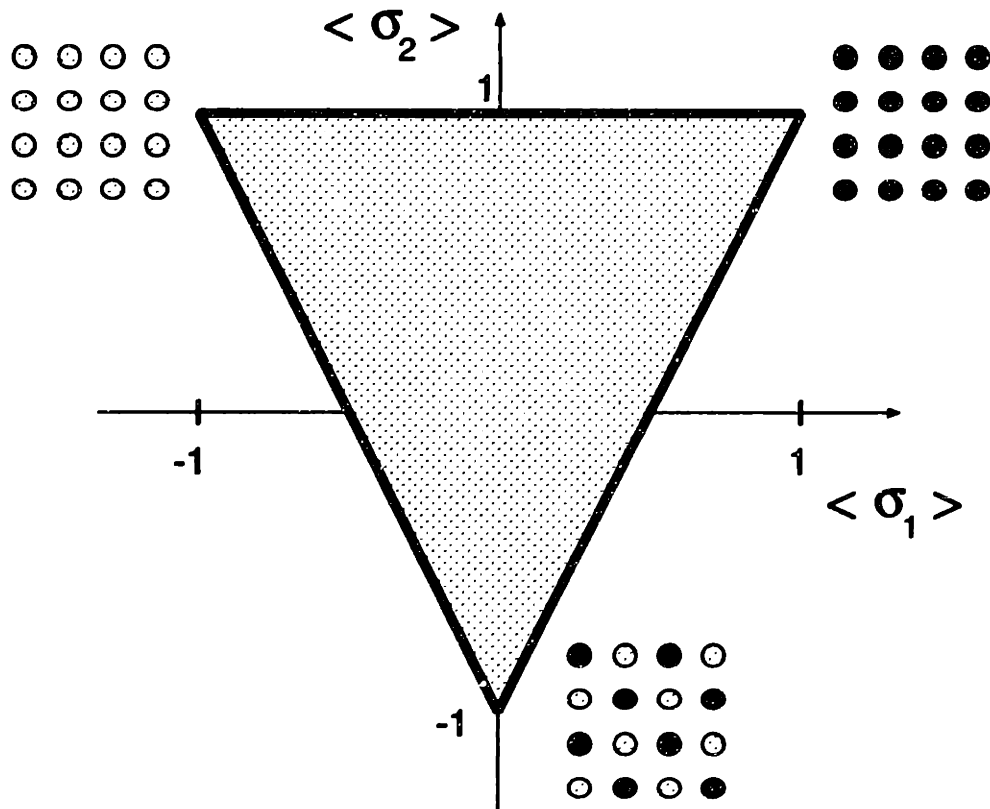


Figure 3-2: Correlation functions of the ground-state structures of the simple-square lattice with point and nearest-neighbor ECI's ( $\langle \sigma_1 \rangle$  is the point correlation function and  $\langle \sigma_2 \rangle$  is the nearest-neighbor pair correlation function). The correlation functions of the ground-state structures are the vertices of the shaded triangle.

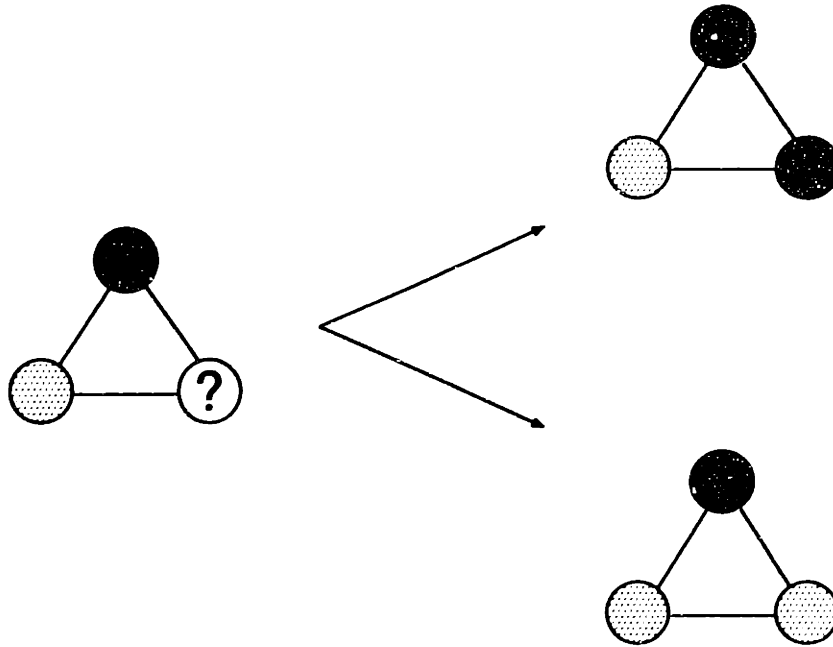


Figure 3-3: Frustration effect in the triangular lattice with nearest-neighbor pair interactions. If the ECI is positive, then the number of A-B nearest-neighbor pairs has to be maximized in order to minimize the energy of the system. However, due to the topology of the triangular lattice, not all nearest-neighbor pairs can be of the A-B type.

To obtain such a value for the averaged cluster function, it is necessary that all nearest-neighbor pairs be of the type A-B. This is impossible in the triangular lattice, as shown in figure 3-3, due to the presence of triangles of nearest-neighbor pairs.

In the triangular lattice, contrary to what happens in the simple-square lattice, not all the points inside the triangle with vertices  $(-1, +1)$ ,  $(0, -1)$ , and  $(+1, +1)$ , in the space of point and nearest-neighbor correlation functions, correspond to physically realizable configurations  $\vec{\sigma}$ . It can be proved that the exact region in correlation-function space of realizable configurations is the polytope shown in figure 3-4. The proof of this statement, and more examples of simple ground-state problems can be found in reference [41].

The constraints that reduce the region of possible correlation functions for a given lattice and interaction range are generally referred to as “frustration” effects. We will refer to the polytope<sup>3</sup> of averaged-cluster functions corresponding to realizable (or “constructible”) configurations as the “configurational polytope” of the problem under study. Since the energy is a linear function of the averaged cluster functions, the vertices of the configurational polytope are the possible ground-state structures

<sup>3</sup>A *polytope* is a bounded *polyhedron*. A *polyhedron*, in turn, is defined as the intersection of a finite number of semi-spaces, or as the set of points in space that satisfy a finite set of linear inequalities.



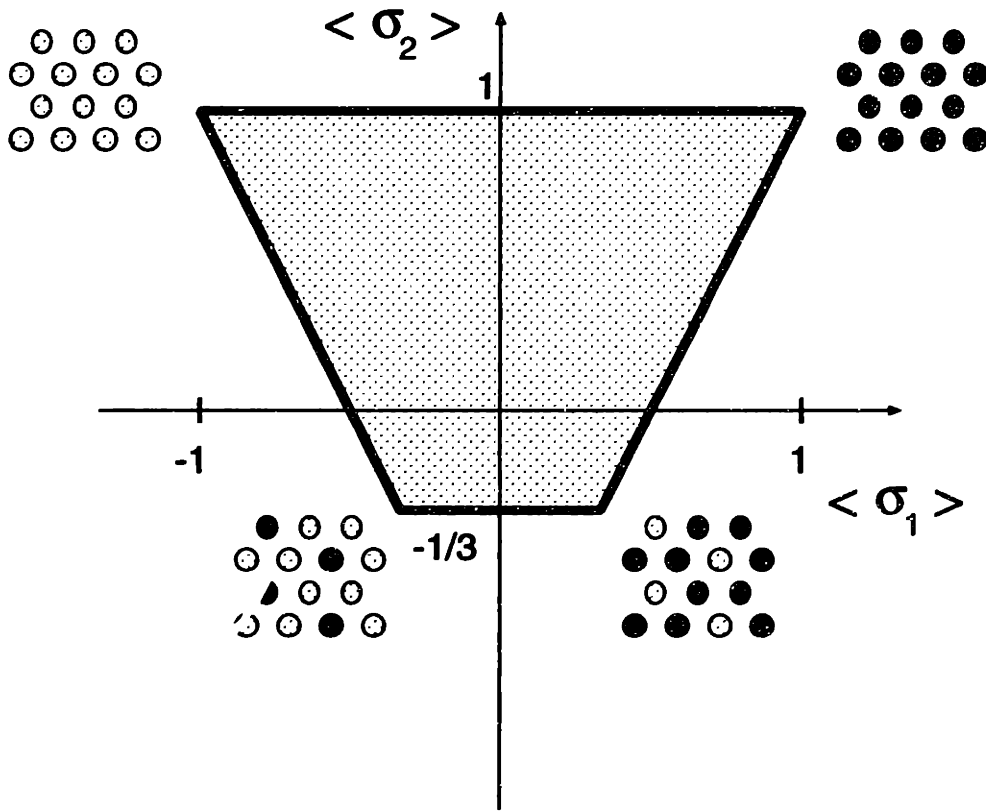


Figure 3-4: Configurational polytope of the triangular lattice with nearest-neighbor ECI's. The vertices of the polytope correspond to the possible ground-state structures.

of the system. We can now restate the ground-state problem as the *search for the vertices of the configurational polytope*.

The name “configurational polytope” could be misleading, since the region of the space of lattice-averaged cluster functions that corresponds to constructible configurations does not need to be a polytope. In fact, for the two-dimensional honeycomb lattice with first- and second-neighbor interactions, such region is defined by an infinite number of linear inequalities (see page 115 in reference [41]). In spite of this, we will use the term “configurational polytope,” but keeping in mind that the region we are referring to might not be a polytope.

An important property of the configurational polytope is that it is *convex*. This follows from the fact that if two points, corresponding to configurations  $\vec{\sigma}_1$  and  $\vec{\sigma}_2$ , are inside the configurational polytope, then all the points on the segment that joins those two points correspond to configurations  $\vec{\sigma}$  that can be obtained from phase-separated mixtures of  $\vec{\sigma}_1$  and  $\vec{\sigma}_2$ . We will exploit this property to develop the enumeration method in section 3.3.1.

## 3.2 The polytope method

### 3.2.1 The method

The *polytope method* is a systematic way of finding linear constraints on the correlation functions  $\langle \sigma_\alpha \rangle$ . Any point in correlation-function space, not satisfying one or more of these constraints corresponds to an “inconstructible” set of correlation functions (i.e., there is no configuration  $\vec{\sigma}$  with those correlation functions). A schematic representation of these constraints and the exact configurational polytope are shown in figure 3-5.

The inequalities of the polytope method are constructed to represent the frustration effects on a subset of sites of the lattice. This group of lattice points is usually called the “maximal cluster,”  $\beta_{max}$ , of the polytope method.<sup>4</sup> To impose the constraints on the correlations functions, we require that the probability of any configuration on the maximal cluster be positive. The probability of finding configuration  $J$  on any cluster equivalent by symmetry to the maximal cluster  $\beta_{max}$  can be expressed as a linear combination of the correlation functions of subclusters of  $\beta_{max}$  as [42, 41]:

$$P_{\beta_{max}}(J) = \frac{1}{2^{n_{\beta_{max}}}} \left[ 1 + \sum_{\alpha \subseteq \beta_{max}} v_{\beta_{max}\alpha}(J) \langle \sigma_\alpha \rangle \right], \quad (3.4)$$

where the sum is over the non-empty symmetry-independent (by the symmetry of the lattice) subclusters  $\alpha$  of the maximal cluster  $\beta_{max}$  (we will note by  $n$  the number of such symmetry-distinct subclusters),  $n_{\beta_{max}}$  is the number of sites in cluster  $\beta_{max}$ ,

---

<sup>4</sup>This maximal cluster of the polytope method,  $\beta_{max}$ , should not be confused with the truncation of the cluster expansion, usually symbolized with  $\alpha_{max}$ .

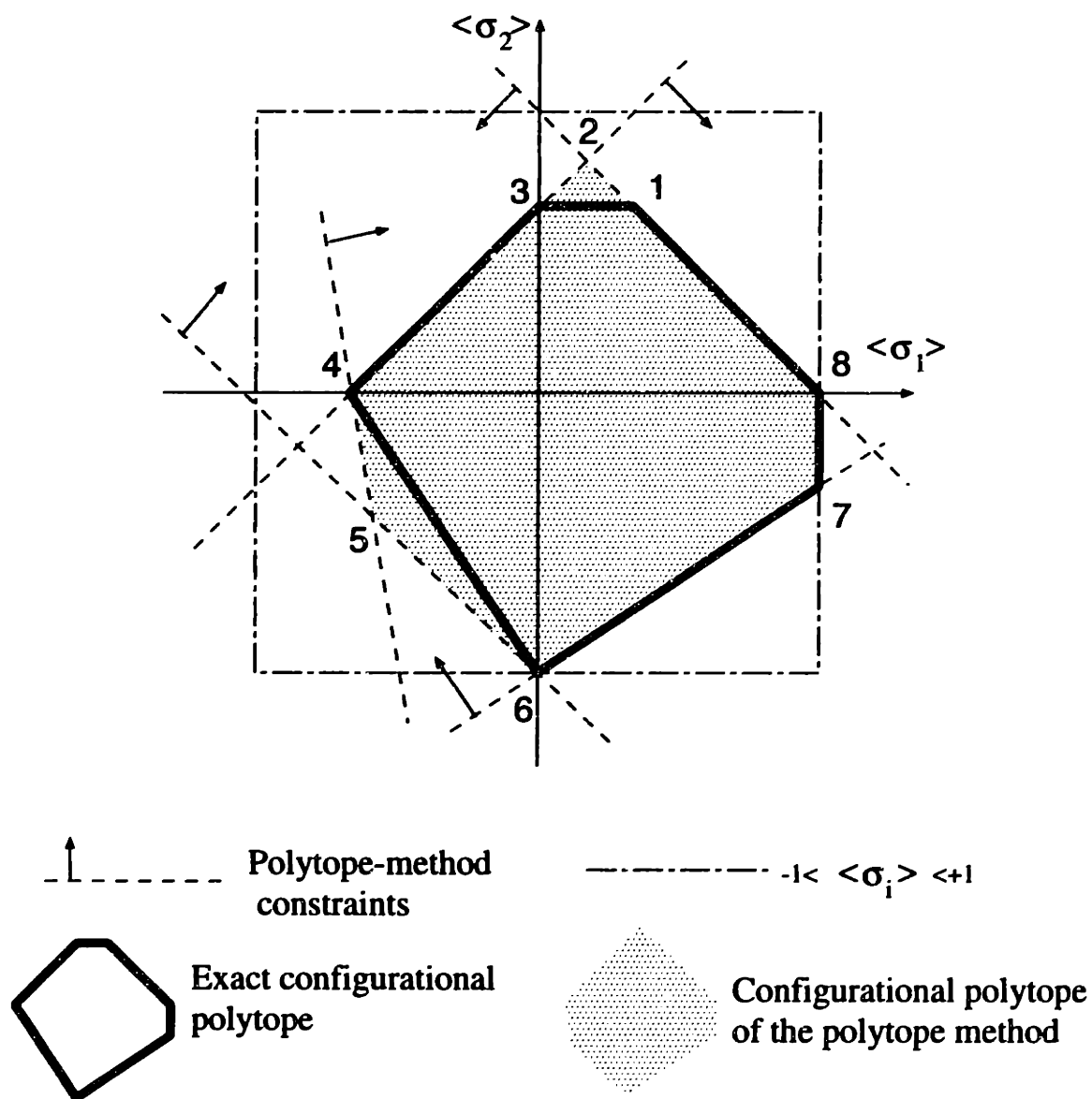


Figure 3-5: Schematic representation of the polytope method for the determination of the possible ground states of a lattice model. Every point inside the exact configurational polytope corresponds to one or more configurations on the lattice (constructible points), while there is no configuration with correlation functions outside the exact configurational polytope (inconstructible points). The constraints of the polytope method define a polytope that contains the exact solution, but may also contain inconstructible points (e.g., vertices 2 and 5). In other words, the polytope method approaches the exact solution from outside in the space of the correlation functions.

and the so-called *v-matrix*  $v_{\beta_{max}\alpha}(J)$  is defined as:

$$v_{\beta_{max}\alpha}(J) \equiv \sum_{\substack{\gamma \in \Omega(\alpha) \\ \gamma \subseteq \beta_{max}}} \sigma_{\gamma}(J), \quad (3.5)$$

where  $\Omega(\alpha)$  is the set (sometimes referred to as the “orbit”) of clusters equivalent to cluster  $\alpha$  by the symmetry of the lattice. The computation of the *v-matrix* can be automated using group-theoretical techniques [42]. The number ( $m$ ) of independent probabilities  $P_{\beta_{max}}(J)$  is equal to the number of configurations  $J$  on cluster  $\beta_{max}$  that are distinct under the point-group symmetry of the cluster (and not of the lattice). An example of the calculation of the probabilities of configurations on a triangular cluster using equation 3.4 in the triangular lattice, and the correspondent *v-matrix* using equation 3.5 is shown in figure 3-6.

Any configuration on the lattice ( $\vec{\sigma}$ ) must satisfy  $0 \leq P_{\beta_{max}}(J) \leq 1$ . Since by construction, the probabilities in equation 3.4 are normalized ( $\sum_J P_{\beta_{max}}(J) = 1$ ) [41], it suffices to require  $P_{\beta_{max}}(J) \geq 0$ .

The set of inequalities  $P_{\beta_{max}}(J) \geq 0$  defines a polytope in the space of correlation functions on the subclusters of the maximal cluster  $\beta_{max}$ . For example, if  $\beta_{max}$  is the nearest-neighbor triangle in the triangular lattice, then the inequalities are defined in the space of the correlation functions on the triangle, pair, and point clusters (see figure 3-6).

If the point-group symmetry of the cluster is such that all the sites of the cluster are equivalent (e.g., in the fcc lattice the tetrahedron and octahedron clusters shown in figure 3-7) then  $m = n + 1$  and the polytope is a simplex.<sup>5</sup> If not all the points of the cluster are equivalent by the point-group symmetry of the cluster (e.g., the 10-point, 13-point, and 14-points clusters in fcc, shown in figure 3-7), then  $m > n + 1$  and the polytope is more complicated. In this case, the vertices of the polytope can be found using vertex enumeration techniques, well developed in the field of combinatorial geometry [62].

The vertices of the polytope defined by  $P_{\beta_{max}}(J) \geq 0$  are the possible ground states of the system. Since the coordinates of these vertices are correlation functions on the subclusters of the maximal cluster  $\beta_{max}$ , they will be possible ground states when the Hamiltonian is defined in this same space. In other words, when the cluster expansion is truncated to retain *exactly* the correlation functions corresponding to subclusters of  $\beta_{max}$ .

By definition, the exact configurational polytope is inside the polytope defined by  $P_{\beta_{max}}(J) \geq 0$  (see figure 3-5). When these two polytopes are identical, the polytope method has produced the exact solution of the ground-state problem. Otherwise, one or more of the vertices of the polytope defined by  $P_{\beta_{max}}(J) \geq 0$  are outside the exact configurational polytope (e.g., vertices 2 and 5 in figure 3-5), and therefore do

---

<sup>5</sup>A simplex in  $n$  dimensions is a polytope with  $n + 1$  faces, and  $n + 1$  vertices. The vertices of a simplex are obtained by solving the set of linear equations that results from all the  $n$ -subsets of faces of the polytope.

Maximal cluster		Spin 								
Non-empty subclusters ( $\alpha$ )										
Orbits ( $\gamma$ )										
Configurations ( $J$ )	$\sigma_\gamma$	$\Sigma \sigma_\gamma$	$\sigma_\gamma$	$\sigma_\gamma$	$\sigma_\gamma$	$\Sigma \sigma_\gamma$	$\sigma_\gamma$	$\sigma_\gamma$	$\sigma_\gamma$	$\Sigma \sigma_\gamma$
J1	+1	<b>+1</b>	+1	+1	+1	<b>+3</b>	+1	+1	+1	<b>+3</b>
J2	-1	<b>-1</b>	+1	-1	-1	<b>-1</b>	-1	+1	+1	<b>+1</b>
J3	+1	<b>+1</b>	-1	-1	+1	<b>-1</b>	-1	-1	+1	<b>-1</b>
J4	-1	<b>-1</b>	+1	+1	+1	<b>+3</b>	-1	-1	-1	<b>-3</b>

$$P(J_1) = \frac{1}{8}(1 + 1\langle\sigma_3\rangle + 3\langle\sigma_2\rangle + 3\langle\sigma_1\rangle) \geq 0$$

$$P(J_2) = \frac{1}{8}(1 - 1\langle\sigma_3\rangle - 1\langle\sigma_2\rangle + 1\langle\sigma_1\rangle) \geq 0$$

$$P(J_3) = \frac{1}{8}(1 + 1\langle\sigma_3\rangle - 1\langle\sigma_2\rangle - 1\langle\sigma_1\rangle) \geq 0$$

$$P(J_4) = \frac{1}{8}(1 - 1\langle\sigma_3\rangle + 3\langle\sigma_2\rangle - 3\langle\sigma_1\rangle) \geq 0$$

Figure 3-6: Example of the calculation of the  $v$ -matrix and probability constraints for the triangular maximal cluster in the two-dimensional triangular lattice. The bold numbers on the table constitute the  $v$ -matrix, obtained through equation 3.5. The probabilities of the configurations  $J$  on the maximal cluster are linear combinations of the correlation functions. The coefficients of these linear functions are the rows of the  $v$ -matrix. The condition of positive probability implies then a linear constraint on the correlation functions (shown below the table).

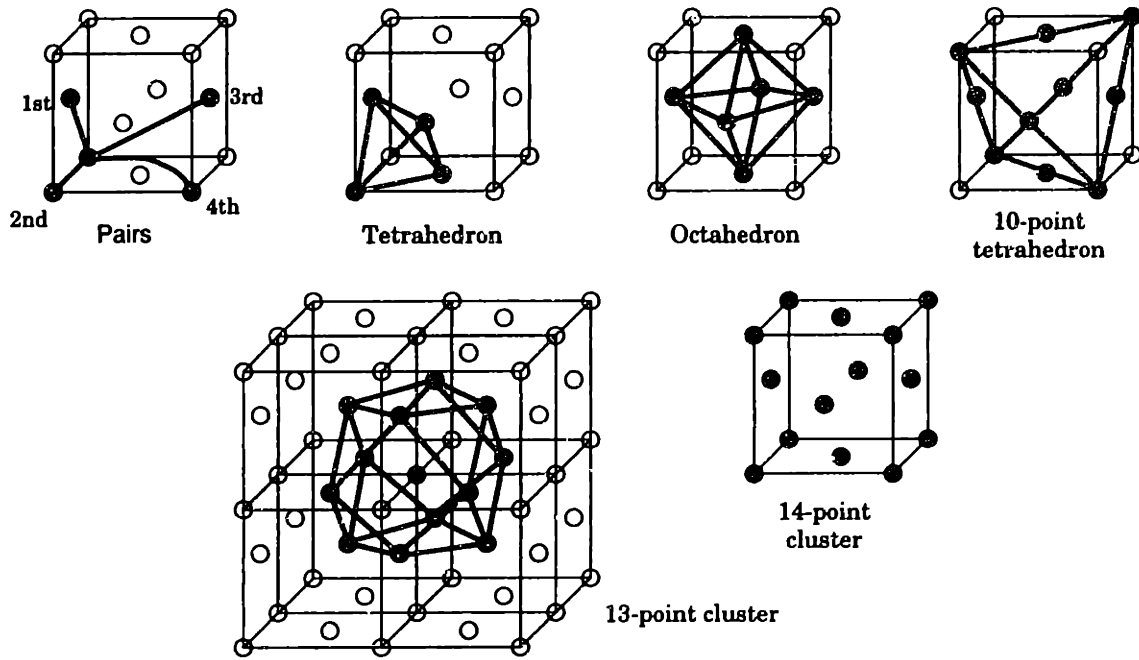


Figure 3-7: Definitions of clusters on the fcc lattice. The 14-point cluster is composed of all the atoms in a conventional fcc unit cell and the 13-point cluster by one atom and its 12 nearest neighbors.

not correspond to constructible structures. In this case, the frustration effects on the maximal cluster  $\beta_{max}$  (that give rise to the constraints  $P_{\beta_{max}}(J) \geq 0$ ) are not enough to account for all the frustration effects on the lattice and a larger maximal cluster is required.

The terms that are kept in the truncated cluster expansion do not need to coincide with the subclusters of the maximal cluster of the polytope method. For example, one may want to study the ground states of a lattice model on the two-dimensional triangular lattice with nearest-neighbor interactions. Since the nearest-neighbor pair cluster is not enough to account for the frustration on the triangular lattice, the nearest-neighbor triangle is necessary as maximal cluster for the polytope method. The linear constraints derived from this maximal cluster depend not only on the point and pair correlation functions (included in the cluster expansion), but also on the triplet correlation function.

In general, the constraints are formulated on a higher dimensional space (hereafter referred to as the *high-dimensional* space) than the space spanned by the correlation functions kept in the cluster expansion (hereafter, the *low-dimensional* space). In this case, it is necessary to enumerate the vertices of the polytope in the high-dimensional space, and then project them down to the low-dimensional space. Only the points on the convex hull<sup>6</sup> of this set of points are possible ground-state structures. The

<sup>6</sup>The convex hull of a set of points is the smallest convex region of space that contains all the

flowchart in figure 3-8 summarizes the steps of the polytope method.

The coordinates of the vertices of the convex hull in the low dimensional space are the correlation functions of the candidate ground-state structures. If there is no configuration  $\vec{\sigma}$  with the correlation functions of a given vertex, then that vertex is in-constructible. In this case the constraints on the maximal cluster  $\beta_{max}$  are not enough to account for all the frustration effects on the lattice, and a larger maximal cluster is needed. The process has to be iterated until all the vertices of the low-dimensional convex hull can be constructed, in which case the ground-state problem has been solved exactly. If a configuration  $\vec{\sigma}$  can be found with the correlation functions of a given vertex, then that configuration is an *exact* ground state of the system. In other words, that vertex is part of the exact configurational polytope and will not be removed by frustration constraints generated by any cluster.

In some ground-state problems, it is convenient to define the frustration constraints on more than one maximal cluster simultaneously. In this case, the high-dimensional space is spanned by the subclusters of all the maximal clusters (some of which may be shared by two or more of the maximal clusters). The rest of the procedure is exactly the same as in the case of just one maximal cluster. For example, for the binary fcc alloy with first- and second-neighbor ECI's, the constraints on the tetrahedron and octahedron clusters (see figure 3-7) are enough to account for all the frustration effects, and to solve the ground-state problem exactly.

Once the exact configurational polytope has been found, the range of values of the ECI's that make a given vertex of the exact configurational polytope the actual ground state of the system can be obtained by analyzing the faces of the polytope that contain that vertex [41]. The normal vectors of those faces form (in dual space) a cone such that any set of ECI's inside the cone makes the original vertex the ground state of the system.

It is important to note that the polytope method does not impose any restriction on the size of the unit cell of the ground-state structures. In fact, the size of the unit cell of the ground-state structure can be much larger than the interaction range in the cluster expansion of the energy. An example of such phenomenon can be found in the honeycomb lattice with first- and second-neighbor interactions [41]. This lattice presents an infinite sequence of ground-state configurations with increasing unit-cell size, even for a fixed interaction range.

Other methods based on similar ideas to the ones used for the development of the polytope method have been discussed in the literature. They include the so-called "cluster" method of Allen and Cahn [63] and the method of geometrical inequalities by Kanamori [64].

### 3.2.2 Successes of the polytope method

The polytope and similar methods have been applied successfully to several ground-state problem in alloys. A summary of the applications of this kind of methods to

---

points. If the set of points is finite, then the convex hull is the smallest polytope which vertices are points in the set.

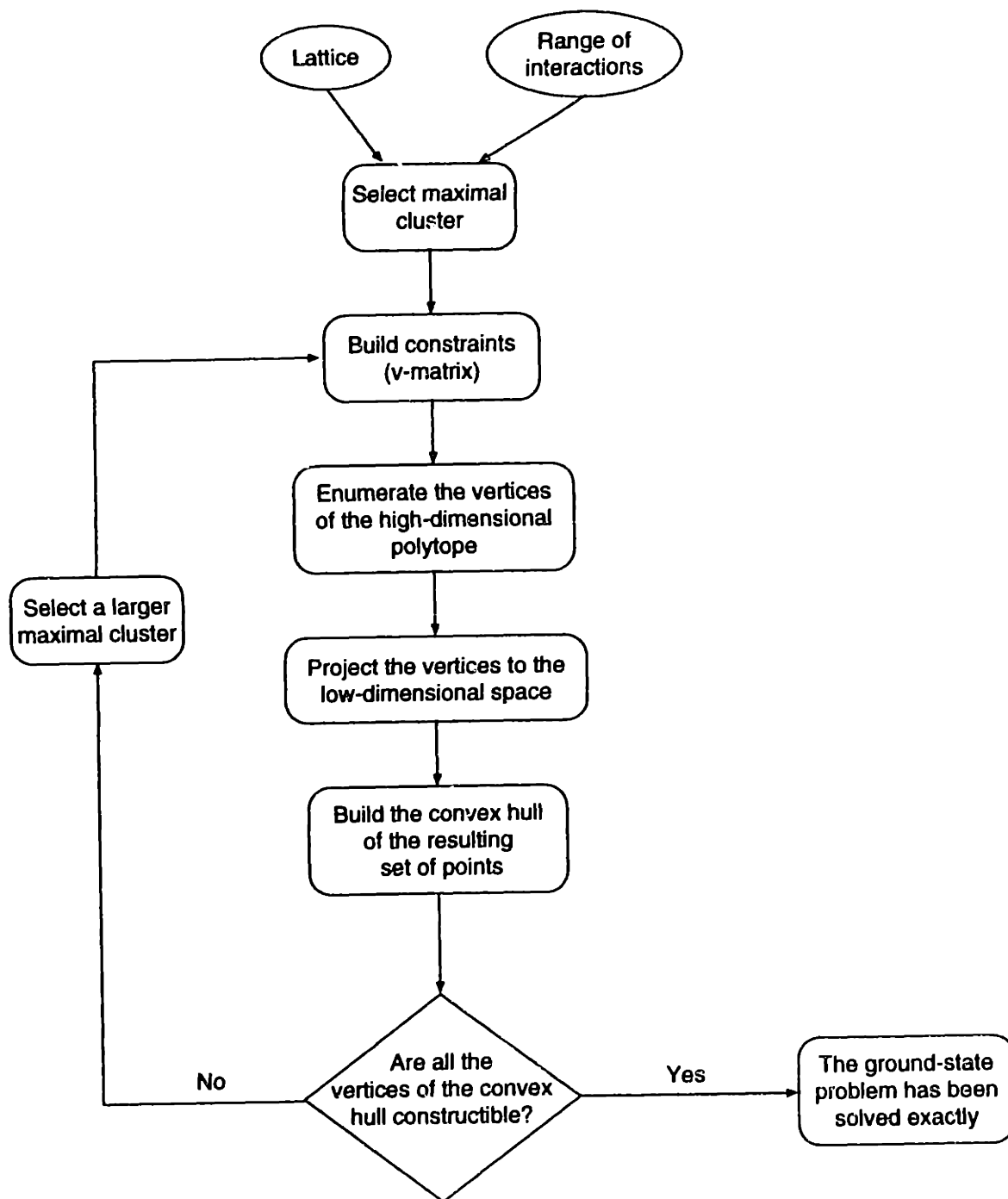


Figure 3-8: Steps for the determination of the ground-state structures of a lattice model using the polytope method.



Lattice	ECI's		Solution	Number of g.s. struc. <sup>c</sup>	Year	Ref.
	Pairs <sup>a</sup>	Multib. <sup>b</sup>				
bcc	2 <sup>nd</sup>	–	Exact	4	1966	[64]
bcc <sup>d</sup>	5 <sup>th</sup>	–	Approx.	17	1986	[65]
bcc-ternary	2 <sup>nd</sup>	–	Exact	6	1992	[66]
fcc	2 <sup>nd</sup>	–	Exact	9	1966	[64, 63]
fcc	2 <sup>nd</sup>	TO	Approx.	16	1981	[67]
fcc	4 <sup>th</sup>	–	Approx.	39	1977	[3]
hcp	2 <sup>nd</sup>	–	Exact	9	1976	[68]
hcp	2 <sup>nd</sup>	TO	Approx.	32	1993	[69]

Table 3.1: Summary of solutions of the ground-state problem for some three-dimensional lattices using the polytope or similar method. The results are for binary alloys, unless otherwise stated.

<sup>a</sup>From the nearest-neighbor pair to the pair shown, unless otherwise stated.

<sup>b</sup>TO: includes all the multisite ECI correspondent to subclusters of the tetrahedron and octahedron clusters (see figure 3-7).

<sup>c</sup>Only distinct ground-state structures are included. If a structure can be obtained from another structure by an exchange of the A and B atomic species, then these two structures are considered as one structure in this table.

<sup>d</sup>The 4<sup>th</sup> neighbor was not included in this study.

the solution of the ground-state problems on the fcc, bcc, and hcp three-dimensional lattices is shown in table 3.2.2. A more comprehensive review can be found in reference [41].

As can be seen in table 3.2.2, exact solutions could not be found for any of these lattices for alloys with more than two pair ECI's. Two different types of approximate solutions are possible. In the first type, some *ad-hoc* approximation is made. This is the case of reference [3] for the fcc binary alloy with first- through fourth-neighbor ECI's where the nearest-neighbor ECI was assumed to be dominant, greatly simplifying the problem. In the second type, one or more of the vertices resulting from the polytope method are inconstructible, and therefore a larger maximal cluster should be considered to remove them from the polytope.<sup>7</sup>

Through the use of state-of-the-art vertex enumeration techniques we have approximately solved two more ground-state problems. The summary is shown in table 3.2. In the next two sections these solutions are explained in detail.

<sup>7</sup>When constraints on larger clusters are considered to remove an inconstructible vertex, they can generate other vertices not present in the previous solution. The constructibility of these new vertices has to be verified and the procedure repeated until all the vertices of the polytope are constructible.

Lattice	ECI's		Solution	Number of g.s. struc. <sup>b</sup>	Year	Ref.
	Pairs <sup>a</sup>	Multib.				
fcc	4 <sup>th</sup>	–	Approx.	27	1993	[11] <sup>c</sup>
fcc-ternary	2 <sup>nd</sup>	–	Approx.	31	1994	[70] <sup>d</sup>

Table 3.2: New solutions of ground-state problems obtained in this thesis using the polytope method.

<sup>a</sup>From the nearest-neighbor pair to the pair shown, unless otherwise stated.

<sup>b</sup>Only distinct ground-state structures are included. If a structure can be obtained from another structure by an exchange of the A and B atomic species, then these two structures are considered as one structure in this table.

<sup>c</sup>See section 3.2.3.

<sup>d</sup>See section 3.2.4.

### 3.2.3 Application of the polytope method to fcc binary alloys with first- through fourth-neighbor pair interactions

#### The problem

Taking the symmetry of the lattice into account and keeping the point and pairs interactions up to the fourth-neighbor distance, the cluster expansion of the energy is

$$E(\vec{\sigma}) = V_1 \langle \sigma_1 \rangle + \sum_{i=1}^4 m_{2,i} V_{2,i} \langle \sigma_{2,i} \rangle, \quad (3.6)$$

where  $\langle \sigma_1 \rangle$  is the lattice average of the spin (or point correlation function),  $\langle \sigma_{2,i} \rangle$  is the lattice average of the  $i^{\text{th}}$  neighbor pair cluster function (or pair correlation function),  $V_1$  is the point ECI,  $V_{2,i}$  are the pair ECI's (see figure 3-7), and  $m_{2,i}$  are the number of  $i^{\text{th}}$  neighbor pairs per lattice site on the fcc lattice ( $m_{2,1} = 6$ ,  $m_{2,2} = 3$ ,  $m_{2,3} = 12$ , and  $m_{2,4} = 6$ ).

#### Previous results

The fcc lattice with only nearest- and next-nearest-neighbor pair interactions has been analyzed by different authors [64, 63, 67]. The exact solution of this problem contains 9 distinct non-degenerate structures. Since this number can not account for all the superstructures of fcc observed in nature to be ground states of binary alloy systems, it is necessary to include more terms in the cluster expansion of the energy.

For binary alloys on the fcc lattice, the most comprehensive search for ground-state structures was done by Kanamori and Kakehashi [3]. They considered pair interactions up to the fourth-neighbor distance (equation 3.6) assuming that the nearest-neighbor ECI was dominant. Under this condition, the nearest-neighbor

correlation function is minimum for a given concentration of the alloy. Using the method of geometrical inequalities, they found 39 non-degenerate distinct ground-state structures. The assumption of a dominant nearest-neighbor interaction in their work excluded some known structures, like the CuPt family.

As described above, the polytope method was applied successfully to the ground-state problem on the fcc lattice with first and second nearest-neighbor interactions [67], using the regular tetrahedron and octahedron as clusters to account for the frustration (see figure 3-7). In order to include third and fourth neighbors in the analysis, one has to choose larger clusters. The simplest cluster that contains these interactions and some of the frustration effects is the 10-point tetrahedron shown in figure 3-7.

### Constraints on the 10-point cluster

We carried out a ground-state search following the steps in the flowchart in figure 3-8. The 10-point tetrahedron was used as the maximal cluster to account for the frustration of the first four neighbor correlation functions in fcc. This cluster has 85 distinct subclusters and 90 symmetry-independent configurations. We solved the vertex enumeration problem in 85 dimensions with 90 constraints obtaining 323,188 vertices. These points in correlation-function space were then projected down to the five dimensions spanned by the point and first four neighbor pair correlation functions. To determine the structures that can be ground states with only these interactions one has to build the convex hull of this set of points. Due to the high degeneracy of the set of points (many points lie on faces of the convex hull), we could only find a lower bound of 1,288 for the number of vertices of the low-dimensional convex hull.

We tested the constructibility of these 1,288 vertices using the method described in appendix A and allowing for a maximum of 20 atoms in the primitive unit cell. We could construct only 27. The other 1,261 vertices are either not constructible or their primitive unit cells contain more than 20 atoms. Since the later alternative is not likely, this means that the 10-point tetrahedron is not big enough to account for all the frustration of the correlation functions considered.

### Constraints on larger clusters

One may consider selecting a larger cluster to account for frustration. To evaluate the feasibility of this approach, we compared the complexity of the problem including 3 interactions (point and two pair ECI's) in the tetrahedron-octahedron approximation and including 5 interactions (point and four pair ECI's), using several possible maximal clusters (shown in figure 3-7). Table 3.3 contains the results of this study.

The number of vertices in the ground-state polytopes can be estimated using several methods. The maximum possible number of vertices of a polytope defined by  $m$  constraints in  $n$  dimensions is given by [53]:

$$f(m, n) = \binom{m - \lfloor \frac{n+1}{2} \rfloor}{m - n} + \binom{m - \lfloor \frac{n+2}{2} \rfloor}{m - n}, \quad (3.7)$$

pair ECI's max. cl. (fig. 3-7)	1 <sup>st</sup> & 2 <sup>nd</sup> TO	1 <sup>st</sup> – 4 <sup>th</sup> 10–point	1 <sup>st</sup> – 4 <sup>th</sup> 13–point	1 <sup>st</sup> – 4 <sup>th</sup> 14–point	1 <sup>st</sup> – 4 <sup>th</sup> 13 & 14–pt.
$m$	15	90	288	554	842
$n$	10	85	280	544	742
$f(m, n)$	378	$3 \cdot 10^6$	$9 \cdot 10^{12}$	$1 \cdot 10^{18}$	$4 \cdot 10^{104}$
$g(m, n)$	94	$1 \cdot 10^6$	$4 \cdot 10^{12}$	$6 \cdot 10^{17}$	$6 \cdot 10^{101}$
Avis' estim.	N/A	$2 \cdot 10^6$	$2 \cdot 10^{12}$	N/A	N/A
Vertices highD	43	323, 188	unsolved	unsolved	unsolved
Vertices lowD	15	> 1, 288	unsolved	unsolved	unsolved
construc.	15	very few	unsolved	unsolved	unsolved
comp. time	10 sec	1 day	too long	...	...

Table 3.3: Size of the ground–state problem in the polytope method for different ranges of the interactions and clusters used to account for the frustration of the fcc lattice. The vertices in the high–dimensional space correspond to the polytope before being projected to the correlation space of the interactions in the truncated cluster expansion, while the vertices in the low–dimensional space are the possible ground states of the truncated Hamiltonian.

where  $\lfloor x \rfloor$  indicates that  $x$  is rounded down to the nearest integer. On the other hand, the expected number of vertices for a random polytope is a smaller number, given by [53]:

$$g(m, n) = \binom{m}{n} 2^{n-m}. \quad (3.8)$$

For large values of  $m$  and  $n$ , there is a very large variability in the number of vertices of a polytope. Therefore, the above two estimates of the number of vertices may not be very reliable to quantify the complexity of the problem. Furthermore, the constraints derived from the polytope method are not random. In fact, they present a high degree of degeneracy (a vertex of a polytope in  $n$  dimensions is degenerate when it is contained in more than  $n$  faces of the polytope). To produce a better estimate of the size of the ground–state problem, David Avis developed an unbiased procedure to estimate the number of vertices in a given vertex enumeration problem [71]. The results of all these estimations are shown in table 3.3.

It is clear from table 3.3, that the perspectives of solving the ground–state problem on the fcc lattice with first– through fourth–neighbor interactions by using larger clusters to account for the frustration effects are not very promising. The increase in complexity of the polytope method when larger clusters need to be considered makes the calculations prohibitively expensive.

One of the shortcomings of the polytope method is that there is no *a-priori* method to know what cluster is large enough to account for the frustration effects of a given interaction range. However, it is relatively easy to find *some* vertices of the low–dimensional convex hull, by solving linear programming problems [53]. We

performed these calculations and found that even using the constraints on the 13- and 14-point clusters, most of the low-dimensional vertices are inconstructible. Therefore, even if computers became several orders of magnitude faster and we solved the vertex enumeration problem for the 13- and 14-point clusters, we would not find the exact solution of the ground-state problem. This realization led us to the development of an alternative method to find ground-state structures (the *enumeration method*), described in section 3.3.

### 3.2.4 Application of the polytope method to fcc ternary alloys with first- and second-neighbor pair interactions

Whereas binary alloy systems have been studied extensively, both experimentally and theoretically, much less is known for three-component systems. No systematic compilation of ternary phase diagrams exists (although one has been started [72]) and only a few attempts have been made to compute ternary phase diagrams with first-principles models [73, 74, 75, 76].

In this section, we apply the polytope method to find the possible ground-state structures of a ternary lattice model on the fcc lattice with only nearest- and next-nearest-neighbor pair interactions. In the binary case, only 9 distinct ground-state structures are possible with this interaction range [41, 63, 65, 67]. This number increases dramatically when extending the interaction range to the fourth neighbor distance [11, 3], as shown in sections 3.2.3 and 3.3.2. A recent study on the ground states in a ternary *bcc* lattice model indicated that only a few real ternary structures could be stabilized with nearest- and next-nearest-neighbor pair interactions [66]. Whether this is also the case for fcc ternary alloys is not known.

To solve this ternary ground-state problem, we will apply the polytope method (see section 3.2), but first we need to generalize the concepts developed so far to ternary systems.

#### Ternary cluster expansion

In section 2.1, we have shown that the configuration-dependent properties of a *binary* alloy can be conveniently described by a cluster expansion. The occupation of a site of the lattice is represented by a spin variable,  $\sigma_i$ , that takes on the value +1 (-1) when site  $i$  is occupied by an  $A$  ( $B$ ) atom. To describe ordering in a *ternary* system a three-state occupation variable is needed. The obvious choice is a “spin 1” model, although more symmetric state variables in the complex plane can be used as well [45]. In the following we will adopt the simple three state spin model and represent  $A$ ,  $B$ , or  $C$  occupation of a lattice site by the spin value +1, 0, and -1.

Similarly to what is used in computations on binary systems, we can expand the energy of a ternary systems in a complete basis of cluster functions. Sanchez [34] suggested to use orthogonal Chebyshev polynomials in  $\sigma_i$  and  $\sigma_i^2$ . The orthogonality of the basis functions leads to a simple, but powerful, definition of the ECI's: They are the projection of  $E(\vec{\sigma})$  onto cluster function  $\sigma_\alpha$ . This definition has been judiciously followed in one of the methods to compute these effective interactions

from first principles [40, 39] and its feasibility for ternary systems has recently been demonstrated as well [76]. In this ground-state study, we will however, choose a set of basis functions suggested by Inden [77], and in a limited form by Taggart [78], as this basis is more apt for ground state models. In the  $S$  basis, as we will refer to it, the cluster functions are simple products of  $\sigma_i$  and  $\sigma_j^2$ . Consider two clusters  $\beta$  and  $\gamma$  on the lattice, with  $\gamma$  completely in  $\beta$ . The ternary cluster function  $\Phi_{\beta,\gamma}$  is defined as:

$$\Phi_{\beta,\gamma} \equiv \prod_{i \in \beta} \sigma_i \prod_{j \in \gamma} \sigma_j = \prod_{i \in \beta - \gamma} \sigma_i \prod_{j \in \gamma} \sigma_j^2. \quad (3.9)$$

The set of all cluster functions for all combinations  $(\beta, \gamma)$  forms a complete set in the space of all configurations. Although this basis is not orthonormal, it is desirable for ground-state work as the values of the cluster functions are always integer in the  $S$  basis.

In its most general form, the Hamiltonian (or energy) of the ternary system can be expanded in the  $S$  basis as:

$$E(\vec{\sigma}) = \sum_{\beta} \sum_{\gamma \subseteq \beta} V_{\beta,\gamma} \Phi_{\beta,\gamma}. \quad (3.10)$$

Limiting the interaction range to nearest-neighbor (NN) and next-nearest-neighbor (NNN) pairs, the last equation can be written explicitly:

$$\begin{aligned} E(\vec{\sigma}) = & V_0 + \sum_i H^\sigma \sigma_i + \sum_i H^{\sigma^2} \sigma_i^2 + \\ & \sum_{i,j}^{\text{NN}} V_1^{\sigma\sigma} \sigma_i \sigma_j + \sum_{i,j}^{\text{NN}} V_1^{\sigma\sigma^2} (\sigma_i \sigma_j^2 + \sigma_i^2 \sigma_j) + \sum_{i,j}^{\text{NN}} V_1^{\sigma^2\sigma^2} \sigma_i^2 \sigma_j^2 + \\ & \sum_{i,j}^{\text{NNN}} V_2^{\sigma\sigma} \sigma_i \sigma_j + \sum_{i,j}^{\text{NNN}} V_2^{\sigma\sigma^2} (\sigma_i \sigma_j^2 + \sigma_i^2 \sigma_j) + \sum_{i,j}^{\text{NNN}} V_2^{\sigma^2\sigma^2} \sigma_i^2 \sigma_j^2. \end{aligned} \quad (3.11)$$

Equation 3.11 is the most general Hamiltonian for a three state spin model with NN and NNN interactions. In a more restricted form it is known as the Blume-Emery-Griffith model used for the study of superfluidity in helium, liquid crystal mixtures and electronic conduction models [79]. As the effective interactions have the symmetry of the underlying lattice, equation 3.10 can be averaged over the whole lattice to get the energy per lattice site:

$$\frac{E(\vec{\sigma})}{N} = \sum'_{\beta} \sum'_{\gamma \subseteq \beta} m_{\beta,\gamma} V_{\beta,\gamma} \langle \Phi_{\beta,\gamma} \rangle. \quad (3.12)$$

The primed sum indicates that one only sums over the types of clusters that are distinct, considering the symmetry of the lattice. The coefficient  $m_{\beta,\gamma}$  represents the number of clusters equivalent to  $(\beta, \gamma)$  per lattice site and the correlation function,  $\langle \Phi_{\beta,\gamma} \rangle$ , is the average value of the cluster functions defined on all those clusters.

## Application of the polytope method

As described in section 3.1, to find the ground states of our ternary system, equation 3.12 has to be minimized with respect to the values of the correlation functions. These correlation functions are linearly constrained to represent states of ordering that are physically realizable.

To find the constraints on the correlation functions, the probability  $P_\alpha(J)$ , for configuration  $J$  to occur on the maximal cluster  $\alpha$  can be expanded linearly in the correlation functions defined on the clusters that are completely contained in  $\alpha$ :

$$P_\alpha(J) = \sum'_{\beta \subset \alpha} \sum'_{\gamma \subset \beta} Z_{\beta,\gamma}(J) \langle \Phi_{\beta,\gamma} \rangle. \quad (3.13)$$

Only correlation functions on clusters contained in  $\alpha$  appear in the expansion, and  $Z_{\beta,\gamma}(J)$  is the “v-matrix.”<sup>8</sup> Requiring that  $P_\alpha(J)$  be positive gives the desired inequality constraints between the correlation functions. All probabilities sum to 1 by construction. On the tetrahedron, 14 symmetry-distinct correlation functions and 15 atom configurations can be defined. For the octahedron there are 55 correlation functions and 56 distinct configurations. Combined, the two clusters define a polytope bounded by 71 distinct hyperplanes in a 60-dimensional space. The vertices of this polytope are the possible ground states that can be stable with all interactions that can be defined in the tetrahedron and octahedron clusters. To find the constraints between only the correlation functions that appear in equation 3.11, all other correlation functions need to be eliminated from the 71 constraints. This can be done by projecting the vertices of the polytope in the 60-dimensional space down to the 8-dimensional space spanned by the correlation functions of interest and determining the convex hull of all the projected points (see flowchart in figure 3-8).

Although the above is the correct procedure, we decided to introduce an approximation to make the problem more easily solvable. We determined the projections of the polytopes derived from the constraints on the tetrahedron and octahedron onto the 8-dimensional space separately and then computed the intersection of these two polytopes. For the binary ground-state enumeration this gives the exact result. Compare, for example, the results of Ducastelle and Finel [41, 65] (in which the polytopes generated by the tetrahedron and octahedron clusters are intersected in the low-dimensional space) with those obtained by Sanchez and de Fontaine [67] (in which the intersection is done in the high-dimensional space). This approximation is further discussed in page 83. The vertices of the intersected polytope are the ground states we are interested in. The 8-dimensional projections of the tetrahedron and octahedron polytopes were characterized respectively by 36 and 699 faces. Six of the faces of the tetrahedral polytope also appear in the projection of the octahedral polytope so that the intersected polytope is defined by 729 hyperplanes. The vertices of this polytope are the possible ground states of the ternary NN-NNN fcc lattice model.

Enumerating the vertices of a polytope for which the bounding hyperplanes are

---

<sup>8</sup>The derivation of the ternary v-matrix coefficients can be found in the appendix of reference [70].

given is a well known problem in combinatorial geometry [62] that has received much attention for its applications in operations research. Most methods developed, however, are not practical to enumerate vertices of ground-state polytopes as these are usually characterized by a high degeneracy.

To enumerate the vertices of our ternary ground-state polytope, both the double description algorithm and the reverse search algorithm were used. The **double description** method [80] is an incremental algorithm that computes all vertices of a polytope by sequentially adding each hyperplane to the polytope computed in the previous step. Although this method must store all vertices of the intermediate polytopes, it can deal with degeneracy quite well. The **reverse search** method [81], on the other hand, only requires storage space for the input data, making it very useful for large problems. The main idea of this method is to reverse the simplex algorithm for linear programming [53]. Its drawback is that many duplicates of the same vertex can be generated when degeneracy is present. While both methods successfully generated all the vertices of the polytope, the double description method seems to be more appropriate for these computations because of the high degeneracy and moderate size of the inequality system. For larger systems, however, the reverse search method may become the only feasible algorithm for vertex enumeration.

## Results

The ground-state polytope we found is highly degenerate and consists of 4,862 vertices in the 8-dimensional space spanned by the correlation functions. Some of the vertices found correspond to structures that can be transformed into each other by permutations of the A, B and C species. If these are considered to be the same structure, the total number of distinct structures is 980. Nine of these have only two types of atoms and correspond to the ground-state structures of the binary problem.

To test the constructibility of the 971 vertices with ternary composition, we used the method described in appendix A. The only assumption made is that the primitive unit cell of the structure has less than a specified number of atoms. The method explores all the possible unit cells up to the maximal size. Setting the maximum size to 32 atoms, only 31 of the distinct vertices could be constructed. The size distribution of the unit cells of the constructible structures is shown in figure 3-9, while two-dimensional projections of the unit cells of these structures are drawn in figure 3-10.

## Discussion

We found that only very few vertices of the ground-state polytope corresponded to constructible structures. There are two possible reasons for this: either the vertices are truly inconstructible or their primitive unit cells have more than 32 atoms. Given the fact that no structures were found with more than 16 atoms in the primitive unit cell, and only one structure with more than 8 atoms, it is unlikely that many of the 940 vertices that we could not construct correspond to real structures with unit cells larger than 32 atoms. We will therefore consider all 940 vertices as inconstructible



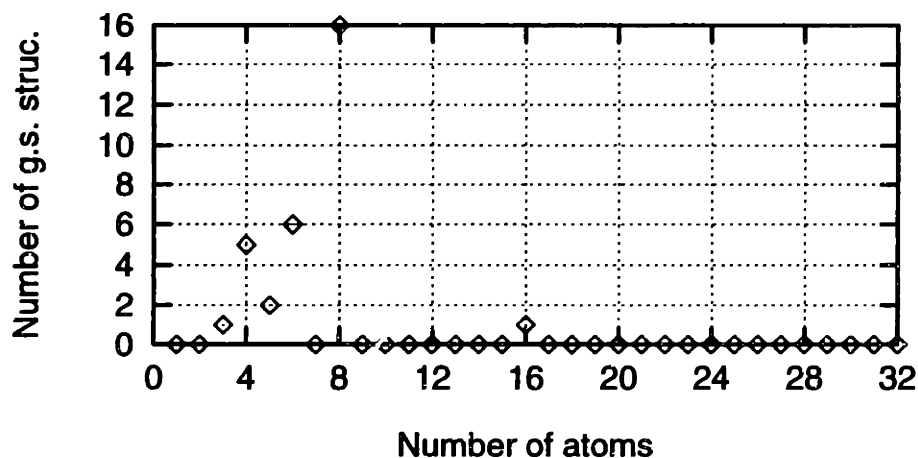


Figure 3-9: Size distribution of the ternary ground-state structures found with the polytope method and constructed using the method of appendix A.

Structure	Prototype	Space Group	Pearson Symbol	Atoms in unit cell
4a	$\text{Cu}_2\text{NiZn}$	$P4/mmm$	tP4	4
4b	$\text{CdPt}_2\text{Zn}$	$P4/mmm$	tP4	4
4c	$\text{Rh}_2\text{SnCo}$	$P4_2/ncm$	tP16	4

Table 3.4: Experimental prototypes have been found for three of the structures shown in figure 3-10.

even though we have not proved this. The vertices that can be constructed are true ground states of the NN and NNN Hamiltonian since they can never be removed by constraints derived from considering larger clusters. For some of the structures with small unit cells we have found experimental evidence in real ternary systems. Structure 4a, which is the only ternary ground state possible if the interactions are limited to the nearest-neighbor distance, has been observed in  $\text{Cu}_2\text{NiZn}$  [82]. The structure is similar to the binary  $L1_0$ , but with the minority atoms ordered in one of the (001) planes. A different secondary ordering occurs in structure 4c which corresponds to the  $\text{CdPt}_2\text{Zn}$  phase. In this structure, Cd and Zn segregate each to their own (001) plane, alternating with pure Pt (001) planes. Structure 4b is the  $\text{Rh}_2\text{SnX}$  phase, where X can be Co, Cr, Fe, or V. This ordered phase can be considered as the antiphased variant of the  $\text{Cu}_2\text{NiZn}$  structure. Table 3.4 lists, the space group, number of atoms in the unit cell, and prototype for these three structures.

The search for prototypes corresponding to our ground states is hampered by the lack of detailed experimental information. For many ternary compounds the occupation of each site has not been determined unambiguously so that they can not be compared with the pictures in figure 3-10. However, most often there is

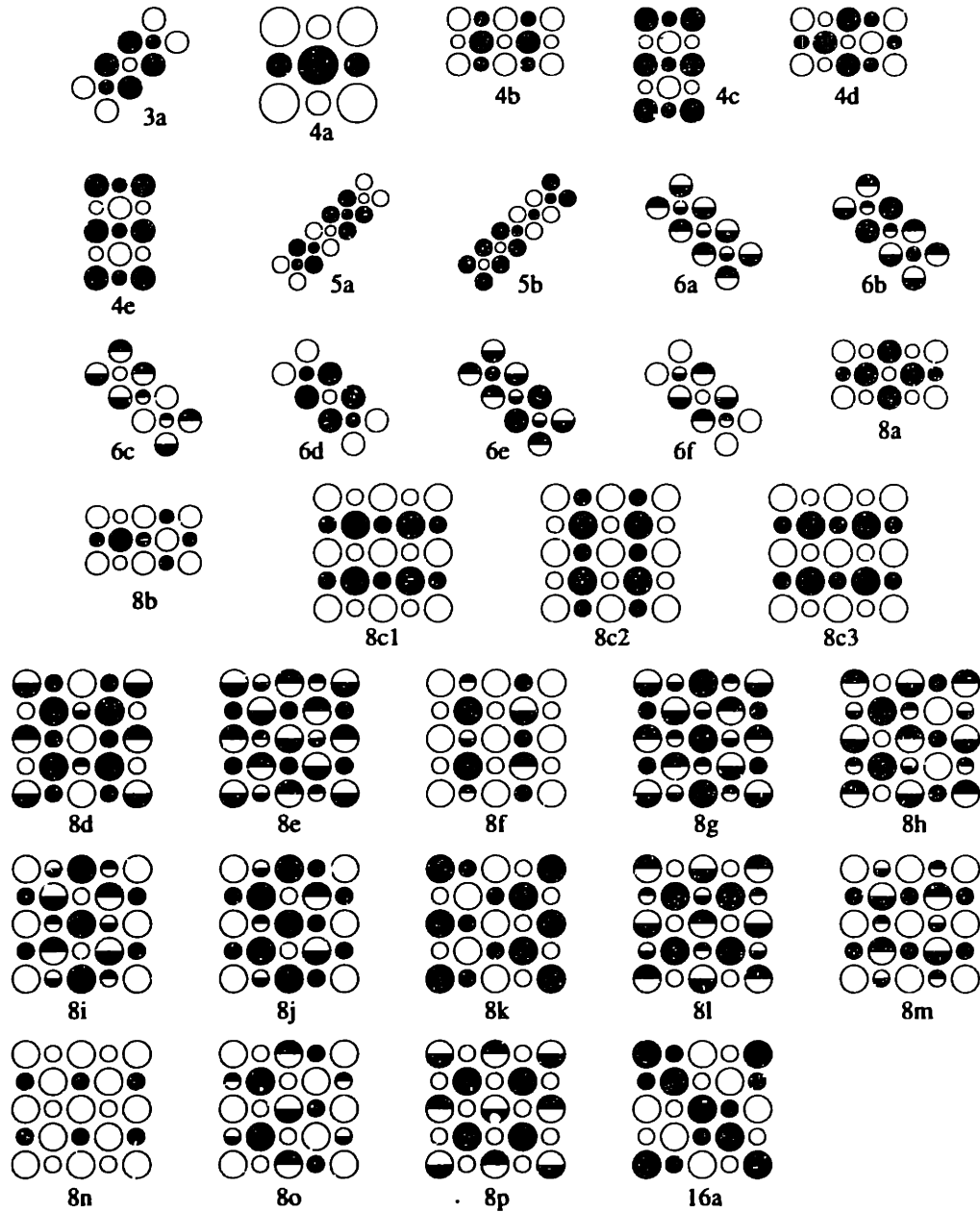


Figure 3-10:  $\{001\}$  projections of the ternary ground-state superstructures of fcc with first- and second-neighbor interactions. White, grey and black circles correspond to A, B and C atoms respectively. Large circles are in  $\{00n\}$  planes, and small ones in  $\{00n + 1/2\}$  planes. Half-shaded circles correspond to atoms alternating in the  $[001]$  direction, while circles with a shaded quadrant correspond to particles occupying every fourth site in the  $[001]$  direction. Rotations of the shaded parts indicate different  $\{00z\}$  planes. The structures are labelled with the number of atoms in their primitive unit cells and letters to distinguish between structures with the same number of atoms. Structures 8c1, 8c2 and 8c3 correspond to the same vertex in the configurational polytope and have the same energy for the range of interactions used.

simply no experimental data available for a ternary system. Since the interaction range we considered here is not at all exceptional (most systems have significant effective interaction up to at least the second neighbor distance), many of the ground states in figure 3-10 should be found in real ternary systems. Maybe this ground-state enumeration can assist experimentalists in their determination of the structure ternary fcc compounds.

In contrast to the success of the tetrahedron–octahedron ground–state analysis for the binary alloys, the ternary analysis produces a large number of inconstructible vertices, indicating that frustration effects on clusters beyond the tetrahedron and octahedron need to be accounted for. The applicability of the polytope method rests on the presumption that frustration effects can be sampled in the local environment around a lattice point. If this is not so, large clusters have to be used to formulate the correct constraints and the method quickly becomes infeasible. In section 3.2.3, we have already found this to be the case for the binary ground–state problem as soon as one tries to go beyond the second neighbor interaction distance [11]. Considering that the problem presented here already tested the limits of vertex–enumeration methods, it seems unlikely that the polytope method, in the form used here, will be tractable to solve the second neighbor ternary ground–state problem exactly. Of course, many first–principles computations of the ECI's have indicated that, in binary systems, interactions are typically significant up to the fourth neighbor distance, and there is no reason to believe that this will be any different in a ternary expansion. Alternative methods, like the *enumeration method*, described in section 3.3, might be the only practical alternative to obtain information on the possible ground states of a lattice model.

### **When to project to the low–dimensional space?**

As discussed above (page 79), when the constraints on the averaged cluster functions are generated with more than one maximal cluster, there are two ways of combining these constraints to generate the configurational polytope in the low–dimensional space spanned by the cluster functions retained in the cluster expansion.

The first procedure is to enumerate the vertices of the polytopes generated by the different clusters in their respective high–dimensional space. Once these vertices are known, they are projected down to the low–dimensional space. After building the convex hulls of these sets of points, a set of constraints in the low–dimensional space is found for each cluster (the constraints are the faces of the convex hull). When all these constraints are combined, a new vertex enumeration problem is solved to obtain the vertices of the configurational polytope in the low–dimensional space. In this first procedure, the intersection of the constraints of the different maximal clusters is done in the low–dimensional space.

The second procedure is to generate the polytopes in the high–dimensional space, extend them to the space union of the spaces of all the maximal clusters, and perform the intersection of the polytopes in this high–dimensional space. After all the vertices have been found, they are projected down to the low–dimensional space. The convex hull of this set of points is the configurational polytope of our problem.

It can be easily proved that, in general, the first procedure results in a configurational polytope that is less restrictive than the one obtained with the second procedure. Therefore, the second procedure is a better approximation of the exact configurational polytope than the first. However, as mentioned above, for *binary* fcc alloys with nearest- and next-nearest-neighbor ECI's both procedures result in the same low-dimensional configurational polytope [41, 65, 67]. To decide whether the same is true for ternary alloys, we solved the vertex enumeration problem for *ternary* alloys using the second procedure, to compare the results with the ones obtained with the first procedure (described above in this section).

The full vertex enumeration problem, with the tetrahedron and octahedron as maximal clusters, has 71 constraints in 60 variables in the high-dimensional space. The solution of this vertex-enumeration problem consists of 3,149,579 vertices.<sup>9</sup> To compare the results with the previous solution, we projected these vertices down to the 8 dimensions corresponding to the averaged cluster functions on the point cluster and nearest- and next-nearest-neighbor pair clusters.

Of the 980 distinct structures of the solution obtained using the first procedure, only 154 are in the new solution. The other 826 vertices have been cut off by the tighter constraints of this better approximation. Of course, the 31 ternary and 9 binary vertices for which a structure could be constructed, are not removed by the new constraints. (These structures are *exact* ground-states.)

Contrary to what occurs for the binary problem, the two possible procedures described above to generate the configurational polytope from the constraints on more than one maximal cluster do not produce the same solution for the ternary problem. Since there are, at least, 114 inconstructible vertices in the new solution,<sup>10</sup> the second procedure does not result in the exact solution of the problem either, and constraints on larger clusters would be necessary.

## 3.3 The enumeration method

### 3.3.1 The method

The enumeration method exploits the fact that the configurational polytope is convex (see section 3.1.2) and is based on the assumption that the ground-state configurations  $\vec{\sigma}$  have small unit cells. The main idea is to systematically enumerate *all* the possible configurations with small unit cells and then build the convex hull of their

---

<sup>9</sup>This solution was obtained by Ambros Marzetta, Komei Fukuda, and collaborators [83] at the Swiss Federal Institute of Technology, in Zurich, Switzerland. They used a parallel version of the reverse-search vertex-enumeration code developed by David Avis, at McGill University, in Montreal, Canada [81]. The code ran for 4.5 days on a NEC parallel computer with 64 processors. This would correspond to approximately 130 days of CPU time on a regular workstation. These statistics correspond to February 1996. Since the results are very recent, we only present here *preliminary* analysis of the data.

<sup>10</sup>These 114 inconstructible vertices correspond to the 154 vertices present in both solutions, minus the 40 constructible structures found in the solution using the first procedure (31 ternary and 9 binary structures).

correlation functions, to approximate the exact configurational polytope, and avoid the inconstructibility problem in the polytope method. The enumeration method consists of 3 steps:

1. Let  $N$  be the number of atoms in the primitive unit cell of a periodic configuration on the lattice. Enumerate all possible primitive unit cells with, at most,  $N_{max}$  atoms. Two unit cells are considered to be different when the lattices they define are not mapped into each other by any of the symmetry elements of the full space group of the parent lattice (fcc in our case).
2. Find all the distinct configurations  $\vec{\sigma}$  of A and B atoms in the lattice, for each of the unit cells in step 1. In general, there are  $2^N$  configurations in a unit cell with  $N$  atoms. Some of them will actually be the same configuration. To determine when two configurations are distinct, we use the following procedure. First, decide the set of effective cluster interactions to use in the energy expansion. For all the possible configurations each unit cell, compute the correlation functions on these clusters. Since we are keeping only a few terms in the energy expansion, the correlation functions we compute do not uniquely define the configuration. If a set of correlation functions occurs more than once, keep only the one corresponding to the configurations with smallest unit cell.<sup>11</sup> For a given set of ECI's, the correlation functions computed determine all the possible values for the energy within the assumption of maximum size of the unit cell made in step 1.
3. To obtain the ground-state configurations, find the convex hull of all the points in the space of correlation functions. The vertices of this convex hull correspond to the configurations that can be ground states; while the normals of the faces of the convex hull adjacent to a given vertex define the cone in interaction space that makes that configuration the ground state of the system. Configurations which lie inside the convex hull can not be ground states with any value of the set of interactions selected to expand the energy of the alloy, while configurations on the faces are ground states only with a range of interactions of zero volume, and therefore not likely to be found in real systems (except for those on 1-D faces, i.e., edges, that are always degenerate with a phase mixture of the two phases defining the edge).

The assumption of maximum size of the unit cell of the ground-state configurations is based on the fact that most known solutions to ground-state problems contain only configurations with "small" unit cells. For example, figure 3-12 shows the number of configurations with a given number of atoms in the unit cell for the ground states obtained by Kanamori and Kakehashi [3]. In their ground-state study,

---

<sup>11</sup>It could (and in fact does) happen that two different configurations with the same volume have the same set of correlation functions. In this case we only keep one set of correlation functions to compute the ground states, but keep in mind that these two configurations will be degenerated within the approximation used.

only two configurations have more than 16 atoms in the unit cell. The enumeration method is based on the assumption that for a given interaction range, the size of the configurations that can be ground states is not larger than a maximum value. This is a plausible assumption in fcc for interactions up to the fourth neighbor distance. A schematic representation of the approximate solution to the ground-state problem with the enumeration method is shown in figure 3-11.

A more limited version of this approach was applied in reference [84]. This study only deals with the ground-state configurations for a given set of interactions (and not the general ground-state problem) and only included about 32,000 configurations (up to 15 atoms in the unit cell).

### **3.3.2 Application of the enumeration method to fcc binary alloys with first- through fourth-neighbor pair interactions**

We used the enumeration method to search for the ground states in fcc with first to fourth neighbor ECI's. Some results are shown in figures 3-13 and 3-14.

We enumerated all the unit cells (step 1) with up to 20 atoms in the unit cell (see figure 3-13-a). As expected, this number increases with increasing size, showing peaks for number of atoms with many integer factors and valleys for prime number of atoms.

We computed the point and the 4 pair correlation functions for all the configurations with up to 20 atoms in the unit cell. The results are shown in figure 3-13-b.

To build the convex hull (step 3) we took all the enumerated configurations except for those with 17 and 19 atoms in the unit cell that were left out because of constraints in the computer memory available. The convex hull of the resulting set of 398,823 points consists of 900 points corresponding to 468 distinct configurations with a size distribution shown in figure 3-13-c. Although the number of ground-state configurations is still increasing with volume, this increase is much slower than the increase in the total number of configurations (figure 3-13-d) supporting (but not proving) the assumption of a finite maximum volume for the ground-state configurations.

Our results are not exact because there may be ground-state configurations with more than 20 atoms in the unit cell. Including larger configurations in the analysis could remove some of the 468 configurations. Our set of possible ground-state configurations contains all the configurations reported by Kanamori and Kakehashi [3], except for the two configurations with more than 20 atoms in the unit cell (see figure 3-12). Comparing our results with the 39 configurations found by Kanamori and Kakehashi, we see that although their assumption of minimum nearest-neighbor correlation function seems to have some physical basis, it leaves out many configurations.

Among the 468 configurations found, 60 have 8 or less atoms in the primitive unit cell. Of these simple configurations, 22 coincide with configurations found by Kanamori and Kakehashi [3]. Two dimensional projections of the new 38 configurations with less than 8 atoms in the unit cell are shown in figure 3-14. They include the CuPt type and other configurations likely to be found in nature.

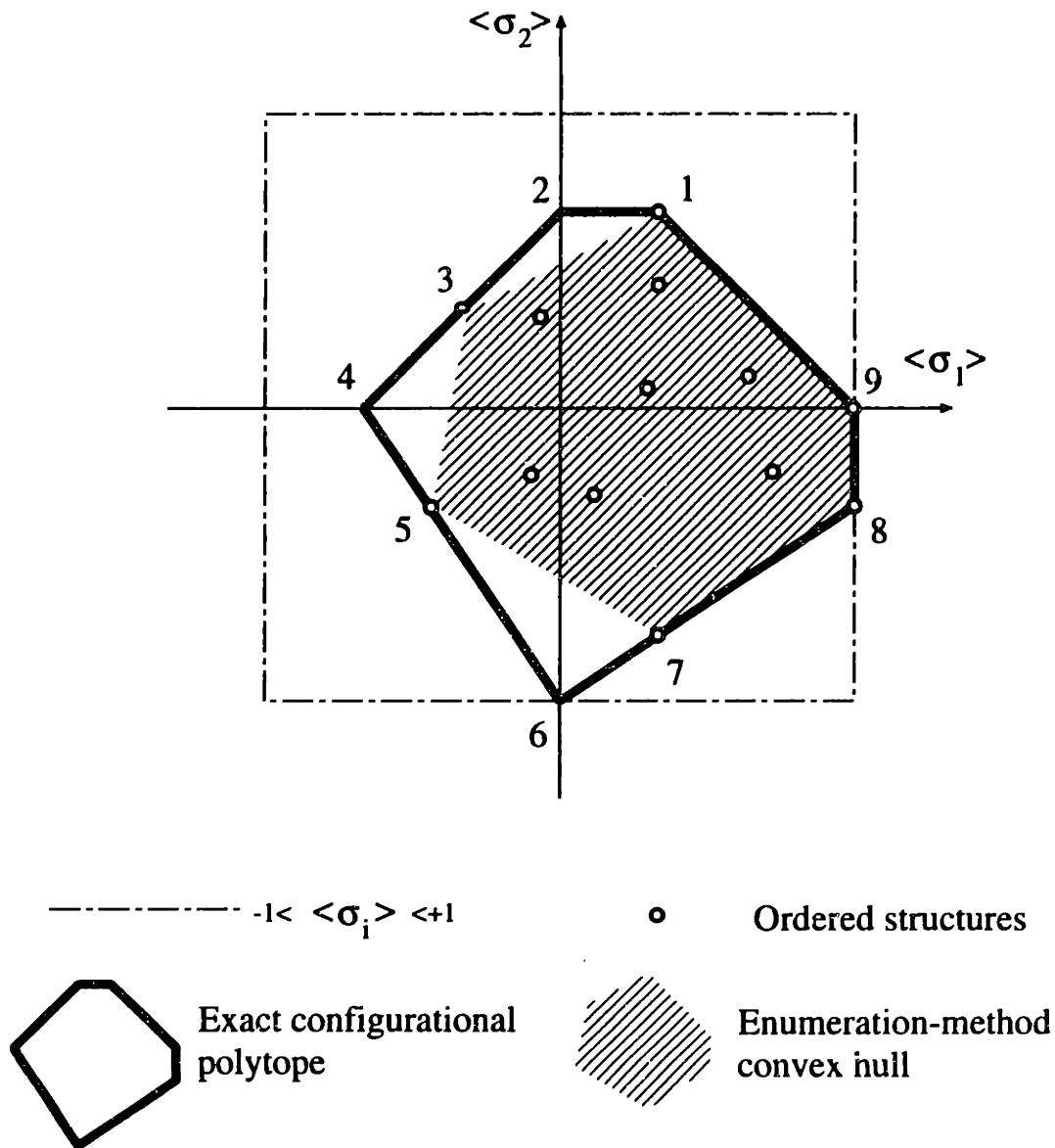


Figure 3-11: Schematic representation of the enumeration method for the determination of the possible ground states of a lattice model. Every point inside the exact configurational polytope corresponds to one or more configurations on the lattice (constructible points), while there is no configuration with correlation functions outside the exact configurational polytope (inconstructible points). The polytope of the enumeration method is the convex hull of the set of points in correlation-function space correspondent to ordered configurations with small unit cells. Since by construction all the vertices of the enumeration-method polytope correspond to constructible configurations, the exact solution is approached from inside in the enumeration method. Vertices 2, 4, and 6 in this example correspond to unit cells with more than  $N_{max}$  atoms and therefore are not obtained with the enumeration method. Compare this figure with the schematic representation of the polytope method in figure 3-5.

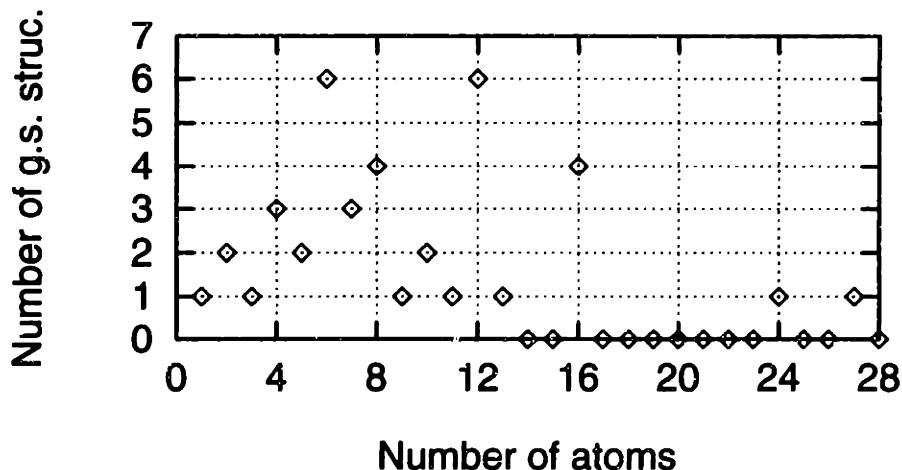


Figure 3-12: Size distribution of the ground-state configurations found by Kanamori and Kakehashi in reference [3].

The enumeration method proved to be more powerful than the polytope method to approach problems with high frustration. The correlation functions are computed from actual configurations and therefore the constructibility problem is avoided.

The results we have obtained, allowed us to show that the assumption of dominant nearest-neighbor interaction is very restrictive. The number of ground-state configurations increases by an order of magnitude when this restriction is released and all possible values of the ECI's are allowed.

### 3.4 Conclusions

The solution of the ground-state problem in substitutional alloys is a very important part of the calculation of the thermodynamical properties and phase diagram of these systems. Very well developed methods have been used to solve the ground-state problem in the past, for models that included very few interaction parameters. Now that more realistic studies of alloy systems have become possible (due to the increase in computational power), longer interaction ranges are used. We have shown in this chapter that the complexity of the *polytope method* to find ground-state configurations increases with the interaction range in such a way that the problem becomes unsolvable when more than second-neighbor interactions are included in the alloy Hamiltonian. The increase in complexity is such that, even with computers orders-of-magnitude faster than the computers available today, we will not be able to use the traditional methods to solve the ground-state problem.

In spite of this observation, we were able to obtain *approximate* solutions of two ground-state problems on the fcc lattice: binary alloys with first- through fourth-neighbor pair interactions and ternary alloys with first- and second-neighbor pair interactions. Although the solutions are approximate, and most configurations are “in-



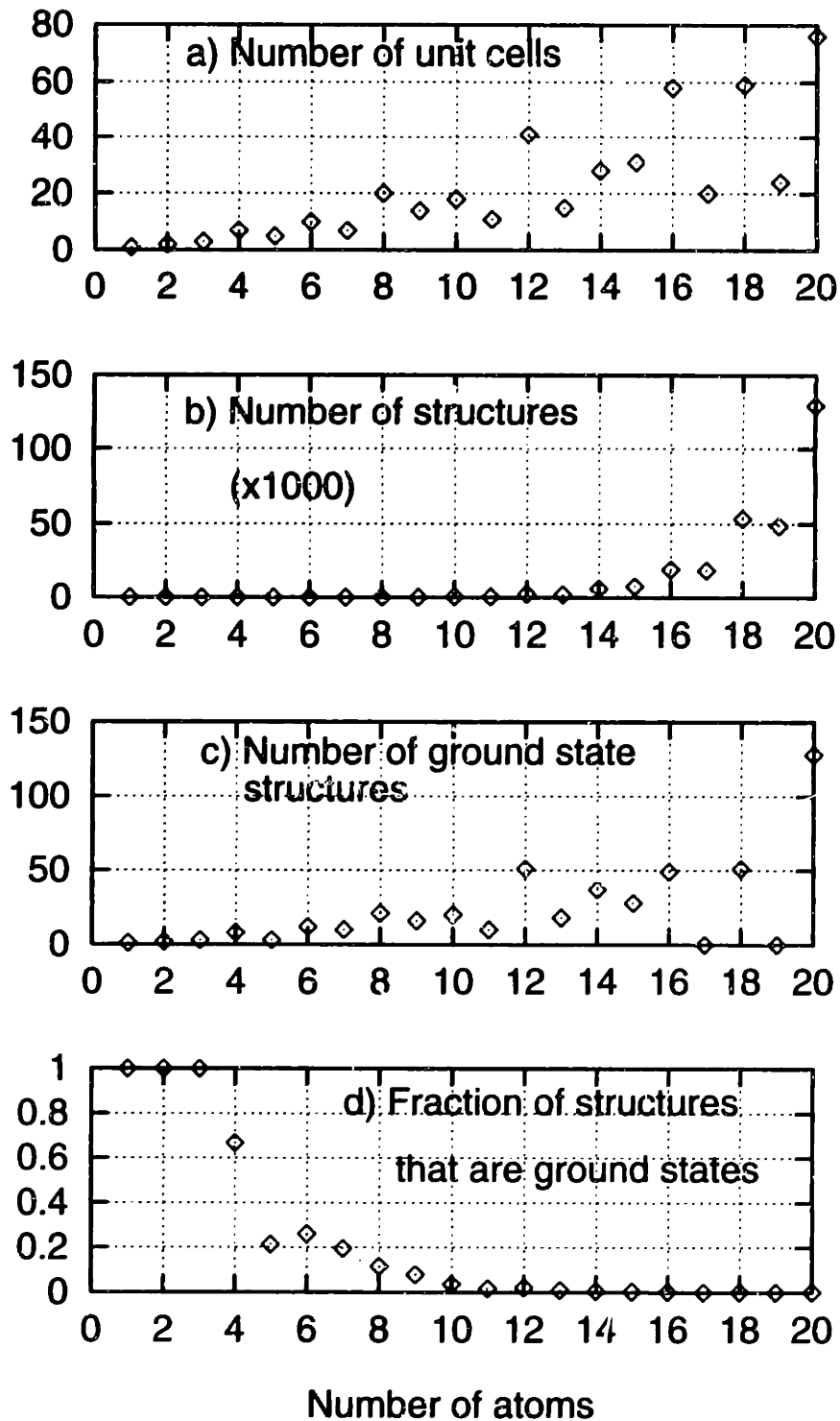


Figure 3-13: Results of the enumeration method applied to the fcc lattice with four pair interactions.

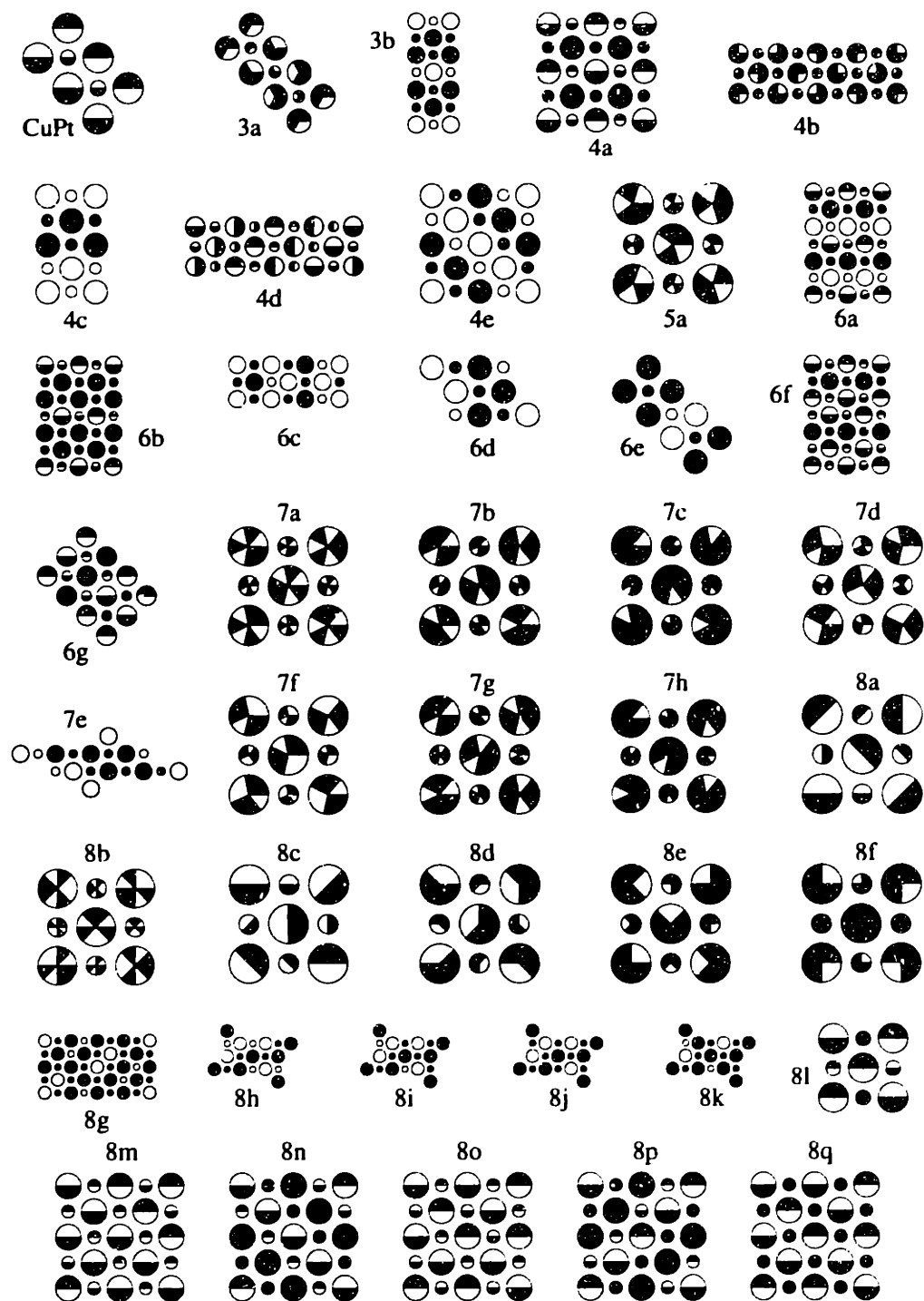


Figure 3-14: Projections on the (001) plane of the new ground-state configurations with up to 8 atoms per unit cell. Each configuration is labeled according to the number of atoms in its primitive unit cell. Refer to the conventions in figure 3-10.

constructible,” several configurations could be identified as solutions of the ground-state problem. To be able to solve these problems, we had to use state-of-the-art vertex-enumeration techniques. To our knowledge, these polytope-method solutions of ground-state problems are the largest obtained so far.

For the ternary problem we found 31 ordered structures. For four of these structures we found prototypes in nature. Some of the other structures are very simple and likely to be found in nature. The total number of vertices we found ( $> 1,288$  for the binary and 4,862 for the ternary problems) is much larger than any previous ground-state study. These results are therefore quite unexpected.

To overcome the limitation of the polytope method when long-range interactions are necessary to model the alloy system, we developed a new method, that we call *enumeration method*, that solves the ground-state problem *approximately* for *any interaction range*. The method avoids the inconstructibility problem by generating actual configurations of atoms and building the convex hull of the resulting points in correlation-function space to approximate the configurational polytope. We applied the enumeration method to the binary ground-state problem on the fcc lattice with first- through fourth-neighbor pair interactions. We found an order-of-magnitude increase in the number of possible ground-state configurations with respect to previous approximate solutions.

Although the solutions of the ground-state problems found in this thesis are approximate, the new possible ground-state configurations will assist both the theorist and the experimentalist. As shown in chapter 1, the knowledge of the ground-state configurations is an important step for the theoretical models of phase stability in alloy systems. As new models for binary alloys with more than first- and second-neighbor pair interactions are developed, and the studies of ternary alloys become computationally feasible, the ground-state results we found will become very useful. On the other hand, the experimental characterization of ordered configurations in multicomponent alloys is a difficult task that can benefit from the “menu” of configurations that can be stabilized with a simple set of interactions.

### 3.5 Future perspectives

There are still some possibilities to be explored to make the polytope method useful for alloys with long-range interactions. As we presented the method in this thesis, the constraints on the correlation-functions are formulated in a high-dimensional space. Once the vertices of this high-dimensional polytope are found, they are projected down to the low-dimensional space of the correlation functions (for which the ECI's are non-zero in the cluster expansion). The convex hull of the the resulting set of points constitutes the solution of the ground-state problem. One of the reasons for the dramatic increase in complexity in the polytope method is the fact that the constraints are formulated in the high-dimensional space, requiring the solution of very large vertex-enumeration problems. The polytope method could be improved by finding a systematic procedure to obtain the low-dimensional constraints directly, avoiding the enumeration of the vertices in the high-dimensional space. Some of the

alternative methods [63, 64], achieve this goal at the expense of leaving some of the constraints out, and therefore not finding the exact solutions of the ground-state problem.

Another possibility to avoid the construction of the full polytope in the high-dimensional space would be to only generate the constraints that are violated by a polytope in the low-dimensional space. Preliminary developments of this idea are very promising [61].

Finally, it is an open question whether the configurational polytopes of the problems we attacked have a finite number of vertices or present an infinity of ground-state configurations (as in the two-dimensional honeycomb lattice with first- and second-neighbor pair interactions). If the latter is true, the polytope method is bound to fail because regardless of the maximal cluster used to account for the frustration effects, the number of constraints is always finite. Completely new approaches would be necessary in this case.

# Chapter 4

## Lattice vibrations and phase stability: Formalism and trends

The lattice models described in chapters 2 and 3 naturally account for the substitutional excitations in alloys. For example, the change in energy when the occupation of a site of the alloy changes is easily computed with the generalized Ising Hamiltonian or cluster expansion of the energy. However, the exact partition function of the alloy contains other excitation modes, such as lattice vibrations or electronic excitations, that do not seem to fit in the framework of the lattice model. In fact, for a long time it was believed that the lattice model could not account for these other excitation modes or even relaxations of the atoms away from the ideal lattice sites (see, for example, reference [29]). In this chapter, we show that these effects *can* be taken into account in a lattice model, and that the inclusion of the vibrational degrees of freedom in the studies of phase stability can be important to obtain even qualitative agreement with experimental observations.

Under some assumptions, the *exact* quantum-mechanical Hamiltonian of a binary<sup>1</sup> alloy can be mapped onto the Hamiltonian of a lattice model. The description of these assumptions and the procedure to obtain the lattice Hamiltonian are described in section 4.1. We argue that, of all the non-substitutional excitations, the lattice vibrations may be the most important to understand phase stability in alloys. In section 4.2, a one-dimensional model alloy, for which analytical results are obtained, is used to illustrate the inclusion of the lattice vibrations in the cluster expansion of the alloy Hamiltonian. Finally, the size of the effect of the lattice vibrations on phase stability in alloys is studied in section 4.3. In the next two chapters, we apply the newly developed formalism to the study of systems modeled with classical potentials (chapter 5) and with first-principles techniques (chapter 6).

---

<sup>1</sup>In chapters 4, 5, and 6, we will develop and apply the formalism to include the lattice vibrations in the studies of phase stability of *binary* alloys. The extension to *multicomponent* alloys is conceptually straightforward.

## 4.1 Coarse-graining of the partition function

### 4.1.1 From the continuous to the lattice Hamiltonian

Consider the quantum-mechanical partition function of a binary alloy composed of  $N_A$  and  $N_B$  atoms of the  $A$  and  $B$  species respectively:<sup>2</sup>

$$Z(T) = \sum_j \exp(-\beta E_j), \quad (4.1)$$

where the sum is over *all* the possible quantum-mechanical eigenstates  $j$  of the Hamiltonian of the system,  $E_j$  is the eigenenergy of state  $j$ ,  $T$  is the absolute temperature, and  $\beta = 1/k_B T$ , where  $k_B$  is the Boltzmann constant. The Hamiltonian of the alloy is an explicit function of the coordinates of all the nuclei and electrons in the system. Its eigenstates include microstates that can be associated with different states of matter: crystalline, amorphous, liquid, and gaseous phases. Therefore, it is difficult to envision how the partition function of equation 4.1 could be computed as the partition function of a lattice model. In fact, it *cannot* if one is interested in describing *all* the possible states of the system.

Since we are only interested in the solid phases of the alloy, we can approximate the partition function. At the temperatures for which the stable phases of the alloy are crystalline, the contribution to the partition function of non-crystalline microstates is negligible, and the sum in equation 4.1 can be restricted to crystalline states. The crystalline microstates of the alloy can, in turn, be grouped according to the “parent” lattice  $L$  on which the  $A$  and  $B$  species of the alloy order (e.g., fcc, bcc, hpc, etc.). We will further assume that every microstate of lattice  $L$  can be associated with a configuration  $\vec{\sigma}$  of the  $A$  and  $B$  atoms on that lattice. Under all these assumptions, the partition function can be computed as:

$$Z(T) = \sum_L \sum_{\vec{\sigma} \in L} \sum_{j \in \vec{\sigma}} \exp(-\beta E_j). \quad (4.2)$$

The first sum in equation 4.2 is over all the possible parent lattices  $L$  that compete for stability in the system of interest. If we are studying an alloy in which the stable phases can be thought of as the ordering of  $A$  and  $B$  atoms on just one lattice (e.g., Cu-Au system on the fcc lattice described in section 1.2), then the sum over lattices  $L$  reduces to one term (e.g., fcc). In more general alloy systems, such as Cu-Zn (also described in section 1.2), more terms will be necessary in the sum over parent lattices.<sup>3</sup> In this thesis, we are interested in substitutional alloys with only one stable parent lattice in all the composition range. Therefore, the sum over lattices  $L$  will

---

<sup>2</sup>The partition function of the alloy will be computed in the ensemble of constant temperature and pressure. Since we will not be dealing with transformations when the pressure is changed, we will assume  $P = 0$  to avoid the pressure-dependence in all the thermodynamic quantities.

<sup>3</sup>For first-principles calculations with no experimental input, there is no *a-priori* knowledge of the stable parent lattice or lattices. In this case the sum over lattices in equation 4.2 should include all the parent lattices likely to be stable.

not be included in the rest of the treatment. Our results, however, can be extended to alloys based on more than one parent lattice.

The second sum in equation 4.2 is over all possible arrangements  $\vec{\sigma}$  of the  $A$  and  $B$  atoms on the lattice  $L$ . These arrangements are the  $2^N$  possible states of a binary lattice model with  $N$  sites. Finally, the last sum in equation 4.2 includes all the eigenstates of the quantum-mechanical Hamiltonian of the alloy that are associated with (or mapped onto) the arrangement  $\vec{\sigma}$  on lattice  $L$ . These states include the state with the atoms at their ideal location on the lattice sites, but also small deviations away from the ideal sites, vibrational states around these sites, different electronic states for that location of the ions (the electronic ground state and excited states), magnetic excitations, etc. The only requirement is that the mapping microstate  $\rightarrow \vec{\sigma}$  be unique, i.e., a given microstate can only be associated with one substitutional state.

We define the “ $\vec{\sigma}$ -ensemble” as the set of microstates of the alloy that are mapped onto configuration  $\vec{\sigma}$ . Since the substitutional degrees of freedom evolve with much longer time scales than the degrees of freedom of the  $\vec{\sigma}$ -ensemble, we assume that an ergodic sampling of the the microstates of the  $\vec{\sigma}$ -ensemble is achieved before the system changes configuration  $\vec{\sigma}$ .<sup>4</sup> In appendix B, we perform a quantitative analysis of the limitations of this assumption studying a “toy” model system for which analytical results are obtained. This ergodicity allows us to define the free energy in the  $\vec{\sigma}$ -ensemble as:

$$F(\vec{\sigma}, T) = -\frac{1}{\beta} \ln \left\{ \sum_{j \in \vec{\sigma}} \exp(-\beta E_j) \right\}. \quad (4.3)$$

Combining this definition with equation 4.2, we can rewrite the partition function of the substitutional alloy as:

$$Z(T) = \sum_{\vec{\sigma}} \exp(-\beta F(\vec{\sigma}, T)). \quad (4.4)$$

Equation 4.4 is the partition function of a lattice model with lattice Hamiltonian  $F(\vec{\sigma}, T)$ . With the above assumptions, we have succeeded in recasting the complex partition function of equation 4.1 onto the simpler partition function of a lattice model (equation 4.4). Expression 4.4 is usually referred to as the “coarse-grained” partition function of the system. Only the substitutional degrees of freedom are *explicitly* represented in the lattice Hamiltonian. All the other degrees of freedom have been

---

<sup>4</sup>For example, the typical vibrational frequencies in solid materials are of the order of  $10^{13}$  Hz, which corresponds to vibrational periods of  $\sim 10^{-13}$  seconds. On the other hand, the changes of configuration  $\vec{\sigma}$  are related to atomic jumps (diffusion) and take place in time scales orders-of-magnitude longer (sometimes even reaching the millisecond time scales). However, there are some “pathological” systems, where this assumption is not valid. For example, some super-ionic conductors like Ag-I in which the Ag ions form an almost liquid-like state in the interstitial sites of the I lattice [85]. For this system, the time scale of changes in the Ag distribution in the interstitial sites is similar to the vibrational period. There are also some systems for which long-lived electronic excitations are possible [86]. For these systems, there is not a well defined free energy in the  $\vec{\sigma}$ -ensemble, and other treatments are necessary. See appendix B for more details.

“integrated out.”<sup>5</sup>

Besides the simplifying assumptions, the complexity of the original quantum-mechanical problem is *hidden* in the calculation of the free energy of the  $\vec{\sigma}$ -ensemble, i.e., the lattice Hamiltonian  $F(\vec{\sigma}, T)$ . Contrary to the usual lattice models, the lattice Hamiltonian of the alloy is temperature-dependent because it includes not only the energy of the configuration  $\vec{\sigma}$  on the lattice, but also the free energy that depends on all the excitations of the system that do not change the substitutional state  $\vec{\sigma}$  of the lattice model (i.e., the  $\vec{\sigma}$ -ensemble). We now discuss how this free energy can be approximated with some further assumptions.

### 4.1.2 The $\vec{\sigma}$ -ensemble free energy

The  $\vec{\sigma}$ -ensemble free energy can be explicitly written as:

$$F(\vec{\sigma}, T) = E_0(\vec{\sigma}) + F^{vib}(\vec{\sigma}, T) + F^{elec}(\vec{\sigma}, T) + F^{mag}(\vec{\sigma}, T) + \text{coupling terms}, \quad (4.5)$$

where  $E_0(\vec{\sigma})$  is the eigenstate with lowest energy, or ground state, of the  $\vec{\sigma}$ -ensemble, and the other contributions are the vibrational, electronic, and magnetic free energies of the  $\vec{\sigma}$ -ensemble, and coupling between the different excitation modes.

In the early studies of phase stability of substitutional alloys [29], the *free energy* of equation 4.5 was approximated by the *energy* of the system with the atoms at the ideal lattice sites. It was later realized that the atomic relaxations away from ideal lattice sites<sup>6</sup> could be accounted for by fitting effective cluster interactions to reproduce the energy of relaxed structures (see chapters 1 and 2). Including the atomic relaxations improved the agreement of the theory with the experimental observations. In our framework, we can interpret this improvement as a consequence of a better approximation of the  $\vec{\sigma}$ -ensemble free energy: when the relaxations are taken into account, one obtains the correct value of  $E_0(\vec{\sigma})$ . Our goal is to develop systematic ways of including non-zero temperature contributions to the  $\vec{\sigma}$ -ensemble free energy to further improve the models of alloy phase stability.

No criteria are known to predict in general which of the above contributions to the  $\vec{\sigma}$ -ensemble free energy is the most important to determine ordering tendencies in substitutional alloys. In this thesis, we have chosen to develop the formalism to include the lattice vibrations, based on the following observations:

- Coupling between different types of excitations is small at low enough temper-

---

<sup>5</sup>The idea of integrating out fast degrees of freedom is not new, but it has only recently been used to solve problems in materials science, such as calculations of ferroelectric phase transitions [87, 88, 89] and the calculation of the effects of lattice vibrations on alloy phase stability presented in this thesis.

<sup>6</sup>The relaxations to minimize the energy of an atomic configurations are usually classified in two groups: global and local relaxations. The global relaxations include the volume and shape of the unit cell, while the local relaxations include the relative positions of the atoms inside the unit cell. For studies at constant pressure (usually  $P = 0$ ), the volume of the configurations has to be relaxed to minimize the energy.



atures.

- If we consider non-magnetic insulator systems, the only term that contributes significantly is the lattice vibrations (for temperatures much lower than the electronic band-gap, the electronic excitations can be ignored). In other words, of all excitation modes in the  $\bar{\sigma}$ -ensemble free energy, the lattice vibrations are always present while the electronic and magnetic contributions can be neglected for some systems.
- The possibility of excited electronic states in *metallic* systems could play an important role in influencing phase stability. However, recent studies of the Cd-Mg system [31] with very crude approximations for the vibrational and electronic excitations indicate that, for this system, the electronic contribution is negligible when compared with the lattice vibrations. In spite of this observation in the Cd-Mg system, the electronic excitations may contribute significantly to the ordering tendencies of *some systems*, and should therefore also be included in a *complete* treatment of the alloy thermodynamics. Some efforts in this direction have been made by Wolverton and Zunger [90], who showed that the short- and long-range order in the Ni-V and Pd-V systems are affected by the electronic excitations.
- For simple alloy systems, such as Ag-Cu, the correct topology of the fcc substitutional phase diagram is predicted with models that neglect the non-zero temperature contributions to the  $\bar{\sigma}$ -ensemble free energy. However, the quantitative agreement with experiment is improved if the lattice vibrations are included in the model [30].
- Most structural transformations in elements (e.g., a close-packed low-temperature phase to a bcc high-temperature phase) are driven by differences in vibrational free energies [91, 92, 93, 94]. This fact suggests that the vibrational contribution to the free energy in alloys must be included in the computation of phase diagrams that are based on more than one parent lattice, to get even *qualitative* agreement with experiment.
- It has been shown experimentally that for the Ni-Al, Fe-Al, Fe-Cr, and Cu-Au systems [4, 5, 6, 7, 8] the change of vibrational free energy in order-disorder and segregating phase transformations of substitutional alloys can be comparable in magnitude to the change in the configurational entropy. This means that the inclusion of the lattice vibrations in the studies of the phase transformations in these systems would greatly alter the predictions.
- The effect of the vibrational free energy is known to be important to understand the ordering tendencies of adsorbate atoms and molecules. For example, the order-disorder transition temperature of CO on Pt(111) is predicted to be lowered by a factor of 2 when the lattice vibrations are included in the model [95]. The site selection of CO on Ni(100) shows similar behavior [96].

From the above considerations, we conclude that the predictive power of the theoretical and computational models of alloy phase stability can be greatly improved if we account for the lattice vibrations when studying ordering tendencies. In the rest of this thesis we will develop and apply the formalism to include the *lattice vibrations* in the calculation of alloy phase diagrams, ignoring the other contributions to the  $\vec{\sigma}$ -ensemble free energy.

When the only non-substitutional degrees of freedom in the  $\vec{\sigma}$ -ensemble are the lattice vibrations, the  $\vec{\sigma}$ -ensemble free energy reduces to:

$$F(\vec{\sigma}, T) = E_0(\vec{\sigma}) + F^{vib}(\vec{\sigma}, T) \quad (4.6)$$

In the next section we analyze the second term on the r.h.s. of this equation.

### 4.1.3 The vibrational free energy

In the Born–Oppenheimer or adiabatic approximation [16], the electrons are assumed to respond instantaneously to any movement of the much heavier ions.<sup>7</sup> This means that the electronic density of states is determined by the positions of the ions, and therefore the total potential energy of the crystal is only a function of the ionic positions.<sup>8</sup> The potential energy of the system in substitutional state  $\vec{\sigma}$  can be expanded around the ground-state geometry of the  $\vec{\sigma}$ -ensemble as:

$$\begin{aligned} V(\vec{\sigma}; \vec{u}(1), \dots, \vec{u}(N)) &= E_0(\vec{\sigma}) + \sum_{\alpha\beta l l'} \frac{1}{2} \Phi_{\alpha\beta}(\vec{\sigma}; l, l') u_{\alpha}(l) u_{\beta}(l') \\ &+ \sum_{\alpha\beta\gamma l l' l''} \frac{1}{6} \Phi_{\alpha\beta\gamma}(\vec{\sigma}; l, l', l'') u_{\alpha}(l) u_{\beta}(l') u_{\gamma}(l'') + \dots, \end{aligned} \quad (4.7)$$

where  $\vec{u}(i) = \vec{R}(i) - \vec{R}_0(i)$  is the displacement of ion  $i$  away from the position of lowest energy in configuration  $\vec{\sigma}$ ,  $E_0$  is the ground-state energy of the  $\vec{\sigma}$ -ensemble, the Greek subindices label the cartesian components of the displacements, and  $l$ ,  $l'$ , and  $l''$  label atoms on the lattice sites.  $\Phi_{\alpha\beta}(l, l')$  and  $\Phi_{\alpha\beta\gamma}(l, l', l'')$  are the second and third derivatives of the potential energy with respect to the displacements:

$$\Phi_{\alpha\beta}(l, l') = \frac{\partial^2 V}{\partial u_{\alpha}(l) \partial u_{\beta}(l')} \quad (4.8)$$

$$\Phi_{\alpha\beta\gamma}(l, l', l'') = \frac{\partial^3 V}{\partial u_{\alpha}(l) \partial u_{\beta}(l') \partial u_{\gamma}(l'')} \quad (4.9)$$

The tensor  $\Phi_{\alpha\beta}(l, l')$  ( $\alpha, \beta = x, y, z$ ) is usually referred to as the (harmonic) “atomic force (or spring) constant tensor.” Each of its components is an “atomic force (or

<sup>7</sup>In general, the ions are the nuclei of the atoms. However, when frozen core techniques are used the ions are the nuclei with the frozen set of core electrons attached to them.

<sup>8</sup>This total potential energy is temperature-dependent due to the electronic excitations. This effect is one of the “coupling terms” in equation 4.5, and will be neglected in our treatment.

spring) constant.” The explicit dependence of the force constants with configuration  $\vec{\sigma}$  is shown in equation 4.7.

The harmonic approximation consists of keeping just the first two terms on the r.h.s. of equation 4.7. This is a good approximation for low enough temperatures, typically well below the melting temperature of the material.<sup>9</sup> There are many binary alloy systems for which the phase transformations between different solid-state phases occur at temperatures low enough so that the harmonic approximation is a good representation of the ionic motion [97]. We will assume harmonicity in the rest of this thesis, keeping in mind that the anharmonic corrections (third and higher order terms on the r.h.s. of equation 4.7) might become important at high temperatures.

The solution of the *classical* dynamics of the system in the harmonic approximations consists of a set of independent harmonic oscillators. For a periodic arrangement  $\vec{\sigma}$  with  $r$  atoms in the unit cell, the frequencies  $\omega$  of the system are obtained solving the equation [98]:

$$\mathbf{D}(\vec{k})\vec{u}(\vec{k}) = \omega^2(\vec{k})\vec{u}(\vec{k}) \quad (4.10)$$

where  $\vec{k}$  are vectors in the Brillouin zone of reciprocal space, and the elements of the dynamical matrix  $\mathbf{D}$  are defined as:

$$D_{\alpha\beta}^{KK'}(\vec{k}) = \frac{1}{\sqrt{M_K M_{K'}}} \sum_L \Phi_{\alpha\beta}^{KK'}(L, 0) e^{-i\vec{k} \cdot \vec{R}(L)}, \quad (4.11)$$

where  $K$  and  $K'$  label the  $r$  atoms in the unit cell,  $L$  labels the unit cells ( $L = 0$  is the unit cell at the origin of coordinates),  $\vec{R}(L)$  is the position of the unit cell  $L$ , and  $M_K$  is the mass of the atom  $K$  in the unit cell.

Quantization of the normal modes leads to the quantum-mechanical Hamiltonian for the lattice vibrations:

$$H = \sum_{j=1}^{3r} \sum_{\vec{k}} \hbar\omega_j(\vec{k}) \left[ n_j(\vec{k}) + \frac{1}{2} \right], \quad (4.12)$$

where the first sum is over the  $3r$  branches of the dispersion relations  $\omega_j(\vec{k})$ , the second sum is over all the vectors  $\vec{k}$  of the Brillouin zone,  $\hbar$  is the Plank constant, and  $n_j(\vec{k})$  is the integer occupation number of the oscillator of the  $j^{\text{th}}$  branch evaluated at  $\vec{k}$ . The resulting *vibrational* free energy per atom, for an alloy with  $N$  sites, can be obtained by analytically summing the partition function [98]:

$$\frac{F^{\text{vib}}(\vec{\sigma}, T)}{N} = \int_0^\infty \left\{ \frac{1}{2} \hbar\omega + k_B T \ln [1 - \exp(-\beta \hbar\omega)] \right\} g(\vec{\sigma}, \omega) d\omega, \quad (4.13)$$

---

<sup>9</sup>For some systems the harmonic approximation is accurate up to the melting temperature. Since melting is a first-order transition, at the melting temperature the solid and liquid states are very different, allowing for harmonic behavior in the solid state in spite of the highly anharmonic characteristics of the liquid phase.

where the vibrational density of states (VDOS) per atom is defined as:

$$g(\vec{\sigma}, \omega) = \frac{1}{N} \sum_{j=1}^{3r} \sum_{\vec{k}} \delta[\omega - \omega_j(\vec{k}, \vec{\sigma})], \quad (4.14)$$

where  $\delta[x]$  is the Dirac delta function, and the dispersion relations  $\omega_j(\vec{k})$  depend on the substitutional configuration  $\vec{\sigma}$  of the alloy.

It will prove useful for our analysis to study the temperature dependence of the vibrational free energy in equation 4.13. The low- and high-temperature limits are:

$$\text{low } T \rightarrow \frac{F^{\text{vib}}(\vec{\sigma}, T)}{N} = \frac{\hbar \overline{\omega}(\vec{\sigma})}{2} - \sum_{n=0,1,\dots} \zeta(n+1) \frac{g_n(\vec{\sigma})}{\hbar^{n+1}} (k_B T)^{n+2} \quad (4.15)$$

$$\begin{aligned} \text{high } T \rightarrow \frac{F^{\text{vib}}(\vec{\sigma}, T)}{N} &= -k_B T \ln(k_B T) + \overline{\ln(\omega)}(\vec{\sigma}) k_B T \\ &+ \frac{\hbar^2 \overline{\omega^2}(\vec{\sigma})}{24} (k_B T)^{-1} \\ &- \frac{\hbar^4 \overline{\omega^4}(\vec{\sigma})}{2880} (k_B T)^{-3} + \mathcal{O}(T^{-5}), \end{aligned} \quad (4.16)$$

where  $\overline{\omega^n}$  is the  $n^{\text{th}}$  moment of the VDOS, defined as  $\overline{\omega^n}(\vec{\sigma}) \equiv \int_0^\infty \omega^n g(\vec{\sigma}, \omega) d\omega$ , for  $n > 0$  and the  $0^{\text{th}}$  moment is defined as  $\overline{\ln(\omega)}(\vec{\sigma}) \equiv \int_0^\infty \ln(\omega) g(\vec{\sigma}, \omega) d\omega$ ,  $g_n(\vec{\sigma})$  is the  $n^{\text{th}}$  derivative of the VDOS at the origin, and  $\zeta(n)$  is the Riemann zeta function [99].

To obtain the coefficients of the high-temperature expansions of the vibrational free energy it is not necessary to diagonalize the dynamical matrix, because the moments of the VDOS can be obtained as traces and determinants of the dynamical matrix [100]:

$$\begin{aligned} \text{high } T \rightarrow \frac{F^{\text{vib}}(\vec{\sigma}, T)}{N} &= -k_B T \ln(k_B T) + \frac{\ln \det D(\vec{\sigma})}{2} k_B T \\ &+ \frac{\hbar^2 \text{Tr} D(\vec{\sigma})}{24} (k_B T)^{-1} \\ &- \frac{\hbar^4 \text{Tr} D^2(\vec{\sigma})}{2880} (k_B T)^{-3} + \mathcal{O}(T^{-5}). \end{aligned} \quad (4.17)$$

In order to compute the vibrational free energy, it is important to note that the atomic force constants have to be computed as the second derivatives of the energy in the *fully relaxed geometry* (i.e., for the atoms at the positions of ground state of the  $\vec{\sigma}$ -ensemble). Otherwise, unstable modes with “imaginary” frequencies (i.e.,  $\omega^2 < 0$ ) will be present, making the use of the above formulae impossible.

#### 4.1.4 The vibrational effective cluster interactions

To be able to easily evaluate the lattice Hamiltonian of equation 4.6, we need a fast way of computing the ground-state energy ( $E_0$ ) and vibrational free energy ( $F^{\text{vib}}$ ) for many substitutional configurations  $\vec{\sigma}$  of the alloy. It was shown in chapter 2

that the cluster expansion technique provides a convenient way of parameterizing the dependence of any function of the configuration  $\vec{\sigma}$ . In particular, we showed (see equation 2.12) that the calculation of the ground-state energy of the  $\vec{\sigma}$ -ensemble  $E_0$  can be conveniently parameterized with a few effective cluster interactions (ECI's)  $V_\alpha$ :

$$\frac{E_0(\vec{\sigma})}{N} = \sum'_{\alpha \leq \alpha_{max}} m_\alpha V_\alpha \langle \sigma_\alpha \rangle(\vec{\sigma}), \quad (4.18)$$

where  $\alpha_{max}$  symbolizes the truncation of the cluster expansion,  $m_\alpha$  is the number of clusters per lattice site that are equivalent to cluster  $\alpha$  by the symmetry of the lattice,  $\langle \sigma_\alpha \rangle$  is the average of the cluster functions over the equivalent clusters (or “correlation functions”), and the prime indicates that the summation is only performed over non-equivalent clusters  $\alpha$ . An analogous procedure can be carried out for the lattice Hamiltonian including the vibrational free energy:

$$\frac{F(\vec{\sigma}, T)}{N} = \sum'_{\alpha \leq \alpha_{max}} m_\alpha (V_\alpha^{chem} + V_\alpha^{vib}(T)) \langle \sigma_\alpha \rangle(\vec{\sigma}), \quad (4.19)$$

where the *total* ECI's are the sum of the *chemical* ECI's (CECI's) originated in the cluster expansion of the ground-state energy, and the  $T$ -dependent *vibrational* ECI's (VECI's) that parameterize the vibrational free energy. The calculation of the CECI's was analyzed in detail in chapter 2.

To obtain the VECI's to parameterize the low- and high-temperatures limits of the vibrational free energy (equations 4.15 and 4.16), it is sufficient to cluster-expand the coefficients in the expansion that depend on  $\vec{\sigma}$  (e.g., the moments and derivatives of the VDOS). The first term in the high-temperature expansion ( $-T \ln T$ ) does not depend on the configuration  $\vec{\sigma}$  and therefore does not affect the ordering tendencies of the alloy (it only contributes to the empty-cluster term of the cluster expansion, which is only important if more than one parent lattice competes for stability). At high temperature, the VECI's are linear in  $T$ . On the other hand, at  $T = 0K$ , the VECI's are determined by the zero-point vibration. The first power in  $T$  in the low-temperature limit is  $d + 1$ , where  $d$  is the dimensionality of the system (because for  $n < d$ ,  $g_n$  vanishes).

The first configuration-dependent term in the high-temperature expansion of the VECI's is independent of the masses of the system, i.e., two systems with the same chemical interactions but different masses have the same high-temperature VECI's. This results from the fact that, for a system with  $N$  atoms, and composition  $c$  of B atoms, the masses can be factored out of the determinant of the dynamical matrix (we do not need to assume periodicity for this result):

$$\det \mathbf{D} = \frac{1}{(M_A^{1-c} M_B^c)^{3N/2}} \det \Phi. \quad (4.20)$$

Then, the masses cancel out in the formation value of the logarithmic average of the

frequencies:

$$\Delta \overline{\ln(\omega)} = \frac{1}{2N} \ln \left[ \frac{\det \Phi}{(\det \Phi_A)^c (\det \Phi_B)^{1-c}} \right], \quad (4.21)$$

where  $\Phi$ ,  $\Phi_A$ , and  $\Phi_B$  are the matrices of second derivatives of the energy for the configuration with composition  $c$ , the pure-A, and the pure-B configurations respectively.

In the next section, we study a simple one-dimensional alloy to illustrate the applicability of the cluster expansion to parameterize the vibrational properties, and to analyze the importance of the different temperature dependent terms.

## 4.2 The vibrating binary chain

Consider a one dimensional alloy of  $A$  and  $B$  atoms of masses  $M_A$  and  $M_B$ . Each nearest-neighbor pair is connected with an ideal spring of constant  $\gamma_{AA}$ ,  $\gamma_{BB}$ , or  $\gamma_{AB}$ , depending on the occupation of the pair. The dynamical matrix is symmetric tridiagonal with elements  $D_{ii} = (\gamma_{i-1,i} + \gamma_{i,i+1})/M_i$  and  $D_{ii+1} = -\gamma_{i,i+1}/\sqrt{M_i M_{i+1}}$ .

We solved [101] the high-temperature form of the VECI's exactly, using equation 4.16 and the dynamical matrix for the linear chain defined above. After lengthy algebra the final result for the nearest-neighbor VECI is:<sup>10</sup>

$$\begin{aligned} V_{2,1}(T) = & \frac{1}{8} \ln \left[ \frac{\gamma_{AA}\gamma_{BB}}{\gamma_{AB}^2} \right] T \\ & + \frac{1}{48} \left\{ \frac{\gamma_{AA}}{M_A} + \frac{\gamma_{BB}}{M_B} - \gamma_{AB} \left[ \frac{1}{M_A} + \frac{1}{M_B} \right] \right\} T^{-1} \\ & - \frac{1}{5760} \left\{ 3 \left[ \frac{\gamma_{AA}}{M_A} \right]^2 + 3 \left[ \frac{\gamma_{BB}}{M_B} \right]^2 - 2\gamma_{AB}^2 \left[ \frac{1}{M_A^2} + \frac{1}{M_B^2} + \frac{1}{M_A M_B} \right] \right\} T^{-3} \\ & + \mathcal{O}(T^{-5}). \end{aligned} \quad (4.22)$$

The first term in the r.h.s. of equation 4.22 was already obtained by Bakker [102] and Matthew *et al.* [103]. Similar derivations show that all the other VECI's for the linear chain model (second- and further-neighbor pairs and multiplets) vanish in the infinite-temperature limit. As a consequence, the cluster expansion is convergent at high temperatures.

The low temperature coefficients can not be solved exactly but a good approximation can be obtained by analyzing the elastic limit. We replace the binary chain by an effective monatomic chain. The effective atom in this chain is constructed so that the effective chain has the same elastic properties as the binary configuration we are interested in. The values of  $\mu_1$  and  $g_n$  can then be expressed in terms of the lattice-averaged cluster functions on the point cluster ( $\langle \sigma_1 \rangle$ ) and the nearest-neighbor pair cluster ( $\langle \sigma_{2,1} \rangle$ ). After linearizing  $\mu_1$  and  $g_n$  around the chain with random occupation

---

<sup>10</sup>To simplify the notation, the Boltzmann and Plank constants,  $k_B$  and  $\hbar$  respectively, are set to unity for the study of the binary chain.

( $\langle\sigma_1\rangle = 0$ ,  $\langle\sigma_{2,1}\rangle = 0$ ) we obtain:

$$\begin{aligned}
V_{2,1}(T) = & -\frac{2}{\pi}\alpha_-\alpha_+^{-3/2}M^{-1/2} \\
& -\frac{\zeta(0)}{4\pi}\alpha_-\alpha_+^{-1/2}M^{1/2}T^2 \\
& -\frac{3\zeta(2)}{64\pi}\alpha_-\alpha_+^{1/2}M^{3/2}T^4 + \mathcal{O}(T^6),
\end{aligned} \tag{4.23}$$

where

$$\begin{aligned}
\alpha_{\pm} &= \frac{1}{\gamma_{AA}} + \frac{1}{\gamma_{BB}} \pm \frac{1}{\gamma_{AB}} \\
M &= \frac{M_A + M_B}{2} \\
\zeta(0) &= 1.645 \\
\zeta(2) &= 1.082.
\end{aligned}$$

To test the two approximations made to obtain equation 4.23, i.e., the elastic limit and the linearization, we performed numerical calculations of the VECI's on chains of 10,000 to 50,000 atoms, averaging over 150 configurations, using the “negative-eigenvalue” method developed by Dean [104]. We computed  $V_2(T = 0\text{K})$  numerically for 137 different sets of the parameters of the system ( $M_A$ ,  $M_B$ ,  $\gamma_{AA}$ ,  $\gamma_{BB}$ ,  $\gamma_{AB}$ ). In figure 4-1 the numerical results are compared with those in equation 4.23. Reasonable agreement is obtained. Equation 4.23 fails to predict the ordering tendencies at low  $T$  of isotopic disordered chains, i.e., those chains for which all the spring constants are equal, and only the masses of the two species differ (we will further discuss isotopic systems in chapter 5).

To estimate the temperature range for which equations 4.22 and 4.23 are valid, we computed  $V_2(T)$  numerically for a linear chain with  $\gamma_{AA} = 1$ ,  $\gamma_{BB} = 3$ ,  $\gamma_{AB} = 1.2$ ,  $M_A = 1$ ,  $M_B = 1.5$ . Figure 4-2 shows the results. The Debye temperatures for pure  $A$ , pure  $B$  and ordered  $AB$  structures are shown in the temperature axis. The slight difference in the slope at high  $T$  is due to numerical errors, while the differences at low  $T$  are due to the approximations introduced to derive equation 4.23. It can be seen that two terms in the high- $T$  limit and two terms in the low- $T$  limit suffice to represent the temperature dependence of the VECI at all temperatures.

Most of the important features of alloy phase diagrams occur at temperatures that are generally of the order or larger than the Debye temperatures of the system. From figure 4-2 we then expect that the first term in the high- $T$  expansion will dominate the VECI's. The value of the VECI for this example is a sizable fraction of the temperature (recall  $k_B = 1$ ), and therefore will significantly affect the phase diagram. In the rest of this thesis, we will assume that the leading high-temperature term is enough to describe the VECI's accurately. This allows us to write the lattice

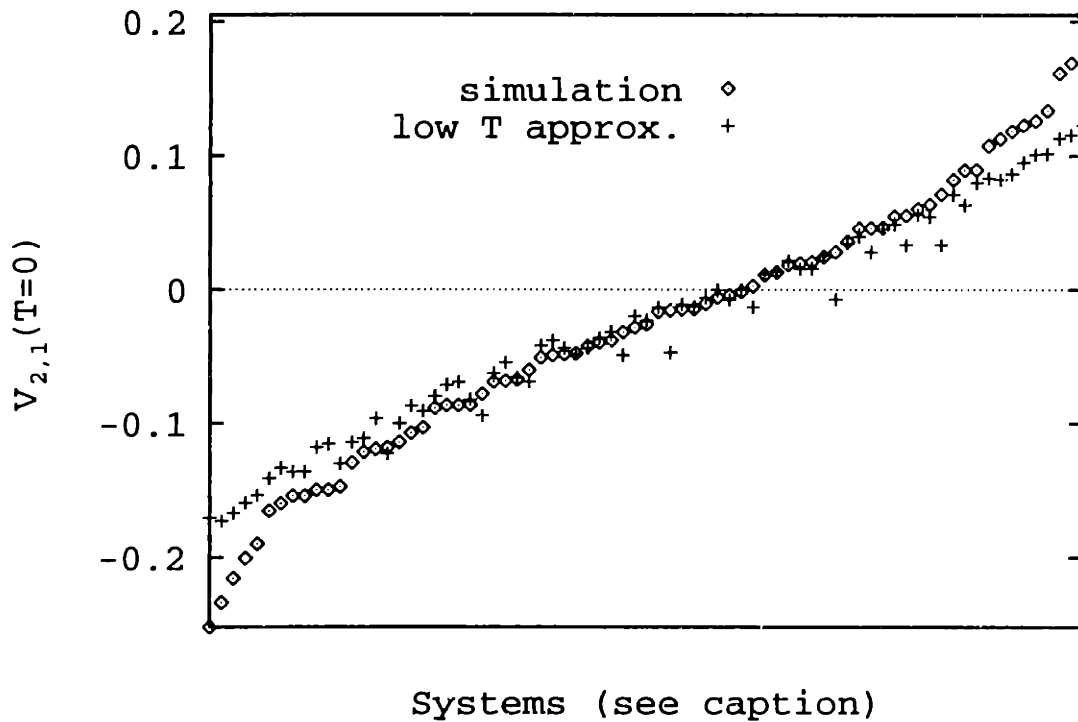


Figure 4-1: Comparison of the zero-temperature nearest-neighbor pair VECI computed with equation 4.23 and numerical results. The 137 different systems scan the sets of parameters  $0.3 < \gamma_{BB}, \gamma_{AB} < 3$  and  $1 < M_B < 3$ , while keeping  $\gamma_{AA} = 1$  and  $M_A = 1$ . The systems are ordered in the horizontal axis in increasing value of  $V_2$  as obtained numerically. It can be seen that equation 4.23 underestimates the absolute value of the VECI for large VECI's.



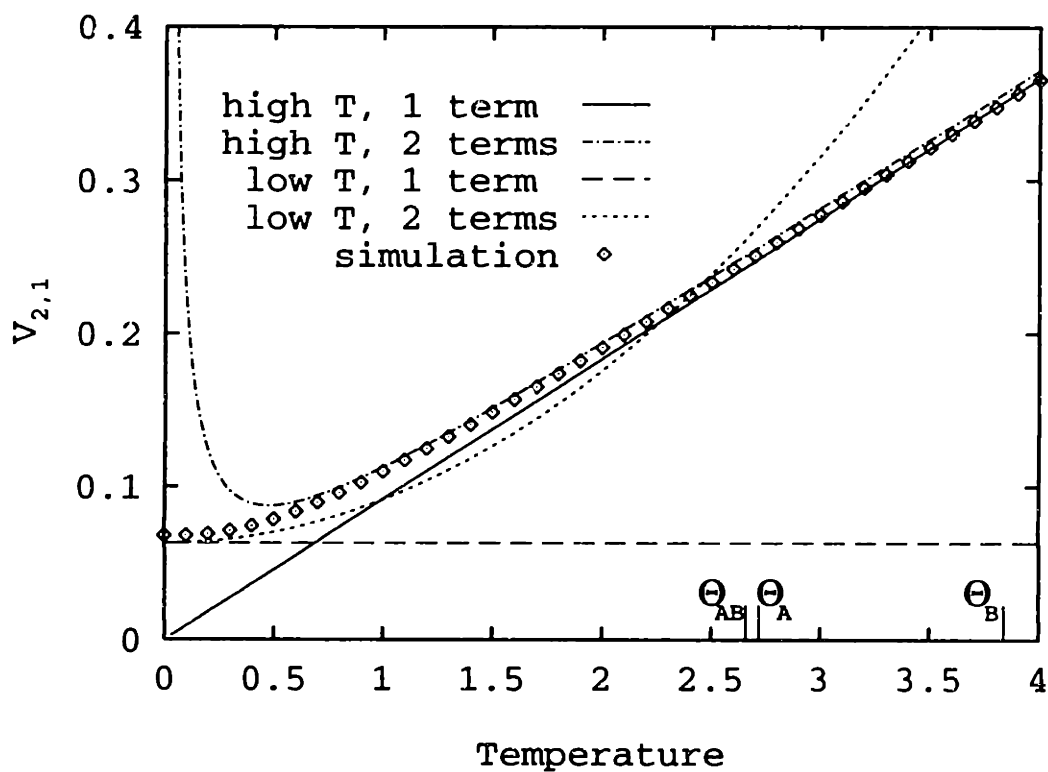


Figure 4-2: Nearest-neighbor VECI as a function of temperature for a linear chain with  $\gamma_{AA} = 1$ ,  $\gamma_{BB} = 3$ ,  $\gamma_{AB} = 1.2$ ,  $M_A = 1$ ,  $M_B = 1.5$ . Debye temperatures for different configurations are also indicated.

Hamiltonian as

$$\frac{F(\vec{\sigma}, T)}{N} = \sum'_{\alpha \leq \alpha_{max}} m_{\alpha} (V_{\alpha}^{chem} + V_{\alpha}^{vib} k_B T) \langle \sigma_{\alpha} \rangle(\vec{\sigma}), \quad (4.24)$$

where we have redefined the VECI  $V_{\alpha}^{vib}$  to be the coefficient of the cluster expansion of  $\mu_0$  (recall from page 100,  $\mu_0 = \overline{\ln(\omega)}$ ) and therefore  $V_{\alpha}^{vib}$  is temperature independent (within the harmonic approximation).

The leading term of the VECI at high  $T$  is independent of the masses of the atoms for the linear chain (see equation 4.22). This result is also valid for an alloy in any number of dimensions. From the leading term in equation 4.22, we see that if the spring constant between the  $A$  and  $B$  atoms is smaller than the geometrical average of the spring constants between like atoms, the vibrations will induce ordering in the alloy, while phase separation will be favored otherwise. On the other hand, an arithmetic average for  $\gamma_{AB}$  would induce ordering. The importance of the lattice vibrations can be illustrated by considering the change in the predicted transition temperatures for ordering and phase-separating systems (see section 4.3) and the limit of the short-range order (SRO) parameter at infinite temperature.

It is generally assumed that, in the infinite-temperature limit, the Warren-Cowley SRO parameter<sup>11</sup> ( $\alpha_j$ ) vanishes, based on the fact that the completely disordered state has the highest configurational entropy. This is valid only when the ECI's approach a constant value at high  $T$ . From the derivation above, we see that if the lattice vibrations are considered, the vibrational entropy introduces a linear  $T$  dependence in the ECI's at high  $T$ . It can be easily shown that, in that case,  $\alpha_j$  will approach a finite non zero value when  $T \rightarrow \infty$ . This value can be predicted if the leading configuration-dependent high temperature term of the VECI's is known (equation 4.16). This possible behavior of the SRO was already pointed out by Miller [106] and some experimental evidence to support it is available for Ni-Fe [107] and Ni-Cu [108] alloys.

### 4.3 The size of the effect of lattice vibrations on phase stability

In the previous section, we showed that the leading high-temperature term is the most important contribution to the VECI's for the temperatures of interest in substitutional alloys. In this section, we will assume that only this term is kept in the VECI's.

---

<sup>11</sup>The Warren-Cowley SRO parameter is defined as [105]

$$\alpha_j = \frac{\langle \sigma_0 \sigma_j \rangle - \langle \sigma_0 \rangle^2}{1 - \langle \sigma_0 \rangle^2},$$

where  $\sigma_0$  and  $\sigma_j$  are the spin variables at the origin and site  $j$  respectively, and  $\langle \rangle$  denotes thermal average (not to be confused with the lattice average, for which the same symbol is used). When the occupation of the sites is completely uncorrelated  $\langle \sigma_0 \sigma_j \rangle = \langle \sigma_0 \rangle \langle \sigma_j \rangle = \langle \sigma_0 \rangle^2$  and  $\alpha_j = 0$ , otherwise  $\alpha_j \neq 0$ .

A rough estimate of the effect of the lattice vibrations on the phase diagram of a substitutional binary alloy can be obtained [109] by assuming that only the nearest-neighbor pair ECI is non-zero in the Hamiltonian of the alloy,

$$F(\vec{\sigma}, T) = (V^{chem} + V^{vib}k_B T)m_2 \langle \sigma_2 \rangle, \quad (4.25)$$

where  $V^{chem}$  and  $V^{vib}$  are the chemical and vibrational nearest-neighbor pair ECI obtained by cluster expanding  $E_o$  and  $\overline{\ln(\omega)}$  respectively,  $\langle \sigma_2 \rangle$  is the lattice average of the cluster functions on the nearest-neighbor pairs of the lattice, and  $m_2$  is the number of nearest-neighbor pairs per lattice site (e.g.,  $m_2 = 6$  for fcc and  $m_2 = 4$  for bcc). The transition temperatures at composition 1/2 for systems with only nearest neighbor ECI are given by  $T_c = \alpha |V|/k_B$ , where  $\alpha$  is a numerical constant that only depends on the underlying lattice and on whether the system is ordering or segregating [42]. For the fcc lattice,  $\alpha = 1.7$  for ordering systems and  $\alpha = 9.8$  for segregating systems, while for bcc,  $\alpha = 6.5$  regardless of the ordering tendency (the bcc lattice is not *frustrated* in the nearest-neighbor approximation).

The size of the effect of the lattice vibrations can be expressed as the ratio between the transition temperatures computed with and without considering the vibrations as

$$\frac{T_c^{chem+vib}}{T_c^{chem}} = \frac{1}{1 \mp \alpha V^{vib}}, \quad (4.26)$$

where the “−” and “+” correspond to ordering and segregating systems respectively. Due to the linear dependence on temperature of the VECI, the result in equation 4.26 only depends on the sign of  $V^{chem}$  (i.e., on the ordering tendency of the system) and not on its actual value. In other words, for a rough estimate of the *relative* change in transition temperatures with the lattice vibrations, it is enough to compute the vibrational ECI,  $V^{vib}$ . The predicted values of the relative change in transition temperatures,  $(T_c^{chem+vib} - T_c^{chem})/T_c^{chem}$ , according to equation 4.26 are shown in figure 4-3 as a function of  $V^{vib}$  for fcc and bcc alloys.

Estimates of the effect of vibrations on the phase stability of real materials can be made using the experimental results of Fultz *et al.* [4, 5, 6, 7, 8]. They measured differences in vibrational entropy between different configurations of several alloys. These differences allow us to obtain an estimate for the value of the nearest-neighbor vibrational ECI, assuming a short range cluster expansion, and recalling that  $\Delta S^{vib} = -k_B \Delta \overline{\ln(\omega)}$  in the high-temperature limit. The resulting estimates for the change in transition temperature at composition 1/2 are shown in figure 4-3. Note that for the alloy systems studied, all transition temperatures are reduced by the lattice vibrations (this includes both ordering and segregating systems). In chapter 5 we analyze whether the trend of *lowering* the transition temperatures in figure 4-3 can be explained.

It is clear from figure 4-3, that the effect of the lattice vibrations on the transition temperatures can be significant. Although using only nearest-neighbor interactions makes this a rough estimate, the truncation of the cluster expansion is not expected to bias the estimate towards larger effects. Therefore, lowering transition temperatures by 30% might not be uncommon.

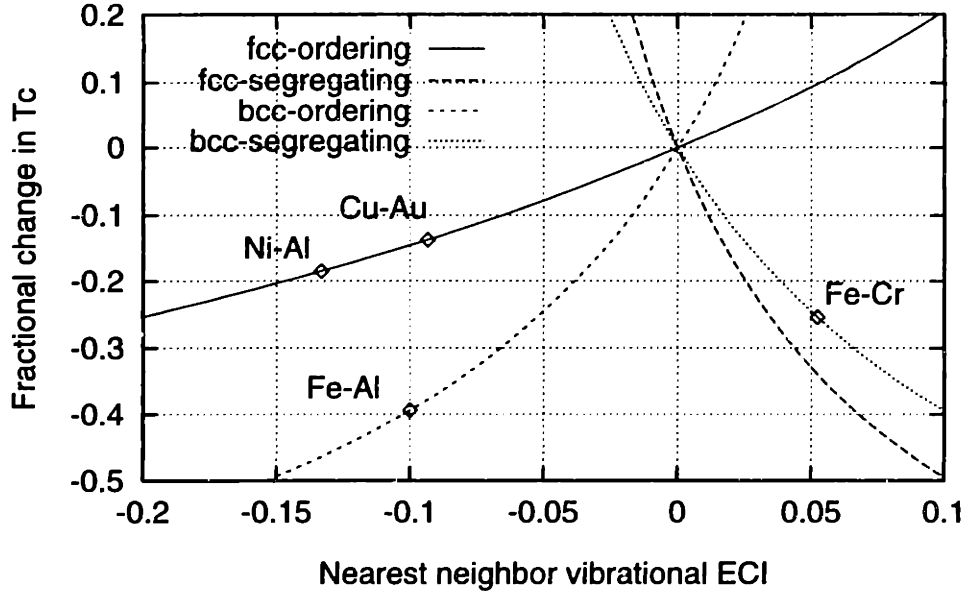


Figure 4-3: Rough estimate of the effect of lattice vibrations on the predicted phase stability for some alloys systems. The vibrational ECI for the other systems were estimated from experimental measurements of vibrational entropy [4, 5, 6, 7, 8].

Since the order of magnitude of the vibrational effect only depends on the vibrational ECI's, it can be argued that the effect will be largest for systems where the A-B bonding is very different in nature from the A-A or B-B bonding. This is the case, for example, in transition-metal aluminides that have highly "asymmetric" bonding. The two transition-metal aluminides, considered in figure 4-3 present a relatively large vibrational effect on the phase stability of the system, supporting the above argument.

## 4.4 Conclusions

In this chapter, we showed that that lattice model of a substitutional alloy can accommodate non-substitutional degrees of freedom by coarse-graining the alloy Hamiltonian. This is done by integrating out the fastest degrees of freedom. The resulting Hamiltonian is temperature-dependent and includes the effects of the excitations that do not change the substitutional state  $\vec{\sigma}$  (i.e., lattice vibrations, electronic promotions, magnetic excitations, and coupling between them). Based on theoretical and experimental results, we argued that the lattice vibrations are the most important of these excitation modes to be included in the studies of alloy phase stability.

We developed the formalism to include the lattice vibrations in the lattice model Hamiltonian in the harmonic approximation. A very simple one-dimensional alloy was used to illustrate the formalism. Finally, a very simple argument was used to estimate the size of the effect of the vibrations on the predicted phase diagrams. As a result of this calculation, large effects can be expected.

# Chapter 5

## Lattice vibrations and phase stability: Classical–potential models

The calculation of the contribution of lattice vibrations to the ordering tendencies in binary alloys requires a model of the energetics of the system. The atomic force constants, which are the second derivatives of the energy with respect to atomic displacements away from the equilibrium positions (see equations 4.10 and 4.11), are needed to obtain the vibrational frequencies and harmonic free energy of the system. There are two possible approaches to model the energetics of a collection of atoms: classical potentials and quantum–mechanical energy methods.

When using classical potentials, the energy of the system is parameterized with respect to the positions of the atoms, using diverse functional forms. The parameters of these functions can be obtained by fitting to experimental properties or to first-principles results. They are relatively easy to use, and are suitable to study large collections of atoms. However, their predictive capability is limited.

On the other hand, with quantum–mechanical techniques, the electronic problem is modeled by solving the Schrödinger (or Dirac) equation under some simplifying assumptions. When no empirical input is used, these methods are *ab initio* and can have great predictive power.

In this chapter, we will apply simple classical–potential models to study the effect of the lattice vibrations to phase stability of binary alloys. The simplicity of these models, allows us to compute the vibrational effective interactions (VECI's) for the model systems without any assumptions beyond the harmonic approximation. The use of the more powerful quantum–mechanical methods to compute the VECI's is deferred to chapter 6.

In section 5.2, we study mixtures of isotopes of the same element, where the ordering tendencies are due *only* to vibrational effects (there is no chemical effect). A very simple model of the Ar–Kr system is analyzed in section 5.3. The temperature–composition phase diagram is computed with and without the effect of the lattice vibrations. We also analyze the vibrational spectrum to assess what frequencies are responsible for the observed ordering effects. Finally, the trends of the contribution

of lattice vibrations to the ordering tendencies with respect to changes in chemical affinity and in size mismatch between the atomic species are analyzed in section 5.4.

## 5.1 Classical potentials

The use of classical pair and multibody potentials to describe the energetics of a collection of atoms is reviewed in appendix C. In this chapter, we will use the Lennard-Jones (LJ) pair potentials. The contribution to the total energy of the system of a pair of atoms at distance  $r$  interacting with a LJ potential is:

$$V^{(2)}(r) = \epsilon \left[ \left( \frac{\rho}{r} \right)^{12} - 2 \left( \frac{\rho}{r} \right)^6 \right], \quad (5.1)$$

where the parameters  $\rho$  and  $\epsilon$  correspond to the distance of minimum energy between two atoms and their binding energy at that distance respectively. For simple monatomic systems, these two parameters can be fitted to the lattice constant and cohesive energy of the elemental solid.

Although the classical-potential models are not a reliable tool to make quantitative predictions, they are useful to study qualitative behavior of model systems. With that spirit in mind, we use them in this chapter to analyze the effect of lattice vibrations on phase stability of alloys.

## 5.2 The “isotopic” alloy

Two isotopes (A and B) of the same element only differ in the number of neutrons in the nucleus. Their chemical properties are therefore almost identical<sup>1</sup> and hence the chemical ECI's are negligible. Neglecting the vibrations in the study of phase stability, all the configurations have the same probability, even at  $T = 0\text{K}$ , and the system shows complete miscibility at all temperatures. The different masses of the two isotopes will, however, influence the vibrational properties. The vibrational density of states is not the same for different configurations of the isotopes on a lattice, generating  $\vec{\sigma}$ -dependent vibrational free energies. This vibrational free energies will determine the ordering tendencies in the system. We will consider the vibrational free energy in the harmonic approximation.<sup>2</sup>

---

<sup>1</sup>There are small chemical differences due to subtle effects. The non-zero volume of the nucleus affects the “ $1/r$ ” electrostatic potential. Since the volume of the nucleus depends on number of neutrons, small corrections to the energy levels of the electrons are expected. For example, first order perturbation theory predicts corrections  $\sim 10^{-8}$  eV for the hydrogen atom [110]. The other possible effect is the so-called hyperfine structure of the electronic energy levels. The nuclear spin (which depends on the number of neutrons in the nucleus) couples with the electrons shifting the electronic states. The corrections are also of the order of  $10^{-8}$  eV [110]. As we will see, the vibrational effect that we will study is larger than these effects. This justifies neglecting the chemical effects in isotopic systems.

<sup>2</sup>When the zero-point vibrations show anharmonic behavior, the mass of the atom determines the amplitude of these vibrations, producing an effective change in the size of the atom. In these

The problem of ordering tendencies in isotopic systems was already studied in the 1950's by Prigogine *et al.* [111, 112], and Dyson [113]. In reference [111], Prigogine *et al.* studied an isotopic linear binary chain (similar to the one studied in section 4.2) with fixed nearest-neighbor spring constants and applied second order perturbation theory in the difference of the masses of the atoms from a reference chain with all the atoms with the average mass. These results were extended to three dimensional lattices in reference [112]. They proved that any mixture of two isotopes of the same element will segregate in thermodynamical equilibrium to a region of pure A and a region of pure B. The predicted transition temperatures at composition 1/2 are very low, in the milli-Kelvin range. In this section, we will illustrate the isotopic effects by performing numerical studies on isotopic mixtures of rare-gas atoms modeled with Lennard-Jones potentials, using the formalism developed in chapter 4.

In the previous chapter, we showed that the leading term in the high-temperature expansion of the vibrational free energy (i.e.,  $\Delta \overline{\ln(\omega)} k_B T$ ) was sufficient to accurately represent the VECI's in binary alloys. The case of isotopic alloys is rather different due to the lack of chemical interactions. As shown in chapter 4, the value of  $\Delta \overline{\ln(\omega)}$  is independent of the masses of the atoms forming the alloy. Therefore,  $\Delta \overline{\ln(\omega)} = 0$  for isotopic systems, and the VECI's for isotopic system vanish when  $T \rightarrow \infty$ . Due to the small values of the ECI's in isotopic systems, the main contribution to the ordering tendencies originates in the zero-point vibrations of the system (first term in the low-temperature expansion, equation 4.15). Retaining only that term, the  $\vec{\sigma}$ -ensemble free energy reduces to

$$\frac{F^{vib}(\vec{\sigma}, T)}{N} = \frac{\hbar \bar{\omega}(\vec{\sigma})}{2}, \quad (5.2)$$

where  $\bar{\omega}(\vec{\sigma})$  is the average frequency per atom of the system in configuration  $\vec{\sigma}$ .

We studied isotopic mixtures of the two most common isotopes of Ne, Ar, Kr, and Xe, using the following Lennard-Jones parameters, fitted to the experimental cohesive energy and lattice parameters of the fcc solids [114]:

Pair	$\rho$ (Å)	$\epsilon/k_B$ (K)
Ne-Ne	3.07	36.0
Ar-Ar	3.82	120.7
Kr-Kr	4.10	162.5
Xe-Xe	4.47	232.1

The LJ potential functions were truncated at  $1.1\rho$ , allowing only nearest-neighbor atoms to interact.

---

cases, there is a change in the bonding characteristics, and therefore a chemical effect is expected. This effect is important for light atoms, for which the amplitude of vibrations is large.

For every isotopic mixture, we computed  $\bar{\omega}$  for 5 different ordered arrangements of the light and heavy isotopes on the fcc lattice:<sup>3</sup> pure A, pure B, L1<sub>0</sub>, A-rich L1<sub>2</sub>, and B-rich L1<sub>2</sub>. The calculations were done using the equivalent to 60 special fcc k-points for the average over the Brillouin zone (see appendix D). With these values, we constructed a cluster expansion of  $\bar{\omega}$  using the Connolly-Williams method [35]. We truncated the cluster expansion keeping only the subclusters of the nearest-neighbor tetrahedron (see figure 5-4 in page 118). For these isotopic systems, we find that the multibody VECI's are much smaller than the pair VECI and will therefore be neglected. The lattice Hamiltonian, or  $\vec{\sigma}$ -ensemble free energy with only nearest-neighbor VECI is:

$$\frac{F^{vib}(\vec{\sigma}, T)}{N} = m_2 V_2 \langle \sigma_2 \rangle, \quad (5.3)$$

where the VECI  $V_2$  is the cluster expansion coefficient of  $\hbar\bar{\omega}/2$ ,  $m_2$  is the number of nearest-neighbor pairs per lattice site ( $m_2 = 6$  in the fcc lattice), and  $\langle \sigma_2 \rangle$  is the lattice average of the nearest-neighbor cluster functions. For our systems  $V_2 < 0$ . Therefore, these isotopic systems are phase separating.

The transition temperature at composition 1/2 for phase separating fcc alloys modeled with only nearest-neighbor interactions is  $T_c \sim 9.8|V_2|/k_B$  [42]. If we write  $\epsilon$  in eV,  $M_A$  in atomic units,  $\rho$  in Å, then the transition temperature (in Kelvin) is

$$T_c = 235 \frac{|\nu_2|}{\rho} \sqrt{\frac{\epsilon}{M_A}}, \quad (5.4)$$

where  $\nu_2$  is the nearest-neighbor cluster-expansion coefficient of the average frequency (in THz), for a system with  $\epsilon = 1\text{eV}$ ,  $\rho = 1\text{Å}$ , and  $M_A = 1\text{a.u.}$  Figure 5-1 shows the dependence of  $\nu_2$  on the mass ratio ( $M_B/M_A$ ). The resulting transition temperatures for the rare-gas isotopic mixtures are shown in table 5.1. Due to the non-linear behavior of  $|\nu_2|$  vs.  $M_B/M_A$ , the transition temperature is more sensitive to the mass ratio than to the other parameters of the system (compare  $T_c$  for the Ne and Ar mixtures with  $T_c$  for the Kr and Xe mixtures).

The transition temperatures are so low that the slow kinetics will prevent the system to reach equilibrium. It is therefore unlikely that these results be verified by experimental techniques. Furthermore, the results have no technological implication (i.e., isotopic systems will not segregate in any reasonable time). This problem is, nonetheless, very interesting from the theoretical point of view. It shows that phase-separating tendencies can be generated by the lattice vibrations alone, without any "chemical" effect. As shown in chapter 4, the main contribution to the ordering tendencies due to the lattice vibrations is due to the atomic spring constants, and not to the mass. Since in isotopic systems, there is no dependence of the spring constants with configuration, the only contribution is the mass "disorder" and therefore the effect is small. Prigogine and collaborators [112] found for a transition temperature

---

<sup>3</sup>The L1<sub>0</sub> is a superstructure of fcc in which planes of A and B atoms are stacked in the (001) direction. In the L1<sub>2</sub> superstructure of fcc, one of the species occupies the corners of the fcc cube while the other species is located in the faces of the cube.



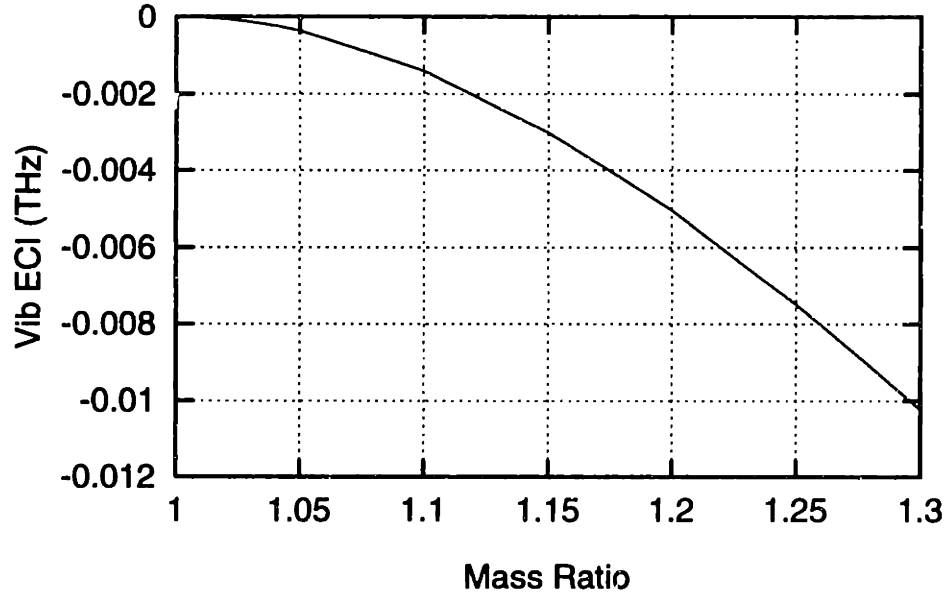


Figure 5-1: Cluster expansion coefficient of the average frequency  $\bar{\omega}$  for a system with  $\epsilon = 1\text{eV}$ ,  $\rho = 1\text{\AA}$ , and  $M_A = 1\text{a.u.}$  as a function of the isotopic mass ratio  $M_B/M_A$

Atom	$M_A$	$M_B$	$M_B/M_A$	$T_c$ (mK)
Ne	20	22	1.100	1.3
Ar	36	40	1.111	1.7
Kr	84	86	1.024	0.065
Xe	129	132	1.023	0.053

Table 5.1: Transition temperatures at composition 1/2 of isotopic mixtures. The masses of the two most abundant isotopes are in atomic units and the temperatures in  $10^{-3}$  Kelvin.

Pair	$\rho$ (Å)	$\epsilon/k_B$ (Kelvin)
Ar–Ar	3.87	114.1
Ar–Kr	3.88	164.0
Kr–Kr	4.11	156.4

Table 5.2: Parameters of the Lennard–Jones potentials used to model the Ar–Kr system, from [12].

for the Ne isotopic mixture of 0.7mK. The difference between this result and our prediction is due to the fact that in reference [112] the mean–field approximation was used to obtain  $T_c$ .

### 5.3 The Ar–Kr system

The elements of group VIII of the periodic table (Ne, Ar, Kr, and Xe) have closed shells of electrons and exhibit simple van–der–Waals type of bonding. Due to this simple bonding, the LJ potentials are a good representation of the energetics of assemblies of these atoms. In particular, mixtures of Ar and Kr have been studied using three LJ pair potentials to model the Ar–Ar, Ar–Kr, and Kr–Kr interactions. The parameters of the pure elements were fitted to reproduce the crystal structures and the cutoff vibrational frequency, while the Ar–Kr potential parameters were adjusted to reproduce atomic collision experiments [12]. These potentials have already been used to study vibrational properties of rare–gas mixtures using the molecular dynamics method [115]. The parameters of the potentials are shown in table 5.2.<sup>4</sup> To simplify the calculations, the potential functions were truncated at  $r = 2.5\rho$ .

With these potentials, the crystal structure that minimizes the cohesive energy of the pure rare–gas solids is hexagonal closed packed (hcp). However, the relative difference in cohesive energy between the hcp and fcc structures is only  $\sim 10^{-4}$ , which is too small to provide an explanation of the observed structures. In fact, the fcc arrangement is seen to form both in nature and in simulations.<sup>5</sup> We will therefore model the Ar–Kr mixtures as arrangements of the atoms on the fcc lattice. Since there is a sizable difference in atomic radii between Ar and Kr atoms ( $\sim 6\%$ ), relaxations away from the ideal lattice sites will be taken into account.

<sup>4</sup>The parameters of the Lennard–Jones potentials for the Ar–Ar and Kr–Kr interactions are slightly different from the ones used to study the isotopic systems in section 5.2 because they were fitted to different experimental properties.

<sup>5</sup>It has been recently argued that certain lattice defects, possible in the fcc lattice but not in the hcp lattice, may explain why the observed structure is not the minimum–energy structure [116].

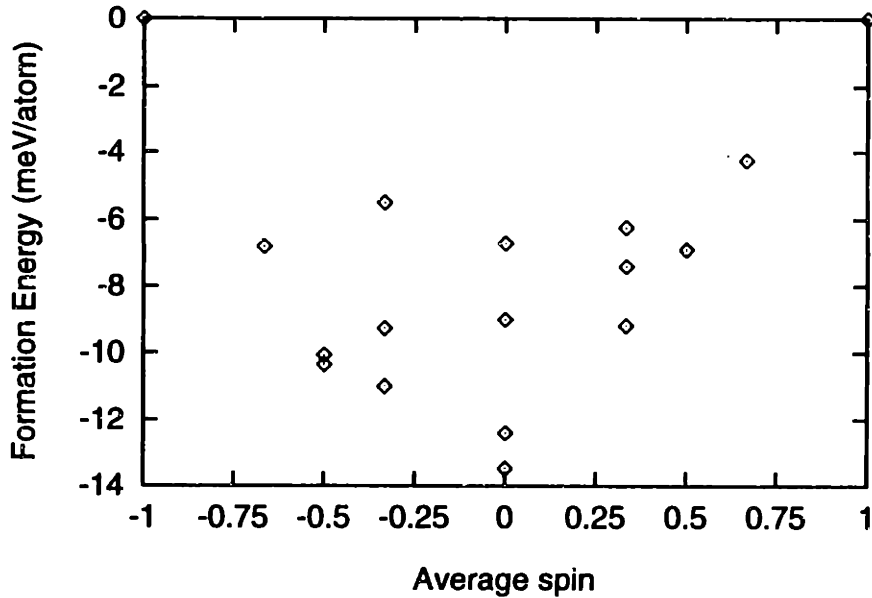


Figure 5-2: Formation energies of the selected ordered structures in the Ar–Kr system. Average spin of  $-1$  ( $1$ ) corresponds to pure Ar (Kr).

### 5.3.1 The phase diagram

To analyze the effect of the lattice vibrations on the phase stability of the model system, we studied a set of 16 ordered structures with up to 8 atoms in the unit cell. Since the expected transition temperatures are of the order of the Debye temperatures of the system, only the configuration-dependent first term in the high-temperature expansion of the vibrational free energy (see equation 4.16) will be kept. Therefore, for each structure we need to compute  $\Delta E$  and  $\Delta \ln(\omega)$ . The direct<sup>6</sup> energy and vibrational frequencies of the 16 structures were computed after relaxing the structures both locally<sup>7</sup> and globally<sup>8</sup> to minimize their energy. The results of these calculations are shown in table 5.3 and figures 5-2 and 5-3.

With the knowledge of the potential function, the calculation of the dynamical matrix of equation 4.11 is straightforward. The dynamical matrix has to be diagonalized to obtain the vibrational frequencies for a given point in the Brillouin zone (see equa-

<sup>6</sup>We will refer to any quantity computed directly from the energy method (e.g., potential functions, Schrödinger equation, etc.) as the “direct” value of that quantity. On the other hand, when the same quantity is cluster-expanded, its value can be recomputed with the cluster expansion. In general, the cluster expansion is truncated and the “cluster-expanded” value will be different from the “direct” value.

<sup>7</sup>Local relaxations include the fractional coordinates of the atoms inside the unit cell of the ordered structure.

<sup>8</sup>Global relaxations include the size and shape of the unit cell. In particular, it was shown in reference [117] that the value of  $\Delta \ln(\omega)$  is very sensitive to the volume relaxations.

Struc.	Comp.	$\Delta E$	$\overline{\Delta \ln(\omega)}$	Ref.
L1 <sub>1</sub>	ArKr	-9.02	.0624	[41]
L1 <sub>0</sub>	ArKr	-13.48	.1940	[41]
L2 <sub>0</sub>	ArKr	-6.70	.0780	[41]
L1 <sub>2</sub>	Ar <sub>3</sub> Kr	-10.07	.1965	[41]
L1 <sub>2</sub>	ArKr <sub>3</sub>	-6.88	.0184	[41]
DO <sub>22</sub>	Ar <sub>3</sub> Kr	-10.35	.2048	[41]
DO <sub>22</sub>	ArKr <sub>3</sub>	-6.89	.0281	[41]
A <sub>2</sub> B <sub>2</sub>	ArKr	-12.40	.1648	[41]
MoPt <sub>2</sub>	Ar <sub>2</sub> Kr	-10.99	.1837	[41]
MoPt <sub>2</sub>	ArKr <sub>2</sub>	-9.20	.0828	[41]
A <sub>2</sub> B	Ar <sub>2</sub> Kr	-9.28	.1172	[41]
A <sub>2</sub> B	ArKr <sub>2</sub>	-7.40	.0071	[41]
A <sub>5</sub> B	Ar <sub>5</sub> Kr	-6.79	.1345	[41]
A <sub>5</sub> B	ArKr <sub>5</sub>	-4.25	-.0061	[41]
G3a	Ar <sub>2</sub> Kr	-5.51	-.0134	[11]
G3a	ArKr <sub>2</sub>	-6.23	.0365	[11]

Table 5.3: Direct formation energy ( $\Delta E$ ) (in meV/atom) and logarithmic average of the vibrational frequencies ( $\overline{\Delta \ln(\omega)}$ ) (dimensionless) for the 16 ordered configurations on the fcc lattice in the Ar–Kr system, modeled with LJ potentials. The structures are identified by either their prototype structure, their Strukturbericht notation, or a conventional name. The composition is expressed by the chemical formula of the structure. The fifth column contains the reference number where a picture of the structure can be found.

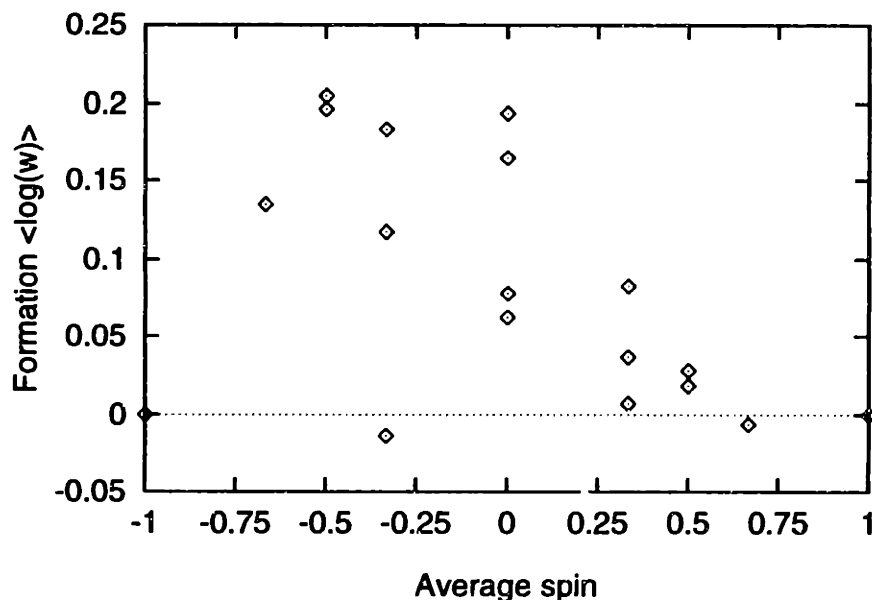


Figure 5-3: Formation of the logarithmic average of the frequencies of the selected ordered structures in the Ar–Kr system. Average spin of  $-1$  ( $1$ ) corresponds to pure Ar (Kr).

tion 4.10). To perform the integrals over the Brillouin zone to compute  $\overline{\ln(\omega)}$ , we used the equivalent of 408 special fcc points obtained with the Chadi–Cohen scheme [13]. The resulting relative integration error in  $\Delta\overline{\ln(\omega)}$  is less than  $10^{-3}$ .

To compute the chemical and the vibrational ECI’s we used the Connolly–Williams approach [35]. We truncated the cluster expansion to include the cluster functions corresponding to all the subclusters of the tetrahedron and octahedron clusters on the fcc lattice. Figure 5-4 shows pictures of these clusters. The resulting ECI’s are shown in figure 5-5.

Both the chemical and vibrational ECI’s decay rapidly with increasing distance between the sites of the cluster and increasing number of sites in the cluster. This is a signature that the local environments determine the properties we are computing. Presumably, the ECI’s for larger clusters are even smaller and therefore the cluster expansion can be truncated without introducing much error. To assess the quality of the cluster expansion, we need to compare the direct and cluster-expanded values of  $\Delta E$  and  $\Delta\overline{\ln(\omega)}$ . In figures 5-6 and 5-7 we show this comparison for the 16 ordered structures of table 5.3. It can be seen that the values of  $\Delta E$  and  $\Delta\overline{\ln(\omega)}$  are accurately reproduced by the cluster expansions. Although convergence studies for the cluster expansion of  $\Delta E$  have been widely reported in the literature [37, 52, 118, 38, 49], a comprehensive study of the convergence of the cluster expansion of  $\Delta\overline{\ln(\omega)}$  is still lacking.

Once the cluster expansion of the  $\sigma$ -ensemble free energy is known, the free energy of any configuration  $\vec{\sigma}$  on the lattice can be computed by evaluating the cluster

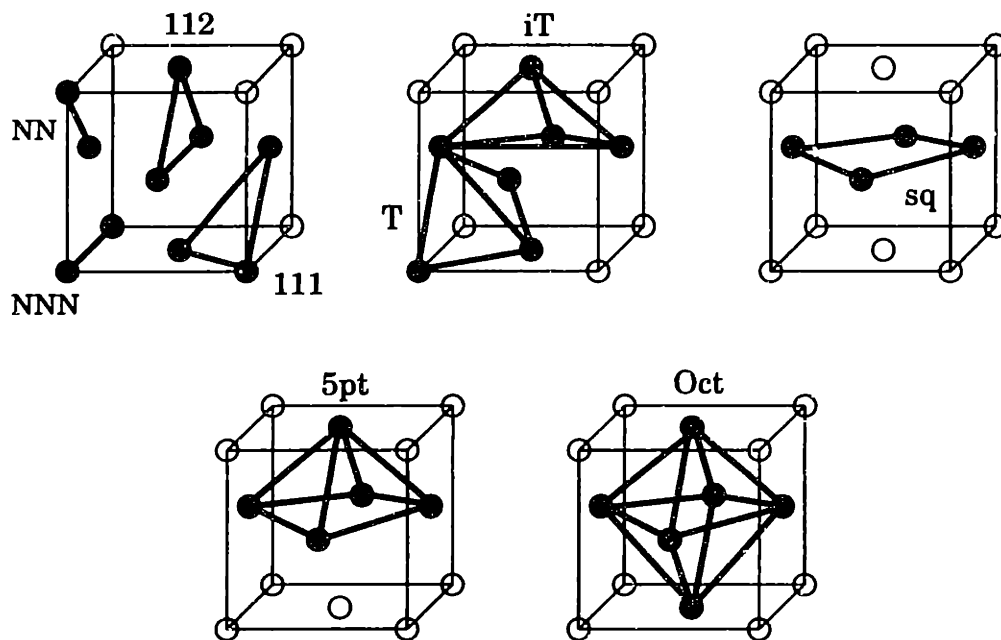


Figure 5-4: Subclusters of the tetrahedron and octahedron clusters on the fcc lattice. The “point” subcluster is not shown.

expansion:

$$F(\vec{\sigma}, T) = \sum_{\alpha \in \text{TO}} (V_{\alpha}^{\text{chem}} + V_{\alpha}^{\text{vib}} k_B T) m_{\alpha} \langle \sigma_{\alpha} \rangle, \quad (5.5)$$

where the sum is over all the subclusters of the tetrahedron and octahedron (TO) clusters, shown in figure 5-4. We used the cluster variation method [22, 41] (CVM) in the tetrahedron–octahedron approximation to compute the free energies of the possible stable phases of the system. By performing a common–tangent construction, the equilibrium phase diagram of the system can be obtained. The resulting phase diagrams with and without the effect of the lattice vibrations are shown in figure 5-8.

The  $L1_0$  structure is the lowest energy structure in the system (see table 5.3) and the  $L1_0$  phase is present in the phase diagram. Other ordered phases are in the ground state line (see figure 5-2) and therefore are expected to be stable at lower temperatures. The lattice vibrations modify the phase diagram only quantitatively, reducing the transition temperature for the order–disorder phase transition by 12%.

The Debye temperature of Ar is approximately 90K. Kr is expected to have a somewhat larger Debye temperature. Since the transition temperatures are slightly lower than the Debye temperatures, the second configuration–dependent term in the high temperature expansion of the vibrational free energy (equation 4.16) may be necessary to get an accurate assessment of the effect of vibrations on the phase diagram. To estimate the error of using only the leading term in the high–temperature expansion, we computed the temperature dependence of the contribution of the lattice vibrations to the total ECI’s for the first– and second–neighbor pairs and the “111”

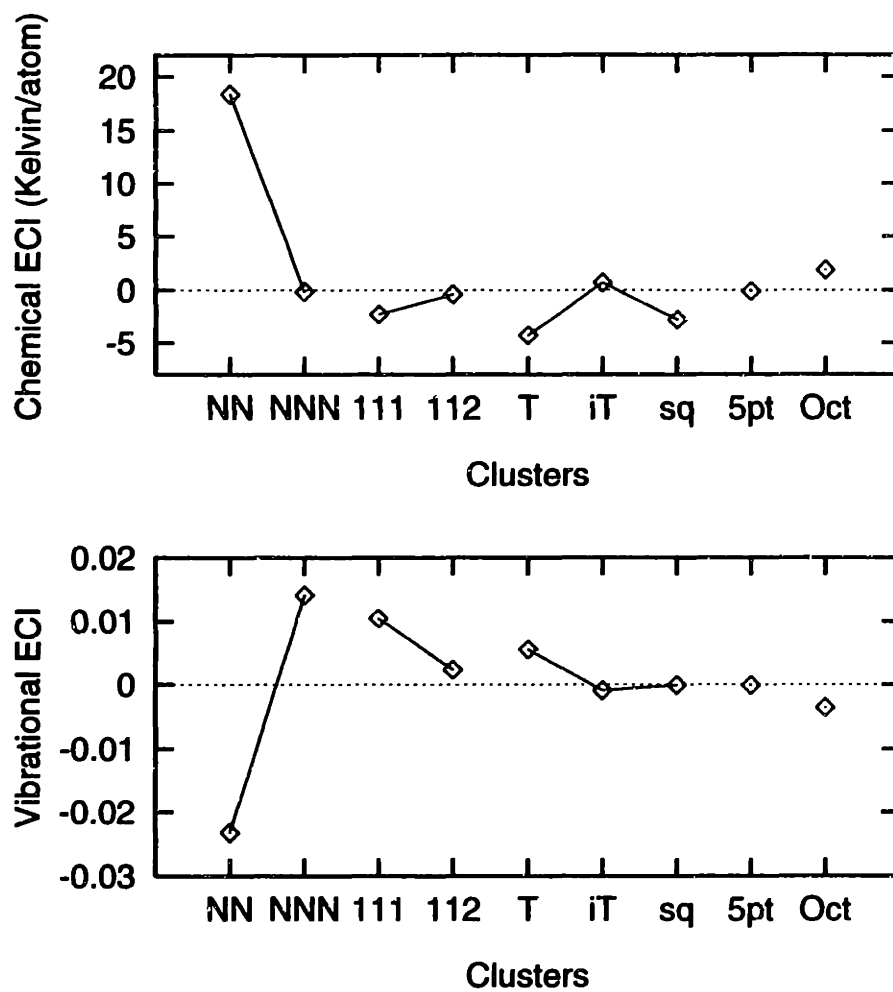


Figure 5-5: Chemical and vibrational effective cluster interactions for the Ar-Kr system. The labels of the clusters are explained in figure 5-4. The energy is expressed in units of temperature (Kelvin), which is obtained from the units of energy dividing by the Boltzmann constant.

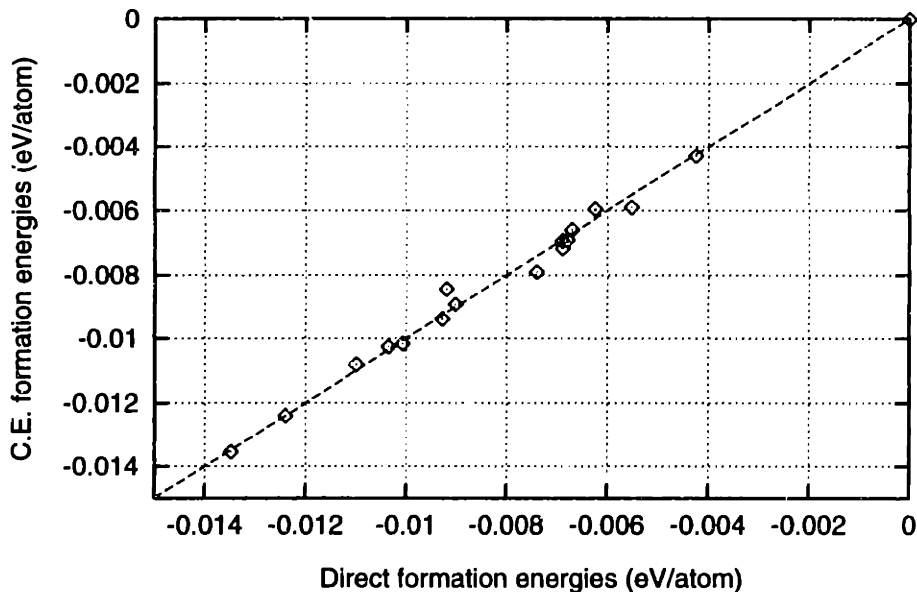


Figure 5-6: Comparison of the direct and cluster-expanded (C.E.) energies for the 16 ordered structures studied in the Ar-Kr system. The closer the points are to the dashed line, the better the fit.

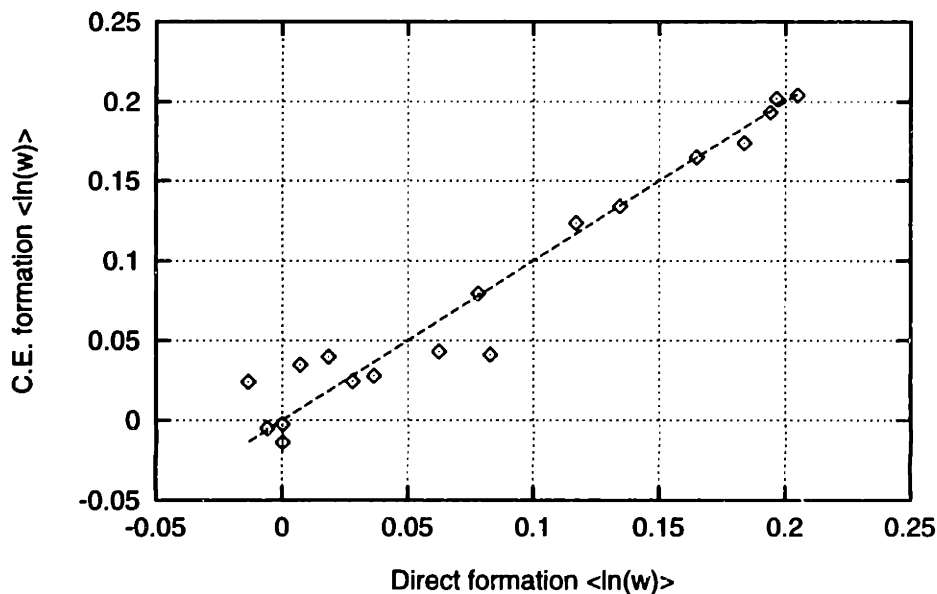


Figure 5-7: Comparison of the direct and cluster-expanded (C.E.) values of  $\overline{\Delta \ln(w)}$  for the 16 ordered structures studied in the Ar-Kr system. The closer the points are to the dashed line, the better the fit.



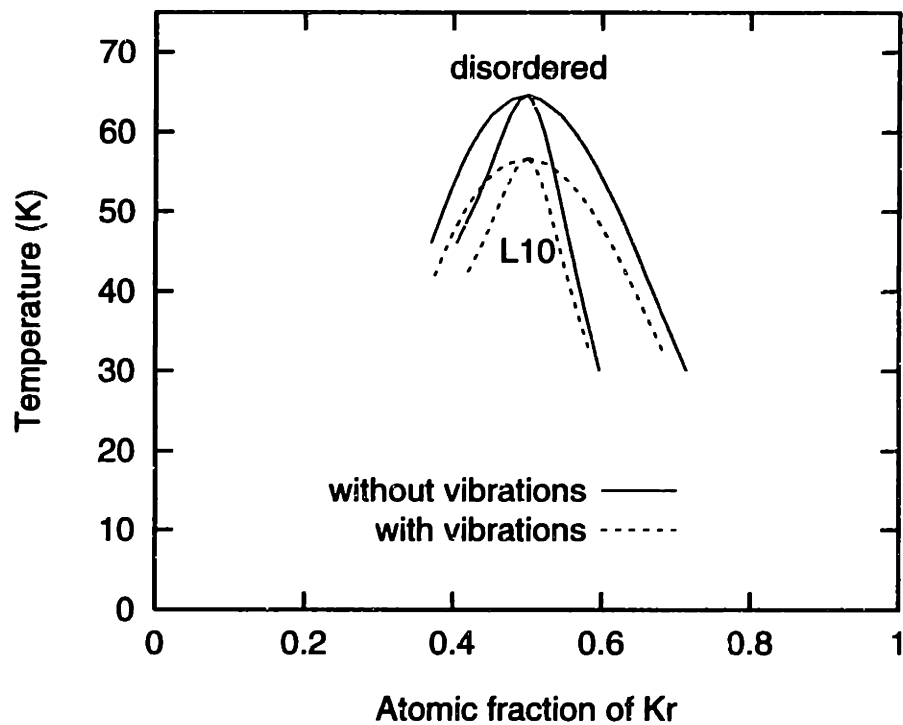


Figure 5-8: Phase diagram of the Ar-Kr system computed with the ECI's of figure 5-5 and using the cluster variation method in the tetrahedron-octahedron approximation. The lattice vibrations reduce the order-disorder transition temperature of the  $L1_0$  phase by 12%.

triplet, using 1, 2, and 3 terms in the high-temperature expansion. The results are shown in figure 5-9. The error in the vibrational contribution to the total ECI's due to only keeping the first term is of 7%, 6%, and 8% for these three clusters respectively. The corrections to the first term in the VECI's would change the order-disorder temperature by less than one degree. We conclude that, even for the Ar-Kr system, where the Debye temperatures are higher than the order-disorder transition, keeping the leading term in the high-temperature expansion of the VECI's gives enough accuracy for the calculation of the phase diagram.

### 5.3.2 What frequencies are responsible for $\overline{\Delta \ln(\omega)}$ ?

As it will become apparent in chapter 6 when we study first-principles approaches, it is important to investigate what part of the frequency spectrum is responsible for the reported values of  $\overline{\Delta \ln(\omega)}$ . To answer this question, we define [109] for every structure the function:

$$s(\omega) \equiv \ln(\omega)\Delta g(\omega), \quad (5.6)$$

where  $\Delta g(\omega)$  is the formation value of the vibrational density of states (VDOS). Then the value of  $\overline{\Delta \ln(\omega)}$  can be obtained as the area under the curve  $s(\omega)$ , i.e.,

$$\overline{\Delta \ln(\omega)} = \int_0^\infty s(\omega)d\omega. \quad (5.7)$$

The values of  $s(\omega)$  were computed using the VDOS obtained with the equivalent to 408 fcc Chadi-Cohen k-points and smoothed with a 0.02 THz-wide Lorentzian. The results are shown in figure 5-10.

It can be seen from these figures that the contribution of  $s(\omega)$  to  $\overline{\Delta \ln(\omega)}$  is, in most cases, larger in the high frequency optical region of the spectrum than in the low frequency acoustical modes. This is in agreement with recent experimental findings in the Fe-Al system [6]. This observation has important consequences for the applicability of some of the approximate methods (see section 6.2).

## 5.4 Trends

By generalizing the Ar-Kr model system to a mixture of A and B atoms interacting through general Lennard-Jones potentials, we can analyze how the effect of the lattice vibrations on phase stability changes, when changing the size mismatch and chemical affinity of the alloy species [109]. In principle, this is achieved by systematically varying the parameters that define the LJ potentials (i.e.,  $\epsilon_{AA}$ ,  $\rho_{AA}$ ,  $\epsilon_{AB}$ ,  $\rho_{AB}$ ,  $\epsilon_{BB}$ , and  $\rho_{BB}$ ) and computing the vibrational effective interactions for different set of parameters. For simplicity, we evaluated the effects of the lattice vibrations by computing  $\overline{\Delta \ln(\omega)}$  for just one ordered structure ( $L1_0$ ).

Without losing generality, we can set  $\epsilon_{AA} = 1$  and  $\rho_{AA} = 1$  (recall that the value of  $\overline{\Delta \ln(\omega)}$  is independent of the energy and length scales). A power expansion of  $\overline{\Delta \ln(\omega)}$  for  $L1_0$  can be constructed numerically around  $\epsilon_{AB} = 1$ ,  $\rho_{AB} = 1$ ,  $\epsilon_{BB} = 1$ ,

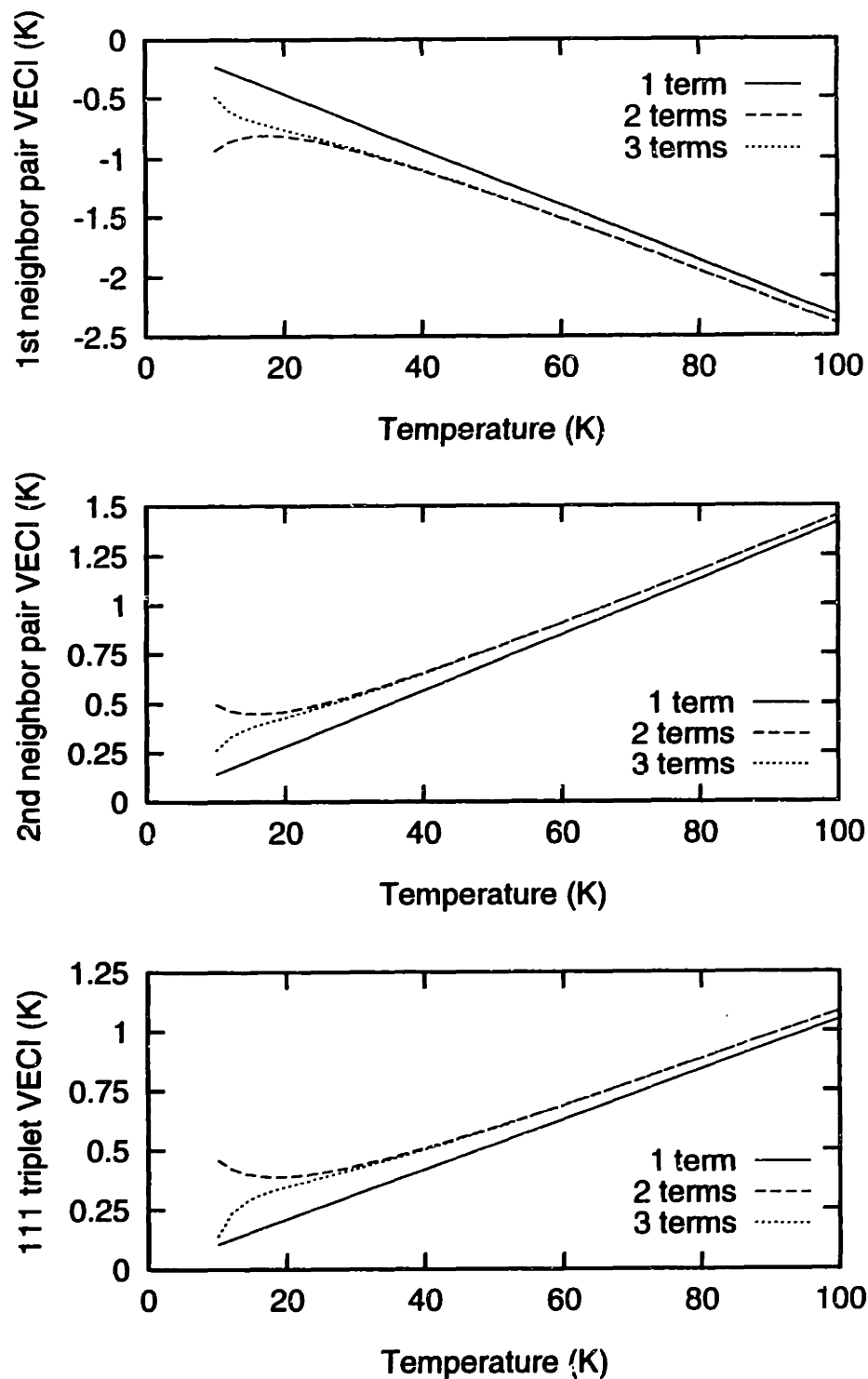


Figure 5-9: Temperature-dependent contribution of the lattice vibrations to the total ECI's in the Ar-Kr system. The number of terms refers to the configuration-dependent terms in equation 4.16.

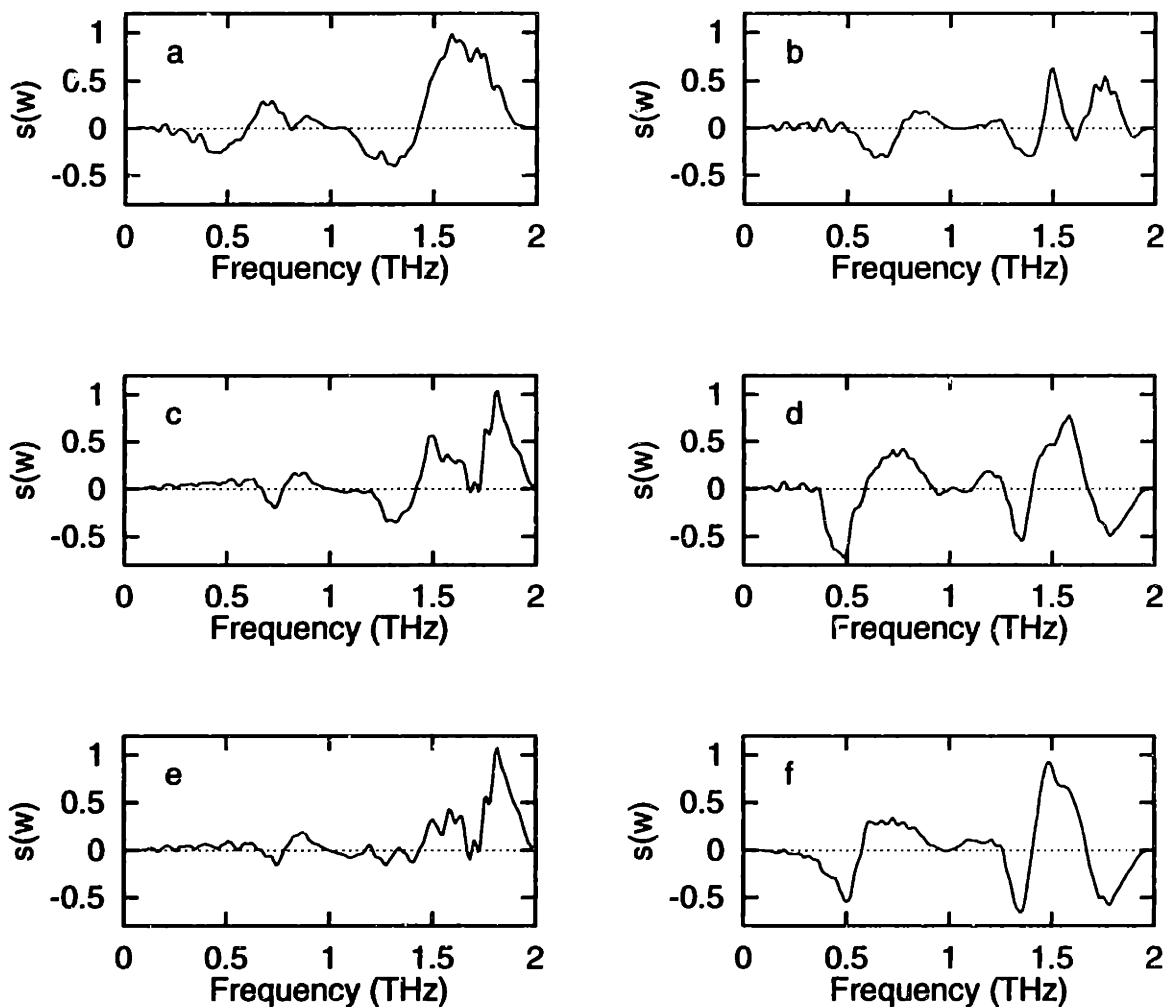


Figure 5-10: Contribution to the formation value of the logarithmic average of the frequencies for some ordered configurations in the Ar-Kr system. The plots correspond to the following structures in the Strukturbericht notation: a)  $L1_0$ , b)  $L1_1$ , c) Ar-rich  $L1_2$ , d) Kr-rich  $L1_2$ , e) Ar-rich  $DO_{22}$ , and f) Kr-rich  $DO_{22}$ .

and  $\rho_{BB} = 1$ . The linear term of the expansion does not depend on the four variables independently, but only on  $\Delta\epsilon \equiv \epsilon_{AB} - (\epsilon_{AA} + \epsilon_{BB})/2$  (“chemical affinity”) and  $\Delta\rho \equiv \rho_{AB} - (\rho_{AA} + \rho_{BB})/2$  (“size mismatch”):

$$\overline{\Delta\ln(\omega)}_{L1_0} \approx 0.84\Delta\epsilon - 2.86\Delta\rho. \quad (5.8)$$

For an ordering system, a positive value of  $\overline{\Delta\ln(\omega)}$  reduces the ordering tendency of the system. A similar expression can be computed for the formation *energy* of  $L1_0$ :

$$\Delta E_{L1_0} \approx -4.70\Delta\epsilon + 4.05\Delta\rho. \quad (5.9)$$

A negative value of  $\Delta E_{L1_0}$  corresponds to an ordering tendency. Equations 5.8 and 5.9 divide the parameter space  $(\Delta\epsilon, \Delta\rho)$  in four areas (see figure 5-11). In the unshaded areas,  $\Delta E_{L1_0}$  and  $\overline{\Delta\ln(\omega)}_{L1_0}$  have opposite sign and the effect of the lattice vibrations is to reduce the (ordering or segregating) transition temperature. In a small area of parameter space (shaded areas in figure 5-11) vibrations tend to increase the transition temperature.

An intuitive argument indicates that the lattice vibrations may *lower* the transition temperatures. In ordering systems, A–B bonds have lower energy than the average of the A–A and B–B bonds. *Usually* lower energy correlates with stiffer bonds and therefore lower vibrational entropy. This lower entropy will make the ordered structure less stable and hence its transition temperature will be lower. A similar argument can be applied to segregating systems with the same conclusion (the effect of lattice vibrations would be to reduce the transition temperature in miscibility gaps). Although this simplified picture is true for most of the parameters in figure 5-11, it breaks down in the shaded area, showing that there may be systems for which the lattice vibrations *increase* the transition temperatures. Of course, the reason for the failure of the above argument is that lower energy for a chemical bond does not *always* correlate with stiffer (higher vibrational frequency) bonds.

The results obtained in this section are based on just one ordered structure in a very simple system, modeled with pair potentials. These results may not be valid for other system. They should only be considered as a guideline for analyzing simple cases.

## 5.5 Conclusions

In this chapter, we have shown that the effect of the lattice vibrations on phase stability of substitutional alloys can be computed without much effort when the energetics of the system can be modeled with classical potentials. The straightforward evaluation of the potential functions and their derivatives allow the calculation of the atomic spring constants. Once the spring constants are known, the dynamical matrix at any point in reciprocal space and the vibrational density of states for any configuration  $\vec{\sigma}$  can be evaluated. By performing a cluster expansion of the vibrational free energy, the vibrational effective interactions are obtained.

We applied these concepts to the study of isotopic mixtures, showing that the

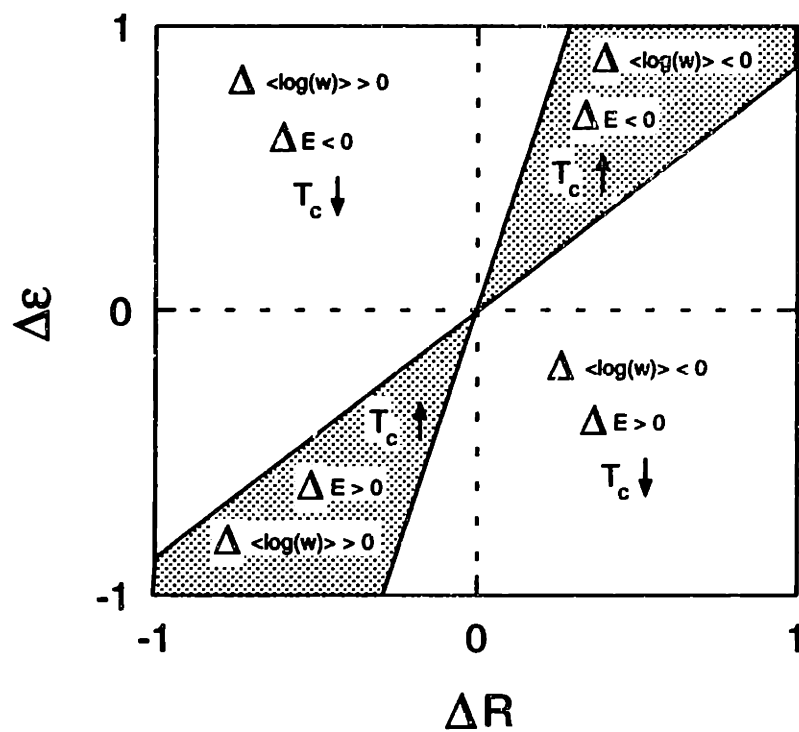


Figure 5-11: Trends in the effect of lattice vibrations on phase stability. The shaded region corresponds to the set of LJ parameters that define systems in which the lattice vibrations tend to increase the transition temperatures.

vibrational effect alone can induce ordering tendencies. Any isotopic mixture will be phase separating, but the transition temperatures are in the milli-Kelvin range, and therefore these transitions are not expected to be observed in the laboratory.

A very simple model of the energetics of mixtures of Ar and Kr was used to study the phase diagram of the binary alloy on the fcc lattice. If only the energy is cluster expanded, then the phase diagram shows an order-disorder transition from the  $L1_0$  phase to the disordered alloy at  $T_c \sim 64\text{K}$ . If the lattice vibrations are included in the  $\bar{\sigma}$ -ensemble free energy, then the transition temperature is predicted to be  $T_c \sim 56\text{K}$ . In other words, the lattice vibrations reduce the predicted transition temperature by  $\sim 12\%$ . We found that the most important contribution to the vibrational effective interactions originates in the medium to high frequency part of the spectrum.

By extending the model of Ar-Kr alloys to general binary alloy modeled with Lennard-Jones potentials, we studied the trends of the effect of the lattice vibrations on phase stability with respect to chemical affinity and size mismatch between the alloy species. We found that for most systems the vibrations will lower the transition temperatures, in agreement with an intuitive description of the effect of vibrations. However, there are some combinations of chemical affinity and size mismatch for which the lattice vibrations are expected to increase the transition temperatures.

As described in appendix C, the classical potential models are not a reliable tool to make quantitative predictions about properties the potentials were not fitted to. For instance, in spite of the simple bonding of the rare gases the potentials used here for Ar and Kr had to be improved with multibody corrections to reproduce other solid-state properties [12]. The calculations in this chapter have to be regarded as *qualitative* predictions about the systems studied. To be able to make reliable *quantitative* predictions, first-principles approaches have to be used. In chapter 6, we analyze the approximate schemes that have been used in the literature to study the effect of lattice vibrations from first principles, and develop a more reliable method that we apply to the study of Si-Ge alloys.





# Chapter 6

## Lattice vibrations and phase stability: First-principles methods

In order to make quantitative predictions of the effect of lattice vibrations on phase stability in substitutional alloys, we need to understand the important contributions and trends and to develop the techniques for computing the effect from first principles. In chapter 4, we developed the formalism through which the lattice vibrations can be included in the effective Hamiltonian of a lattice model to study alloy phase stability. Then, in chapter 5, we used simple classical potentials and model systems to analyze the effect of the vibrations on phase stability and study the trends with respect to changes in chemical affinity and size mismatch between the alloy species. In this chapter, we will develop the quantum-mechanical “machinery” needed to complement the above formalism and understanding, and be able to make reliable quantitative predictions about real alloy systems.

First, in section 6.1, we study the MgO–CaO pseudobinary system. The bonding in this oxide mixture is highly ionic, allowing the use of a *relatively* simple first-principles technique to compute the vibrational frequencies. The effect of the vibrational free energy on the phase diagram is assessed. The explicit calculation of the vibrational frequencies in more complex systems, such as intermetallic and semiconductor alloys, is beyond the available computational power and approximate techniques have to be used. The most common of these techniques are the Debye and Einstein approximations, that we review and evaluate in sections 6.2 and 6.3 respectively. We conclude that neither of these techniques provides a practical and reliable tool to compute the effect of lattice vibrations on phase stability of alloys. We discuss alternative approaches in section 6.4. We develop a new technique based on the calculation of a limited number of real-space spring constants in detail in section 6.5. In section 6.6, we apply the new method to study the vibrational free energy in Si–Ge alloys. Finally, the conclusions of this chapter are discussed in section 6.7.

## 6.1 The MgO–CaO pseudobinary system

Both CaO and MgO form the rocksalt structure, which consists of two inter-penetrating fcc sublattices. The cations (Ca or Mg) occupy one of the sublattices, while the anions (O) occupy the other sublattice. When the two oxides are mixed together, the Ca and Mg atoms substitute each other on the cation sublattice. Since Ca and Mg have the same valence, no charge-compensating defects are necessary, and the anion sublattice remains fully occupied. Therefore, all the substitutional disorder occurs in the cation fcc sublattice, and the configurational thermodynamics of the system can be studied with a binary lattice model.

Although considerable miscibility is observed in the MgO–CaO system, no ordered structures are thermodynamically stable and the phase diagram is a eutectic. Since the eutectic temperature is relatively high ( $T_e \sim 2600\text{K}$ ), the first configuration-dependent term in the high-temperature expansion of the vibrational free energy is enough to represent the VECI's. The total ECI on cluster  $\alpha$  can then be expressed as:

$$V_\alpha(T) = V_\alpha^{\text{chem}} + k_B T V_\alpha^{\text{vib}} . \quad (6.1)$$

To determine the values of the chemical ECI we used the Connolly–Williams method [35]. We computed the energy of structures with a number of different cation arrangements. The energies were computed using the first-principles self-consistent potential-induced breathing method (SCPIB) [119, 120]. The SCPIB is a modified version of the electron-gas model of Gordon and Kim [121]. Within the latter scheme, the total energy of the crystal is expressed as the sum of the self-energy of each ion plus the interatomic interaction energy. The SCPIB extends this approach by allowing spherically symmetric relaxations of the ion's charge density in response to the Madelung potential (the so-called “breathing” effect). In its present form, its use is restricted to highly ionic systems where the non-spherical components of the electronic charge density are negligible. This method has more recently been called the spherical self-consistent atomic deformation method (SSCAD) [119, 120]. Due to the assumptions about the electronic density, the SCPIB is well suited for calculations in highly ionic systems with spherical charge densities, such as MgO–CaO. The energies of all structures were minimized with respect to all lattice parameters and internal degrees of freedom. The cluster expansion used in the fit was well converged with pair interactions up to the sixth cation-cation neighbor, three three-body and two four-body chemical ECI's [122].

To compute the VECI's, the vibrational frequencies of ordered structures were computed at 2,992 fcc Chadi–Cohen special k-points (see appendix D and reference [13]). To compute the VECI's we used the Connolly–Williams method [35] fitting the nearest-neighbor pair and triangle VECI's to the value of  $\overline{\Delta \ln(\omega)}$  of two cubic ordered structures with 31 Ca (Mg) atoms and 1 Mg (Ca) atom. The elements of the dynamical matrix were obtained indirectly from the SCPIB wave functions with a method developed by Boyer and Stokes [123].

The free energy of the resulting lattice model was computed by applying a combination of Monte Carlo simulation and the cluster variation method (CVM). The

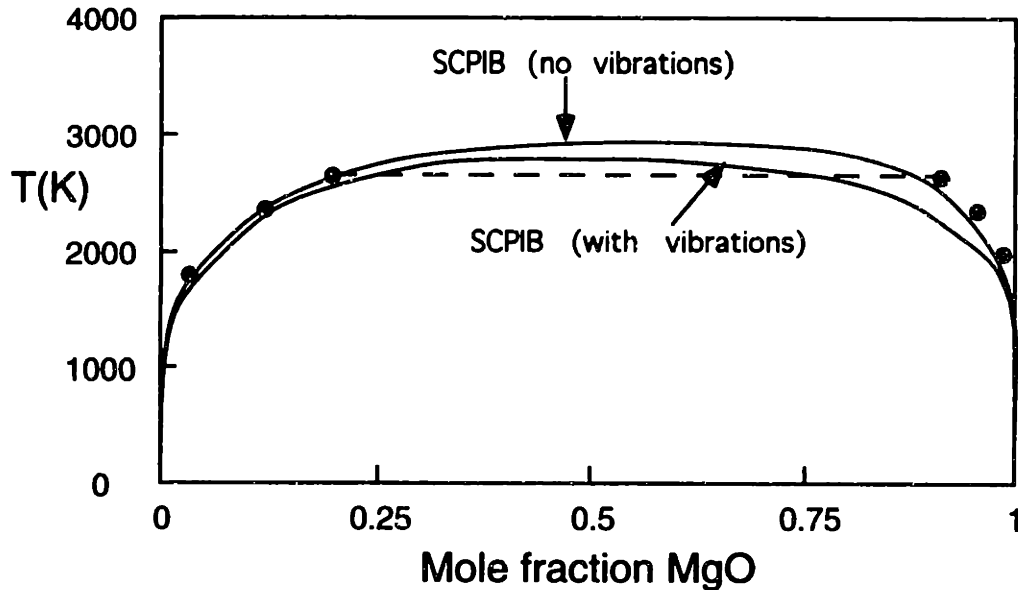


Figure 6-1: Solid part of the CaO–MgO phase diagram computed with and without vibrational effects. A few experimental data points [9] are represented with filled circles.

resulting phase diagrams, with and without the effects of the lattice vibrations, display a miscibility gap and are shown in figure 6-1. As only the solid state part is computed, the region above the experimentally observed eutectic temperature (dashed line) is metastable. Considering the fact that no adjustable parameters were used in the calculation, the agreement with the experimental solubility limits is remarkable. The effect of vibrations is to increase solubility limits. In this particular system the vibrational ECI's are small. The consolute temperature of the miscibility gap is lowered by about 10%, reducing the agreement with the experimental data. The correction due to the vibrations is asymmetric: The increase in solubility of CaO in MgO is much greater than the increase in solubility of MgO in CaO.

It was recently shown [124], using the first-principles pseudopotential method, that the SCPIB underestimates the formation energies of ordered structures in the MgO–CaO system by approximately  $\sim 15\%$ . This correction to the SCPIB chemical ECI's would bring the predicted phase diagram *with* the effect of the lattice vibrations in agreement with experimental observations.

To determine the contribution to  $\overline{\Delta \ln(\omega)}$  of different parts of the frequency spectrum, we computed the values of  $s(\omega)$ , defined in page 122, for five ordered structures. The results are shown in figure 6-2. Similarly to what we found for the Ar–Kr system in section 5.3.2, the low frequencies of the spectrum do not contribute significantly to  $\overline{\Delta \ln(\omega)}$ . For the MgO–CaO system, the intermediate frequencies of the spectrum have the largest contribution to  $\overline{\Delta \ln(\omega)}$ . We will use this result to evaluate the approximate first-principles schemes in section 6.3.

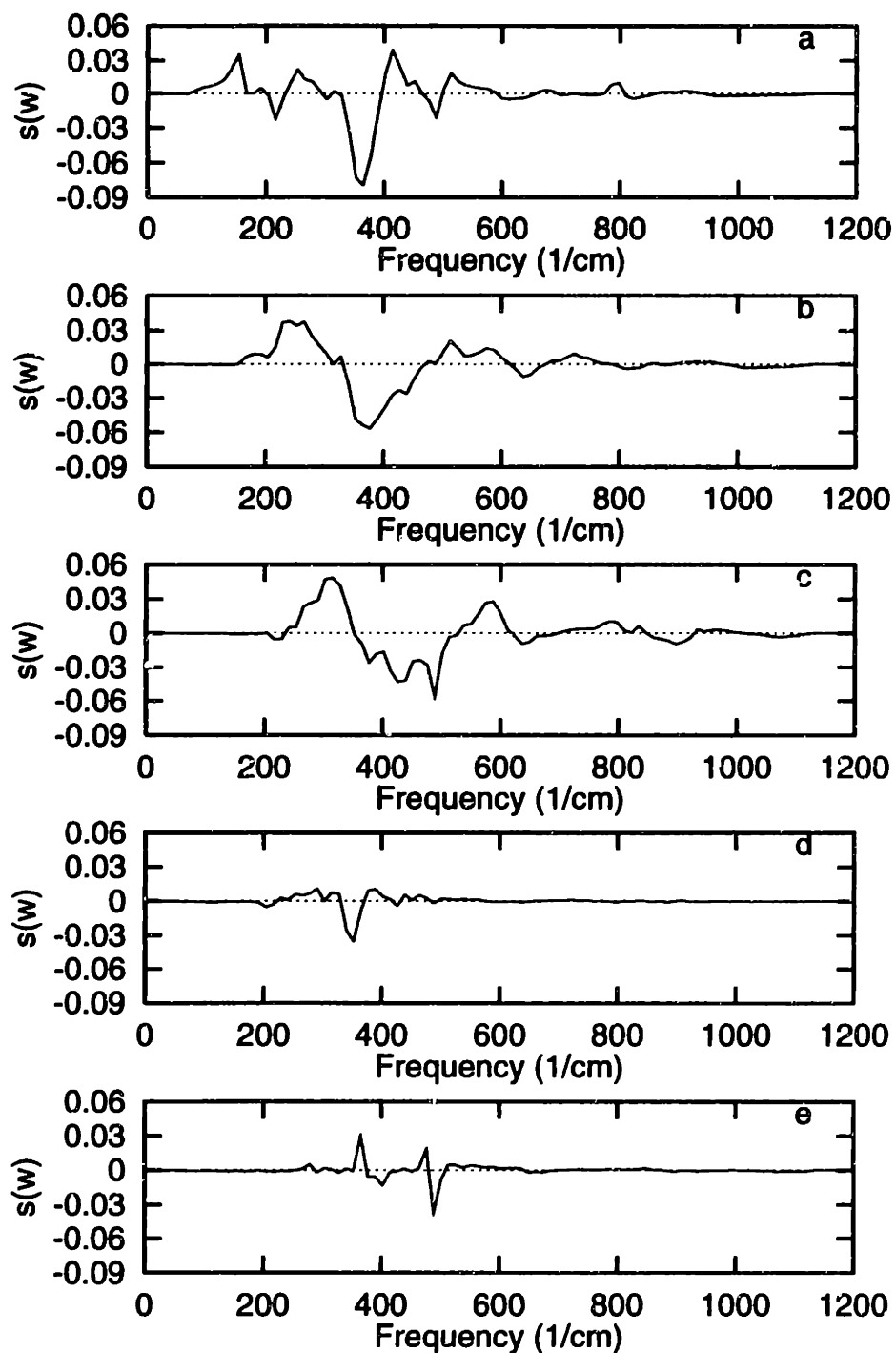


Figure 6-2: Contribution to  $\Delta \overline{\ln(\omega)}$  for some ordered structures in the MgO-CaO system. The plots correspond to the following structures: a) Ca-rich  $L1_2$ , b)  $L1_0$ , c) Mg-rich  $L1_2$ , d)  $2 \times 2 \times 2$  Ca cell with one Mg impurity, and e)  $2 \times 2 \times 2$  Mg cell with one Ca impurity.

We have successfully predicted the MgO–CaO phase diagram without any experimental input. Although the effect of the lattice vibrations for this system is not very large, it is necessary to include the VECI's in the lattice Hamiltonian to make accurate predictions of the solubility limits at the eutectic temperature. Using the SCPIB method, the vibrational frequencies at a large number of k-points can be computed for relatively complex ordered configurations. This success can not be easily imitated for other systems with more complex bonding, such as intermetallic or semiconductor alloys. The highly ionic character of the bonding in the MgO–CaO system allows the use of the SCPIB method, which is less computer-time demanding than the methods necessary to make accurate predictions in more complex systems. For this reason, approximate schemes, that do not require the calculation of the dynamical matrix, have been applied extensively. We describe the most popular of these approximations in section 6.2 and evaluate their performance in section 6.3.

## 6.2 Approximate schemes

The calculation of  $\Delta \overline{\ln(\omega)}$  for several ordered structures of binary alloys with complex bonding from first principles is beyond the current computer power because it amounts to computing the full phonon dispersion relations for structures with complex unit cells. For this reason, simplified models have been developed in recent years to make these calculations tractable. In this section, we review these simplified schemes. Models based on the Debye approximation of the vibrational density of states are reviewed in section 6.2.1, while local harmonic or “Einstein” approximations are described in section 6.2.2. In section 6.3, we assess the accuracy of these approximations using a simple model system for which the exact results can be computed.

### 6.2.1 Debye model

In the Debye model, the solid is considered as an elastic continuum with the same elastic constants as the true solid. The vibrational density of states is then parabolic, with a cutoff frequency,  $\omega_D$ , given by the condition that the total number of frequencies should equal the  $3N$  degrees of freedom of the ions. The Debye temperature is defined as  $\theta_D = \hbar\omega_D/k_B$ , and can be computed as [125]:

$$\theta_D = \frac{2\pi\hbar}{k_B} \left( \frac{9}{4\pi} \frac{N}{V} \right)^{1/3} \left\{ \int \left[ \frac{1}{c_1^3} + \frac{1}{c_2^3} + \frac{1}{c_3^3} \right] \frac{d\Omega}{4\pi} \right\}^{-1/3}, \quad (6.2)$$

where  $c_1$ ,  $c_2$ , and  $c_3$  are the three speeds of sound in a given direction of propagation,  $N/V$  is the atomic number density, and the integral is over all the possible directions. If the elastic constants ( $C_{ij}$ ) and density ( $\rho$ ) of the material are known, the speeds of

sound can be computed solving the secular equation [125]:

$$\begin{vmatrix} \Gamma_{11} - \rho c^2 & \Gamma_{12} & \Gamma_{13} \\ \Gamma_{12} & \Gamma_{22} - \rho c^2 & \Gamma_{23} \\ \Gamma_{13} & \Gamma_{23} & \Gamma_{33} - \rho c^2 \end{vmatrix} = 0, \quad (6.3)$$

where the coefficients  $\Gamma_{ij}$  depend on the direction cosines ( $m$ ,  $n$ , and  $l$ ) of the propagation vector through:

$$\begin{aligned} \Gamma_{11} &= l^2 C_{11} + m^2 C_{66} + n^2 C_{55} + 2mnC_{56} + 2nlC_{15} + 2lmC_{16} \\ \Gamma_{22} &= l^2 C_{66} + m^2 C_{22} + n^2 C_{44} + 2mnC_{21} + 2nlC_{46} + 2lmC_{26} \\ \Gamma_{33} &= l^2 C_{55} + m^2 C_{44} + n^2 C_{33} + 2mnC_{34} + 2nlC_{35} + 2lmC_{45} \\ \Gamma_{12} &= l^2 C_{16} + m^2 C_{26} + n^2 C_{45} + mn(C_{46} + C_{25}) + nl(C_{14} + C_{56}) + lm(C_{12} + C_{66}) \\ \Gamma_{13} &= l^2 C_{15} + m^2 C_{46} + n^2 C_{35} + mn(C_{45} + C_{36}) + nl(C_{13} + C_{55}) + lm(C_{14} + C_{56}) \\ \Gamma_{23} &= l^2 C_{56} + m^2 C_{24} + n^2 C_{34} + mn(C_{44} + C_{23}) + nl(C_{36} + C_{45}) + lm(C_{25} + C_{46}). \end{aligned} \quad (6.4)$$

Assuming a Debye-like distribution of frequencies, the vibrational free energy of an ordered structure  $\vec{\sigma}$  can be computed [126] once  $\theta_D$  is known for that configuration. The resulting high-temperature limit of the vibrational free energy has the same form as equation 4.16 with:

$$\overline{\ln(\omega)}_{Debye} = 3 \ln \left( \frac{k_B \theta_D}{\hbar} \right) - 1. \quad (6.5)$$

Some of the effects of anharmonicity (e.g., thermal expansion) can be taken into account by using the Debye-Grüneisen model [127]. Since we are only evaluating the approximations to reproduce the harmonic behavior, these effects will not be considered.

In most studies where *ab-initio* methods are used, computing all the elastic constants is very difficult and further approximations are necessary. Assuming constant transverse and longitudinal sound velocity, given by  $c_t = (L/\rho)^{1/2}$  and  $c_l = (S/\rho)^{1/2}$ , where  $\rho$  is the density, and using empirical relationships between the bulk modulus and the shear ( $S$ ) and longitudinal ( $L$ ) moduli (valid for nonmagnetic cubic elements), Moruzzi, Janak and Schwarz [127] derived the following approximation to equation 6.2:

$$\theta_D = 0.617(6\pi^2)^{1/3} \frac{\hbar}{k_B} \left[ \frac{v^{1/3} B}{M} \right]^{1/2}, \quad (6.6)$$

where  $v$  is the average volume per atom,  $M$  is the average atomic weight and  $B$  is the bulk modulus obtained from the binding curve as:

$$B = v \left. \frac{\partial^2 u}{\partial v^2} \right|_{v_0}, \quad (6.7)$$

where  $u$  is the energy per atom and  $v_0$  is the equilibrium value of  $v$ .

We will refer to this scheme to approximate the Debye model as the Moruzzi-Janak-Schwarz (MJS) approximation. The MJS approximation has been widely used

in the studies of alloy thermodynamics. Studies of binary (Ag–Cu [30], Co–Pt [128], Au–Ni [129], Ni–Al [130], Ti–Al [131], Au–Cu, Au–Pd, and Au–Ag [132], Cd–Mg [31]), pseudobinary (InP–InSb [133], GaAs–InAs [134]), and ternary (Ru–Nb–Zr [135]) alloys have been reported in the literature.

The popularity of the MJS scheme is due to its simplicity: the quantities needed (volume and bulk modulus) are by-products of the calculation of the relaxed formation energies for the ordered structures. However, its validity for the calculation of *formation* free energies in alloys has not been demonstrated. For an ordered structure with composition  $c$ , the formation value of the coefficient of the leading term in equation 4.16 in the MJS scheme is:

$$\Delta \overline{\ln(\omega)}_{MJS} = \frac{3}{2} \left[ \ln \left( \frac{B}{B_A^c B_B^{1-c}} \right) + \ln \left( \frac{r}{r_A^c r_B^{1-c}} \right) + \ln \left( \frac{M_A^c M_B^{1-c}}{cM_A + (1-c)M_B} \right) \right], \quad (6.8)$$

where  $r$  is the average Wigner-Seitz radius of the structure (i.e.,  $v = 4\pi r^3/3$ ).

As pointed out in section 4.1.4, the exact value of  $\Delta \overline{\ln(\omega)}$  is independent of the atomic masses of the A and B atoms. Both the Debye and MJS approximations fail to reproduce this property (see equations 6.2 and 6.8). An *ad-hoc* way of fixing this deficiency is to drop the last term in equation 6.8. We will refer to this scheme as the modified MJS (mMJS) approximation. To our knowledge the mMJS approximation has not been reported before.

## 6.2.2 Local harmonic model

In the local harmonic (LH) model [136, 137], every atom is assumed to vibrate independently from the other atoms, as if the rest of the structure were frozen at its equilibrium position. The vibrational density of states is then approximated by a set of delta functions at the Einstein frequencies of each atom. This is equivalent to neglecting the elements in the dynamical matrix outside the  $3 \times 3$  block diagonal. With this simplification, the problem of diagonalizing the  $3N \times 3N$  dynamical matrix is reduced to the diagonalization of  $N$   $3 \times 3$  matrices. This model has been used to compute thermodynamic and structural properties of perfect crystals [137], point defects [138], grain boundaries [137], interfacial segregation [139], and phase transitions at surfaces [140].

In the LH approximation the second moment of the vibrational density of states,  $\overline{\omega^2}$ , is obtained exactly. The second moment can be related to the trace of the dynamical matrix  $D$  through [98]  $\overline{\omega^2} = \text{Trace}(D)/N$ . The trace of  $D$  is preserved by the LH approximation making  $\overline{\omega^2}_{LH} = \overline{\omega^2}_{exact}$ . The other moments necessary to compute the free energy (most importantly  $\overline{\ln(\omega)}$ ) are approximate in the LH model.

In the next section we define a model system for which  $\overline{\ln(\omega)}$  can be computed

Set#	$\epsilon_{AB}$	$\rho_{AB}$	$\epsilon_{BB}$	$\rho_{BB}$
1	1.437	1.003	1.371	1.062
2	1.185	1.031	1.371	1.062
3	0.813	1.031	1.371	1.062
4	0.813	1.000	1.000	1.000
5	1.000	0.974	1.000	1.000

Table 6.1: Sets of Lennard–Jones parameters for the model alloy systems. In all cases,  $\epsilon_{AA} = 1$  and  $R_{AA} = 1$  without loss of generality. Set number 1 corresponds to a simplified model of the Ar–Kr system [12].

exactly. Using this model system, we compare the exact results with those obtained using the approximations described in this section.

### 6.3 Evaluation of simplified models

To be able to assess the performance of the schemes reviewed in section 6.2, we need to define a model system for which the exact and approximated VECI’s can be computed [109]. We chose a set of 5 model alloy systems on the fcc lattice. Similarly to the models used in sections 5.3 and 5.4, the A and B atoms of the alloy interact through Lennard–Jones (LJ) pair potentials.

The values of the LJ parameters used in the calculations are summarized in table 6.1. The values of the atomic masses used were  $M_A = 39.95$  a.u. and  $M_B = 83.80$  a.u. (resembling Ar and Kr), unless otherwise stated. The geometry (unit cell shape and size, and the internal coordinates of the atoms) of all the ordered structures was optimized to minimize the energy.

To perform the integrals over the Brillouin zone to get  $\overline{\ln(\omega)}$ , we used the equivalent of 408 special fcc points obtained with the Chadi–Cohen scheme [13]. The resulting relative integration error in  $\Delta\overline{\ln(\omega)}$  is less than  $10^{-3}$ .

To condense the results for the 5 model systems, we computed the averages of  $\Delta E$  and  $\Delta\overline{\ln(\omega)}$  for 16 ordered structures. These are the same structures used in section 5.3 to study the Ar–Kr system. The results are shown in table 6.2.

For the same set of ordered structures, we computed  $\Delta\overline{\ln(\omega)}$  using the Debye, MJS, mMJS, and LH models. Figure 6-3 shows a detailed comparison of the performance of these models for the first set of LJ parameters in table 6.1. A summary of the results for the other sets of LJ parameters is shown in table 6.3.

It can be seen from table 6.3 that the performance of the models varies between the various sets of LJ parameters. However, the local harmonic model systematically outperforms the other models, for the fcc–LJ alloys studied. The magnitude of the LH error in  $\Delta\overline{\ln(\omega)}$  is acceptable (compare tables 6.2 and 6.3) for a first attempt at including the lattice vibrations in the free energy models. However, the implementation of the LH model with first–principles approaches is not straightforward. In fact,



Set#	Average	Average
	$\Delta E$	$\overline{\Delta \ln(\omega)}$
1	-0.8610	0.0931
2	0.0735	-0.0816
3	1.4379	-0.3270
4	0.6887	-0.1345
5	0.0038	0.0218

Table 6.2: Average values of  $\Delta E$  and  $\overline{\Delta \ln(\omega)}$  for the 16 ordered structures considered, using the sets of LJ parameters of table 6.1. The energies are in units of  $\epsilon_{AA}$ .

Set#	RMS error of approximations			
	Debye	MJS	mMJS	LH
1	0.1378	0.0403	0.0848	0.0321
2	0.1036	0.0255	0.0780	0.0190
3	0.1442	0.0524	0.0907	0.0280
4	0.0891	0.0877	0.0050	0.0026
5	0.1047	0.0744	0.0175	0.0092

Table 6.3: Root mean square (RMS) error of the prediction of the value of  $\overline{\Delta \ln(\omega)}$  for 16 ordered structures using the Debye, MJS, mMJS, and LH models, for the sets of LJ parameters shown in table 6.1.

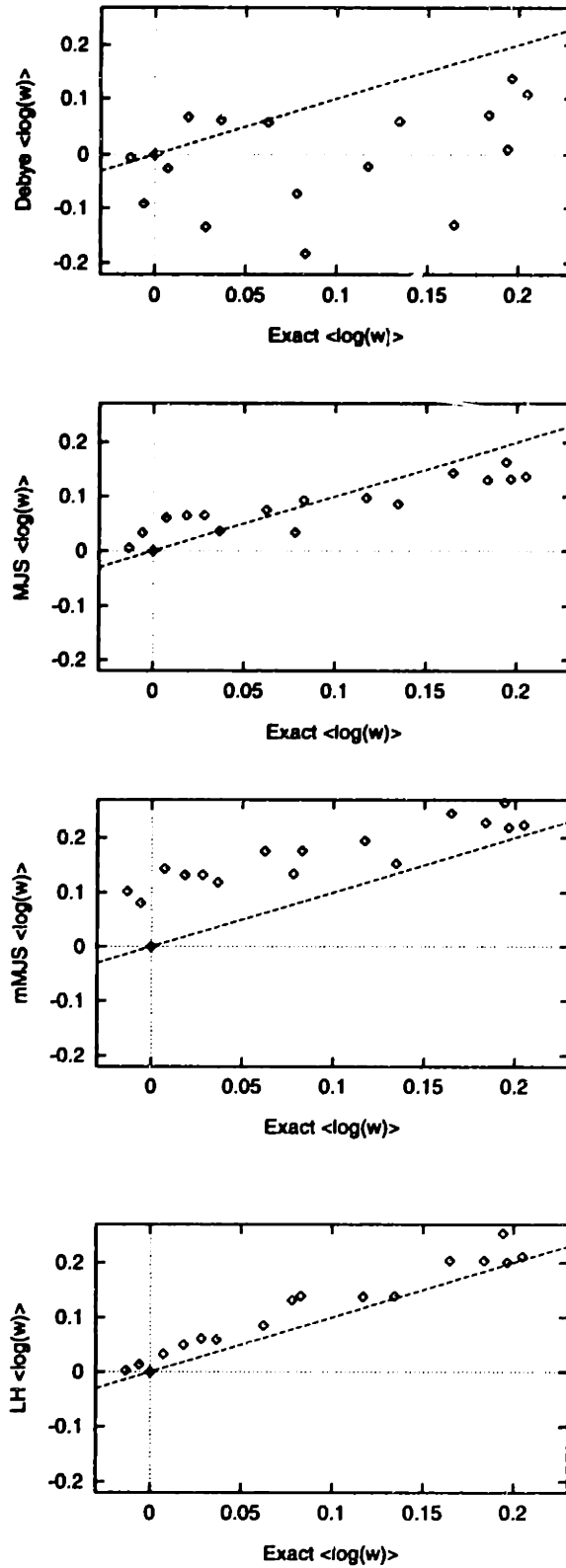


Figure 6-3: Comparison of the exact value of  $\Delta \ln(\omega)$  with the prediction of the Debye, MJS, mMJS, and LH models for the 16 ordered structures. The closer the points lie to the dashed line, the better the approximation.

the calculation of the Einstein frequencies of the atoms in the unit cell of a given structure is almost as difficult as the calculation of all the spring constants (from which, the exact value of  $\overline{\ln(\omega)}$  can be obtained).

The LH model is a very useful technique to approximate the vibrational properties of non-periodic systems (e.g., defects, surfaces, interfaces) modeled with classical potentials. In these cases, the dynamical matrix is easily obtained, while finding its eigenvalues is difficult because of the lack of periodicity. The LH model greatly facilitates this diagonalization as described in section 6.2.2. In the case of simple ordered structures of binary alloys, modeled with first-principles methods, the difficult part of the problem is to obtain the dynamical matrix, while its diagonalization is simplified by the aid of Bloch's theorem. For all these reasons, the LH model, although quite accurate, is not practical for first-principles calculations of vibrational properties of alloys.

The performance of the approximations based on the Debye model (Debye, MJS, and mMJS) is not as good as the LH model (see table 6.3). The errors are comparable in magnitude to  $\Delta\overline{\ln(\omega)}$ . Although the MJS and mMJS models are approximations to the Debye model, the former perform systematically better than the later for the cases studied. We do not understand this behavior.

We identified three sources of error in the Debye and MJS models: contribution of high frequency vibrations to  $\Delta\overline{\ln(\omega)}$ , lack of sampling of certain spring constants, and mass effects.

As noted in sections 5.3.2 and 6.1, the high-frequency part of the vibrational spectrum has a very important contribution to  $\Delta\overline{\ln(\omega)}$ . Since the Debye and MJS models are based on the elastic properties, they lack information about this part of the spectrum. On the other hand the LH model is a better approximation to the optical modes. This could explain the better performance of the LH model.

The value of the bulk modulus used as input in the MJS model does not depend on some of the atomic spring constants. For example, in a cubic structure, the bulk modulus only depends on the central spring constants, but not on the off-diagonal elements of the spring constant tensors. In cases where these off-diagonal elements contribute significantly to  $\Delta\overline{\ln(\omega)}$ , the MJS model will fail to capture the essential features of the system.

The third source of error in the Debye and MJS models is the dependence of  $\Delta\overline{\ln(\omega)}$  on the atomic masses of the constituent atoms. As pointed out in section 4.1.4, the exact value of  $\Delta\overline{\ln(\omega)}$  is independent of  $M_A$  and  $M_B$ , while the predicted value in the Debye and MJS models depends on the masses through equations 6.2 and 6.8. It can be shown that the contribution of the masses in both models has exactly the same form. Figure 6-4 illustrates the size of this effect for an alloy at composition 1/2 as a function of the mass ratio. It can be seen that for an alloy of mass ratio 2 (roughly the Ar-Kr case) the effect of the masses is of the order of the total value of  $\Delta\overline{\ln(\omega)}$  (see table 6.2), making the predictions of these models unreliable. The *ad-hoc* correction introduced in the mMJS model improved the results for some cases, but it is not consistently better than the MJS model.

We conclude that neither the Debye nor the LH model provides a practical and accurate tool for the calculation of the effect of the lattice vibrations on phase stability

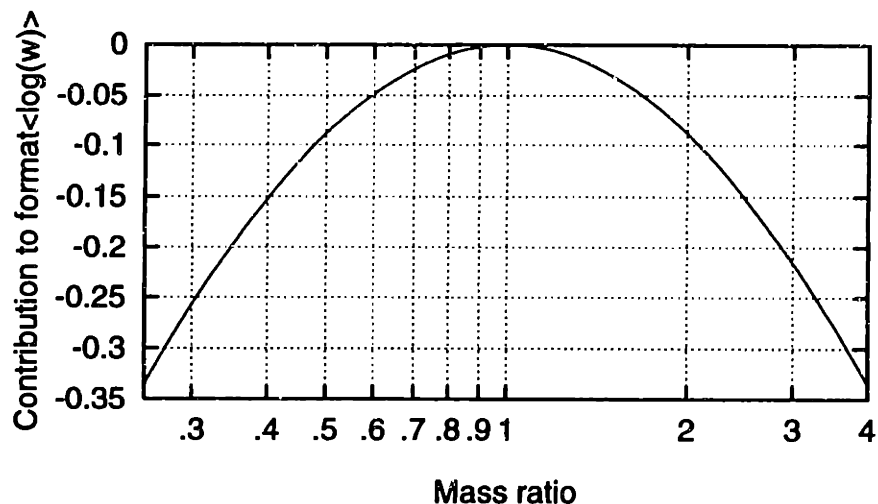


Figure 6-4: Contribution of the masses to the value of  $\overline{\Delta \ln(\omega)}$  in the MJS and Debye models, for an alloy of composition 1/2, as a function of the mass ratio,  $M_A/M_B$ .

of alloys from first principles. In the next section, we explore other possible approaches that, although more complicated than the Debye model, may provide the solution to our problem.

## 6.4 Alternative frameworks for *ab-initio* calculations

We showed in section 6.3 that neither the local harmonic nor the Debye-like models provide the framework for first-principles calculations of the effect of lattice vibrations on the phase stability of alloys. The LH model is relatively accurate, but its implementation in first-principles calculations is difficult, whereas the Debye-like models are of very easy implementation, but the predictions they make are not reliable. Therefore, alternative approaches are needed. In this section, we explore methods that could make the calculations both feasible and accurate.

With the aid of the Hellmann–Feynman theorem [141] for the calculation of forces on atoms, frozen phonon techniques [142, 143] can be used to compute the dynamical matrix at high-symmetry  $k$ -points. These calculations are feasible with first-principles methods and have been reported for several systems (see for example [143]). An important question to answer is how many  $k$ -points are needed to obtain a converged value for  $\overline{\Delta \ln(\omega)}$ . To address this question, we computed the  $k$ -point convergence of  $\overline{\Delta \ln(\omega)}$  for some of the structures studied in previous sections for the first set of LJ parameters in table 6.1 (Ar–Kr system).

For the pure elements, the  $k$ -points were chosen according to the Chadi–Cohen

Chadi-Cohen iteration	Structures					
	fcc	L1 <sub>0</sub>	L1 <sub>1</sub>	L2 <sub>0</sub>	L1 <sub>2</sub>	DO <sub>22</sub>
1	2	2	4	2	1	1
2	10	12	15	6	4	3
3	60	80	102	40	20	20
4	408	576	748	288	120	144

Table 6.4: Number of k-points for the different ordered structures as a function of the iteration number in the Chadi-Cohen scheme [13].

scheme [13]. For the ordered structures, the k-points corresponded to the equivalent set of k-points in reciprocal space. Of course, due to the different symmetry and unit cell of the ordered structures, the actual number of *distinct* k-points varied with the ordered structures. Table 6.4 summarizes the number of distinct k-points for the ordered structures for different number of iterations in the Chadi-Cohen scheme.

We computed  $\overline{\Delta \ln(\omega)}$  for some of the ordered structures as a function of the iteration in the Chadi-Cohen scheme to select the k-points. The convergence results are shown in figure 6-5. It can be seen that convergence of the formation values within 1% is achieved for the third set of k-points. However, if only the first iteration is used, the convergence error in  $\overline{\Delta \ln(\omega)}$  is less than 0.016. This corresponds to less than 20% of the average value of  $\overline{\Delta \ln(\omega)}$ . The simplicity of the Lennard-Jones system studied precludes the extrapolation of this convergence property to more complex systems, for which a quantum-mechanical method is necessary. However, if the fast convergence of  $\overline{\Delta \ln(\omega)}$  is a general feature, it will open the road for first-principles frozen phonon calculations at a very few, high-symmetry k-points, for the calculation of vibrational free energy of alloys.

A second possibility to use first-principles approaches is to exploit the recent advances in linear response methods [144, 145], based on the pseudopotential method (for a review of the pseudopotential method, see [20]). The linear response method can be used to compute the phonon frequencies of specific ordered structures. The linear response function, which is the “expensive” part of the calculation, has to be computed for each configuration of atoms separately. The current computing power would allow only calculations of this sort for very few, high-symmetry ordered structures. For simple systems, where a few ordered structures are enough to obtain a reliable cluster expansion of  $\overline{\Delta \ln(\omega)}$ , this method can provide a viable approach for first-principles calculations.

For systems where the pseudopotentials of the two atoms forming the alloy are similar enough, the identity of the atoms can be treated as a perturbation in the linear response method. The reference state is a virtual crystal formed by a “virtual” atom sitting at the ideal lattice sites. The virtual atom is described with a pseudopotential equal to the arithmetic average of the pseudopotentials of the real atoms. For these systems, the linear response calculations are greatly simplified, because with the

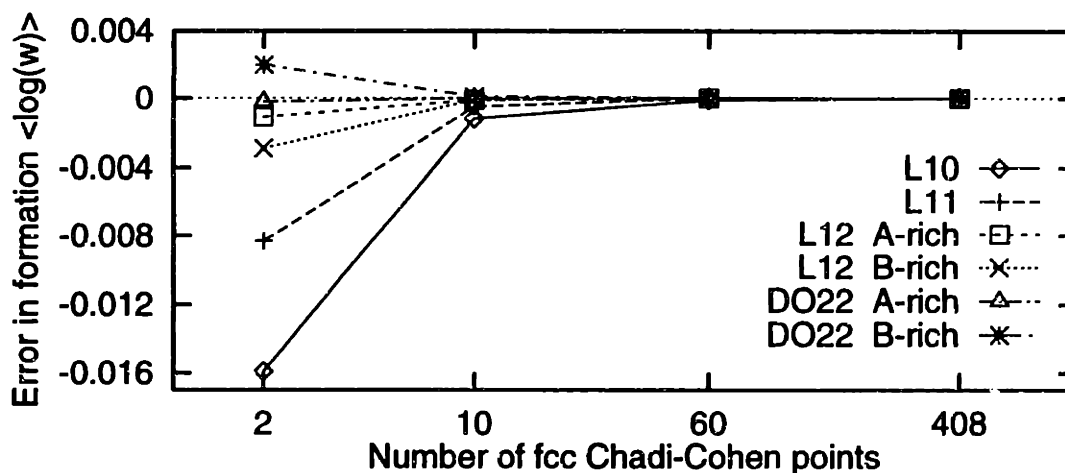


Figure 6-5: Convergence error in  $\Delta \overline{\ln(\omega)}$  as a function of the number of fcc Chadi-Cohen k-points.

calculation of only one response function, we can obtain the geometries of relaxed structures, formation energies, and phonon frequencies of ordered and disordered configurations. It has been successfully applied to the Si-Ge system [146].<sup>1</sup> In most cases, however, the pseudopotentials of the two species are not similar enough for a perturbative treatment of the atomic identity. This is the case, for instance, in metallic alloys and oxide mixtures.

A third option for first-principles calculations would involve an extension of the method recently proposed by Wei and Chou [147]. With this method, one obtains the real-space spring constant tensors by computing the forces on atoms of perturbed unit cells and inverting the resulting set of equations. This approach has been very successful in computing the phonon frequencies and thermodynamic properties of elemental semiconductors [147, 148, 149]. It is very computer intensive because it requires the calculation of forces for several low-symmetry large unit cells, in order to obtain *all* the non-negligible spring constants. These unit cells would become even larger and of lower symmetry for ordered configurations of an alloy. However, the knowledge of *all* the spring constants is not really necessary for the calculation of  $\Delta \overline{\ln(\omega)}$ . In fact,  $\Delta \overline{\ln(\omega)}$  is an integrated quantity over the density of states and therefore does not depend on the fine details of the phonon dispersion relations. Exploiting this fact, we developed a hierarchy of approximations to get  $\Delta \overline{\ln(\omega)}$ . This new approach is explained in the next section.

<sup>1</sup>The similarity of the pseudopotentials of Si and Ge allowed these calculations.

## 6.5 A proposed new approach

As discussed in the previous section, the new approach is based on an extension of the method proposed by Wei and Chou [147] to obtain the real-space spring constant tensors. In their method, the spring constants are fitted to reproduce the forces on atoms of perturbed structures. If the atoms are perturbed slightly from their equilibrium positions, the potential energy of the system can be written as (recall equation 4.7):

$$\begin{aligned}
 V(\vec{u}(1), \dots, \vec{u}(N)) &= E_0 + \sum_{\alpha\beta l l'} \frac{1}{2} \Phi_{\alpha\beta}(l, l') u_{\alpha}(l) u_{\beta}(l') \\
 &+ \sum_{\alpha\beta\gamma l l' l''} \frac{1}{6} \Phi_{\alpha\beta\gamma}(l, l', l'') u_{\alpha}(l) u_{\beta}(l') u_{\gamma}(l'') \\
 &+ \mathcal{O}(u^4),
 \end{aligned} \tag{6.9}$$

where  $\vec{u}(l) = \vec{R}(l) - \vec{R}_0(l)$  is the displacement of ion  $l$  away from the position of lowest energy,  $\Phi_{\alpha\beta}(l, l')$  is the harmonic spring constant tensor element along directions  $\alpha$  and  $\beta$  of the  $l$  and  $l'$  atoms of the crystal, i.e.,  $\Phi_{\alpha\beta}(l, l') = \partial^2 V / \partial u_{\alpha}(l) \partial u_{\beta}(l')$ , and  $\Phi_{\alpha\beta\gamma}(l, l', l'')$  and higher order terms represent the anharmonic contribution to the energy. The  $\alpha$  component of the force on atom  $l$  is the negative derivative of the above potential energy:

$$\begin{aligned}
 F_{\alpha}(l; \vec{u}(1), \dots, \vec{u}(N)) &= - \frac{\partial V(\vec{u}(1), \dots, \vec{u}(N))}{\partial u_{\alpha}(l)} \\
 &= - \sum_{\beta l'} \Phi_{\alpha\beta}(l, l') u_{\beta}(l') \\
 &\quad - \sum_{\beta\gamma l' l''} \Phi_{\alpha\beta\gamma}(l, l', l'') u_{\beta}(l') u_{\gamma}(l'') \\
 &\quad + \mathcal{O}(u^3).
 \end{aligned} \tag{6.10}$$

If the displacements are small, the anharmonic terms can be neglected and the forces on the atoms of a perturbed structure are linear combinations of the elements of the spring constants tensors. By computing the forces on the atoms for a few perturbed structures, a set of linear equations for the spring constant tensors is obtained. If the number of equations is larger than the number of parameters of the spring constant tensors, the numerical values of  $\Phi_{\alpha\beta}(l, l')$  can be obtained by a least-squares procedure [150].

With this method, Wei and Chou computed vibrational and thermodynamic properties of Si and Ge [147, 148, 149] in very good agreement with experimental observations. They used the pseudopotential method [20] and the Hellmann-Feynman theorem [141] to compute forces. To obtain accurate dispersion relations, the spring constant tensors up to the eighth neighbor were computed. This amounts to 31 parameters, for which calculations of forces for several big perturbed supercells are needed. The calculations of the forces using the pseudopotential method are compu-

tationally intensive, requiring tens or hundreds of CPU hours on a supercomputer (in 1995).

To apply this method to study alloys, we would need to perform the calculations on several ordered configurations  $\vec{\sigma}$  to be able to cluster expand the vibrational free energy. Since in these structures the unit cells are larger and the symmetry is lower than in the pure elements, the calculations are more demanding. This precludes the use of the method as developed by Wei and Chou to our problem.

However, the problem is simplified by fact that we are only interested in the value of  $\overline{\Delta \ln(\omega)}$  for the different configurations  $\vec{\sigma}$  and not in the fine details of the dispersion relations and VDOS. While obtaining *all* the non-negligible force constant elements is necessary to reproduce the fine details of the dispersion relations,<sup>2</sup> only a few parameters may be enough to characterize  $\overline{\Delta \ln(\omega)}$ , which is an integrated quantity over the density of states. To test this hypothesis, we developed a hierarchy of approximations to compute  $\overline{\Delta \ln(\omega)}$  for an ordered configuration  $\vec{\sigma}$ . The steps of this procedure are summarized in flowchart of figure 6-6. We now describe the steps of the flowchart in detail.

There are two criteria for selecting the ordered structures for which  $\overline{\Delta \ln(\omega)}$  will be computed. First, the structures should be suitable for the construction of the cluster expansion of  $\overline{\Delta \ln(\omega)}$ . For instance, the averaged cluster functions on the clusters for which we want to compute the VECI's should not be linearly dependent (this would difficult the Connolly-Williams [35] procedure to obtain the VECI's). This criterion has been discussed extensively in the literature (see reference [153, 36] and references therein) and will not be further analyzed here. The second criterion is that the number of atoms in the unit cell of the structures should be small and the structures should have high symmetry. These conditions will make the first-principles calculations of the forces on perturbed atoms feasible.

The space group of the ordered configuration is needed to find the symmetry constraints on the spring constant tensors (see below), and to speed up the first-principles methods to compute the forces on the atoms. There are standard procedures to find the space group of crystals given the unit cell parameters and the coordinates of all the atoms in the unit cell [154].

In most systems, the spring constants decay rapidly with distance. Depending on the system and its crystal structure, first- and second-neighbor spring constants are usually sufficient to account for the most important features of the phonons; while extending the range of spring constants to the fourth or fifth neighbor allows a very fine description of the vibrational modes and frequencies. For our hierarchical method, it is convenient to start with very few spring constant parameters, typically one or two elements of the nearest-neighbor spring constant tensor. As will be discussed later, we will extend this range until we achieve convergence of  $\overline{\Delta \ln(\omega)}$ . For systems where

---

<sup>2</sup>For instance, it is well known that the fifth neighbor spring constants are necessary to reproduce the flatness of the transverse-acoustical mode in Si and Ge [151, 152].



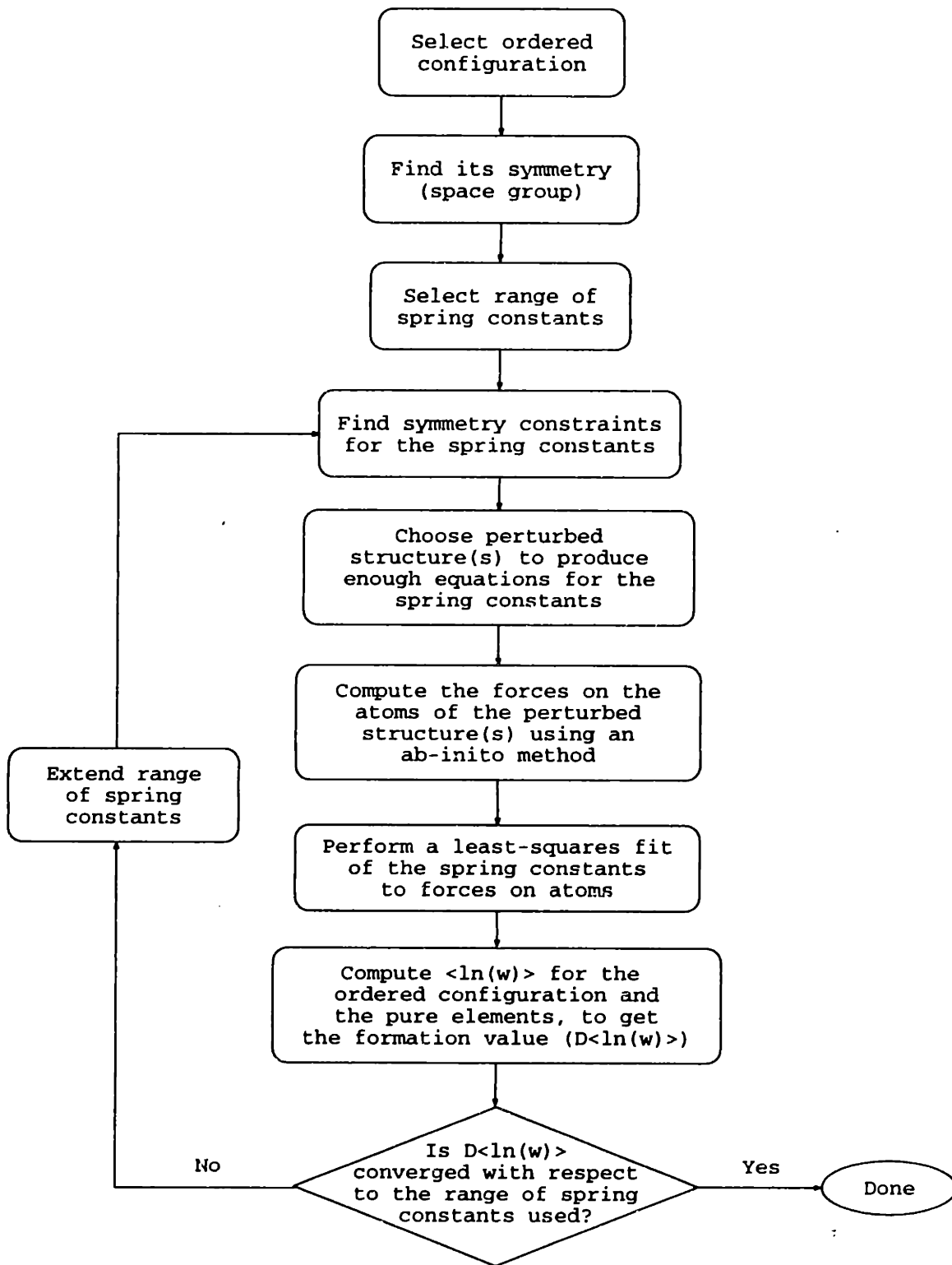


Figure 6-6: Steps for the calculation of  $\Delta \overline{\ln(\omega)}$  (written as  $D\langle \ln(w) \rangle$  in the flow-chart) from first-principles for an ordered configuration  $\vec{\sigma}$  in a substitutional alloy, with the new method.

significant charge transfer between the atoms occurs (such as GaAs), the long range coulombic contribution to the lattice dynamics of the system has to be computed separately from the short range part, through the use of Born effective charges [155].

In general, the nine elements of the spring constant tensor between two atoms are

Find symmetry constraints  
for the spring constants

independent and need to be computed separately.

However, when the atomic pair is part of a crystal with symmetry, not all the elements of  $\Phi_{\alpha\beta}(l, l')$  are independent. The effect of any symmetry element acting on a point in space  $\vec{R}$  can be written as a  $3 \times 3$  real orthogonal matrix (proper or improper rotations)  $\mathbf{S}$  acting on  $\vec{R}$ , plus a rigid translation  $\vec{x}$ . For example, the symmetry element  $(\mathbf{S}|\vec{x})$  maps atom  $l$  onto atom  $l'$  if  $\vec{R}(l') = (\mathbf{S}|\vec{x})\vec{R}(l)$ , i.e.,

$$R_{\alpha}(l') = \sum_{\beta} S_{\alpha\beta} R_{\beta}(l) + x_{\alpha}. \quad (6.11)$$

Furthermore, if the atoms  $l$  and  $l'$  are mapped onto atoms  $L$  and  $L'$  by the symmetry element  $(\mathbf{S}|\vec{x})$ , then the spring constant tensors are related by [98]:

$$\Phi_{\alpha\beta}(L, L') = \sum_{\mu\nu} S_{\alpha\mu} S_{\beta\nu} \Phi_{\mu\nu}(l, l') \quad (6.12)$$

In the special case in which  $(\mathbf{S}|\vec{x})$  maps the  $(l, l')$  pair onto itself, equation 6.12 imposes linear constraints on the values of the elements of the spring constant elements:

$$\Phi_{\alpha\beta}(l, l') = \begin{cases} \sum_{\mu\nu} S_{\alpha\mu} S_{\beta\nu} \Phi_{\mu\nu}(l, l') & \text{if } \vec{R}(l') = (\mathbf{S}|\vec{x})\vec{R}(l) \text{ and } \vec{R}(l) = (\mathbf{S}|\vec{x})\vec{R}(l') \\ \sum_{\mu\nu} S_{\alpha\mu} S_{\beta\nu} \Phi_{\nu\mu}(l, l') & \text{if } \vec{R}(l) = (\mathbf{S}|\vec{x})\vec{R}(l') \text{ and } \vec{R}(l') = (\mathbf{S}|\vec{x})\vec{R}(l) \end{cases}, \quad (6.13)$$

where the second equation is obtained by noting that  $\Phi_{\nu\mu}(l, l') = \Phi_{\mu\nu}(l', l)$ , which expresses the fact that the order in which the second derivatives are taken in the definition of the spring constant tensor (equation 4.8) is not relevant. Once all the constraints are obtained, singular value decomposition techniques [150] can be used to obtain an independent set of parameters of the force constant tensor elements.

The so-called self spring constants,  $\Phi_{\alpha\beta}(ll) = \partial^2 V / \partial u_{\alpha}(l) \partial u_{\beta}(l)$ , can be obtained from all the other spring constants through the use of the ‘‘sum rule’’ that requires that the overall force on the crystal vanish (there are no external forces):

$$\Phi_{\alpha\beta}(ll) = - \sum_{l' \neq l} \Phi_{\alpha\beta}(ll'). \quad (6.14)$$

If this sum rule is used, no extra equations are necessary to obtain the self spring constants, once the other springs are known. Alternatively, the self spring constants can be computed separately from the other spring constants and the sum rule used to verify consistency of the results.<sup>3</sup>

The perturbations of the structures to obtain the forces on the atoms, and hence

---

<sup>3</sup>The deviation away from the sum rule in equation 6.14 provides an estimate of the error in the first-principles method used to compute the forces.

Choose perturbed structure(s) to produce enough equations for the spring constants

the equations for the spring constants, have to be relatively small, so that the harmonic approximation is valid. However, they can not be arbitrarily small because the relative error of the

first-principles method in the values of the forces would increase, making the final assessment of the spring constants inaccurate.

For some structures, there are perturbations for which the first anharmonic corrections to the forces vanish by symmetry.<sup>4</sup> In this case, the first non-zero correction is of higher order and the perturbations can be larger without introducing too much anharmonicity. When this is not the case, we can still isolate the harmonic contribution to the forces from the first anharmonic correction by computing the force for the perturbations  $(\vec{u}(1), \dots, \vec{u}(N))$  and  $(-\vec{u}(1), \dots, -\vec{u}(N))$ :

$$F_{\alpha}(l; \vec{u}(1), \dots, \vec{u}(N)) = - \sum_{\beta l'} \Phi_{\alpha\beta}(l, l') u_{\beta}(l') - \sum_{\beta\gamma l''} \Phi_{\alpha\beta\gamma}(l, l', l'') u_{\beta}(l') u_{\gamma}(l'') + \mathcal{O}(u^3) \quad (6.15)$$

$$F_{\alpha}(l; -\vec{u}(1), \dots, -\vec{u}(N)) = + \sum_{\beta l'} \Phi_{\alpha\beta}(l, l') u_{\beta}(l') - \sum_{\beta\gamma l''} \Phi_{\alpha\beta\gamma}(l, l', l'') u_{\beta}(l') u_{\gamma}(l'') + \mathcal{O}(u^3). \quad (6.16)$$

Subtracting 6.16 from 6.15, we obtain an equation for the spring constants, where the first anharmonic terms are not present:

$$F_{\alpha}(l; \vec{u}(1), \dots, \vec{u}(N)) - F_{\alpha}(l; -\vec{u}(1), \dots, -\vec{u}(N)) = -2 \sum_{\beta l'} \Phi_{\alpha\beta}(l, l') u_{\beta}(l') + \mathcal{O}(u^3) \quad (6.17)$$

The other criterion for the selection of the perturbed structures is that they should provide enough equations for the calculation of the force constant tensor elements that we chose to compute. In general, the perturbed structures are superstructures of the ordered configuration  $\vec{\sigma}$ , where some of the atoms in the unit cell have been slightly moved away from their equilibrium position. One option would be to move all the atoms in the unit cell in a random direction. With this perturbation, the forces will be linear combinations of a large number of spring constant parameters. However, when longer-range spring constants are sought, this random perturbation may not be appropriate, since the relative error in the smaller spring constants will be large. To avoid this problem, the perturbations can be taken so that some forces only depend on long-range spring constants. This can be achieved, for example, by taking a superstructure along a given direction and perturbing only one plane of atoms perpendicular to that direction. In this perturbed structure, the force on

---

<sup>4</sup>The potential function  $V$  has the same symmetry as the crystal. Therefore, if an atom sits on an inversion center, for example, the potential will be an even function of the movement of the atom, making all the even terms in equation 6.10 zero by symmetry.

atoms far from the perturbed plane will only depend on long-range force constants. This will allow an accurate calculation of these spring constants. Examples of these perturbations can be found in references [147, 148, 149], and in section 6.6 below.

The selection of the perturbed structures presents a compromise between the difficulty of computing the forces and the amount of information that we can extract from them. If we choose a perturbation with very low symmetry, the forces will depend of a large number of spring constant parameters and several independent forces will be obtained. For highly symmetric perturbations, very few equations for the spring constant parameters will be obtained; and these equations will only provide information about very few spring constant parameters. Fine-tuning of the perturbed structures, can lead to significantly faster calculations.

To compute the forces on the atoms of the unit cell of the perturbed structure from first principles, the density functional theory (DFT) [17, 18, 19] in the local density approximation (LDA) [18] is usually used to find the electronic density of the system. Once the electronic density is known, the forces on the atoms can be computed using the Hellmann-Feynman theorem [141].

Compute the forces on the atoms of the perturbed structure(s) using an ab-initio method

first principles, the density functional theory (DFT) [17, 18, 19] in the local density approximation (LDA) [18] is usually used to find the electronic density of the system. Once the electronic density is known, the forces on the atoms can be computed using the Hellmann-Feynman theorem [141].

If the number of equations (i.e., the number of independent forces) is the same as the number of parameters of the spring constant tensors to be computed, then a system of linear equations has to be solved. In general, however, we will have more equations than unknowns and a least-squares procedure [150] will be used.

Perform a least-squares fit of the spring constants to forces on atoms

as the number of parameters of the spring constant tensors to be computed, then a system of linear equations has to be solved. In general, however, we will have more equations than unknowns and a least-squares procedure [150] will be used.

Once the spring constants of a given configuration  $\vec{\sigma}$  are known, the calculation of the vibrational frequencies for any k-point is a standard lattice dynamics problem (usually referred to as the Born-von Karman model of lattice dynamics [156, 98]). The value of  $\overline{\Delta \ln(\omega)}$  is obtained by performing an integral over the Brillouin zone. The value of  $\overline{\Delta \ln(\omega)}$  has to be converged with respect to the number of k-points used for this integral. Special ways of selecting the k-points for the ordered configuration  $\vec{\sigma}$  can accelerate this convergence (see appendix D).

Compute  $\langle \ln(\omega) \rangle$  for the ordered configuration and the pure elements, to get the formation value ( $D\langle \ln(\omega) \rangle$ )

the vibrational frequencies for any k-point is a standard lattice dynamics problem (usually referred to as the Born-von Karman model of lattice dynamics [156, 98]).

As shown in figure 6-6, the process has to be iterated including more elements of the force constant tensors, until the value of  $\overline{\Delta \ln(\omega)}$  has converged. The convergence will be faster (less force constant parameters will be needed) when we choose the force constant elements that contribute the most to  $\overline{\Delta \ln(\omega)}$  before the less important ones. Since we do not know this *a-priori*, we follow the following heuristic rule: compute all the non-negligible spring constant tensors for the pure elements (this is usually much easier than computing the same quantities for the ordered structures); then include the spring constants in the calculation of  $\overline{\Delta \ln(\omega)}$  for ordered structures in decreasing absolute value of the correspondent spring constants in the pure elements.

Extend range of spring constants

of the force constant tensors, until the value of  $\overline{\Delta \ln(\omega)}$  has converged. The convergence will be faster (less force constant parameters will be needed) when we choose the force constant elements that contribute the most to  $\overline{\Delta \ln(\omega)}$  before the less important ones.

The new method requires considerable more computational effort than the Debye approximation described in section 6.2.1. However, if enough spring constants are

included to obtain convergence of  $\overline{\Delta \ln(\omega)}$ , the results will be as reliable as the first-principles method used to compute the forces. If it turns out that a few spring constant parameters suffice, the new method will provide a practical tool for the inclusion of the lattice vibrations in the first-principles studies of alloy phase stability.

In the next section, we study the effect of lattice vibrations on the phase stability of Si-Ge alloys. Our objective is to illustrate the method just presented and to test how many parameters of the spring constant tensors are needed to achieve convergence in  $\overline{\Delta \ln(\omega)}$ .

## 6.6 The Si-Ge alloy system

Silicon-germanium alloys are very important technologically. They are currently being investigated as materials for integrated circuits, and very interesting new applications are being developed in the field of quantum-confinement [157]. With the addition of Ge atoms to the traditional Si semiconductor chips, the electrical properties of the system can be fine-tuned to achieve better performance. Both Si and Ge are group-IV elements (4 valence electrons) with very similar bonding properties and atomic size (the size mismatch is only 4%).

Experimentally, the Si-Ge system shows complete miscibility in the solid part of the bulk phase diagram [97], with no ordered structures or phase-separation for temperatures larger than  $\sim 400\text{K}$ . Of course, at lower temperatures, the system will either form ordered structures, or phase-separate into pure Si and pure Ge. The slow kinetics of these processes prevent their experimental observation. Several theoretical studies of the low temperature phase stability in the Si-Ge have been performed [158, 159, 160, 161]. The consensus from these studies is that bulk Si-Ge alloys phase-separate at low temperatures.<sup>5</sup> The predicted consolute temperature of the miscibility gap is somewhere between 150K and 350K. Since these studies did not include the effect of lattice vibrations on the phase diagrams, we decided to apply the method developed in section 6.5 to this problem, to decide whether the above predictions are affected by the lattice vibrations.

Silicon, germanium, and their solid solutions crystallize in the diamond cubic lattice. The conventional unit cell of the diamond lattice is shown in figure 6-7. The coordinates and distances of the first eight neighbors of the atom at the origin are shown in table 6.5. The simplest ordered structure on the diamond lattice is the so-called zinc-blend (ZB) structure that consists of two inter-penetrating fcc lattices of the two species of the alloy (a picture of the ZB structure is shown in figure 6-8).

We will compute  $\overline{\Delta \ln(\omega)}$  for the ZB structure using the method developed in section 6.5, and following the steps in the flowchart in figure 6-6. The space group

---

<sup>5</sup>When Si-Ge alloys are grown epitaxially on Si substrates, the opposite behavior has been observed in experiments and theoretical calculations. Both transmission electron microscope [162, 163] and Raman scattering [163] experiments found a stable rhombohedral structure in epitaxial Si-Ge alloys. First-principles calculations confirmed that when the lattice constant of Si-Ge alloys is constrained by an epitaxial substrate, the same rhombohedral structure has negative formation energy [164].

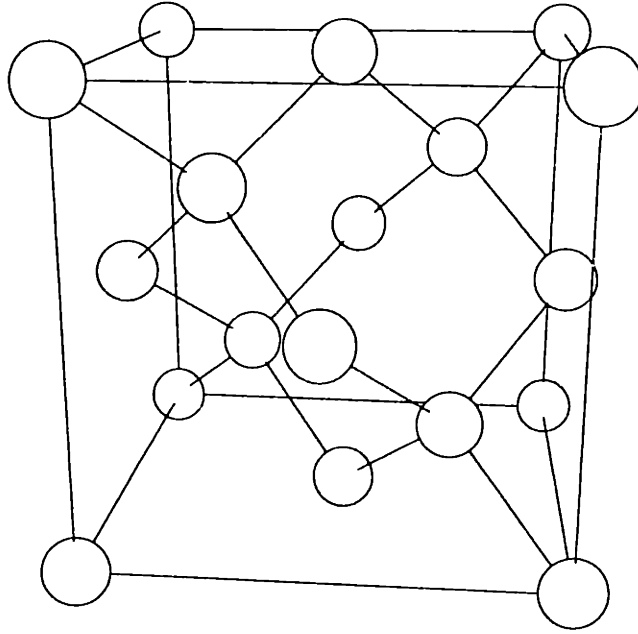


Figure 6-7: Conventional unit cell of the diamond structure. The origin of the systems of coordinates used to describe the atomic positions is conventionally taken at the lower-right atom in the figure. The conventional cell has 8 atoms, while the primitive cell has 2 atoms.

$N$	Distance	Coordinates		
1	0.433	0.25	0.25	0.25
2	0.707	0.50	0.50	0.00
3	0.829	-0.25	-0.25	-0.75
4	1.000	1.00	0.00	0.00
5	1.089	0.75	0.75	0.25
6	1.224	1.00	0.50	0.50
7a	1.299	1.25	0.25	0.25
7b	1.299	-0.75	-0.75	-0.75
8	1.414	1.00	1.00	0.00

Table 6.5: Distances (in units of  $a$ , the conventional-cell lattice constant), and coordinates of the first 8 neighbor atoms to the atom at the origin, in the diamond lattice. Neighbors 7a and 7b are at the same distance to the origin, but are crystallographically distinct.

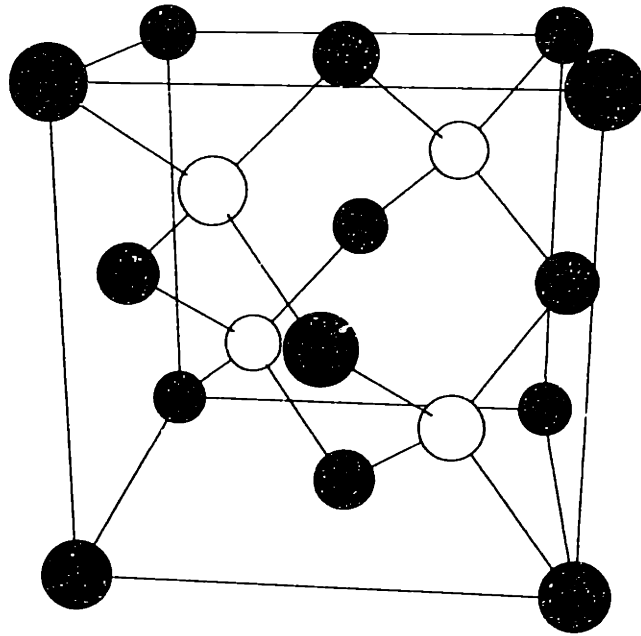


Figure 6-8: Conventional unit cell of the zinc-blend (ZB) ordered structure on the diamond lattice. One of the alloy species (dark-grey shaded atoms) forms an fcc arrangement, while the other (light-gray shaded atoms) occupies half of the tetrahedral interstitial sites, forming another fcc arrangement.

of the diamond structure is  $Fd\bar{3}m$  (227).<sup>6</sup> When the ZB structure is formed, some of the symmetry elements are removed, resulting in space group  $F\bar{4}3m$  (216).

The Si–Ge bond in the alloy has very small ionicity [165], and therefore the use of Born effective charges is not necessary. The spring constant parameters for both Si and Ge decay to less than 1% of the self spring constant, at the eighth–neighbor distance [149]. Since the Si–Ge bond is not very different from the Si–Si or Ge–Ge bonds, we will compute the spring constant parameters up to the eighth–neighbor distance.

We applied the method described in the previous section to obtain the independent spring constant parameters for the diamond symmetry (pure Si and pure Ge) and for the ZB structure. The results for Si and Ge are shown in figure 6.6, and agree with the previously published results [151, 149]. When the symmetry of the crystal is lowered by the ZB ordering, some of the neighbor pairs in the diamond structure become inequivalent by symmetry in the ZB structure. For example, all the second neighbor pairs in the diamond structure are equivalent by symmetry, while there are two distinct second neighbor pairs in the ZB structure: Si–Si and Ge–Ge pairs (see figure 6-8). This effect is usually referred to as the “splitting of the orbit” of the cluster (second neighbor in the example). The splitting of the pairs up to the eighth–neighbor pair, and the resulting spring constant tensors for the ZB structure are shown in table 6.7.

We used four perturbations of the atoms in the Si, Ge, and ZB structures, to compute the forces on the atoms and obtain the equations for the spring–constant parameters of tables 6.6 and 6.7. A summary of the unit cells of the perturbations is shown in table 6.8.

In all the perturbations, the first anharmonic contribution to the forces was either zero by symmetry (first and second perturbations) or taken out of the computed force by computing the negative perturbation as described in the previous section (third and fourth perturbations). To estimate the contribution of the next anharmonic term in the potential (i.e., the term  $\mathcal{O}(u^4)$ ) we computed, for the first perturbation in table 6.8, the forces corresponding to perturbations of  $0.01a$  and  $0.02a$  of the atom at the origin, from which the contribution of the anharmonic term to the force can be computed. The error introduced in the forces by the anharmonic contribution is  $\sim 1\text{meV}/\text{\AA}$ , which is smaller than other errors discussed below.

To compute the forces on the atoms of the perturbed structures we used the pseudopotential method [20] to solve the LDA equations. We used non–local, optimized [166], Kleinman–Bylander [167] pseudopotentials for Si and Ge. For the exchange and correlation potential, the Perdew–Zunger parameterization [168], was used. The wave functions were represented with a plane–wave basis. To verify the accuracy of the pseudopotentials, we computed the lattice constants and bulk moduli of Si, Ge, and ZB, and the formation energy of ZB. The results are compared to other available data in table 6.9. The agreement with measured and computed properties validates the use of these pseudopotentials. To compute the forces on the atoms of

---

<sup>6</sup>The space groups are identified by their conventional name and by their number in the International Tables for Crystallography [14].



N	P	Tensor	N	P	Tensor
self	1	$\begin{pmatrix} a & 0 & 0 \\ 0 & a & 0 \\ 0 & 0 & a \end{pmatrix}$	1	2	$\begin{pmatrix} a & b & b \\ b & a & b \\ b & b & a \end{pmatrix}$
2	4	$\begin{pmatrix} a & c & b \\ c & a & b \\ \bar{b} & \bar{b} & d \end{pmatrix}$	3	4	$\begin{pmatrix} a & c & b \\ c & a & b \\ b & b & d \end{pmatrix}$
4	2	$\begin{pmatrix} a & 0 & 0 \\ 0 & b & 0 \\ 0 & 0 & b \end{pmatrix}$	5	4	$\begin{pmatrix} a & c & b \\ c & a & b \\ b & b & d \end{pmatrix}$
6	5	$\begin{pmatrix} a & b & b \\ c & e & d \\ c & d & e \end{pmatrix}$	7a	4	$\begin{pmatrix} a & \bar{b} & b \\ b & d & c \\ b & c & d \end{pmatrix}$
7b	2	$\begin{pmatrix} a & b & b \\ b & a & b \\ b & b & a \end{pmatrix}$	8	4	$\begin{pmatrix} a & c & b \\ c & a & b \\ \bar{b} & \bar{b} & d \end{pmatrix}$

Table 6.6: Self and pair spring-constant tensors for the first 8 neighbor pairs in the diamond lattice, as shown in table 6.5. For each neighbor (N), the number of independent parameters of the tensor is shown (P), together with the general form of the spring-constant tensor expressed in the cartesian basis.

Diam-Pair	ZB-pairs	Param	Tensor
self	000 – 000 111 – 111	1	$\begin{pmatrix} a & 0 & 0 \\ 0 & a & 0 \\ 0 & 0 & a \end{pmatrix}$
1	000 – 111	2	$\begin{pmatrix} a & b & b \\ b & a & b \\ b & b & a \end{pmatrix}$
2	000 – 220 111 – 331	4	$\begin{pmatrix} a & c & b \\ c & a & b \\ \bar{b} & \bar{b} & d \end{pmatrix}$
3	000 – $\bar{1}\bar{1}\bar{3}$	5	$\begin{pmatrix} a & c & b \\ c & a & b \\ d & d & e \end{pmatrix}$
4	000 – 400 111 – 511	2	$\begin{pmatrix} a & 0 & 0 \\ 0 & b & 0 \\ 0 & 0 & b \end{pmatrix}$
5	000 – 332	5	$\begin{pmatrix} a & c & b \\ c & a & b \\ d & d & e \end{pmatrix}$
6	000 – 422 111 – 533	5	$\begin{pmatrix} a & b & b \\ c & e & d \\ c & d & e \end{pmatrix}$
7a	000 – 511	5	$\begin{pmatrix} a & b & b \\ c & e & d \\ c & d & e \end{pmatrix}$
7b	000 – $\bar{3}\bar{3}\bar{3}$	2	$\begin{pmatrix} a & b & b \\ b & a & b \\ b & b & a \end{pmatrix}$
8	000 – 440 111 – 551	4	$\begin{pmatrix} a & c & b \\ c & a & b \\ \bar{b} & \bar{b} & d \end{pmatrix}$

Table 6.7: Self and pair spring-constant tensors for the first 8 neighbor pairs in the ZB structure. The splitting of the orbits of the diamond pairs is explicitly shown. The pairs are identified by the coordinates of the atoms of a representative pair (in units of  $a/4$ ). For each pair, the number of independent parameters of the tensor is shown (Param), together with the general form of the spring-constant tensor expressed in the cartesian basis.

$N_{\text{atoms}}$	Supercell	Shift	Space group
8	(001)	[001]	Pmm2 (25)
8	(001)	[1 $\bar{1}$ 0]	Pm (6)
8	(111)	[111]	R3m (160)
16	(110)	[001]	Pmm2 (25)

Table 6.8: Perturbations used to compute the forces on the atoms to obtain the equations for the spring constant parameters. In all cases, the unit cells are supercells along the supercell direction given. Only the atom at the origin is perturbed, along the direction shown in the table by  $0.01a$ , where  $a$  is the lattice constant of the conventional cell. The space groups of the perturbed structures are given by their conventional name and their number in the International Tables for Crystallography [14]. Since ZB has the same primitive unit cell as Si and Ge, the perturbations for the three structures are the same. The only difference is that twice as many perturbations were computed for ZB: shifting a Si atom and shifting a Ge atom.

the perturbed supercells, we used the Hellmann–Feynman theorem [141, 142, 143].

To decide the energy cutoff ( $E_c$ ) for the plane–wave basis, we studied simple perturbed unit cells of Si, Ge, and ZB. These perturbations have the same primitive unit cell as the unperturbed structure, but the second atom in the cell is displaced towards the origin by 1% of the lattice constant. The projection of the resulting forces along the  $x$  direction vs.  $E_c$  is shown in figure 6-9. From these results we conclude that the convergence error on the forces is less than 2 meV/Å for an energy cutoff of  $E_c = 300\text{eV}$ .

An estimate of the error in  $\overline{\Delta \ln(\omega)}$  due to the finite energy cutoff in the plane–wave basis, can be obtained by fitting only one spring–constant–tensor parameter for the nearest–neighbor pair, to reproduce the forces shown in figure 6-9. We fitted this spring constant, and computed the value of  $\overline{\ln(\omega)}$ , averaging over 2,992 points in the Brillouin zone. With the values of  $\overline{\ln(\omega)}$  for Si, Ge, and ZB, we computed  $\overline{\Delta \ln(\omega)}$  for ZB as a function of the energy cutoff. The results are shown in figure 6-10. For an energy cutoff of  $E_c = 300\text{eV}$  the error in  $\overline{\Delta \ln(\omega)}$  is less than 0.005 (dimensionless), which will prove to be sufficient for our purposes.

From the above calculations, we conclude that  $E_c = 300\text{eV}$  provides enough accuracy in the calculation of the forces on the atoms. Hereafter, all the calculations are done using this energy cutoff.

From figure 6-10, we note that the convergence of  $\overline{\Delta \ln(\omega)}$  for ZB vs. the energy cutoff is faster than the convergence of the absolute quantities  $\overline{\ln(\omega)}$  for any of the three structures (Si, Ge, and ZB). This is due to cancellations when the formation value is computed. This effect is also present for the calculation of the formation energies, which can be obtained with a much smaller error than the total energies of any structure.

We computed the forces and fitted the spring constant parameters for Si, Ge, and

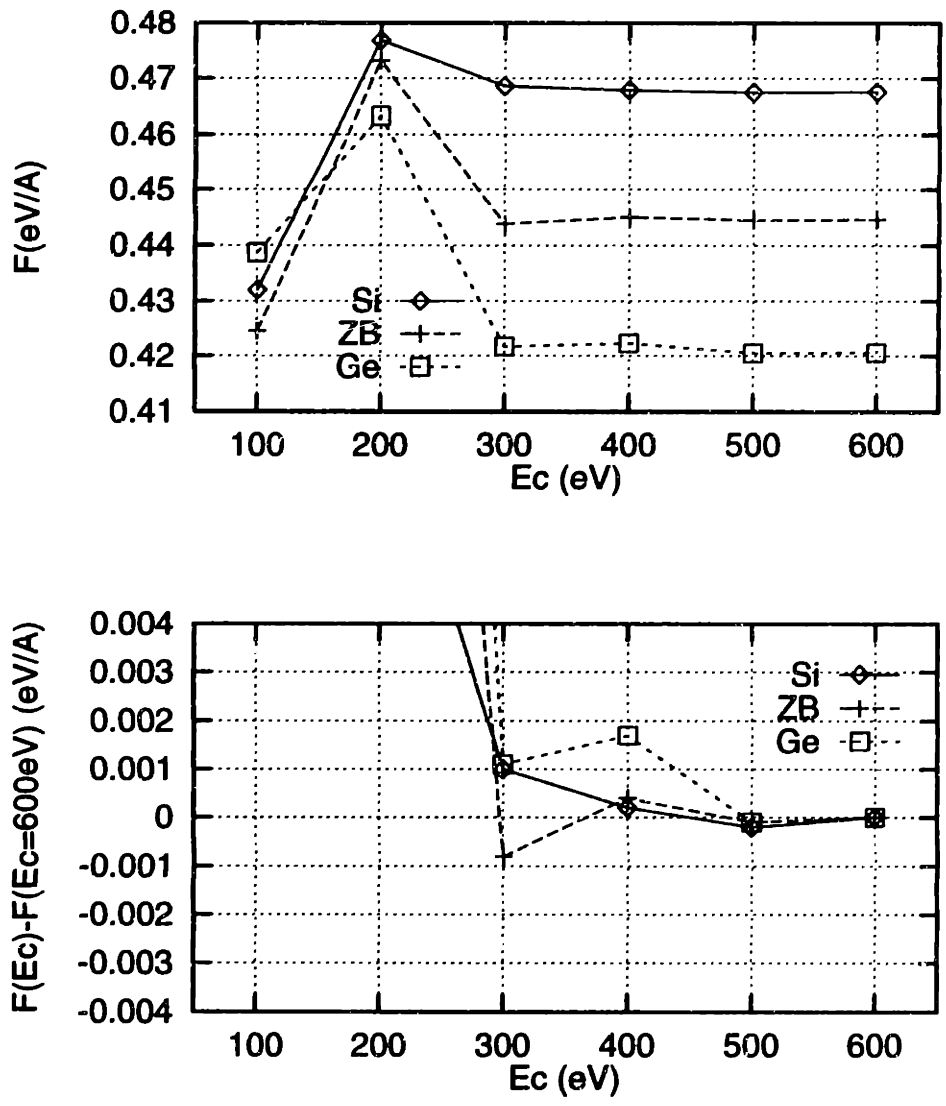


Figure 6-9: Convergence properties of the force along  $x$  for the structures with the nearest-neighbor bonds contracted by 1% of the lattice constant. In the first plot, the absolute value of the forces is shown. In the second, we show the difference between the force computed with a given energy cutoff ( $E_c$ ) and the force at  $E_c = 600$  eV.

Struc.	Property	Our result	Experimental measurements	Other theoretical
Si	$a(\text{\AA})$	5.36	5.43	5.38 [165]
	$B(\text{GPa})$	97	99	98 [165], 95 [164]
Ge	$a(\text{\AA})$	5.57	6.65	5.57 [165]
	$B(\text{GPa})$	81	77	77 [165], 77.5 [164]
ZB	$a(\text{\AA})$	5.46	N/A	5.47 [165]
	$B(\text{GPa})$	88	N/A	87 [165, 164]
	$\Delta E(\text{meV/at})$	14	N/A	10 [165], 12 [169]

Table 6.9: Comparison of the predictions of the pseudopotentials used in this thesis for Si and Ge with experimental results and other theoretical calculations. Experimental measurements for the ZB structure are not available (N/A).

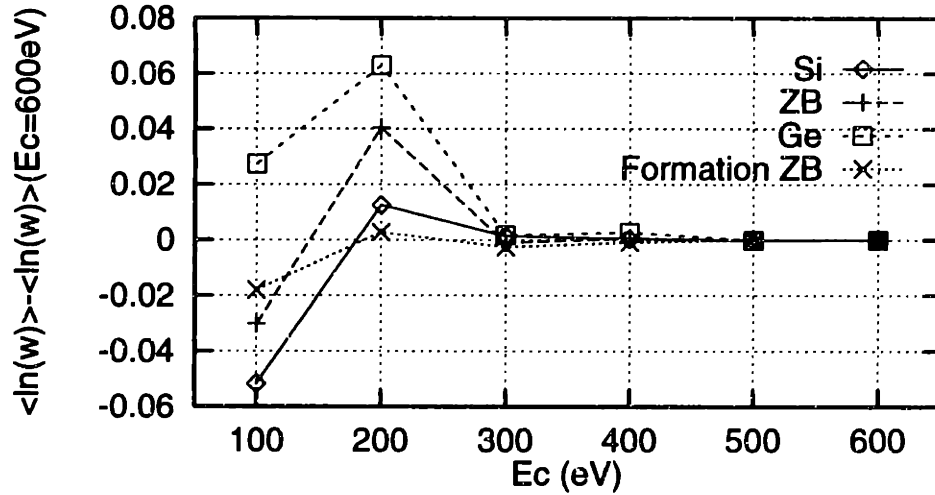


Figure 6-10: Convergence of  $\overline{\ln(\omega)}$  for Si, Ge, and ZB, and  $\Delta \overline{\ln(\omega)}$  for ZB as a function of the energy cutoff ( $E_c$ ) in the pseudopotential calculations. The values of  $\overline{\ln(\omega)}$  were obtained by fitting to only one spring-constant-tensor parameter.

N	Param	Si	Ge	ZB		
				Si-Si	Si-Ge	Ge-Ge
1	a	-3.298	-2.867		-3.073	
	b	-2.355	-2.027		-2.174	
2	a	-0.218	-0.203	-0.245		-0.180
	b	-0.158	-0.123	-0.142		0.157
	c	-0.305	-0.310	-0.346		-0.276
	d	0.426	0.377	0.404		0.387
4	a	-0.017	-0.019	-0.009		-0.027
	b	0.024	0.026	0.030		0.015
5	a	-0.011	0.005		-0.004 a	
	b	0.050	0.051		0.049 b	
					0.054 d	
	c	0.048	0.055		0.049 c	
	d	-0.183	-0.197		-0.186 e	
8	b	-0.017	-0.019	-0.018		0.019
	c	-0.033	-0.037	-0.031		-0.037
	d	0.059	0.068	0.061		0.063

Table 6.10: Spring constant parameters for Si, Ge, and ZB in  $\text{eV}/\text{\AA}^2$ . The labels for the parameters are from tables 6.6 and 6.7. Note that the fifth neighbor spring constant tensor has one more parameter due to the lower symmetry of ZB.

ZB. We choose the 15 spring constant parameters with largest absolute value from reference [149] and only fitted to them, since the limited number of perturbations do not provide enough equations to fit to all the parameters. The fitted parameters included elements of the spring constant tensors for the first, second, fourth, fifth, and eighth neighbors and are shown in table 6.10.

As a test of the parameters obtained, we computed the vibrational density of states (VDOS) for Si. The result is shown in figure 6-11. Our results agree very well with both theoretical calculations of the VDOS [149, 144] and experimental measurements of the dispersion relations [170].

To “close the loop” in the flowchart of figure 6-6, we computed a hierarchy of approximations for the spring constants including from 1 to 15 parameters in the fitting procedure. When all the 15 parameters are included, we obtain the results in table 6.10. When fewer springs are fitted to, the least significant springs in table 6.10 are left out. With the resulting sets of springs, we computed the vibrational frequencies in 2,992 special points in the Brillouin zone, selected with the Chadi-Cohen scheme [13]. We obtain the values of the first three even moments ( $\overline{\ln(\omega)}$ ,  $\overline{\omega^2}$ , and  $\overline{\omega^4}$ ) of the VDOS for Si, Ge, and ZB. The formation values of these moments, as a function of the number of spring constant parameters included in the fit, are shown in figure 6-12.

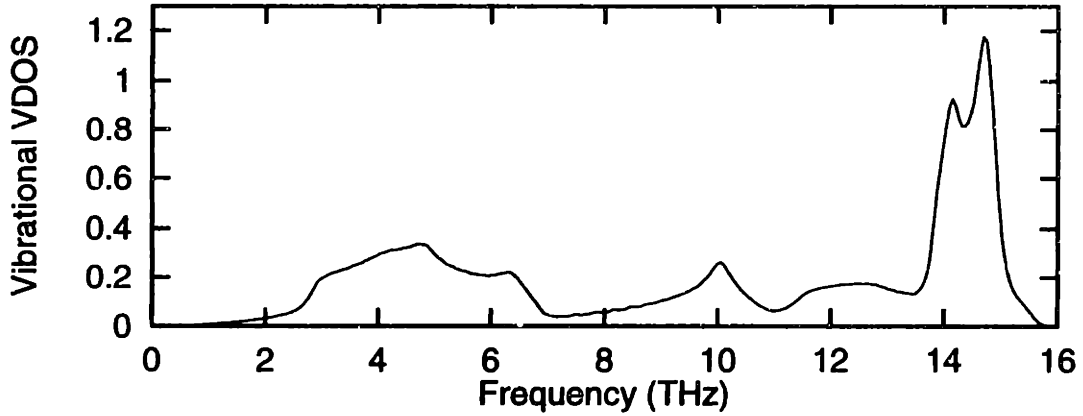


Figure 6-11: Vibrational density of states for Si computed with the 15 force-constant-tensor parameters, shown in table 6.10.

It can be seen in figure 6-12, that the value of  $\overline{\Delta \ln(\omega)}$ , used to compute the high-temperature effect of the lattice vibrations (see equation 4.16), is well converged when as few as 5 or 6 parameters of the force constant tensors are included in the fit to the forces. The remaining oscillation of the value of  $\overline{\Delta \ln(\omega)}$  is consistent with the 0.005 error due to the finite energy cutoff for the plane-wave basis (discussed in page 155). The other two moments of the VDOS,  $\overline{\Delta \omega^2}$  and  $\overline{\Delta \omega^4}$ , show faster convergence, with only 3 parameters being enough to obtain an accurate result. These other moments also contribute to the high-temperature vibrational free energy (see equation 4.16).

To obtain these few parameters, less perturbations with smaller unit cells are sufficient. This reduces the computational cost of the method, opening the road for applications in studies of phase stability of real systems. The error in the converged value of  $\overline{\Delta \ln(\omega)}$  is only due to the first-principles method used to compute the forces, and therefore the new method provides a reliability not present in the other approximate schemes discussed in section 6.2.

To be able to predict the effect of lattice vibrations on the phase stability of Si-Ge alloys, we would need to compute  $\overline{\Delta \ln(\omega)}$  for several structures, to be able to find the vibrational ECI's. However, we can speculate about the vibrational effect on Si-Ge alloys from the results obtained for the ZB structure.

For the ZB structure, both  $\Delta E$  and  $\overline{\Delta \ln(\omega)}$  are positive. This means that, based on this structure alone, the tendency is that the lattice vibrations will *increase* the consolute temperature of the miscibility gap. If this fact is confirmed, the Si-Ge system would be the first real system, to our knowledge, in which the lattice vibrations increase the transition temperature of a phase transition. Although we showed in chapter 5 that this trend is *possible*, it had not been found in any system in nature before.

The value of  $\overline{\Delta \ln(\omega)}$  for ZB is rather small. If the value of  $\overline{\Delta \ln(\omega)}$  for other ordered structures in the Si-Ge system is comparable to the value in ZB, then the effect of the lattice vibrations on the miscibility gap will be to increase the transition temperature

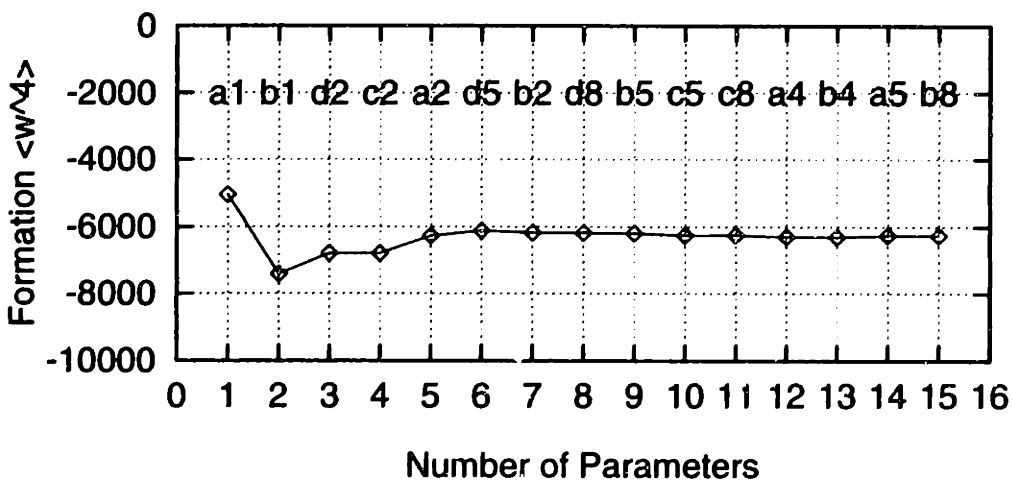
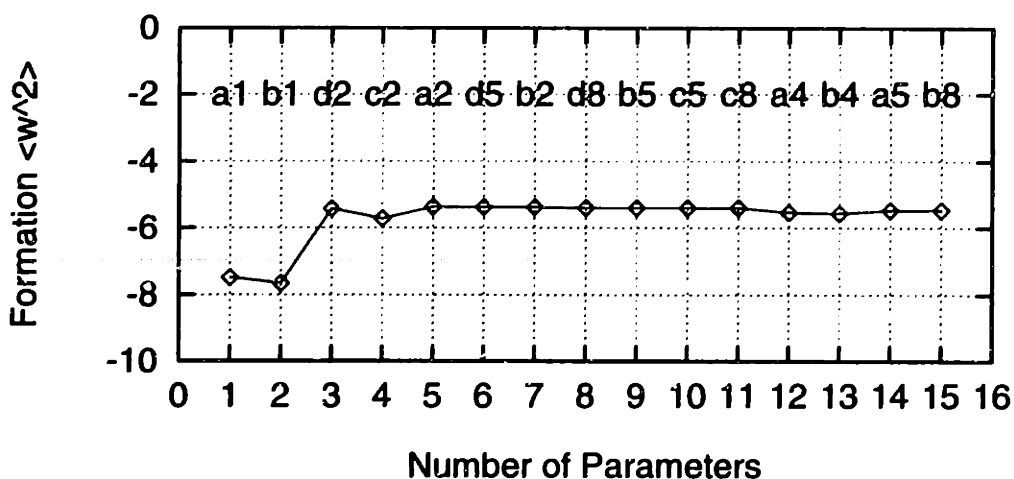
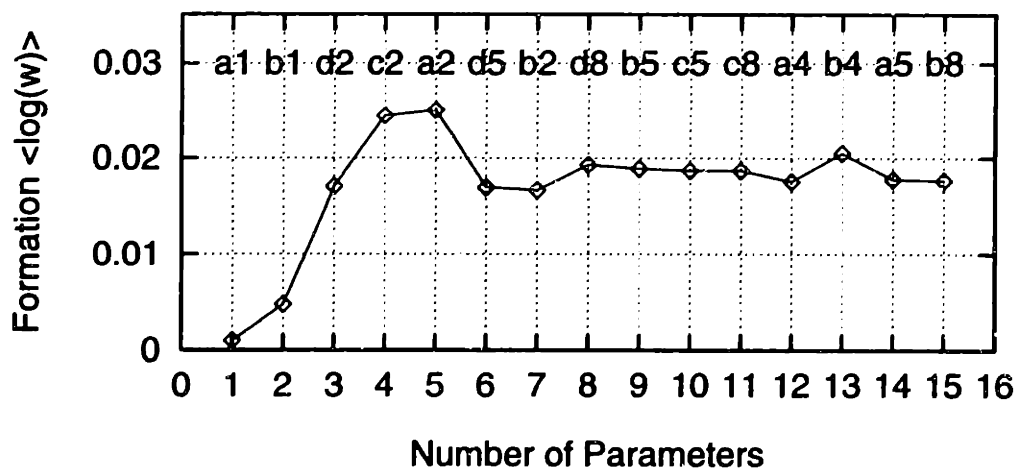


Figure 6-12: Convergence of the formation value of the first three even moments of the VDOS for the zinc-blend configuration in Si-Ge alloys, with respect to the number of spring-constant parameters. The labels of the spring constant parameters correspond to the tensors shown in table 6.6.



by a few percent, therefore not affecting significantly the previous studies of phase stability in this system [158, 159, 160, 161].

## 6.7 Conclusions

In this chapter, we showed that using first-principles methods to compute the effect of the lattice vibrations on phase stability, quantitative agreement with experiment can be obtained. The solubility limits in the MgO–CaO pseudobinary system that we computed compete in accuracy with the laboratory experiments.

To be able to make quantitative predictions in more complex systems, reliable approximations to include the lattice vibrations in the studies of phase stability are necessary. We showed that the Debye approximation can fail to predict the correct trend, and that the Einstein approximation is more accurate, but not practical for first-principles calculations. We developed a new approach based on the calculation of a few spring constant parameters, that although more complex than the Debye model, provides a practical tool to make reliable predictions. We studied the Si–Ge system, and showed that the effect of the lattice vibrations on the miscibility gap can be computed with the new method.



# Chapter 7

## Conclusions

In the last few years, the computational modeling of alloy phase diagrams has evolved from a purely qualitative field to a much more quantitative and reliable discipline. The predictions of the models are starting to rival the accuracy of experimental observations and will continue to do so with the increase in computational power and sophistication of the models. In this thesis, we have contributed to this trend, improving the models and showing that they are capable of predicting accurate thermodynamic properties with as little input as the atomic numbers and masses of the species forming the alloy.

To be able to make reliable predictions, the models have to account for all the important contributions to the free energy of the alloy. For a long time, most studies used lattice models to account for the substitutional degrees of freedom. It was later realized that the relaxation of the atoms away from the ideal lattice sites could also be accounted for in the lattice model. In this thesis, we showed that the lattice model is much more general than previously thought. It can incorporate *any* degree of freedom, with the only assumption that all the microstates of the alloy that contribute significantly to the partition function be uniquely mapped to substitutional states of the lattice. In particular, we argued that the lattice vibrations may be the most important of the non-substitutional excitations to understand the thermodynamics of the alloy. More than half of this thesis was devoted to the development of the formalism to include the lattice vibrations in the lattice models, the understanding of the basic trends, and the applications to real systems.

The most important conclusion of this study is that the lattice vibrations can be accounted for with natural extensions of the lattice models and that the effect on alloy phase stability can be rather large. We predict that changes in the computed transition temperatures of 30% due to the lattice vibrations may not be uncommon. The effect will be large for systems with highly asymmetric bonding, such as transition-metal aluminides. Although the lattice vibrations will in most cases *reduce* the transition temperatures, the opposite may be true for some systems, such as Si-Ge (more calculations are needed to confirm this). In non-magnetic insulators, the lattice vibrations are the *only* important contribution to the free energy besides the substitutional excitations. This means, that models that include the substitutional and vibrational degrees of freedom should be capable of producing quantitatively ac-

curate predictions for these systems. We verified this by computing the MgO–CaO phase diagram in excellent agreement with experimental observations.

If the alloy can be model with classical potentials, the calculation of the effect of the lattice vibrations on the phase stability is straightforward. To illustrate this, we computed the phase diagram of the Ar–Kr system that can be accurately described with simple Lennard–Jones potentials. We predict that the lattice vibrations lower the order–disorder transition temperature of the system by 12%.

Unfortunately, first–principles calculations are needed for most alloy systems. We found that the methods used in the past, such as the Debye model, do not produce reliable estimates of the effect of lattice vibrations on phase stability. These methods, based on just the elastic properties of the alloy, fail to capture the configurational dependence of the vibrational free energy that has important contributions from high frequencies in the phonon spectrum. We developed a method based on the calculation of a few spring constant parameters. This method is more demanding from the computational point of view, but provides a systematic procedure to obtain reliable predictions from first–principles. We showed the feasibility of this method, applying it to Si–Ge alloys.

We have shown that the effect of the lattice vibrations on phase stability can be large. Furthermore, we developed the methodology to include the lattice vibrations in the free energy of the alloy. We believe that the inclusion of the lattice vibrations in the alloy models has to become standard practice, if the predictions are to be reliable.

The analysis of the substitutional energy of the alloy is still a very active area of research. We concentrated on two areas: the parameterization of the energy of the alloy as a function of the substitutional configuration (cluster expansion) and the search for the ground states of the system.

We showed that the traditional methods to find the effective cluster interactions (ECI's) for the cluster expansion of the energy of alloys fail to capture subtle energy differences between ordered structures. If the cluster expansion does not correctly parameterize these energy differences, the ground state line of the system may not be reproduced. In this case, the prediction of stable phases is doomed to fail. We developed a method to obtain the ECI's from the total energies of ordered compounds, that overcomes this limitation. With the new method, we can assess whether a given truncation of the cluster expansion is capable of reproducing the important features of the formation energies of ordered structures in an alloy system. We applied the new method to study Pd–V alloys, in which a large number of ordered structures are close to the ground–state line. Our method proved that in order to reproduce the ground–state line, long–range pair interactions (seventh– or eighth–neighbor ECI's) are necessary. The new method is more involved than the traditional Connolly–Williams technique [35], but should be applied whenever subtle energy differences may play a crucial role in determining the thermodynamics of the alloy.

Once the range of the lattice Hamiltonian is known, it is important to find the ground states of the system. The ground–state structures of the system will be stable a  $T = 0\text{K}$ , and depending on the details of the system may remain stable at high temperatures as well.

In the past, the polyhedron method was used to obtain exact solutions of the

ground-state problem for systems with only a few effective cluster interactions (usually only first- and second-neighbor pair ECI's). We showed that the complexity of the polyhedron method grows with the interaction range in such a way that the exact solution of problems with more than two or three pair interactions is beyond the current or near-future computer power. Therefore, the polyhedron method will not be a practical tool to search for the ground states of alloys with realistic interactions.

To be able to study alloys with long-range interactions, a new approach is needed. We developed a new method, that we call the "enumeration" method, that finds an *approximate* solution of the ground-state problem for *any* interaction range. We showed that the number of possible ground state structures for alloys with more than two or three pair interactions can be much larger than expected from results on simpler systems.

To solve the largest ground-state problem to date, we interacted with researchers in the field of combinatorial geometry (David Avis and Komei Fukuda). This interaction proved to be a very fruitful symbiosis. From the point of view of materials science, the recently developed vertex-enumeration techniques helped us find solutions to new ground-state problems. On the other hand, the creation of highly degenerate vertex-enumeration problems is not straightforward. The unsolved ground-state problems provide a set of stringent test cases for the vertex-enumeration algorithms currently being developed [171] by the mathematicians.

The modeling of phase stability in alloys is at the verge of becoming a reliable tool for making quantitative predictions about real alloy systems. There are already a few examples in which the modeling techniques made predictions before the actual material was studied in the laboratory (for example, see reference [172]). We expect this tendency to grow in the future, when the available computer power increases by one or two orders of magnitude. Whether computer modeling will eventually replace traditional experimentation, we do not know.



# Chapter 8

## Future research

If the predictions of phase stability in substitutional alloys are to become reliable and quantitative, more research is needed in the areas of alloy theory covered in this thesis. In this chapter, we explore the future of alloy theory, and suggest research topics that would improve the current methods to study the thermodynamics of alloys from first principles.

Behind any first-principles calculation of alloy properties there is a quantum-mechanical method to compute energies and forces. So far, these methods have been based on the local density approximation (LDA) [18] to the density functional theory [17, 18, 19]. The LDA is known to predict overbinding in solids, typically underestimating the lattice constant by 1% or 2%. Errors of 10% to 20% in the elastic properties are also common. Currently, generalized gradient corrections to the LDA are being developed [173, 174, 175], but it is still not clear if these techniques will improve the LDA results.

However, the major problem with the quantum-mechanical methods (for our purposes) is not accuracy, but speed. The calculations of relaxed geometries for ordered structures with the most sophisticated methods (FLAPW [176], full-potential LMTO [59, 177], pseudopotentials [20]) are currently limited to structures with very few atoms in the unit cell (typically less than 10 atoms). To study the phase stability of complex alloys, larger unit cells are needed. Due to the " $N^3$ " scaling of these methods, we will not be able to perform these calculations in the near future. There are two options to overcome this difficulty. The first option is to use methods with more "benign" scaling, such as order  $N$  [26, 27]. The second alternative, is to use the sophisticated methods to compute the properties of a few simple structures and then use simple models to interpolate the results for more complex structures. One possible simple model is the tight-binding approximation [114]. Recent results in this direction for oxide mixtures are very promising [178].

The cluster expansion is a very versatile tool to parameterize any function of the configuration of a substitutional alloy. In particular, the calculation of the chemical effective cluster interactions is a very active area of research. In spite of recent controversy [179, 180, 181, 182], the cluster expansion has proved to be a very useful practical tool.

To obtain *exact* solutions of the general ground-state problem with long-range

interactions, a breakthrough is needed. We have shown that the polytope method is not capable of producing the complete solution of a ground-state problem when more than 2 or 3 pair interactions are necessary to model the energetics of the system. The enumeration method we developed can deal with long range interactions, but only generates approximate solutions of the ground-state problem. The polytope method would be improved if the frustration constraints could be generated in the low dimensional space directly, without the need of generating vertices of the high dimensional polytope. Recent progress along this direction is very promising [61].

To make reliable predictions of phase stability on real systems, *all* the important contributions to the free energy of the alloy need to be included. In this thesis, we developed the methodology to account for the lattice vibrations, and showed that the effect can be important and therefore should be included. Recently, the effect of the electronic excitations was also studied [33, 90]. Although the effect is expected to be smaller than the effect of the lattice vibrations in general, it may play an important role in determining the stable phases for some systems.

We applied the formalism we developed to study the effect of the lattice vibrations on the phase stability of three alloy systems: Ar-Kr, MgO-CaO, and Si-Ge. In these three systems, the A-B bonding is not *very* different from the A-A and B-B bonding (the A and B species in these alloys are in the same column of the periodic table), and therefore the effect of the lattice vibrations is not as big as we estimated it to be in intermetallic alloys. It would be interesting to apply our formalism to study systems with very asymmetric bonding, such as transition-metal aluminides. This study would illustrate the effect of lattice vibrations in a system where they are expected to play a very important role in the thermodynamics. We are currently exploring the possibility of computing the effect of the lattice vibrations on the order-disorder transition in Ni<sub>3</sub>Al, with the use of linear response methods, in collaboration with K. Rabe and U. Waghmare (Yale University).

Our results for the Si-Ge system suggest that the lattice vibrations may *increase* the consolute temperature. Since this would be the first real system studied where this is the case, we believe that it would be worth pursuing the calculations to prove it or disprove it.

We studied the thermodynamics of *substitutional* alloys. Most alloys, however, have stable phases that are based on different parent lattices. For these systems, the effect of the lattice vibrations is expected to be very important. Therefore, it would be interesting to include the lattice vibrations in the studies of phase stability of systems such as Cu-Zn (see figure 1-2).

The formalism we developed is based on the harmonic approximation for the lattice vibrations. For alloys that present solid-solid transformations at temperatures close to the melting temperatures, the anharmonic effects may become important. *Part* of the anharmonic effects can be taken into account with the use of the quasi-harmonic approximation [183]. In the quasi-harmonic approximation, the *harmonic* vibrational free energy is computed as a function of unit cell parameters and internal coordinates of the atoms. The geometry is then relaxed to minimize the harmonic free energy at every temperature. With this scheme, thermal expansion effects can be taken into account. Although its implementation for classical-potential and



embedded-atom models is straightforward, it is not clear whether a first-principles approach is feasible due to the complexity of the problem. Further work is needed to clarify this point. To include *all* the anharmonic effects, a combination of molecular dynamics and Monte Carlo simulations is possible. However, this is only practical in systems modeled with classical potentials.

To obtain a complete description of the phase stability of alloys, an understanding of the thermodynamical properties of the liquid phases are necessary. Although the computation of the solid part of the phase diagram is well developed, very little is known about the liquid phases.

Finally, most of the technologically relevant alloys are not binary, but multicomponent alloys. While in this thesis we explored the ground states of ternary alloys, some studies have been done to understand their thermodynamic properties [74, 47]. However, much more work is needed to understand trends and be able to make quantitative predictions in multicomponent alloys.

We have concentrated our efforts in the calculation of *thermodynamic* properties of alloys. Nonetheless, the atomistic modeling of *kinetic* processes, including transport, processing, approach to equilibrium, etc. is also crucial for the development of new materials. But that is another story...



# Appendix A

## Building alloy configurations with specified values of correlation functions

We will consider in this appendix the problem of finding configurations  $\vec{\sigma}$  of two or more species on a lattice with specified values of correlation functions  $\langle\sigma_a\rangle$ . This problem is of importance for the determination of the ground-state structures of lattice models using the polytope method (see section 3.2 and flowchart in figure 3-8). The method to build the structures should be able to either find a structure or decide whether the set of correlation functions do not correspond to any configuration  $\vec{\sigma}$  (i.e., whether the structure is “inconstructible”).

The method we developed is based on two assumptions. The first assumption is that the set of known correlation functions correspond to all the subclusters of a given set of clusters. This assumption is necessary to be able to obtain the probabilities on the configurations on these clusters. The second assumption is that the number of atoms in the primitive unit cell of the sought configuration is less than a given number  $N_{max}$ . That maximum size depends on the problem to be solved and is determined by the computational power available. For the problems we solved in chapter 3, we assumed that the ground-state structures are periodic with less than 32 atoms in the primitive unit cell.<sup>1</sup>

The method consists of the following steps:

1. Find all the distinct unit cells for the possible superstructures on the parent lattice, with up to  $N_{max}$  atoms in the primitive unit cell. Two unit cells are considered distinct if the lattices they define cannot be mapped onto each other by any of the symmetry elements of the space group of the parent lattice (e.g., fcc). The results of this search of unit cells for the fcc lattice are shown in figure A-1.

---

<sup>1</sup>The assumption of a finite size of the ground-state structures may seem very restrictive. However, in most solutions of ground-state problems reported in the literature, the unit cells of the structures are relatively small, very rarely with more than 16 atoms.

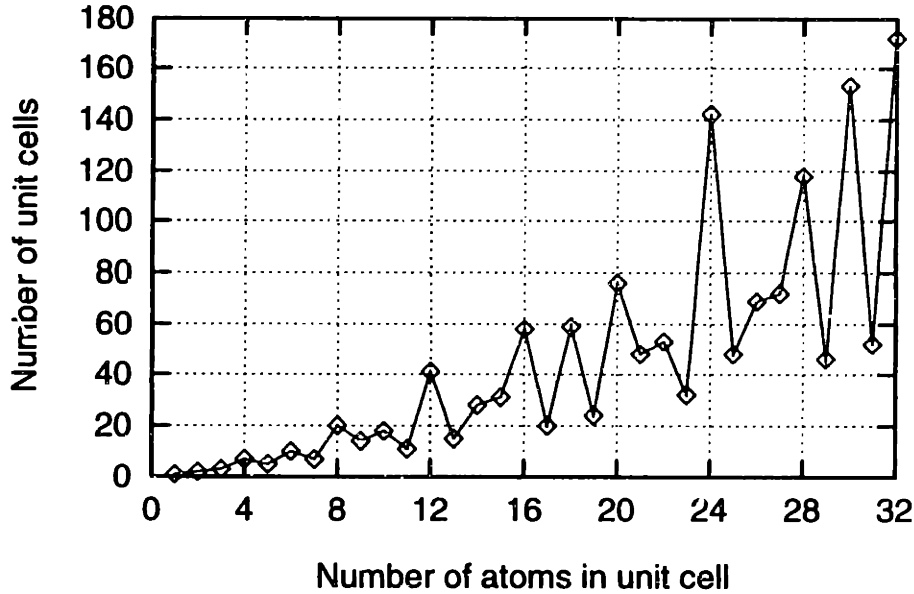


Figure A-1: Number of distinct unit cells of superstructures of fcc, as a function of the number of atoms in the cell.

2. Compute the probability  $P_\beta(J)$  of occurrence of the configurations  $J$  on the cluster(s)  $\beta$  for which the correlation functions  $\langle\sigma_\alpha\rangle$  are known for all its(their) subclusters  $\alpha$ . This is done for binary alloys using the relationship:

$$P_\beta(J) = \frac{1}{2^{n_\beta}} \sum_{\alpha \subseteq \beta} v_{\beta\alpha}(J) \langle\sigma_\alpha\rangle, \quad (\text{A.1})$$

where  $v_{\beta\alpha}(J)$  is the  $v$ -matrix defined in chapter 3 (equation 3.5). The extension for multicomponent alloys is straightforward [70].

3. Find the number of atoms in the unit cell that are consistent with the above probabilities. For example, if the point correlation function is  $1/2$  then the number of atoms in the unit cell has to be a multiple of 4.
4. Starting with the smallest possible unit cell, scan the possible unit cell sizes in increasing order.
5. For every possible size of unit cell, scan all the possible unit cells, and try to build the structure with the given set of probabilities of the selected clusters. To do this, we first choose a configuration with non-zero probability and put it on the lattice. Then, using a “branching” algorithm, put the other configurations with non-zero probability on the lattice. The overlap between different configurations and the periodic boundary conditions restrict the allowed choices of configurations. If, at some point in the branching algorithm a configuration which has zero probability is generated, then the branch of the algorithm is terminated. The procedure is carried on until a structure is found or all the

branches of the tree are terminated.

If after all the unit cells with up to  $N_{max}$  atoms have been explored no structure is found, then the set of correlation functions do not correspond to *any* structure with at most  $N_{max}$  atoms. Although this is not proof of inconstructibility, if  $N_{max}$  is large enough, it is very unlikely that correlation functions derived from the polytope method correspond to a configuration  $\vec{\sigma}$  on the lattice.



# Appendix B

## The Ising mapping of the alloy Hamiltonian: a toy model

One of the assumptions we made in section 4.1 is that every configuration on the lattice,  $\vec{\sigma}$ , has a well defined free energy. In other words, that there is a well defined free energy in the ensemble of constant  $\vec{\sigma}$ . This is a reasonable approximation for systems in which the time scale of the excitations within the ensemble of constant  $\vec{\sigma}$  is much faster than the timescale of changes in  $\vec{\sigma}$ . Our goal is to estimate the size of the error due to this approximation, by studying a very simple model.

Consider one particle in a one-dimensional potential defined by:

$$V(x) = \begin{cases} \gamma_B x^2/2 + 2(\gamma_B(E_m - E_0))x + E_m & x \leq 0 \\ \gamma_A x^2/2 + 2(\gamma_A E_m)x + E_m & x > 0 \end{cases} \quad (\text{B.1})$$

The geometrical meaning of the parameters is shown in figure B-1.

This potential can be thought of as a very simplified description of the energetics of an alloy system, when only two configurations,  $\vec{\sigma}_A$  and  $\vec{\sigma}_B$ , are considered. The Ising mapping of this problem would correspond to assigning the lattice configuration  $\vec{\sigma}_A$  when the coordinate of the particle is positive and  $\vec{\sigma}_B$  when it is negative. To evaluate the error in the thermodynamic properties computed with such Ising mapping, we will compute the probability of the system being in  $\vec{\sigma}_A$  using an *exact* approach and the *Ising* solution of the “lattice” Hamiltonian. In the Ising mapping, each configuration is assigned a free energy according to:

$$\begin{aligned} F(\vec{\sigma}_A, T) &= F_{harm}(\omega_A, T) \\ F(\vec{\sigma}_B, T) &= E_0 + F_{harm}(\omega_B, T), \end{aligned} \quad (\text{B.2})$$

where  $\omega_A \equiv \gamma_A^{1/2}$  and  $\omega_B \equiv \gamma_B^{1/2}$  are the vibrational frequencies of the system in state *A* and *B* respectively (assuming unitary mass), and  $F_{harm}(\omega, T)$  is the vibrational free energy of an oscillator with frequency  $\omega$ , here computed in the classical approximation.

The probability of the system to be found in  $\vec{\sigma}_A$  can be easily computed from the

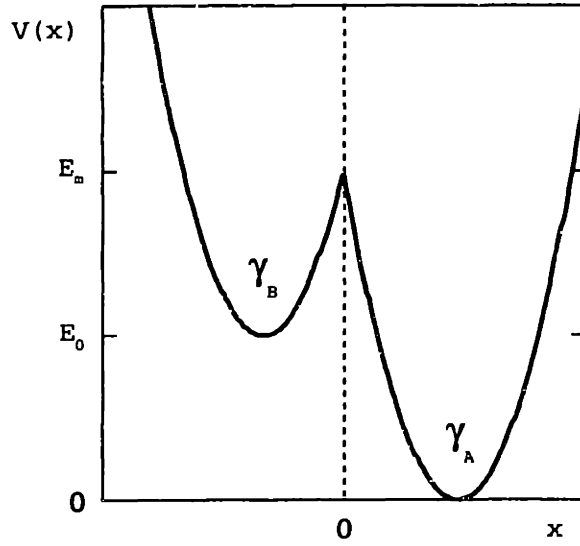


Figure B-1: One-dimensional potential used to study the accuracy of the Ising mapping of the alloy Hamiltonian. The parameters  $\gamma_A$  and  $\gamma_B$  are the second derivatives of the potential at the minima.

above free energies, obtaining:

$$P_A(\text{Ising}) = \frac{\omega_B}{\omega_B + \omega_A e^{-E_0/T}}. \quad (\text{B.3})$$

The exact probability of  $\vec{\sigma}_A$  (i.e.,  $x > 0$ ) can be computed by integrating the classical partition function of the system defined by the potential in equation B.1:

$$P_A(\text{Exact}) = \frac{\omega_B}{\omega_B + \frac{\text{erfc}\left[-\sqrt{\frac{E_m - E_0}{T}}\right]}{\text{erfc}\left[-\sqrt{\frac{E_m}{T}}\right]} \omega_A e^{-E_0/T}}, \quad (\text{B.4})$$

where  $\text{erfc}(x)$  is the complementary error function.

As expected, the exact result (equation B.4) reduces to the Ising approximation (equation B.3) in the limit of  $E_m \rightarrow \infty$ . In this limit, the barrier between the two configurations is infinitely high and the system will be ergodic in each configuration. In this case, the free energies in equation B.2 are well defined, justifying the Ising mapping.

As the "migration" energy  $E_m$  is lowered, the exact solution deviates from the Ising approximation. In this case, the residence time of the system in one configuration is not long enough for the system to sample all the phase space associated with that configuration. Figure B-2 shows the exact values of  $P_A$  for the special case  $\omega_A = \omega_B$ ,



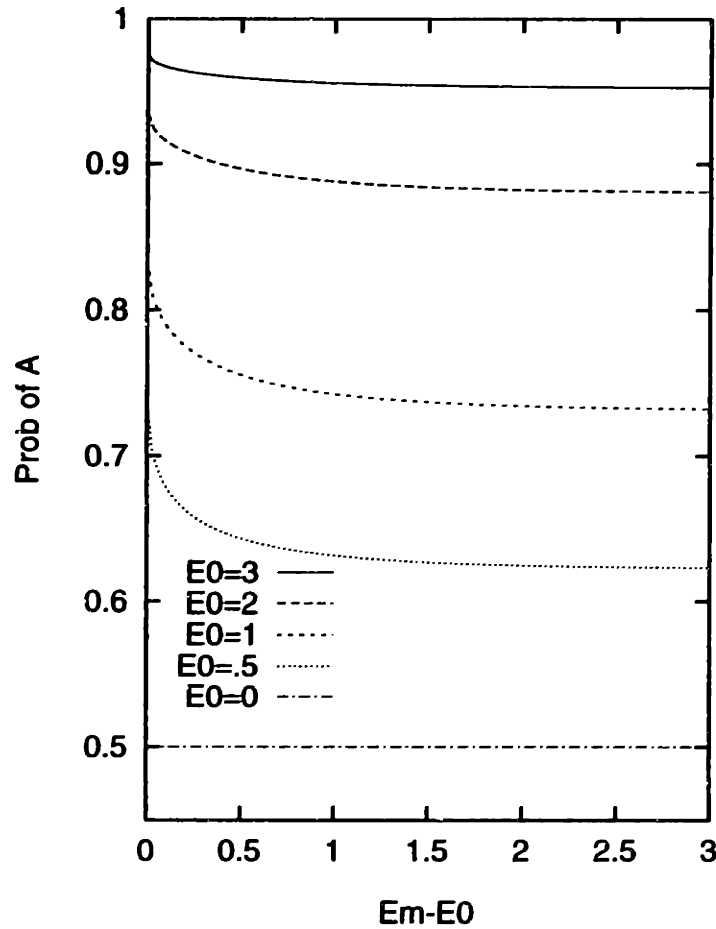


Figure B-2: Exact probability of finding the system in  $\vec{\sigma}_A$ , as a function of the migration barrier,  $E_m - E_0$ , for different values of the “spin flip energy,”  $E_0$ , when  $\omega_A = \omega_B$ . Both energies are expressed in units of the temperature,  $T$ . The asymptotic value for large  $E_m - E_0$  corresponds to the Ising solution of equation B.3.

as a function of the migration barrier,  $E_m$ , for different values of  $E_0$ .

In our model system, the Ising mapping underestimates the probability of the lower energy state,  $\vec{\sigma}_A$ . This is not due to the vibrational free energy, but to the non-ergodicity of the system in each Ising configuration  $\vec{\sigma}$ . The size of the error depends on the migration barrier.

A *rough* estimate of the Ising error in the predicted transition temperatures can be computed by comparing equations B.3 and B.4. We can define an energy  $E_1$  such that equation B.4 has the same form as the Ising expression B.3 with  $E_1$  as the energy change between states  $\vec{\sigma}_A$  and  $\vec{\sigma}_B$  instead of  $E_0$ .  $E_1$  is the “spin flip energy” in an Ising model that would produce the exact value of  $P_A$  (note that  $E_1$  is temperature-dependent). If the temperature of a phase transition in the *real system*<sup>1</sup> is proportional to the energy scales, then we can estimate the ratio of transition

<sup>1</sup>Note that our very simple model system does not exhibit a phase transition. It is only being used to estimate the behavior of more complex systems.

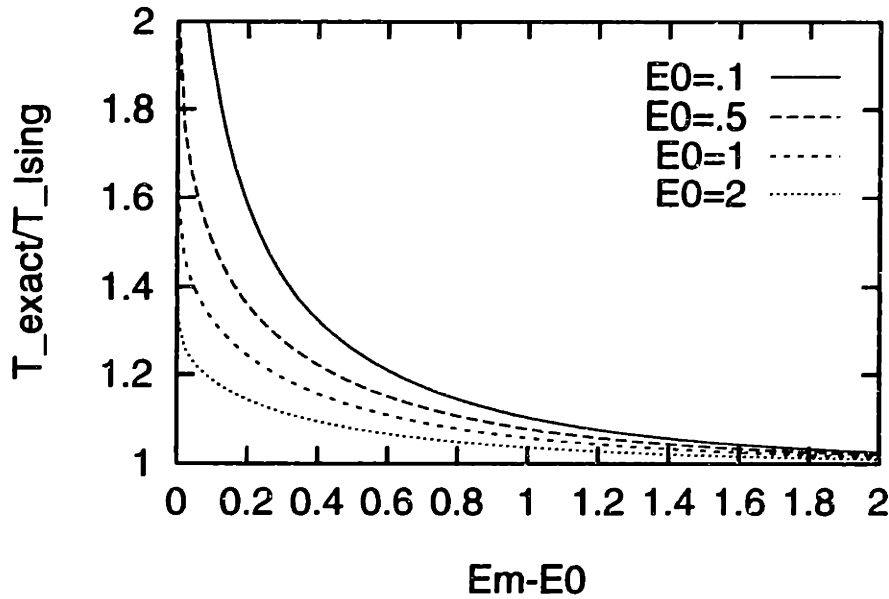


Figure B-3: Rough estimate of the error in the transition temperature of a phase transition due to the Ising mapping of the alloy Hamiltonian. The ratio of transition temperatures is shown as a function of the migration barrier,  $E_m - E_0$ , for different values of the “spin flip energy,”  $E_0$ , when  $\omega_A = \omega_B$ . Both energies are expressed in units of the temperature,  $T$ .

temperatures,  $T_{Exact}/T_{Ising}$  as:

$$\frac{T_{Exact}}{T_{Ising}} = \frac{E_1}{E_0} = 1 + \frac{T}{E_0} \ln \frac{\operatorname{erfc} \left[ -\sqrt{\frac{E_m}{T}} \right]}{\operatorname{erfc} \left[ -\sqrt{\frac{E_m - E_0}{T}} \right]}. \quad (\text{B.5})$$

Figure B-3 shows the ratio between the exact and Ising transition temperatures, for different values of the “spin flip energy,”  $E_0$ , as a function of the migration energy,  $E_m - E_0$ . It is interesting to note that the transition temperatures are systematically underestimated by the Ising model, for our *very simple* model system. The Ising model of our system underestimates the stability of the low energy state ( $\bar{\sigma}_A$  in our system).

To compute the size of the error of the Ising model for real systems, we estimated the values of  $E_0$  and  $E_m$ , from experimental measurements, or modeling studies of the energetics of some alloy systems.

The AgI compound undergoes a phase transition at  $T \sim 420\text{K}$  to a high-temperature phase (called the  $\alpha$  phase) in which the I ions form a bcc lattice and the Ag ions occupy the interstitial sites [184, 85] At high temperatures, the Ag ions are highly mobile, showing a quasi-liquid behavior. This behavior is due to the low migration barrier between the tetrahedral sites for the Ag ions. We estimate the migration barrier to be of the order of 0.2 to 0.3 eV from molecular dynamics results [184, 85] at  $T = 1000\text{K}$ . Then  $E_m \sim 3T$ . Since at this temperature the Ag atoms are completely

disordered, the association energy of Ag atoms (which is related to  $E_0$ ) has to be much lower than this temperature. For any reasonable guess of  $E_0$  the error in the transition temperature due to the Ising mapping is at most 2%. Note that AgI is probably one of the most difficult systems to model with the Ising mapping due to the small migration barrier of the Ag atoms, and therefore a short time between configuration changes. In spite of this we found that the error of the Ising mapping is only of a few percent, which is much smaller than errors induced by other approximations (e.g., method to compute the energy of different configurations).

In Si-Ge alloys, typical spin-flip energies are of the order of .01 eV [164], while migration barriers (e.g., with the concerted exchange mechanism [185]) are of the order of 4 eV. Since the predicted consolute temperature for the Si-Ge miscibility gap is  $T_c \sim 200\text{K}$  [160], we get  $E_m \sim 250$  and  $E_0 \sim 0.6$ , both in units of  $T_c$ . The resulting error in the Ising mapping for Si-Ge alloys is too small to be computed:  $T_c(\text{Exact})/T_c(\text{Ising}) = 1 + x$ , with  $x < 10^{-100}$ !

By using a very simple model system, we studied the error in the predicted transition temperatures of alloy phase transformations, due to the assumption that every substitutional configuration  $\vec{\sigma}$  of the alloy has a well defined free energy. We conclude that, for most systems of interest, the error is negligible. Even for systems that present relatively small migration barriers, such as AgI, the error in the transition temperature would only be of a few percent.



# Appendix C

## Classical potentials

The effect of the lattice vibrations on the phase stability of substitutional alloys can be easily computed if the system is modeled with classical potentials. In this appendix, we review some of the functional forms used to model the interaction of atoms.

A materials system is composed by nuclei and electrons. The Born–Oppenheimer approximation allows us to assign a well defined energy to an atomic system as a function of only the coordinates of the nuclei. Since the electrons are much lighter than the nuclei ( $M_e/M_n \sim 10^{-4}$ ), their quantum–mechanical state responds almost instantaneously to any change in the positions of the nuclei. These considerations allows us to write the potential energy of the system as function of the nuclei coordinates alone:

$$V = V(\vec{R}_1, \dots, \vec{R}_N), \quad (\text{C.1})$$

where  $\vec{R}_i$  are the positions of the nuclei. In this appendix, we review the functional forms used in the literature for  $V(\vec{R}_1, \dots, \vec{R}_N)$ , and how to obtain their parameters with empirical approaches.

The simplest approach, is to assume a functional form for  $V(\vec{R}_1, \dots, \vec{R}_N)$  and try to capture the physics of the system by a wise choice of this form and of the parameters in it. According to the type of function used, the methods can be classified as shown in figure C-1 [10]. Here, we will only review the pair and cluster potentials. The reader is referred to reference [10] for a description of the functionals.

### C.1 Pair potentials

The pair potential energy functions have the following form:

$$V(\vec{R}_1, \dots, \vec{R}_N) = V_0 + \frac{1}{2} \sum_{i,j} V^{(2)}(|\vec{R}_i - \vec{R}_j|) \quad (\text{C.2})$$

The functional form of  $V^{(2)}$  is usually chosen according to the kind of atom that is being modeled. In any case,  $V^{(2)}$  should have some general features. When atoms  $i$  and  $j$  are very far apart, their contribution to the energy of the system should be small and therefore we expect  $V^{(2)}(r)$  to decay to zero at large values of  $r$ . On the

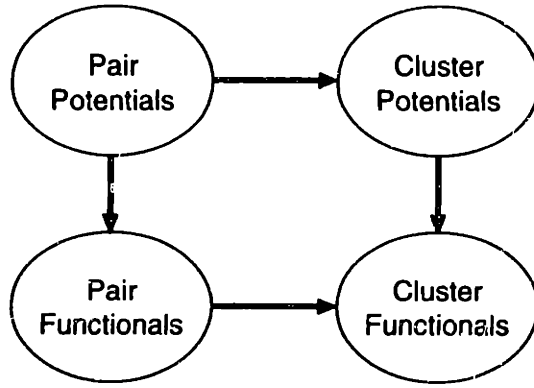


Figure C-1: Possible types of energy functions and functionals for the description of the energy of an assembly of atoms. After figure 1 in reference [10]. The arrows point in the direction of increasing complexity

other hand, when atoms  $i$  and  $j$  are very close together, they strongly repel each other because of both electrostatic and quantum effects.

A review of both empirical and fundamental approaches to obtain pair potentials for specific systems can be found in reference [186]. Some “popular” functional forms are:

- Hard spheres:

$$V^{(2)}(r) = \begin{cases} \infty & r \leq a \\ 0 & r > a \end{cases} \quad (\text{C.3})$$

- Potential wells:

$$V^{(2)}(r) = \begin{cases} \infty & r \leq a \\ -\epsilon & a < r \leq b \\ 0 & r > b \end{cases} \quad (\text{C.4})$$

- The Buckingham potentials:

$$V^{(2)}(r) = Ae^{-Br} - \frac{C}{r^6} - \frac{D}{r^8}, \quad (\text{C.5})$$

where the terms can be interpreted as:

- exponential repulsion: overlap of electronic clouds,
- $r^{-6}$ : induced dipole – induced dipole interactions [187],
- $r^{-8}$ : quadrupole–quadrupole interactions.

This potential function diverges to  $-\infty$  at the origin and is sometimes truncated with a hard-sphere core.

- The Lennard–Jones potential [188]. The functional form is:

$$V^{(2)}(r) = \frac{A_n}{r^n} - \frac{A_m}{r^m}. \quad (\text{C.6})$$

Usually  $n = 12$  and  $m = 6$ , but also  $n = 8$  and  $m = 4$  have been used [128]. This potential was originally proposed to explain the variation of viscosity with temperature in gases. Due to the simple functional form, the second virial coefficient can be computed analytically. Although the repulsive part has no theoretical justification, its simple form made it very popular to model not only rare gases [12], but also some properties of metals [189].

- The Morse potential. The functional form is:

$$V^{(2)}(r) = De^{-2\alpha(r-r_0)} - 2De^{-\alpha(r-r_0)}. \quad (\text{C.7})$$

Morse [190] proposed this potential to account for the energy levels of diatomic molecules, and used spectroscopic data for different molecules to obtain the parameters of the potential. It was later found that the Buckingham form gives a better interpretation of the spectroscopic data. Although originally devised for molecules, the functional form proposed by Morse has been extensively used for solids. The three parameters of the Morse potential, can be fitted to the lattice constant, cohesive energy and compressibility. Values of the parameters for several metals can be found in page 56 of reference [186]. For these metals, the “predicted” equation of state agrees well with experiment, but the elastic constants show some deviation.

- The Coulomb potential. Of course, the electrostatic contribution to the energy is known exactly to be the Coulomb potential of the form:

$$V^{(2)}(r) = \frac{Z_i Z_j}{r}, \quad (\text{C.8})$$

where  $Z_i$  and  $Z_j$  are the ionic charges on ions  $i$  and  $j$  respectively. Due to the extended interaction range, special techniques need to be used to perform the summations to get the Coulombic energy of a solid–state system [191].

- For some simple ionic crystals, the electrostatic contribution can be supplemented with a Born–Mayer potential of the form:

$$V^{(2)}(r) = Ae^{-Br} \quad (\text{C.9})$$

to avoid collapsing the crystal under the electrostatic attraction.

- “Shell models” have been developed to include polarizability effects in ionic materials [192].
- A myriad of other functional forms for pair potentials has been proposed and used for different kinds of materials.

### C.1.1 Limitations of pair potentials

Independently of the functional form, the pair potentials fail to reproduce some general features of the energetics of condensed systems:

- In general, the pair potential that describes the interaction of two atoms in vacuum is very different from what you need to understand the solid phases. This is seen, e.g., in Ni and Si [10], where the cohesive energy ( $E_c$ ) as a function of coordination is not what is expected from a pair potential model. If only nearest-neighbor atoms interact,  $E_c$  is linear with the coordinations number for a system modeled with a pair potential.
- Vacancy formation energy: Ignoring relaxation, the vacancy formation energy in a pair potential model must equal the cohesive energy per atom. In most metals, the vacancy formation energy is less than half the cohesive energy per atom. In general, lattice relaxation effects can account for only 15% of the difference. The rest of the difference is due to multibody effects, not present in the pair-potential description.
- Elastic constants: For cubic materials at zero pressure, pair potentials predict some relationships between the elastic constants, e.g.,  $C_{12} = C_{44}$ . In transition metals and semiconductors, this is violated by 30% or more.
- Stable crystal structures: Open crystal structures (e.g., diamond cubic, simple cubic, etc.) are unlikely to be stabilized with pair potentials.
- Relaxation at surfaces: in metals, simple pair potentials predict outward surface relaxation, whereas experiments show inward relaxation.

## C.2 Multibody potentials

To overcome the problems of the pair potentials, one could include higher order terms, i.e., terms of the form  $V^{(3)}(\vec{R}_i, \vec{R}_j, \vec{R}_k)$ . The general trend indicates that this approach is much more successful for semiconductors than for metals. The 3- and 4-body interactions allow for the inclusion of bond-bending and torsion effects in the energy that are of critical importance in covalent materials, such as semiconductors or organic compounds. Bonding in metals is more complex and functionals, such as the embedded atom method [193, 194], are necessary.

The Stillinger-Weber potential for silicon [195] is probably one of the most used multibody potentials. Its functional form depends on seven parameters that were fitted to obtain a stable diamond structure and to get a reasonable melting temperature and radial distribution function in the liquid phase.

There are numerous functional forms for multibody potentials in the literature. In commercial software,<sup>1</sup> the most general potential has tens of terms and tens of

---

<sup>1</sup>In commercial software packages and in the field of organic chemistry, the pair and multibody potentials are often referred to as "force fields."



parameters. To be able to obtain the parameters for these potentials, we need to fit them to observed experimental properties or first-principles calculations. Some of the properties often fitted to are:

- Lattice constants.
- Cohesive energy.
- Bulk modulus and elastic constants.
- Equation of state (energy vs. volume curve).
- Phonon frequencies.
- Stable crystal structure(s).
- Surface energy and relaxation.
- Surface reconstruction.
- Liquid pair correlation functions.
- Non-ideal behavior of a gas (e.g., the second virial coefficient).
- Dislocations: structure, formation energy, migration energy.
- Point defects (vacancies, interstitials): formation energy and relaxations.
- Native states in polymers.
- etc., etc. . . .

In general, empirical pair and multibody potentials contain very little physical information about the system to be studied, and should therefore be regarded as a tool to interpolate between the few known properties the potentials are fitted to. An alternative approach is to obtain potentials from quantum-mechanical perturbation theory (see, e.g., the book by Hafner [196] for a review of first-principles potentials for *s-p* bonded metals, and references [197] and [198] for *d*-electron transition metals), in which case, the model has more reliable predicting capabilities.



# Appendix D

## Generating k-points to perform integrals over the Brillouin zone

### D.1 Introduction

Often we need to perform integrals over the Brillouin zone (BZ) in reciprocal space of the form

$$I = \Omega^{-1} \int_{BZ} f(\vec{k}) d\vec{k}, \quad (\text{D.1})$$

where  $\Omega$  is the volume of the BZ. These integrals are needed to compute, e.g., the electronic density from the wave functions in a periodic system (for self-consistent LDA), the total energy from the electronic bands, the electronic density of states from the bands, or the vibrational density of states from the phonon dispersion relations.

In general, these integrals are done numerically, by sampling the value of  $f(\vec{k})$  at a well chosen set of  $\vec{k}_i$  with weights  $\omega_i$ , or

$$I \approx \sum_{i=1,N} \omega_i f(\vec{k}_i), \quad (\text{D.2})$$

$$\text{with } \sum_{i=1,N} \omega_i = 1. \quad (\text{D.3})$$

We now discuss different methods of choosing the set of k-points for primitive cells and for superstructures.

### D.2 Primitive cells

#### D.2.1 Brute Force

Easy choices are a uniform grid of points in the BZ, or a set of random points. In both cases all the points are assigned equal weights. These are easy choices, but it is usually necessary to use a large number of k-points ( $\sim 1,000$  or more) to get converged values for the integrals. For the cases when these integrals are the time-consuming part of the code, it is worth using better chosen k-points.

level	fcc	bcc	sc	tet	orth
1	2	1	1	1	1
2	10	2	4	6	8
3	60	8	20	40	64
4	408	40	120	288	512
5	2,992	240	⋮	⋮	⋮

Table D.1: Number of Chadi–Cohen  $k$ -points for several lattices.

## D.2.2 Using the symmetry

A simple way of improving on the uniform grid is to use the symmetry of the structure to remove the redundant  $k$ -points, adjusting the weights of the remaining ones. This method is a special case of a more general scheme developed by Monkhorst and Pack [199] and generalized and reviewed by Sverre Froyen [200].

## D.2.3 The Chadi–Cohen scheme

There are several ways of choosing the  $k$ -points wisely. The method of Chadi and Cohen [13] is one of the most popular. For every space group, it provides a hierarchy of  $k$ -point sets that consistently improve the approximation. These sets are chosen so that the integral is done exactly for functions  $f(\vec{k})$  that only contain up to a certain Fourier component. As we go up the hierarchy the integral is well approximated for more complex functions. It also uses the symmetry of the BZ to avoid computing redundant  $k$ -points. For details of the method, see the original paper. In table D.1, we list the number of  $k$ -points as we go up the Chadi–Cohen hierarchy for these Bravais lattices.

For fcc the Chadi–Cohen points coincide with the points obtained from a uniform grid using the symmetry (as in D.2.2), using grids of sizes 2, 4, 8, 16, . . .

When the point group of the structure to be studied is a subgroup of the point group of the corresponding Bravais lattice, the Chadi–Cohen points have to be “augmented” using the procedure described below.

## D.3 Superstructures

If the unit cell in real space is a superstructure of a given parent lattice, there is an alternative approach to get the  $k$ -points. The idea is to use an “equivalent” set of  $k$ -points for all the superstructures of a given parent lattice. By “equivalent,” people *usually* mean points that correspond to the same points in the actual reciprocal space.

The procedure to get these  $k$ -points is as follows:

- Obtain the  $k$ -points for the parent lattice, using any of the above schemes (D.2.2 or D.2.3).

- Apply the symmetry elements of the point group of the parent lattice to these  $k$ -points.
- Using the symmetry translations (in reciprocal space) of the superstructure, map all the  $k$ -points back into the Brillouin zone of the superstructure.
- Using the point group elements of the superstructure, remove the redundant  $k$ -points, adjusting the weights of the remaining  $k$ -points.

This same procedure can be used to obtain the Chadi-Cohen points for a structure which has a point group of lower symmetry than its Bravais lattice. In this case, the primitive and super cells would be the same, but the point group of the supercell would be a subgroup of the point group of the Bravais lattice.

Most of the  $k$ -space quantities we are interested in are centro-symmetric (inversion at the origin), even when the space group of the structure does not have an inversion center. Therefore, in most cases, we should include the inversion in the point group.



# Bibliography

- [1] R. Lenzner. The reluctant entrepreneur. *Forbes*, 156:162–166, 1995.
- [2] Furio Ercolessi. MDBNCH: A molecular dynamics benchmark. Universal Resource Locator <http://www.sissa.it/furio/mdbnch.html>.
- [3] J. Kanamori and Y. Kakehashi. Conditions for the existence of ordered structure in binary alloy systems. *Journal de Physique*, 38:C7–274, 1977.
- [4] L. Anthony, J. K. Okamoto, and B. Fultz. Vibrational entropy of ordered and disordered Ni<sub>3</sub>Al. *Physical Review Letters*, 70:1128, 1993.
- [5] B. Fultz, L. Anthony, L. J. Nagel, R. M. Nicklow, and others. Phonon densities of states and vibrational entropies of ordered and disordered Ni<sub>3</sub>Al. *Physical Review B*, 52:3315–21, 1995.
- [6] L. Anthony, L. J. Nagel, J. K. Okamoto, and B. Fultz. Magnitude and origin of the difference in vibrational entropy between ordered and disordered Fe<sub>3</sub>Al. *Physical Review Letters*, 73:3034, 1994.
- [7] B. Fultz, L. Anthony, J. L. Robertson, R. M. Nicklow, and others. Phonon modes and vibrational entropy of mixing in Fe–Cr. *Physical Review B*, 52:3280–5, 1995.
- [8] L. J. Nagel, L. Anthony, and B. Fultz. Differences in vibrational entropy of disordered and ordered Cu<sub>3</sub>Au. *Philosophical Magazine Letters*, 72:421–7, 1995.
- [9] Y. Yin and B. B. Argent. The phase diagrams and thermodynamics of the ZrO<sub>2</sub>–CaO–MgO and CaO–MgO systems. *Journal of Phase Equilibria*, 14:588–600, 1993.
- [10] A. E. Carlsson. Beyond pair potentials in elemental transition metals and semiconductors. *Solid State Physics*, 43:1, 1990.
- [11] G. D. Garbulsky, P. D. Tepesch, and G. Ceder. Ground state analysis on the fcc lattice with four pair interactions. In J. Broughton, P. Bristowe, and J. Newsam, editors, *Materials Research Society Symposium Proceedings*, volume 291, page 259, Boston, 1993.

- [12] M. L. Klein and J. A. Venables. *Rare gas solids*. Academic Press, London, 1976.
- [13] D. J. Chadi and M. L. Cohen. Special points in the Brillouin zone. *Physical Review B*, 8:5747–53, 1973.
- [14] T. Hahn, editor. *International tables for crystallography*. Kluwer Academic Publishers, Dordrecht, 1989.
- [15] R. Lenzner. Whither Moore’s law? *Forbes*, 156:167–168, 1995.
- [16] N. W. Ashcroft and N. D. Mermin. *Solid State Physics*. Saunders College, Philadelphia, 1976.
- [17] P. Hohenberg and Kohn W. Inhomogeneous electron gas. *Physical Review*, 136:864B, 1964.
- [18] W. Kohn and L. J. Sham. Self-consistent equations including exchange and correlation effects. *Physical Review*, 140:1133A, 1965.
- [19] R. O. Jones and O. Gunnarsson. The density functional formalism, its applications and prospects. *Reviews of Modern Physics*, 61:689–746, 1989.
- [20] M. C. Payne, M. P. Teter, D. C. Allan, Arias T. A., and others. Iterative minimization techniques for ab initio total-energy calculations: molecular dynamics and conjugate gradients. *Reviews of Modern Physics*, 64:1045–97, 1992.
- [21] K. Huang. *Statistical mechanics*. John Wiley & Sons, New York, 1987.
- [22] R. Kikuchi. A theory of cooperative phenomena. *Physical Review*, 81:988, 1951.
- [23] K. Binder and D. W. Heermann. *Monte Carlo simulation in statistical physics*. Springer-Verlag, Berlin, 1988.
- [24] M. P. Allen and D. J. Tildesley. *Computer simulation of liquids*. Oxford University Press, New York, 1987.
- [25] R. Car and M. Parrinello. Unified approach for molecular dynamics and density-functional theory. *Physical Review Letters*, 55:2471–4, 1985.
- [26] S. Goedecker. Low complexity algorithms for electronic structure calculations. *Journal of Computational Physics*, 118:261–8, 1995.
- [27] S. Goedecker and L. Colombo. Efficient linear scaling algorithm for tight-binding molecular dynamics. *Physical Review Letters*, 73:122–5, 1994.
- [28] G. Ceder. A derivation of the Ising model for the computation of phase diagrams. *Computational Materials Science*, 1:144, 1993.
- [29] C. M. van Baal. Order-disorder transformations in a generalized Ising alloy. *Physica*, 64:571–86, 1973.



- [30] J. M. Sanchez, J. P. Stark, and V. L. Moruzzi. First-principles calculation of the Ag-Cu phase diagram. *Physical Review B*, 44:5411, 1991.
- [31] M. Asta, R. McCormack, and D. de Fontaine. Theoretical study of alloy phase stability in the Cd-Mg system. *Physical Review B*, 48:748, 1993.
- [32] A. Silverman, A. Zunger, A. Kalish, and J. Adler. Atomic-scale structure of disordered  $\text{Ga}_{1-x}\text{In}_x\text{P}$  alloys. *Physical Review B*, 51:10795–816, 1995.
- [33] C. Wolverton, Alex Zunger, and Z. W. Lu. Long-range versus short-range order in  $\text{Ni}_3\text{V}$  and  $\text{Pd}_3\text{V}$  alloys. *Physical Review B*, 49:16058–61, 1994.
- [34] J. M. Sanchez, F. Ducastelle, and D. Gratias. Generalized cluster description of multicomponent systems. *Physica*, 128A:334, 1984.
- [35] J. W. D. Connolly and A. R. Williams. Density-functional theory applied to phase transformations in transition-metal alloys. *Physical Review B*, 27:5169, 1983.
- [36] Z. W. Lu, S. H. Wei, Alex Zunger, S. Frota-Pessoa, and L. G. Ferreira. First-principles statistical mechanics of structural stability of intermetallic compounds. *Physical Review B*, 44:512, 1991.
- [37] D. B. Laks, L. G. Ferreira, S. Froyen, and A. Zunger. Efficient cluster expansion for substitutional systems. *Physical Review B*, 46:12587, 1992.
- [38] L. G. Ferreira, A. A. Mbaye, and A. Zunger. Chemical and elastic effects on isostructural phase diagrams: the  $\epsilon$ -G approach. *Physical Review B*, 37:10547–70, 1988.
- [39] H. Dreyssé, A. Berera, L. T. Wille, and D. de Fontaine. Determination of effective-pair interactions in random alloys by configurational averaging. *Physical Review B*, 39:2442, 1989.
- [40] C. Wolverton, G. Ceder, D. de Fontaine, and H. Dreyssé. Ab-initio determination of structural stability in fcc-based transition-metal alloys. *Physical Review B*, 48:726, 1993.
- [41] F. Ducastelle. *Order and Phase Stability in Alloys*. North-Holland, Amsterdam, 1991.
- [42] G. Ceder. *Alloy theory and its applications to long period superstructure ordering in metallic alloys and high temperature superconductors*. PhD thesis, University of California at Berkeley, 1991.
- [43] M. J. Buerger. *Elementary crystallography*. MIT Press, Cambridge, 1978.
- [44] D. de Fontaine. Cluster approach to order-disorder transformations. *Solid State Physics*, 47:33–176, 1994.

- [45] P. Cenedese and D. Gratias. Multicomponent formalism in the mean-field approximation: a geometric interpretation of Chebychev polynomials. *Physica A*, 179:277, 1991.
- [46] R. P. McCormack. *Applications of the cluster expansion to substitutional disorder in ternary and hexagonal-close-packed binary alloys*. PhD thesis, University of California at Berkeley, 1994.
- [47] A. J. S. Traiber. *Electronic structure and phase equilibria in ternary substitutional alloys: a tight-binding approach*. PhD thesis, Massachusetts Institute of Technology, 1995.
- [48] C. Wolverton, D. de Fontaine, and H. Drysse. Global volume relaxations and phase stability in disordered Pd-Rh alloys. *Physical Review B*, 48:5766-78, 1993.
- [49] G. Ceder, G. D. Garbulsky, and P. D. Tapesch. Convergent real-space cluster expansion for configurational disorder in ionic systems. *Physical Review B*, 51:11257-61, 1995.
- [50] P. D. Tapesch, G. D. Garbulsky, and G. Ceder. Model for configurational thermodynamics in ionic systems. *Physical Review Letters*, 74:2272-5, 1995.
- [51] Z. W. Lu, D. B. Laks, S. H. Wei, and A. Zunger. First-principles simulated annealing study of phase-transitions and short-range order in transition metal and semiconductor alloys. *Physical Review B*, 50:6642, 1994.
- [52] G. D. Garbulsky and G. Ceder. Linear-programming method for obtaining effective cluster interactions in alloys from total-energy calculations: application to the fcc Pd-V system. *Physical Review B*, 51:67-72, 1995.
- [53] V. Chvatal. *Linear Programming*. W. H. Freeman and Company, Ney York, 1983.
- [54] P. E. A. Turchi, G. M. Stocks, W. H. Butler, D. M. Nicholson, and A. Gonis. First-principles study of ordering properties of substitutional alloys using the generalized perturbation method. *Physical Review B*, 37:5982, 1988.
- [55] G. Ceder, P. D. Tapesch, C. Wolverton, and D. de Fontaine. Ab-initio computation of the fcc Pd-V phase digram. In P. E. A. Turchi and A. Gonis, editors, *Statics and Dynamics of Alloy Phase Transformations*, page 571, New York, 1994. Plenum Press.
- [56] C. Wolverton, G. Ceder, D. de Fontaine, and H. Dreysse. Ab-initio ground-state study with fourth-nearest-neighbor cluster interactions for fcc Pd-V alloys. *Physical Review B*, 45:13105, 1992.

- [57] P. D. Tapesch, G. Ceder, C. Wolverton, and D. de Fontaine. An ab-initio calculation of the Pd-V fcc superstructure phase diagram with fourth nearest neighbor cluster interactions. In J. Broughton, P. Bristowe, and J. Newsam, editors, *Materials Research Society Symposium Proceedings*, volume 291, page 129, Boston, 1993.
- [58] C. Wolverton and A. Zunger. Comparison of two cluster-expansion methods for the energetics of Pd-V alloys. *Physical Review B*, 50:10548-60, 1994.
- [59] H. L. Skriver. *The LMTO Method*. Springer, Berlin, 1984.
- [60] E. Ising. *Z. Phys.*, 31:253, 1925.
- [61] A. van de Walle. Inequality generation for the ground-state problem. Private communication.
- [62] H. Edelsbrunner. *Algorithms in Combinatorial Geometry*. Springer-Verlag, Berlin, 1987.
- [63] S. M. Allen and J. W. Cahn. Ground state structures in ordered binary alloys with second neighbor interactions. *Acta Metallurgica*, 20:423-33, 1972.
- [64] J. Kanamori. Magnetization process in an Ising spin system. *Progress of Theoretical Physics*, 35:16-35, 1966.
- [65] A. Finel. *Contribution a l'etude des effets d'ordre dans le cadre du modele d'Ising: Etats de base et diagrammes de phase*. PhD thesis, Universite Pierre et Marie Curie, 1987.
- [66] A. J. S. Traiber and S. M. Allen. Ground state structures in ordered bcc ternary alloys with second-neighbor interactions. *Acta Metallurgica et Materialia*, 40:1403-8, 1992.
- [67] J. M. Sanchez and D. de Fontaine. *Structure and Bonding in Crystals*, volume II, page 117. Academic Press, New York, 1981.
- [68] T. Kudo and S. Katsura. A method of determining the orderings of the Ising model with several neighbor interactions under the magnetic field and applications to hexagonal lattices. *Progress of Theoretical Physics*, 56:435-49, 1976.
- [69] R. McCormack, M. Asta, D. de Fontaine, G. Garbulsky, and G. Ceder. hcp ising model in the cluster-variation approximation. *Physical Review B*, 48:6767, 1993.
- [70] G. Ceder, G. D. Garbulsky, D. Avis, and K. Fukuda. Ground states of a ternary fcc lattice model with nearest- and next-nearest-neighbor interactions. *Physical Review B*, 49:1-7, 1994.
- [71] David Avis. Estimation of the number of vertices of a polytope. Private communication.

- [72] G. Petzow and G. Effenberg. *Ternary Alloys: a comprehensive compendium of evaluated constitutional data and phase diagrams*. Weinheim, New York, 1992.
- [73] A. Marty, Y. Calvayrac, F. Guillet, and P. Cenedese. Thermodynamics of order in dilute fcc ternary alloys. *Physical Review B*, 44:11640-8, 1991.
- [74] R. McCormack, D. de Fontaine, C. Wolverton, and G. Ceder. Nonempirical phase equilibria in the W-Mo-Cr system. *Physical Review B*, 51:15808-22, 1995.
- [75] A. J. S. Traiber, M. Sluiter, P. E. A. Turchi, and S. M. Allen. Electronic structure and phase stability properties in ternary substitutional alloys. In J. Broughton, P. Bristowe, and J. Newsam, editors, *Materials Research Society Symposium Proceedings*, volume 291, page 437, Boston, 1993.
- [76] C. Wolverton and D. de Fontaine. Cluster expansions of alloy energetics in ternary intermetallics. *Physical Review B*, 49:8627-42, 1994.
- [77] G. Inden and W. Pitsch. Atomic ordering. In R. W. Cohns, editor, *Materials Science and Technology: A Comprehensive Review*, pages 497-552. Weinheim, New York, 1991.
- [78] G. B. Taggart. Generalized flinn operators with applications to multi-component alloys. *Journal of the Physics and Chemistry of Solids*, 34:1917-25, 1973.
- [79] W. Hoston and A. N. Berker. Multicritical phase diagrams of the Blume-Emery-Griffiths model with repulsive biquadratic coupling. *Physical Review Letters*, 67:1027-30, 1991.
- [80] T. S. Motzkin, H. Raiffa, G. L. Thompson, and R. M. Thrall. The double description method. In H. W. Kuhn and A. W. Tucker, editors, *Contribution to the Theory of Games*, pages 81-103. Princeton University Press, Princeton, NJ, 1953.
- [81] D. Avis and K. Fukuda. A pivoting algorithm for convex hulls and vertex enumeration of arrangements and polyhedra. *Discrete and Computational Geometry*, 8:295-313, 1992.
- [82] G. van der Wegen, R. Helmhold, P. Bronsveld, and J. De Hosson. Single crystal neutron diffraction study of the long-range order in Cu<sub>2</sub>NiZn. *Zeitschrift fur Metallkunde*, 74:592-7, 1983.
- [83] A. Brüngger, A. Marzetta, K. Fukuda, and J. Nievergelt. The parallel search bench ZRAM and its applications. Submitted To *Annals of Operations Research*.

- [84] L. G. Ferreira, S. H. Wei, and A. Zunger. Stability, electronic structure, and phase diagrams of novel inter-semiconductor compounds. *International Journal of Supercomputer Applications*, 5:34–56, 1991.
- [85] A. Fukumoto, A. Ueda, and Y. Hiwatari. Molecular dynamics study of ionic motion in  $\alpha$ -AgI. *Solid State Ionics*, 3–4:115–19, 1981.
- [86] W. D. Kingery. *Introduction to ceramics*. John Wiley & Sons, New York, 1960.
- [87] W. Zhong, D. Vanderbilt, and K. M. Rabe. Phase transitions in BaTiO<sub>3</sub> from first principles. *Physical Review Letters*, 73:1861–4, 1994.
- [88] W. Zhong, D. Vanderbilt, and K. M. Rabe. First-principles theory of ferroelectric phase transitions for perovskites: the case of BaTiO<sub>3</sub>. *Physical Review B*, 52:6301–12, 1995.
- [89] K. M. Rabe and U. V. Waghmare. Localized basis for effective lattice Hamiltonians: Lattice Wannier functions. *Physical Review B*, 52:13236–46, 1995.
- [90] C. Wolverton and A. Zunger. First-principles theory of short-range order, electronic excitations, and spin polarization in Ni–V and Pd–V alloys. *Physical Review B*, 52:8813–28, 1995.
- [91] G. Grimvall and I. Ebbsjo. Polymorphism in metals. I. Vibrational free energy. *Physica Scripta*, 12:168, 1975.
- [92] G. Grimvall. Polymorphism in metals. II. Electronic and magnetic free energy. *Physica Scripta*, 12:173, 1975.
- [93] W. Petry, A. Heiming, J. Trampenau, M. Alba, C. Herzig, H. R. Schober, and G. Vogl. Phonon dispersion of the bcc phase of group-IV metals. I. bcc titanium. *Physical Review B*, 43:10933, 1991.
- [94] R. E. Watson and M. Weinert. Contribution of electronic excitations to the entropy of crystals: The relative stabilities of the hcp, fcc, and bcc structures among the transition metals. *Physical Review B*, 30:1641, 1984.
- [95] B. N. J. Persson. Monte Carlo calculations of adsorbate structures and the role of the vibrational entropy in phase transitions at surfaces. *Physical Review B*, 40:7115, 1989.
- [96] A. Grossmann, W. Erley, and H. Ibach. Occupation of adsorption sites controlled by phonon entropy. *Physical Review Letters*, 71:2078–81, 1993.
- [97] T. B. Massalski et al., editors. *Binary alloy phase diagrams*. William W. Scott, Jr.; ASM International, Materials Park, Ohio, 1990.
- [98] A. A. Maradudin, E. W. Montroll, and G. H. Weiss. *Theory of lattice dynamics in the harmonic approximation*. Academic Press, New York, 1963.

- [99] M. Abramowitz and I. A. Stegun, editors. *Handbook of Mathematical Functions*. Dover Publications, New York, 1965.
- [100] L. Salter. On the thermodynamics of crystalline lattices. *Proceedings of the Royal Society. London*, 233:418, 1956.
- [101] G. D. Garbulsky and G. Ceder. Effect of lattice vibrations on the ordering tendencies in substitutional binary alloys. *Physical Review B*, 49:6327–30, 1994.
- [102] H. Bakker. Numerical calculations of the change of the vibrational entropy due to disordering of a one- and two-dimensional ordered binary alloy. *Philosophical Magazine A*, 45:213, 1982.
- [103] J. A. D. Matthew, R. E. Jones, and V. M. Dwyer. The effect of short-range order on the vibrational entropy of one-dimensional chains. *Journal of Physics F: Metal Physics*, 13:581, 1983.
- [104] P. Dean. The vibrational properties of disordered systems: numerical studies. *Reviews of Modern Physics*, 44:127, 1972.
- [105] J. M. Cowley. X-ray measurement of order in single crystals of  $\text{Cu}_3\text{Au}$ . *Journal of Applied Physics*, 21:24, 1950.
- [106] A. Miller. Model for a vibrating disordered binary alloy. *Physical Review B*, 39:3616, 1989.
- [107] S. Lefebvre, F. Bley, M. Fayard, and M. Roth. Neutron diffuse scattering investigation of different states of local order in  $\text{Ni}_{0.765}\text{Fe}_{0.235}$ . *Acta Metallurgica*, 29:749, 1981.
- [108] J. Vrijen and S. Radelaar. Clustering in Cu–Ni alloys: A diffuse neutron-scattering study. *Physical Review B*, 17:409, 1978.
- [109] G. D. Garbulsky and G. Ceder. Contribution of the vibrational free energy to phase stability in substitutional alloys: Methods and trends. *Physical Review B*, 53:8993–9001, 1996.
- [110] C. Cohen-Tannoudji, B. Diu, and F. Laloë. *Quantum Mechanics*. John Wiley & Sons, Paris, 1977.
- [111] I. Prigogine and J. Jeener. Effets isotopiques et propriétés thermodynamiques en phase condensée. I. *Physica*, 20:383–394, 1954.
- [112] I. Prigogine, R. Bingen, and J. Jeener. Effets isotopiques et propriétés thermodynamiques en phase condensée. II. *Physica*, 20:516–520, 1954.
- [113] F. J. Dyson. The dynamics of a disordered linear chain. *Physical Review*, 92:1331–1338, 1953.

- [114] W. A. Harrison. *Electronic Structure and the Properties of Solids*. Dover Publications, New York, 1989.
- [115] S. Goncalves and H. Bonadeo. Molecular-dynamics calculation of the vibrational densities of states and infrared absorption of crystalline rare-gas mixtures. *Physical Review B*, 46:10738–42, 1992.
- [116] B. W. van de Waal. Can the Lennard-Jones solid be expected to be fcc? *Physical Review Letters*, 67:3263–6, 1991.
- [117] G. J. Ackland. Vibrational entropy of ordered and disordered alloys. In G. M. Stocks and P. E. A. Turchi, editors, *Alloy modeling & design*, page 149. The Minerals, Metals & Materials Society, 1994.
- [118] R. Magri, S. H. Wei, and A. Zunger. Ground-state structures and the random-state energy of the Madelung lattice. *Physical Review B*, 42:11388, 1990.
- [119] L. L. Boyer and M. J. Mehl. A self consistent atomic deformation model for total energy calculations: application to ferroelectrics. *Ferroelectrics*, 150:13–24, 1993.
- [120] L. L. Boyer, M. J. Mehl, and M. R. Pederson. Charge transfer effects in  $\text{KNbO}_3$  and sodium. *Ferroelectrics*, 153:7–12, 1994.
- [121] R. G. Gordon and Yung Sik Kim. Theory for the forces between closed-shell atoms and molecules. *Journal of Chemical Physics*, 56:3122–33, 1972.
- [122] P. D. Tepesch et al. A model to compute phase diagrams in oxides with empirical or first-principles energy methods and application to the solubility limits in the CaO–MgO system. To be published in *Journal of the American Ceramic Society*.
- [123] H. Stokes. Computation of the dynamical matrix in the SCPIB method. Private communication.
- [124] A. F. Kohan. Formation energies of ordered structures in the MgO–CaO system, computed with the pseudopotential method. Private communication.
- [125] G. A. Alers. *Physical Acoustics*, volume III-B, page 1. Academic Press, New York, 1965.
- [126] D. C. Wallace. *Thermodynamics of crystals*. John Wiley & Sons, New York, 1972.
- [127] V. L. Moruzzi, J. F. Janak, and K. Schwarz. Calculated thermal properties of metals. *Physical Review B*, 37:790, 1988.
- [128] Chang-Seok Oh, T. Mohri, and Dong Nyung Lee. Phenomenological calculation of the  $\text{L1}_0$ -disorder phase equilibria in the Co–Pt system. *Materials Transactions JIM*, 35:445–50, 1994.

- [129] C. Colinet, J. Eymery, A. Pasturel, A. T. Paxton, et al. A first-principles phase stability study on the Au–Ni system. *Journal of Physics: Condensed Matter*, 6:L47–52, 1994.
- [130] I. A. Abrikosov, A. V. Ruban, D. Ya Kats, and Yu. H. Vekilov. Electronic structure, thermodynamic and thermal properties of Ni–Al disordered alloys from LMTO–CPA–DFT calculations. *Journal of Physics: Condensed Matter*, 5:1271–90, 1993.
- [131] Wei-Tsu Tseng and J. P. Stark. First-principle calculations of solid solubility of titanium in aluminium alloys. *Philosophical Magazine B*, 70:919–26, 1994.
- [132] T. Mohri, S. Takizawa, and K. Terakura. First-principles calculation of heats of formation for Au–Cu, Au–Pd and Au–Ag alloys with thermal vibration effects. *Journal of Physics: Condensed Matter*, 5:1473–80, 1993.
- [133] K. Nakamura and T. Mohri. Non-empirical calculation of thermal vibration effects on the phase stability of InP–InSb alloy. *Modelling and Simulation in Materials Science and Engineering*, 1:143–50, 1993.
- [134] T. Mohri. Theoretical study on the phase stability of a III–V semiconductor alloy. *Progress of Theoretical Physics Supplement*, 115:147–64, 1994.
- [135] J. D. Becker and J. M. Sanchez. First principles phase stability study of the Ru–Nb–Zr system. *Materials Science & Engineering A (Structural Materials: Properties, Microstructure and Processing)*, A170:161–7, 1993.
- [136] R. LeSar, R. Najafabadi, and D. J. Srolovitz. Finite-temperature defect properties from free energy minimization. *Physical Review Letters*, 63:624, 1989.
- [137] A. P. Sutton. Temperature-dependent interatomic forces. *Philosophical Magazine A*, 60:147–59, 1989.
- [138] L. Zhao, R. Najafabadi, and D. J. Srolovitz. Finite temperature vacancy formation thermodynamics: local harmonic and quasiharmonic studies. *Modelling and Simulation in Materials Science and Engineering*, 1:539–51, 1993.
- [139] H. Y. Wang, R. Najafabadi, D. J. Srolovitz, and R. Lesar. Interfacial segregation in Ag–Au, Au–Pd, and Cu–Ni alloys: I. (100) surfaces. *Interface Science*, 1:7–30, 1993.
- [140] R. Najafabadi and D. J. Srolovitz. Order–disorder transitions at and segregation to (001) Ni–Pt surfaces. *Surface Science*, 286:104–15, 1993.
- [141] R. P. Feynman. Forces in molecules. *Physical Review*, 56:340, 1939.
- [142] M. T. Yin and M. L. Cohen. Ab initio calculation of the photon dispersion relation: application to Si. *Physical Review B*, 25:4317–20, 1982.



- [143] K. M. Ho, C. L. Fu, and B. N. Harmon. Microscopic analysis of interatomic forces in transition metals with lattice distortions. *Physical Review B*, 28:6687, 1983.
- [144] P. Giannozzi, S. de Gironcoli, P. Pavone, and S. Baroni. Ab initio calculation of phonon dispersions in semiconductors. *Physical Review B*, 43:7231–42, 1991.
- [145] S. de Gironcoli. Lattice dynamics of metals from density–functional perturbation theory. *Physical Review B*, 51:6773–6, 1995.
- [146] S. de Gironcoli. Phonons in Si–Ge systems: an ab initio interatomic–force–constant approach. *Physical Review B*, 46:2412–19, 1992.
- [147] S. Wei and M. Y. Chou. Ab initio calculation of force constants and full phonon dispersions. *Physical Review Letters*, 69:2799, 1992.
- [148] Siqing Wei, Changlin Li, and M. Y. Chou. Ab initio calculation of thermodynamic properties of silicon. *Physical Review B*, 50:14587–90, 1994.
- [149] S. Wei and M. Y. Chou. Phonon dispersions of silicon and germanium from first–principles calculations. *Physical Review B*, 50:221–6, 1994.
- [150] W. H. Press, S. A. Teukolsky, W. T. Vetterling, and B. P. Flannery. *Numerical recipes in fortran. The art of scientific computing*. Cambridge University Press, Cambridge, 1992.
- [151] F. Herman. Lattice vibrational spectrum of germanium. *Journal of Physics and Chemistry of Solids*, 8:405, 1959.
- [152] Wang Jian, Zhang Kaiming, and Xie Xide. Reinvestigation of the TA modes in Ge and Si in Born–von Karman model. *Solid State Communications*, 86:731–4, 1993.
- [153] L. G. Ferreira, S. Wei, and A. Zunger. First–principles calculation of alloy phase diagrams: The renormalized–interaction approach. *Physical Review B*, 40:3197, 1989.
- [154] Y. Le Page. Computer derivation of the symmetry elements implied in a structure description. *Journal of Applied Crystallography*, 20:264–9, 1987.
- [155] K. Kunc and R. M. Martin. Ab initio force constants in GaAs: a new approach to calculation of phonons and dielectric properties. *Physical Review Letters*, 48:406–9, 1982.
- [156] M. Born and K. Huang. *Dynamical theory of crystal lattices*. Oxford University Press, London, 1956.
- [157] S. C. Jain, editor. *Germanium–silicon strained layers and heterostructures*. Academic Press, Boston, 1994.

- [158] A. Qteish and R. Resta. Thermodynamic properties of Si-Ge alloys. *Physical Review B*, 37:6983-90, 1988.
- [159] P. C. Kelires and J. Tersoff. Equilibrium alloy properties by direct simulation: oscillatory segregation at the Si-Ge(100) $2 \times 1$  surface. *Physical Review Letters*, 63:1164-7, 1989.
- [160] S. de Gironcoli, P. Giannozzi, and S. Baroni. Structure and thermodynamics of Si<sub>x</sub>Ge<sub>1-x</sub> alloys from ab initio Monte Carlo simulations. *Physical Review Letters*, 66:2116-19, 1991.
- [161] P. C. Weakliem and E. A. Carter. Surface and bulk equilibrium structures of silicon-germanium alloys from Monte Carlo simulations. *Physical Review B*, 45:13458-64, 1992.
- [162] A. Ourmazd and J. C. Bean. Observation of order-disorder transitions in strained-semiconductor systems. *Physical Review Letters*, 55:765-8, 1985.
- [163] D. J. Lockwood, K. Rajan, E. W. Fenton, and J. M. Baribeau. Ordering in Si<sub>1-x</sub>Ge<sub>x</sub> crystals. *Solid State Communications*, 61:465-7, 1987.
- [164] J. L. Martins and A. Zunger. Stability of ordered bulk and epitaxial semiconductor alloys. *Physical Review Letters*, 56:1400-3, 1986.
- [165] A. Qteish and R. Resta. Microscopic atomic structure and stability of Si-Ge solid solutions. *Physical Review B*, 37:1308-14, 1988.
- [166] A. M. Rappe, K. M. Rabe, E. Kaxiras, and J. D. Joannopoulos. Optimized pseudopotentials. *Physical Review B*, 41:1227-30, 1990.
- [167] L. Kleinman and D. M. Bylander. Efficacious form for model pseudopotentials. *Physical Review Letters*, 48:1425-8, 1982.
- [168] J. P. Perdew and A. Zunger. Self-interaction correction to density-functional approximations for many-electron systems. *Physical Review B*, 23:5048-79, 1981.
- [169] E. Kaxiras. Private communication.
- [170] G. Nilsson and G. Nelin. Study of the homology between silicon and germanium by thermal-neutron spectrometry. *Physical Review B*, 6:3777-86, 1972.
- [171] David Avis. Private communication.
- [172] D. de Fontaine, G. Ceder, and M. Asta. Low-temperature long-range oxygen order in YBa<sub>2</sub>Cu<sub>3</sub>O<sub>7</sub>. *Nature*, 343:544, 1990.
- [173] D.C. Langreth and M.J. Mehl. Beyond the local-density approximation in calculations of ground-state electronic properties. *Physical Review B*, 28:1809-34, 1983.

- [174] A.D. Becke. Density-functional exchange-energy approximation with correct asymptotic behavior. *Physical Review A*, 38:3098–100, 1988.
- [175] J.P. Perdew, J.A. Chevary, S.H. Vosko, K.A. Jackson, and others. Atoms, molecules, solids, and surfaces: Applications of the generalized gradient approximation for exchange and correlation. *Physical Review B*, 46:6671–87, 1992.
- [176] E. Wimmer, H. Krakauer, M. Weinert, and A.J. Freeman. Full-potential self-consistent linearized-augmented-plane-wave method for calculating the electronic structure of molecules and surfaces: O<sub>2</sub> molecule. *Physical Review B*, 24:864–75, 1981.
- [177] M. Methfessel, C.O. Rodriguez, and O.K. Andersen. Fast full-potential calculations with a converged basis of atom-centered linear muffin-tin orbitals: structural and dynamic properties of silicon. *Physical Review B*, 40:2009–12, 1989.
- [178] A. F. Kohan and G. Ceder. Tight-binding calculation of formation energies in multicomponent oxides: Application to the MgO–CaO phase diagram. To be published in *Physical Review B*.
- [179] M. Asta, C. Wolverton, D. de Fontaine, and H. Dreyssé. Effective cluster interactions from cluster-variation formalism. I. *Physical Review B*, 44:4907–13, 1991.
- [180] C. Wolverton, M. Asta, H. Dreyssé, and D. de Fontaine. Effective cluster interactions from cluster-variation formalism. II. *Physical Review B*, 44:4914–24, 1991.
- [181] A. Gonis, P.P. Singh, P.E.A. Turchi, and X.-G. Zhang. Use of the Ising model in the study of substitutional alloys. *Physical Review B*, 51:2122–31, 1995.
- [182] J.M. Sanchez. Cluster expansions and the configurational energy of alloys. *Physical Review B*, 48:14013–15, 1993.
- [183] S. M. Foiles. Evaluation of harmonic methods for calculating the free energy of defects in solids. *Physical Review B*, 49:14930–8, 1994.
- [184] P. Vashishta and A. Rahman. Ionic motion in  $\alpha$ -AgI. *Physical Review Letters*, 40:1337–40, 1978.
- [185] E. Kaxiras and K. C. Pandey. Contribution of concerted exchange to the entropy of self-diffusion in Si. *Physical Review B*, 47:1659–62, 1993.
- [186] I. M. Torrens. *Interatomic potentials*. Academic Press, New York, 1972.
- [187] A. Dalgarno and W. D. Davison. The calculation of van der Waals interactions. *Advances in Atomic and Molecular Physics*, 2:1, 1966.

- [188] J. E. Lennard-Jones. *Proceedings of the Royal Society*, A106:441, 1924.
- [189] J. Mei, B. R. Cooper, Y. G. Hao, S. P. Lim, et al. New technique for *ab-initio* atomistic potentials and application to thermal expansion of Ni-Cr alloys. In J. Broughton, P. Bristowe, and J. Newsam, editors, *Materials Research Society Symposium Proceedings*, volume 291, pages 15–20, Boston, 1993.
- [190] P. M. Morse. Diatomic molecules according to the wave mechanics. II. Vibrational levels. *Physical Review*, 34:57–64, 1929.
- [191] P. P. Ewald. *Ann. Phys. (Leipzig)*, 64:253, 1921.
- [192] C. R. A. Catlow, C. M. Freeman, M. S. Islam, R. A. Jackson, , and others. Interatomic potentials for oxides. *Philosophical Magazine A*, 58:123–41, 1988.
- [193] M. S. Daw and M. I. Baskes. Embedded-atom method: derivation and application to impurities, surfaces and other defects in metals. *Physical Review B*, 29:6443, 1984.
- [194] M. S. Daw, S. M. Foiles, and M. I. Baskes. The embedded-atom method: a review of theory and applications. *Material Science Reports*, 9:251–310, 1993.
- [195] F. H. Stillinger and T. A. Weber. Computer simulation of local order in condensed phases of silicon. *Physical Review B*, 31:5262–71, 1985.
- [196] Jurgen Hafner. *From Hamiltonians to Phase Diagrams*. Springer-Verlag, Berlin Heidelberg, 1987.
- [197] J. A. Moriarty. First-principles interatomic potentials in transition metals. *Physical Review Letters*, 55:1502, 1985.
- [198] J. A. Moriarty. Analytic representation of multi-ion interatomic potentials in transition metals. *Physical Review B*, 42:1609, 1990.
- [199] H. J. Monkhorst and J. D. Pack. Special points for Brillouin-zone integrations. *Physical Review B*, 13:5188–92, 1976.
- [200] S. Froyen. Brillouin-zone integration by Fourier quadrature: special points for superlattice and supercell calculations. *Physical Review B*, 39:3168–72, 1989.